# Estimation of surface roughness over bare agricultural soil from Sentinel-1 data

Mohammad Choker

# THÈSE POUR OBTENIR LE GRADE DE DOCTEUR DE L'INSTITUT DES SCIENCES ET INDUSTRIES DU VIVANT ET DE L'ENVIRONNEMENT - AGROPARISTECH

N°: 2018 AGPT 0001

**En : Géomatique**

**École doctorale GAIA – Biodiversité, Agriculture, Alimentation, Environnement, Terre, Eau – n°584**
**Portée par l'Université de Montpellier**

**Unité de recherche : TETIS**

## Estimation de la rugosité du sol en milieux agricoles à partir de données Sentinel-1

**Présentée par**
Mohammad CHOKER
**Le 30 Avril 2018**

**Sous la direction de :** Nicolas BAGHDADI et Mehrez ZRIBI

**Devant le jury composé de**

| | |
|---|---|
| **M. Ali KHENCHAF**, Professeur des universités, Lab-STICC UMR CNRS 6285, ENSTA Bretagne, Brest, HDR | Rapporteur, Président |
| **M. Lionel JARLAN,** Professeur des université, Université Paul Sabatier / Ecole Doctorale Sciences de l'Univers, de l'Environnement et de l'Espace (SDUEE), HDR | Rapporteur |
| **M. Hatem BELHOUCHETTE**, Cadre de recherche, Institut Agronomique Méditerranéen Montpellier (IAMM) | Examinateur |
| **Mme Emmanuelle VAUDOUR-DUPUIS,** Maitre de conférences, HDR, AgroParisTech, Centre de Grignon, | Examinatrice |
| **M. Mehrez ZRIBI,** Directeur de recherche, CNRS | Examinateur |
| **M. Nicolas BAGHDADI**, Directeur de recherche, IRSTEA | Examinateur |

AgroParisTech
INSTITUT DES SCIENCES ET INDUSTRIES DU VIVANT ET DE L'ENVIRONNEMENT
PARIS INSTITUTE OF TECHNOLOGY FOR LIFE, FOOD AND ENVIRONMENTAL SCIENCES

UNIVERSITÉ DE MONTPELLIER

# RESUME

La télédétection spatiale est d'une importance primordiale pour la cartographie et la surveillance des problèmes environnementaux. Son intérêt réside dans la capacité des capteurs satellitaires spatiaux à fournir des informations globales et permanentes de la planète, aux échelles locale à globale. La télédétection radar a montré son grand potentiel ces dernières années dans la caractérisation des états de surface du sol. L'état de la surface du sol, et en particulier l'humidité et la rugosité, exerce une influence fondamentale sur la répartition de la pluie entre infiltration, rétention superficielle et ruissellement. Il a un rôle essentiel dans les processus hydrologiques de surface et ceux associés à l'érosion et aux processus d'évapotranspiration. La caractérisation et la prise en compte de ces conditions de surface constituent actuellement un enjeu important pour la modélisation à base physique des processus hydrologiques ou pour le couplage surface-atmosphère. Dans ce cadre et depuis plusieurs années, plusieurs études scientifiques ont montré le potentiel des données micro-ondes actives dans l'estimation de l'état hydrique du sol et de sa rugosité de surface.

Les nouveaux systèmes radar (SAR ″Synthetic Aperture Radar″) ont permis d'ouvrir de nouvelles perspectives pour l'observation de la terre grâce à l'amélioration de la résolution spatiale (métrique sur TerraSAR-X et COSMO-SkyMed) et temporelle (TerraSAR-X, COSMO-SkyMed, Sentinel-1). La disponibilité depuis peu des nouveaux capteurs radar bande C Sentinel-1 (Sentinel-1A et Sentinel-1B) rend indispensable l'évaluation des données Sentinel-1 pour la caractérisation des états de surface du sol et en particulier la rugosité de surface.

Le travail de thèse se structure en trois parties. La première partie consiste à évaluer les modèles de rétrodiffusion de radar les plus utilisés (IEM, Oh, Dubois and AIEM) en utilisant un large ensemble de données de SAR et des mesures expérimentales des paramètres du sol. Cette évaluation permet de trouver le modèle de rétrodiffusion le plus robuste qui simule le mieux le signal radar afin de l'utiliser par la suite dans la procédure d'inversion du signal radar pour estimer la rugosité du sol. Le deuxième axe de recherche de cette thèse consiste à proposer un modèle de rétrodiffusion radar semi-empirique pour les polarisations HH, HV et VV. Ce nouveau modèle sera construit à l'aide d'une grande base de données réelle. Ce nouveau modèle sera également utilisé dans la procédure d'inversion du signal radar pour estimer la rugosité du sol. Le dernier axe de cette thèse consiste à construire une méthode d'inversion du signal radar en utilisant les réseaux de neurones afin d'évaluer le potentiel des données Sentinel-1 pour l'estimation de la rugosité des sols en milieux agricoles. Ces réseaux de neurones seront entraînés à l'aide d'un ensemble de données synthétiques élaborées à partir des modèles de rétrodiffusion radar choisis (IEM calibré par Baghdadi et du nouveau modèle proposé) et validés en utilisant deux ensembles de données: un ensemble de données synthétiques et une base de données réelle (images Sentinel-1 et mesures in situ d'humidité et de rugosité du sol). La base de données réelle a été collectée en Tunisie (Kairouan) et en France (Versailles).

***Mots clés :*** Radar, Sentinel-1, surfaces agricoles, rugosité du sol, modèles de rétrodiffusion radar

# ABSTRACT

Spatial remote sensing is of paramount importance for mapping and monitoring environmental problems. Its interest lies in the ability of space satellite sensors in providing permanent information of the planet, at local, regional and global scales. Also, it provides spatial and repetitive territories visions and ecosystem views. Radar remote sensing has shown great potential in recent years for the characterization of soil surface conditions. The state of the soil surface, in particular moisture and roughness, has a fundamental influence on the distribution of rainfall between infiltration, surface retention and runoff. In addition, it plays an essential role in surface hydrological processes and those associated with erosion and evapotranspiration processes. Characterization and consideration of these surface conditions have been recently considered as an important issue for physically based modeling of hydrological processes or for surface-atmosphere coupling. In this context and for several years, several scientific studies have shown the potential of active microwave data for estimation of the soil moisture and the surface roughness.

New SAR (Synthetic Aperture Radar) systems have opened new perspectives for earth observation through improved spatial resolution (metric on TerraSAR-X and COSMO-SkyMed) and temporal resolution (TerraSAR-X, COSMO-SkyMed, Sentinel-1) . The recent availability of new Sentinel-1 C-band radar sensors (free and open access) makes it essential to evaluate the potential of Sentinel-1 data for the characterization of soil surface conditions and in particular surface roughness.

The work revolves around three parts. The first part consist of evaluation of the most used radar backscattering models (IEM, Oh, Dubois, and AIEM) using a wide dataset of SAR data and experimental soil measurements. This evaluation gives the ability to find the most robust backscattering model that simulates the radar signal with good agreement in order to use later in the inversion procedure of the radar signal for estimating the soil roughness. The second research axe of this thesis consists of proposing an empirical radar backscattering model for HH, HV and VV polarizations. This new model will be developed using a large real dataset. This new model also will be used in the inversion procedure of the radar signal for estimating the soil roughness. The last axe of this thesis consists of producing a method to invert the radar signal using neural networks. The objective is to evaluate the potential of Sentinel-1 data for estimating surface roughness. These neural networks will be trained using wide synthetic dataset produced from the radar backscattering models chosen (IEM calibrated by Baghdadi and the new proposed model) and validated using two datasets: one synthetic dataset and one real (Sentinel 1 images and in-situ measurements). The real datasets are collected from Tunisia (Kairouan) and France (Versailles).

***Keywords:*** Radar, Sentinel-1, agricultural areas, soil roughness, radar backscattering models

# REMERCIEMENTS

Mes profonds remerciements vont avant tout à *M. Nicolas Baghdadi* mon directeur de thèse. Merci *Nicolas* de m'avoir confié ce travail de recherche et de vous être toujours montré à l'écoute, et disponible tout au long de la réalisation de cette thèse. Votre implication et votre disponibilité en toute circonstance, vos conseils avisés, votre exigence, ont été des appuis inestimables. Au même titre, j'adresse mes sincères remerciements à *M. Mehrez Zribi* pour sa participation à la direction de ma thèse, ses bons conseils, et sa sympathie. Avec vous j'ai énormément appris au cours de ces trois années.

Je tiens également à remercier la directrice de l'UMR TETIS *Mme Christiane Weber* de m'avoir accueilli au sein de l'unité TETIS que j'ai eu plaisir à intégrer.

Je souhaiterais aussi particulièrement remercier *M. Mohamad EL-Hajj* pour l'intérêt qu'il est porté à mes travaux, et surtout pour avoir apporté son aide et son conseils à chacune de mes sollicitations.

Je tiens également à remercier *Mme Emmanuelle Vaudour* (UMR ECOSYS, AgroParisTech) et *Mme* Safa Bousbih (INAT) pour leurs soutiens lors des campagnes de terrain. *Mme Emmanuelle Vaudour* a mis à disposition les données in situ sur le site de Versailles (France) et *Mme* Safa Bousbih sur le site de Kairouan (Tunisie).

Mes remerciements s'adressent également à toute l'équipe de la Maison de la Télédétection de Montpellier pour son accueil et son aide. Plus particulièrement à mes collègues *Hassan Bazzi, Ali Nasrallah, Ibrahim El Moussawi, Sarah Zenasni et Lynda Khiali.*

# Table of contents

# List of abbreviations

- **SAR:** Synthetic Aperture Radar
- **mv:** soil moisture
- **H*rms*:** Standard deviation heights
- **L:** Autocorrelation length
- **RMSE:** Root Mean Square Error
- **$R^2$**: Correlation coefficient
- **IEM**: Integral Equation Model
- **AIEM**: Advanced Integral Equation Model
- **IEM_B**: IEM calibrated by Baghdadi
- **GCF**: Gaussian correlation function
- **ECF:** Exponential Correlation function
- **WCM:** Water cloud Model
- **θ :** incidence angle
- **NN:** Neural Network

# List of publications

Several aspects developed during this thesis and have been the subject of publications in peer-reviewed international scientific journals and contributions to conferences. A list of these publications is given bellow:

## 1. Articles published

- **Choker M.,** Baghdadi N., Zribi M., El Hajj M., Paloscia S., Verhoest N., Lievens H., Mattia F., 2017. Evaluation of the Oh, Dubois and IEM models using large dataset of SAR signal and experimental soil measurements. *Water*, 9(38), pp. 1-27, doi: 10.3390/w9010038.
- Baghdadi N., **Choker M**., Zribi M., El Hajj M., Paloscia S., Verhoest N., Lievens H., Baup F., Mattia F., 2016. A new empirical model for radar scattering from bare soil surfaces. *Remote Sensing, vol. 8, Issue 11, pp. 1-14,* doi: 10.3390/rs8110920.
- Baghdadi, N., El Hajj, M., **Choker, M**., Zribi, M., Bazzi, H., Vaudour, E., Gilliot, J.-M., and Ebengo, D.M. 2018. Potential of Sentinel-1 Images for Estimating the Soil Roughness over Bare Agricultural Soils *Sentinel-1, SAR* , Water 10, 131.

## 2. International Conferences

- **Choker M.,** Baghdadi N., Zribi M., El Hajj M., 2017. New semi-empirical radar backscattering model for bare soil surfaces based on the Dubois model. 5th International Symposium on Recent Advances in Quantitative Remote Sensing (RAQRS'V), 18-22 September 2017, Torrent, Valencia, Spain.
- Baghdadi N., **Choker M.,** Zribi M., El Hajj M., Paloscia S., Verhoest N., Lievens H., Baup F., Mattia F., 2017. New empirical model for radar scattering from bare soils. International Geoscience and Remote Sensing Symposium 2017 (IGARSS 2017), 23 - 28 July 2017, Fort Worth, Texas, USA.
- Baghdadi N., El Hajj M., **Choker M.,** Zribi M., Bazzi H., Vaudour E., Gilliot J.M., Mwampongo D.E., 2018. Potential of Sentinel-1 images for estimating the soil roughness over bare agricultural soils. International Geoscience and Remote Sensing Symposium 2018 (IGARSS 2018), Torrent, Valencia, Spain.

# *I. Chapter 1: Introduction*

## I.1 Context

The soil is not just the surface we walk on, build on, nor the land we cultivate; it is the source of our life and a wealth that we must preserve. From the 1950s, the intensification of agricultural land accelerated the processes of soil degradation, thus affecting their biophysical-chemical properties. The first component directly affected by intensification is soil fertility in particular (organic matter and soil structural stability).

Generally, several soil processes could be identified based on specific physical conditions and physical, chemical or biological activities. The soil processes are classified mainly into seven categories (Bockheim and Gennadiyev, 2000): (i) the translocation which is related to physical movements and always in the downward direction, (ii) the Organic Changes which occur mainly on the surface and follow a specific sequence, (iii) the Podzolization which happens in cool, humid climates where the bacterial activity is low, (iv) the gleying which takes place under water-logged and anaerobic conditions, (v) the salinization, (vi) the recarbonatation, (vii) eventually, the desilication that is common in hot-wet tropical and equatorial climates.

The study and modeling of the continental surfaces functioning and their interactions with the atmosphere are essential research subjects to understand the climatic system of the earth. These surfaces constantly exchange the amount of movement, energy, water and chemical constituents, such as carbon, nitrogen, etc… As for continental hydrology, the processes involved in the water cycle and quantifying the exchanges of matter and energy shall be understood. Surface states essentially control the distribution of rainfall between soil storage, underground infiltration, runoff and evapotranspiration. Hydrodynamic characteristics, roughness and vegetation cover are major determinants of hydrological processes (soil water interception and return to the atmosphere), and those associated with erosion (Ambroise, 1999; Auzet et al., 2005).

Runoff and erosion in agricultural soils are major problem for territorial managers. For several years, several regions in Europe have been facing an increase in natural disasters: floods, loss of fertile land, soil degradation and water quality. The soil conditions (i.e. moisture and surface roughness) have an essential role in surface hydrological processes. Runoff occurs when the amount of rain exceeds the infiltration capacity of the soil (Le Bissonnais, 1990; Brun et al., 1990; François, 1988; Zobeck and Onstad, 1987).

Soils with silty texture are particularly sensitive to runoff because they are subjected to crusting phenomenon as a result of episodes (Le Bissonnais and Singer, 1992). The interactions between meteorological conditions, agricultural practices and soil texture cause significant and fast changes in the hydraulic properties of the soil surfaces. The deterioration of soil infiltrability and surface storage capacity is strongly influenced by the phenomena of crusting and degradation of roughness and the genesis conditions of runoff, causing erosive problems (Govers et al., 2000; King and Le Bissonnais, 1992).

Soil moisture is a key parameter in the different processes involved in the hydrological cycle (water cycle). Knowledge of moisture is necessary to assess water resources and to carry out water balances. Information on the spatial distribution of soil moisture optimizes water reassignment during droughts and provides support for flood forecasting and management. From an agronomic point of view, soil moisture is a crucial variable for crop development. Thus, assessing it allows better monitoring and management of irrigation, leading to a more precise farming.

Another characteristic of the soil to be considered is the surface roughness. It is a physical parameter that characterizes the surface state. For agricultural soils, roughness defines the microrelief of the soil surface on the clods scale and is due to small accidents in the field (natural, cultivation techniques or both). Knowing the state of surface roughness is necessary for understanding the different processes. It is a key parameter in the estimation of water storage capacity within the soil horizons as well as modeling runoff. This latter phenomenon has a great influence on the erosion processes (Roose, 1996) and determines the floods following a rainy event.

The evolution in time and space of the physical, hydraulic and geometric properties of soil surfaces is an information that can be integrated into hydrological models for forecasting the water balance and the processes of runoff and erosion (Auzet et al., 2005; Baghdadi et al., 2004; Boiffin, 1984; Casenave and Valentin, 1989; King et al., 2005; Ludwig et al., 1995; Quesney et al., 2000; Weisse et al., 2003). Moreover, soil and water resources' management are key issues, not only from the environmental point of view, but also from a socioeconomic perspective (Condrea and Bostan, 2008).

There are many in situ experimental methods to measure surface soil moisture (Gardner, 1986; Topp et al., 1980). These methods allow precise soil moisture estimates only at the

local scale. Since several years, the scientific community has demonstrated the potential of spatial observation for estimating soil parameters. Spatial remote sensing allows repetitive measurements and provides access to spatial information at scales that can be very fine.

In this context, remote sensing is of paramount importance for mapping and monitoring environmental problems. Its interest lies in the ability of space-based satellite sensors to provide global and permanent information about the planet.

## I.2 State of art

### I.2.1 Remote sensing data for soil characterization

Active microwave remote sensing is specifically well suitable in agricultural fields concerning the characterization of soil surface conditions. Synthetic Aperture Radar (SAR) sensors allow all-weather measurements, independently of weather conditions (cloud cover, day/night…). They use microwave frequencies with wavelengths between 1 mm to 1 m. Theses microwave frequencies are very sensitive to the geometric and dielectric properties which are themselves dependent on surface parameters (roughness, soil moisture, soil composition and vegetation cover). SAR signal also depends on different instrumental parameters (polarization, incidence angle, and radar wavelength).

Studies using radar remote sensing started at the end of the 70s with in-situ or airborne scatterometers (Ulaby et al., 1978). The developments of these studies became more important in the 1990s with satellite and airborne SAR (ERS-1/2, JERS, SIR-C, RADARSAT-1 …). Most studies were carried out in C-band (wavelength ~6 cm), L-band (wavelength ~22 cm), and more recently in X-band (wavelength ~3 cm). Firstly, the satellite SAR sensors that were accessible to the scientific community had an instrumental configuration of mono-polarization and a single incidence angle (ERS-1/2, JERS). The second generation of radar sensors with new instrumental configurations (RADARSAT, ASAR/ENVISAT, PALSAR/ALOS, TerraSAR-X, COSMO-SkyMed, Sentinel-1) allowed the scientific community to gather images in multi-polarization and sometimes polarimetric mode (scattering matrix). These SAR second generation provide images in high spatial resolution (about 1 m for TerraSAR-X and COSMO-SkyMed) and high temporal resolution (up to one image by day). In addition, the launch of the Sentinel-1 C-band SAR, which is based on a constellation of two satellites (A and B units) makes it possible to obtain SAR data for global areas at high spatial and temporal resolutions (spatial resolution of 10 m and time revisit of 6 days over Europe) with free and open access Sentinel satellites. These new SAR sensors with

C-band are suitable for hydrological and agronomic applications (Alexakis et al., 2017; Aubert et al., 2011; Baghdadi et al., 2002a, 2011a, 2012a; Hajnsek et al., 2009; Holah et al., 2005; Paloscia et al., 2008; Srivastava et al., 2003, 2009; Zribi et al., 2005a).

Some low resolution spatial sensors are also suitable for meteorological and climatic applications on a global scale such as, AMSR-E, AMSR2 (microwave radiometers), SMOS, SMAP (L-band microwave radiometers), and ASCAT/METOP (C-band scatterometer). They provide users of soil moisture products with a temporal frequency on few days with a spatial resolution around 25-40 km (Champagne et al., 2016; Chan et al., 2016; Entekhabi et al., 2010; Jackson et al., 2012; Mohanty et al., 2017; Wigneron et al., 2017).

For bare agricultural soils or soils with little vegetation, the radar signal is dependent on the two parameters of the surface: the dielectric constant related to the soil moisture and the surface roughness. Several radar backscatter models have been developed in recent years with the aim to model the backscattering of natural surfaces and to reverse the radar response to find the different parameters of the soil surface. These models depend on the sensor characteristics (incidence, frequency, polarization...) and those of the target (soil moisture and surface roughness). From a perspective of anticipation or coherence of information on various natures, it is essential to rely on models capable for estimating soil parameters. Numerous radar backscattering models have been developed in order to estimate soil parameters (i.e. soil moisture and surface roughness) (Zribi and Dechambre, 2003, Baghdadi et al., 2004, 2006a, 2011b, 2015, 2016a; Chen et al., 2003; Dubois et al., 1995; Fung et al., 1992; Oh, 2004; Oh et al., 1992, 1994, 2002). However, ground measurements of different soil parameters are necessary to calibrate these models in order to have accurate estimations.

### I.2.2 Potential of radar data for monitoring soil conditions

Synthetic Aperture Radar (SAR) data have been used for a long time to estimate and map soil moisture. Several radar backscattering models were developed in order to estimate soil parameters (i.e. soil moisture and surface roughness). The availability of high spatial and temporal resolutions SAR Sentinel-1 data and these models make the intere st to estimate soil parameters accurately. In the case of bare soils (or soils with little vegetation), the estimation of soil moisture and surface roughness was performed by inverting the measured SAR backscatter through SAR backscattering models (both empirical and physical). Unlike physical models, empirical or semi-empirical models need to be calibrated each time the study

area changes by using site-specific in situ measurements and SAR observations. The most commonly semi-empirical models are the models of Oh (Oh, 2004; Oh et al., 1992, 1994, 2002) , Dubois (Dubois et al., 1995) and Baghdadi (Baghdadi et al., 2016a); while, the most popular physical models are Integral Equation Model (IEM) (Fung et al., 1992), IEM calibrated by Baghdadi, called in this thesis "IEM_B" (Baghdadi et al., 2002b, 2004, 2006a, 2011a, 2011b, 2015), and Advanced Integral Equation Model (AIEM) (Chen et al., 2003).

Several studies have been carried out to evaluate and compare the robustness of the backscattering models such as, Oh, Dubois and IEM (original IEM, IEM_B and AIEM). Zribi et al. (1997) evaluated the Oh model and IEM using L-, C- and X-bands SAR data and in situ measurements. Results showed that the IEM provides accurate simulations (RMSE about 2.0 dB) only over smooth surfaces. In addition, for rough surfaces and medium incidence angle, Oh model simulations retrieve backscattering values very close to the measured ones, while showing poor correlation with measured backscattering coefficients over smooth areas. Baghdadi and Zribi (2006) evaluated the backscattering models IEM, Oh and Dubois by using large C-band SAR data and in situ measurements. Results showed that these models frequently tend to over-estimate or under-estimate the radar signal (in the order of 3.0 dB) and the errors on model simulation depend on height surface roughness, *Hrms*, soil moisture, *mv*, and/or incidence angle. Baghdadi et al. (2011b) evaluated the potential of IEM, Oh and Dubois models by using TerraSAR-X images acquired over France and Tunisia and experimental datasets of in situ measurements (*mv* ranged between 5 vol. % and 41 vol. % and *Hrms* between 0.42 cm and 4.55 cm). In this case, the semi-empirical Oh model correctly simulated the backscattering (showing over or under-estimation of the backscatter <1 dB, and RMSE <3 dB), while Dubois model showed a poor correlation between real data and simulations, with RMSE between 2.2 and 4.4 dB and over or under-estimation of the backscatter of about 3.4 dB. In addition, the IEM correctly simulates the backscattering at X-band for *Hrms* < 1.5 cm by using the exponential correlation function and for *Hrms* > 1.5 cm by using the Gaussian correlation function. Panciera et al. (2014) compared the performances of the IEM, Dubois and Oh models by using fully polarized L-band airborne data (incidence angles between 24° and 38°) and in situ measurements (*mv* between 5 vol. % and 39 vol. % and *Hrms* between 1 cm and 7.6 cm) acquired over the study area in southeastern Australia. At HH polarization, the three models simulated the backscattering with almost similar accuracy, showing a mean error between the simulated and the observed backscattering coefficients of about 1.6 dB in absolute value (standard deviation "std" about ±2.5 dB). At

VV polarization, the Oh model resulted to be more accurate than IEM and Dubois models: the mean errors between the simulated and observed backscattering were equal to 4.5 dB (std = ±2.0 dB), 1.7 dB (std = ±2.3 dB), and −0.4 dB (std = ±2.4 dB) for IEM, Dubois, and Oh model, respectively. Moreover, several studies confirmed that the use of the calibrated correlation length, as proposed by Baghdadi et al. (2002, 2004, 2006, 2011a, 2011b, 2015) is able to improve the performance of the IEM at both HH and VV polarizations (Dong et al., 2013; McNairn et al., 2010; Panciera et al., 2014). Dong et al. (2013) used the calibrated correlation length in the AIEM to simulate SAR data in C-band. Results showing that the RMSE reduced from 3.1 to 1.7 dB at HH and VV polarizations and from 31.0 dB to 5.1 dB at HV polarization. Panciera et al. (2014) showed that the use of calibrated correlation length decreases the errors on IEM simulation with a bias equal to about −0.3 dB (standard deviation about ±1.1 dB) at both HH and VV polarizations.

Several studies were done in order to investigate the SAR data for monitoring roughness states over bare agricultural soils. Baghdadi et al., (2002a) examined the potential of the first generation of SAR data (ERS-2 and RADARSAT-1) to estimate surface roughness over bare agricultural soils. Results showed that the use of high incidence angles about 45° are more appropriate to differentiate numerous roughness classes (smooth, medium and rough) over bare agricultural soils. Moreover, Baghdadi et al. (2012a) used neural networks (NNs)techniques to estimate soil moisture *mv* and surface roughness *Hrms* from C-band polarimetric RADARSAT-2 data. Results indicated that the accuracy on the soil roughness estimates was about 0.5 cm using polarimetric data. The estimation is better for *Hrms*-values lower than 2 cm than for *Hrms*-values higher than 2 cm. For higher *Hrms*, the neural networks under-estimate the surface roughness.

## I.3 Plan of the thesis

The general objective of this work is to explore and evaluate the potential of the Sentinel-1 radar sensor to estimate surface roughness over bare agricultural soil. The originality is that few studies have been done to estimate soil roughness from SAR data and never before have been estimated from Sentinel-1 data. The recent launch of Sentinel-1 C-band SAR providing full earth coverage at high spatial and temporal resolutions with free and open access satellite justifies this work.

Thus, the first part of this thesis is to analyze the quality of the most popular radar backscattering models in order to find the model that best fit the SAR measurements. Integral Equation Model "IEM", Integral Equation Model calibrated by Baghdadi "IEM_B", Oh, Dubois, and Advanced Integral Equation Model "AIEM" will be evaluated using a wide dataset of SAR data and experimental soil measurements. The results will show the performance of each model in order to identify the most robust backscattering model that will be used later in the inversion procedure for estimating the soil roughness.

After evaluating the existing radar backscattering models (semi-empirical, empirical and physical) using a wide reference dataset of SAR (Synthetic Aperture Radar) data and experimental soil measurements, a new radar backscattering model will be proposed. The objective is to develop an empirical radar backscattering model. Never before a backscattering model has been built and validated on such a large dataset: wide range of incidence angles (18°-57°), dataset in L, C and X bands, dataset well distributed geographically for regions with different climate conditions (humid, semi-arid and arid sites) and involving many SAR sensors.

The last research part of this thesis consists of proposing a method to invert the radar signal using neural networks technique. The objective is to evaluate the potential of Sentinel-1 data for estimating soil roughness. The best model found in the first part of this thesis and the new empirical model developed in the second part will be used to train and validate neural networks. Finally, the neural networks will be validated using a real dataset composed of Sentinel-1 images and in-situ measurements, collected in Tunisia and France.

This thesis is composed of several chapters. This first chapter is a general introduction that describes the importance of soil parameters and the potential of remote sensing techniques for their monitoring. The second chapter introduces the concept of radar remote sensing technique and describes the interaction of electromagnetic waves with agricultural soils. The soil surface parameters (roughness and moisture content) as well as the different methods for estimating these parameters are described. Next, the most popular radar backscattering models (empirical, semi-empirical and analytical) will be described and evaluated in chapter 3. A new semi-empirical backscattered model will be proposed in chapter 4. Finally in chapter 5, neural networks trained on dataset simulated from radar backscattering models (the IEM modified by Baghdadi and the new proposed model) will be used to estimate the soil roughness from Sentinel-1 radar images. Conclusions and perspectives are presented in chapter 6.

# *II. Chapter 2: Generalities*

## II.1 Introduction

This chapter is an introduction to radar remote sensing, its principle measurement and its instrumental characteristics. Some reminders are introduced in section 2 on electromagnetic waves and their interactions with surfaces in agricultural areas. Section 3 of this chapter describes the descriptive parameters of soil (moisture and roughness). Section 4 shows the sensitivity of radar signal to soil moisture and surface roughness. In this thesis, our study focuses on soils in bare agricultural areas. Thus, to conclude this chapter, the electromagnetic backscattering models are introduced, which simulate the radar signal by linking it to the geophysical parameters of the soil surface, mainly moisture and roughness.

## II.2 Radar remote sensing

Radar is an active sensor for Earth observation, operates in the microwave frequencies of the electromagnetic spectrum (300 MHz to 30 GHz). The principle of radar, for the observation of surfaces, consists of emitting an electromagnetic wave in a selected configuration (frequency, polarization, incidence angle). This wave propagates in space to the observed surface and part of the emitted energy is returned in the direction of observation. It is then said that the energy is backscattered. It is a function of both the characteristics of the system and the nature of the surface (electrical properties and surface state) (Baghdadi and Zribi, 2016).

In the general introduction, we have already mentioned the advantages of the radar. It is used day and night and is almost insensitive to the weather conditions. For the observation of the Earth, most radars are synthetic aperture radars (SARs) which provide images with high and very high spatial resolution (from 1m for TerraSAR-X and CosmoSky-Med to 10 m for Sentinel-1 for example). These new SAR images have made it possible to retrieve surface soil parameters with a high spatial resolution.

### II.2.1 Instrumental Parameters

The main instrumental parameters of radar remote sensing described in this subsection are frequency, polarization and incidence angle.

*II.2.1.1 Radar frequency*

Radar systems operate on the microwave domain. The frequency of the transmitted signal is the number of waves passing through a given point during the interval of one second. It is measured in Hertz. The frequency ranges in the microwave domain (from 0.3 to 300GHz) Wavelength is a measure of the physical distance between peaks of a sine wave propagated in space. Most radar signals have wavelengths measured in centimeters or millimeters. Wavelength and frequency have inverse relationship $= c/\lambda$ : the higher the frequency, the shorter the wavelength. The wavelengths range in the microwave domain between 1m and 1mm.

For the Earth observation, the frequency bands particularly used in radar imagery are summarized in the table II.1.

| **Band** | **Frequency (GHz)** | **Wavelength (cm)** | **Space sensors** |
|---|---|---|---|
| P | 0.3-1 | 100-30 | Biomass (not launched) |
| L | 1-2 | 30-15 | PALSAR/ALOS |
| C | 4.20-5.75 | 7.1-5.2 | ERS, ASAR, RADARSAT, SENTINEL-1, … |
| X | 5.75-10.9 | 5.2-2.7 | TerraSAR-X, Cosmo-SkyMed |

**Table II.1.** The main frequency band used in radar imagery and examples of space sensors (past, present or future).

Using radar images in L, C, and X bands to perform studies for the characterization of the soil surface moisture in agricultural areas, in-situ measurements of soil moisture are taken at a depth between 0 and 10 cm. This measurement depth is related to the penetration depth of the radar wave (δp) that is generally equal to few centimeters in C and X bands. In L-band, this

depth could reach a few dozen cm for very dry soils. Moreover, the penetration depth of the radar signal in C-band decreases from 5 to 1 cm for a clay soil when the soil moisture increases from 10 to 30 vol. % (HH polarization and 15º incidence angle) (Bruckler et al., 1988). Indeed, the thickness of this surface layer depends on the radar wavelength (λ) (more penetration with greater wavelengths) and the dielectric constant of soil (water content and soil composition) (Ulaby et al., 1978):

$$\delta_p \cong \frac{\lambda\sqrt{\varepsilon'}}{2\pi\sqrt{\varepsilon''}} \qquad (2.1)$$

Where ε' is the real part of the dielectric constant and ε" its imaginary part.

The dielectric constant is a physical quantity also known as complex permittivity. The amount of water present in a soil affects its electrical properties and consequently the radar signal. The microwave dielectric constant of soil is related to soil moisture content and to a lesser extent soil texture (Ulaby et al., 1978). This constant is a complex number expressed in the form $\varepsilon=\varepsilon'-j\varepsilon''$. The real part ε' affects the moisture content more, while the imaginary part ε" essentially depends on the electrical conductivity of the soil solution.

*II.2.1.2 Polarization*

The polarization is a property of the electromagnetic wave that describes the orientation of the electric field in the plane perpendicular to the direction of propagation. For radars existing in the Earth observation field, this is a linear polarization in two directions (horizontal and vertical). For example, Sentinel-1 has selectable single polarizations (VV or HH) for the Wave mode and selectable dual polarizations (two polarizations: VV+VH or HH+HV) for all other modes.

*II.2.1.3 Incidence angle*

The incidence angle (θ) is the angle between the incident propagation direction and the normal surface, in the plane of propagation. The first generation of satellite radar had a fixed sight (for ERS-1/2, θ is centered at 23°). Other sensors have been equipped with variable-focus antennas that can acquire images with incidence angles ranging from 20° to 46° for Sentinel-1.

The launch of multi-incidence SAR satellites (ASAR, RADARSAT-1/2, TerraSAR-X, COSMO-SkyMed, Sentinel-1) have allowed to estimate under very limited conditions the soil moisture and surface roughness simultaneously, even though multi-incidence acquisitions actually represent two acquisitions on two different dates. However, it is assumed that the soil parameters have not changed between the two acquisition dates. For this configuration, the radar images are acquired at two different incidence angles, generally one image with a weak incidence ($\theta_{weak}$~20°) and another image with a strong incidence ($\theta_{strong}$~40°) (Baghdadi and Zribi, 2016).

### II.2.2 Radar backscattering coefficient

The backscattering coefficient (σ°) is the usual radar term for the measurement of the backscattering of a target by the radar. It expresses the ratio between the power transmitted by the antenna to the ground and that returned by the target for a given configuration system (polarization, frequency, angle of incidence). It defines the ability of an illuminated surface to reflect incident energy towards the antenna. It is usually expressed in decibels (dB), on a logarithmic scale:

$$\sigma^{o}_{dB} = 10 \cdot \log_{10} (\sigma^{\circ}_{linear}) \qquad (2.2)$$

## II.3 Description of soil parameters

### II.3.1 Soil moisture

Soil moisture is defined as the water contained in the soil. Obtained from rainfall, snowmelt, irrigation, or from the tube of liquid of groundwater. Soil moisture content is an important variable of climatological, hydrological and environmental systems.

The moisture content in the surface layers of the soil is an important parameter for many applications in hydrology, agriculture and meteorology. Soil moisture is one of the few directly observable hydrological variables that play an important role in the water and energy budgets necessary for climate studies. Estimation of soil properties as soil moisture is an important variable for many water management and agricultural applications (Verhoest et al., 2008). Moreover soil moisture information could also be used to predict natural disasters such as flooding and for environment changing such as soil erosions (Lakhankar et al., 2006).

Soil moisture measurements in situ are expensive and take time. Also these measurements might have some problems during the sampling process that make all the measurement incorrect. There are several methods to measure soil moisture, such as the gravimetric method and Time-Domain Reflectrometry (TDR).

### II.3.2 In situ measurements

*II.3.2.1 The gravimetric method*

The gravimetric method consists in first measuring the moisture content of a soil sample taken from a cylinder. The wet content *Wp* (% or $g.g^{-1}$) is calculated using the wet weight *(Ph*: soil weight after sampling) and the dry weight (*Ps*). The dry weight (*Ps*) is obtained by drying the sample from the sampled soil with a temperature of 105 °C for 24 h.

This method determines the wet weight of a soil sample by comparing the wet mass to its dry mass, according to the following equation:

$$Wp(vol.\%) = 100 * \left[\frac{P_h - P_s}{P_h}\right] \quad (2.3)$$

With:

$P_h$: soil moisture mass

$P_s$: dry soil mass

*Wp*: water content in weight %

The moisture volume *mv* (% or $cm^3/cm^3$) is deduced from the wet weight $W_p$ (% or $g.g^{-1}$) by multiplying it by the apparent density of the soil:

$$mv(\%) = D_a . W_p \ (\%) \quad (2.4)$$

$D_a$: apparent density = the dry soil mass / the cylinder volume

*II.3.2.2 The TDR (Time Domain Reflectometry)*

This instrument measures the propagation speed of a microwave signal by waveguides pressed into the soil. This speed is a function of the soil dielectric permittivity, related to the soil water content. For surface measurements, this method is fast with equipment that allows extensive measurements of soil moisture. This instrument can be placed deeply in a horizontal position for automated measurements. It is better to precede a previous calibration of the device by doing a comparison with measurements obtained by the gravimetric method (calibration for each soil type). Moreover, the TDR measurements are not valid for frozen soil where an important drop in the moistures registered by the probe can be observed.

The gravimetric method is considered the most accurate but it requires a lot of effort and time to collect the soil samples. For this reason, soil moisture content is usually measured using a calibrated TDR (Figure II.1). Figure II.1b shows the calibration line of TDR established by expressing TDR measurements as a function of the gravimetric measurements.

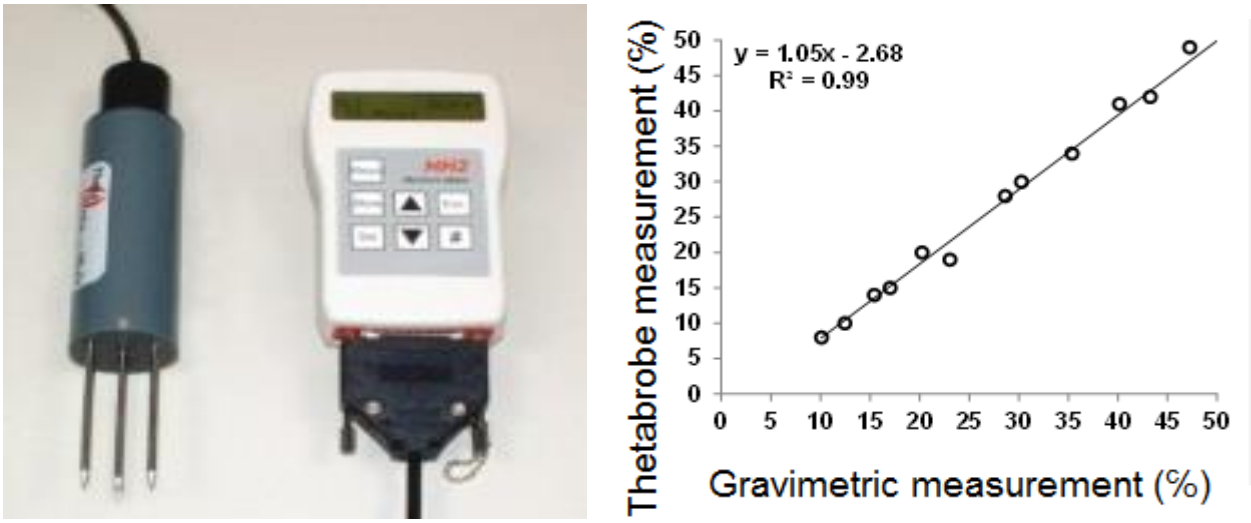


(a) (b)

**Figure II.1.** (a) The Thetaprobe instrument. (b) Thetaprobe calibration curve, black circles represent moisture measurements.

### II.3.3 Surface roughness

Roughness is a parameter that describes the soil microtopography. When the transmitted radar signal interacts with a rough surface, the energy of the wave is reflected in all directions and in particular in the radar's direction. The description of the surface roughness of bare

agricultural soils is based on three parameters: the standard deviation height (*Hrms*), the correlation length (*L*) and the autocorrelation function (Ogilvy and Ogilvy, 1991; Ulaby et al., 1986).

There are several techniques that could be used for soil roughness measurement: pin profilometer (Figure II.2), laser profilometer (Figure II.3), and 3D photogrammetry. The pin profilometer 1D can be represented by a function f(x) = z, where x is on the horizontal axis and z is the profile height with respect to this axis. Moreover, the use of the laser or 3D photogrammetry allows for the most accurate rendering of soil roughness (high spatial resolution) with a precise estimation of the roughness parameters, *Hrms* and *L* (Davidson et al., 2000; Mattia and Le Toan, 1999).

However, the pin profilometer is the very widely used due to cost reasons. Most pin profilometers are 1 or 2 m long with a sampling interval of 0.5, 1, or 2 cm. The measures are often taken in both directions, parallel and perpendicular to the row direction, in order to consider the directional effect of soil tilling (several profiles in each direction). The autocorrelation functions, calculated using different roughness profiles of a reference plot, are averaged, and the roughness parameters *Hrms* and *L* estimated (Baghdadi and Zribi, 2016).

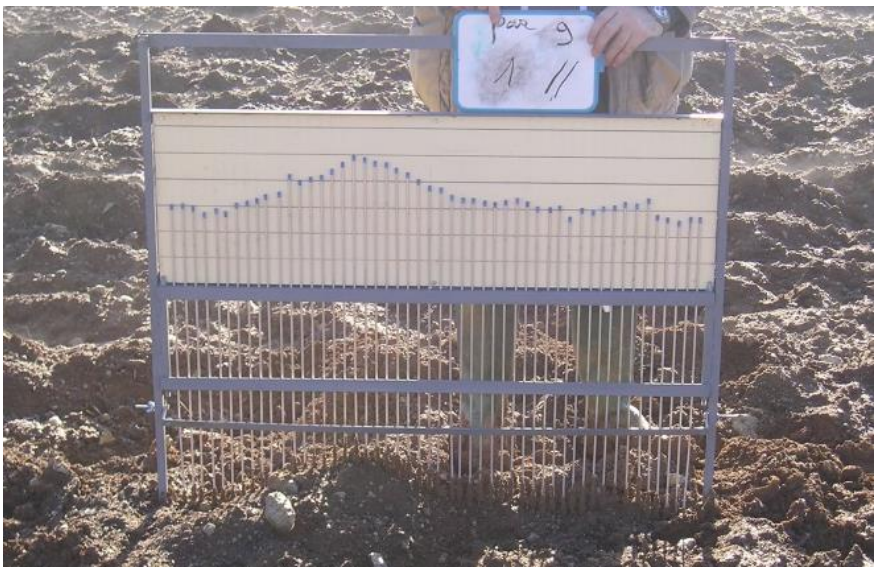

**Figure II.2.** Roughness profile made by a needle profile-meter in the parallel direction to the furrows (1D profile from a pin profilometer: 1 m long and a sampling interval of 2 cm) (Baghdadi and Zribi, 2016).

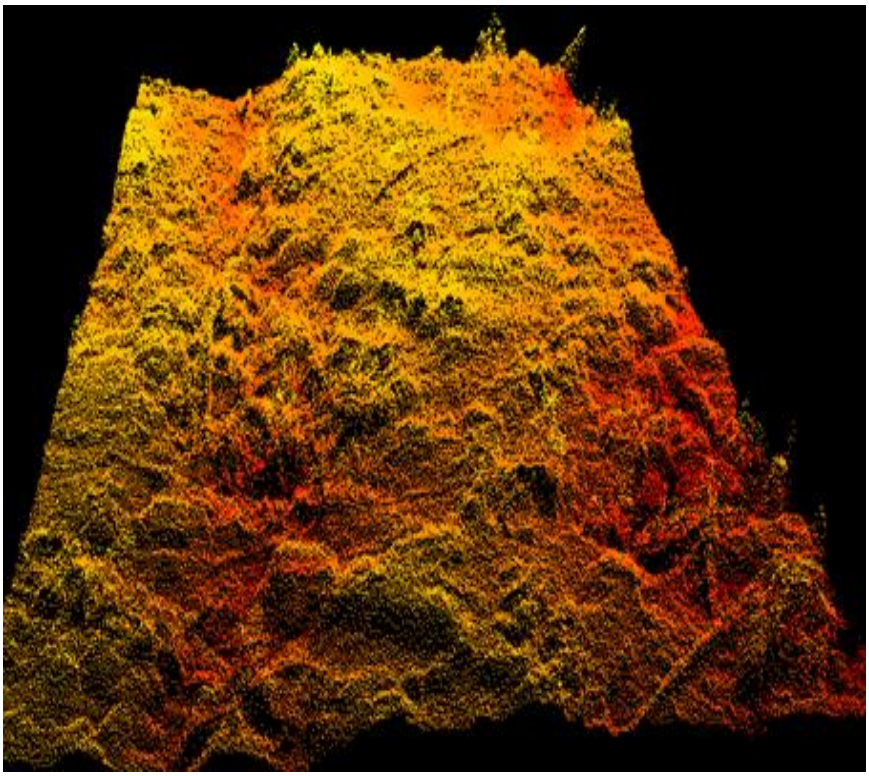

**Figure II.3.** Examples of roughness profile: 3D profile from a laser scanner (Baghdadi and Zribi, 2016).

The standard deviation height (*Hrms*) expresses the vertical variation of the soil roughness. The *Hrms* values depend on the agricultural operations and the rain or snow ground effects. The parameter is defined as follows:

$$Hrms^2 = \langle (z(x) - \langle z \rangle)^2 \rangle \qquad (2.5)$$

Where z (x) is the measured altitude on the x axis, and <z> is the mean height.

The *Hrms* parameter is not sufficient to characterize the soil surface. It does not take into account the relation which may exist between different surface points.

In order to take into account the relationship that may exist between the altitudes of two surface points separated by a distance $u$, we define the autocorrelation function ($\rho(u)$) of the surface and calculating the correlation length $L$:

$$\rho(u) = \left[\frac{\langle\{z(x+u) - \langle z\rangle\}.\{z(x) - \langle z\rangle\}\rangle}{Hrms^2}\right] \qquad (2.6)$$

When u = 0, the distance between the altitudes of two surface points is zero, the correlation between these two points is maximum and the autocorrelation function is one: $\rho(u) = 1$. When $u$ increases, the points move away and become less correlated and the function $\rho(u)$ decreases.

Finally, there is a distance for which the points are considered to be uncorrelated. This distance is the correlation length ($L$). It is defined as the distance (from the origin profile) in which the autocorrelation function equals $e^{-1}$ (Figure II.4). When the roughness is low and the ground is smooth, the autocorrelation function has an exponential shape. Conversely, for high roughness, the autocorrelation function has a Gaussian shape (Ulaby et al., 1982) (Equation 2.7). Zribi (1998) introduced the fractal dimension to the description of the autocorrelation function's shape for bare soils in agricultural fields. For one-dimensional roughness profiles, the autocorrelation functions are defined as follows:

$$\begin{aligned} \rho(x) &= Hrms^2\, e^{-\left(\frac{x}{L}\right)} \quad : \quad \text{exponential} \\ &= Hrms^2\, e^{-\left(\frac{x}{L}\right)^2} \quad : \quad \text{Gaussian} \\ &= Hrms^2\, e^{-\left(\frac{x}{L}\right)^{\alpha}} \quad : \quad \text{fractal} \end{aligned} \qquad (2.7)$$

with $\alpha = -2D+4$, where D is the fractal dimension. When the fractal dimension varies, the shape of the autocorrelation function changes: it goes from an exponential function from for D=1.5 to a Gaussian shape for D=1. The experimental measurements show a fractal dimension between 1.25 and 1.45, where an autocorrelation function power $\alpha$ between 1.1 and 1.5.

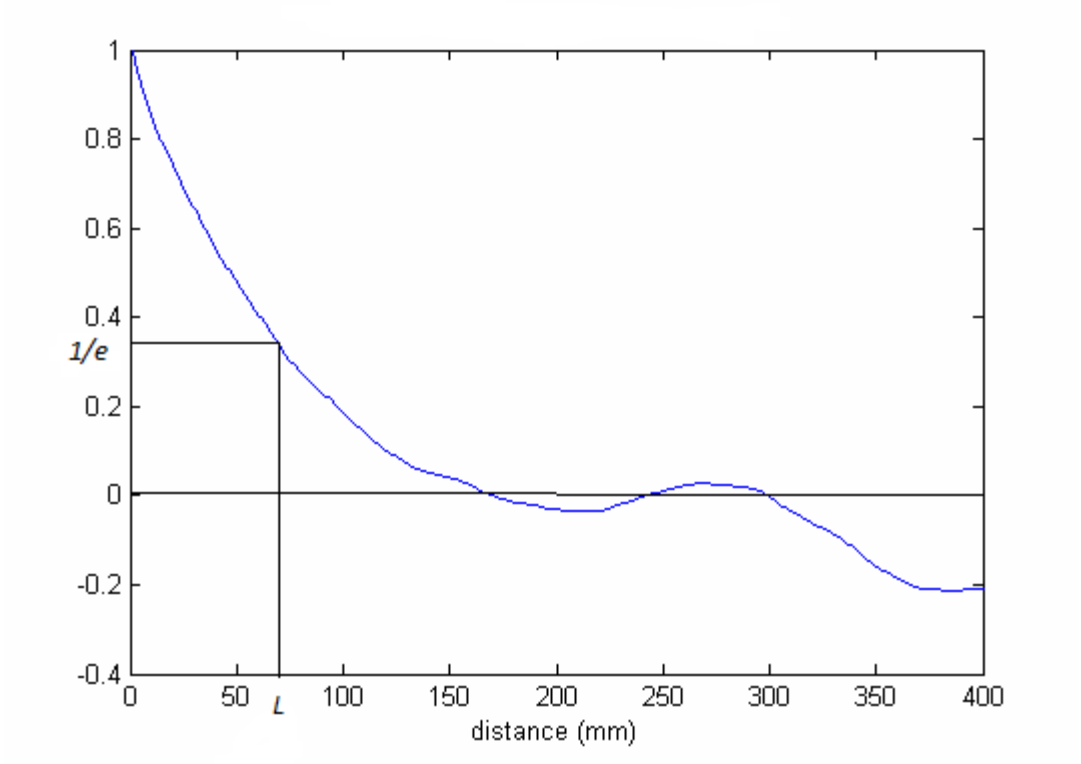


**Figure II.4.** Example of a correlation function, *L* is the correlation length.

The inversion of the radar signal to estimate all surface parameters of the soil (*Hrms*, *L*, *D*, and soil moisture) is impossible without simplifications in the description of the roughness (too many variables and too few observations). In this context, Zribi and Dechambre (2002) proposed a new roughness parameter *Zs* (which equal to $Hrms^2/L$) combining *Hrms* and *L*. This parameter *Zs* takes into account the influence of both surface height variations (*Hrms*) and soil surface slope (*Hrms*/*L*). Low values of *Zs* correspond to low values of *Hrms* and/or large values of *L*, whereas large values of *Zs* correspond to large values of *Hrms* and/or low values of *L*. Smooth soil surfaces are described by a low *Zs* (<0.1 cm), whereas rough soils lead to a large value of *Zs* (>1 cm).

Moreover, Zribi et al. (2014a) proposed a new parameter Zg, which combines the standard deviation of heights *Hrms*, the correlation length *L*, and the shape of the autocorrelation function (described by the power $\alpha$):

$$Zg = Hrms \left(Hrms / L\right)^{\alpha} \quad (2.8)$$

For a fixed value of α, high values of *Zg* correspond to high values of *Hrms* or low values of *L*, and low values of *Zg* correspond to low values of *Hrms* and/or high values of *L*.

In the case of a fixed correlation length *L*, high values of *Zg* correspond to high values of *Hrms* or low values of α, and low values of *Zg* correspond to low values of *Hrms* and/or high values of α. In general, a smooth soil surface is characterized by a low value of *Hrms* and a medium to large value of *L*, thus to a small value of *Zg*. Moreover, rough surface is generally associated with a high value of *Hrms*, a medium to large value of *L*, and a value of α about 1, and thus to a high value of *Zg*. In addition, rough surfaces, corresponding to eroded soils, are often characterized by a high value of *Hrms*, a medium to large value of *L* and a value of α about 2, thus to a medium value of *Zg*.

Several studies (e.g. Lievens et al., 2009; Oh and Kay, 1998) showed that the precision of in-situ measurements root mean surface height (*Hrms*) and correlation length (*L*) are very sensitive to the length and the horizontal resolution Δx of the roughness profiles (Lievens et al., 2009; Oh and Kay, 1998). An underestimation is observed of *Hrms* and *L* using small profiles. Moreover, the estimate correlation length (*L*) increase using roughness profiles with large sampling intervals. For agricultural soils, with about ten profiles measuring 1 m, *Hrms* can be measured with a precision of 10%, while the precision of the estimation of *L* is around 15 to 20% (a more important error for strong *L* values). Measuring *L* and *Hrms* with an error better than 5%, the sampling interval Δx must be smaller than 0.2*L* and 0.5*L* respectively (Oh and Kay, 1998). The *Hrms* values are generally seen between 0.3 cm (very smooth fields that have just been sown) and 4 cm (fields that have just been plowed). The lengths of correlation *L* measured on the agricultural plots are predominantly between 3 and 25 cm.

## II.4 Radar signal sensitivity to soil parameters

### II.4.1 Sensitivity of radar signal to soil roughness

Many studies (Aubert et al., 2011a; Baghdadi and Zribi, 2016; Baghdadi et al., 2008a; Gorrab et al., 2015a) showed that the backscattering radar signal for bare soil increases with the rms surface height (*Hrms*) according to the logarithmic or exponential law. Then after certain

thresholds, the backscattering radar signal becomes constant (Figure II.5). This threshold after which the signal becomes constant depends on the wavelength and the radar's incidence angle. According to several studies, the radar signal rapidly saturates with the soils roughness (*Hrms*) when the wavelength and or the incidence angle are weak. This saturation of the radar signal occurs when *kHrms* is higher than 1 (where k is the radar wave number = $2\pi/\lambda$) (Figure II.5). Moreover, this saturation corresponds to *Hrms* values of 4 cm in L-band, 1 cm in C-band and around 0.5 cm in X-band (Baghdadi and Zribi, 2016). Figure II.5 also illustrates the dynamic weakness of the radar backscattering coefficient in two cases, first in the case of weak incidence angles (variation of 7 dB for 20º-25º, Figure II.5a), than in the case of strong incidence angles (variation of 10 dB for 45º-50º, Figure II.5b).

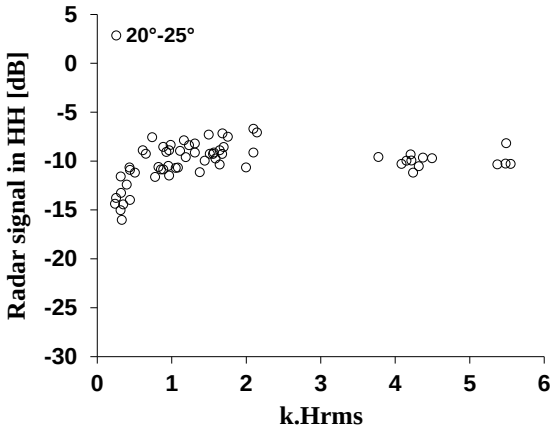


(a)

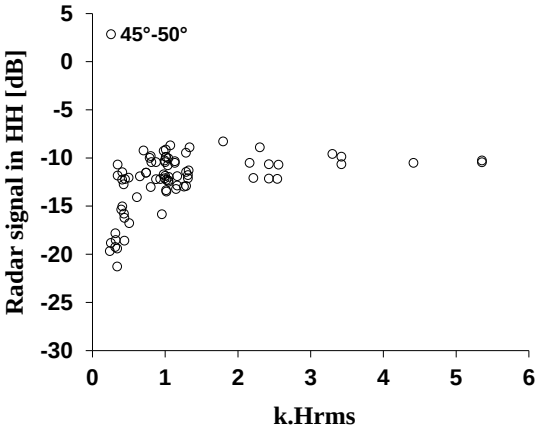


(b)

**Figure II.5.** Sensitivity of the radar signal to soil roughness. SAR sensors in C and L bands were used. The signal is represented as a function of *kHrms* (Baghdadi and Zribi, 2016).

### II.4.2 Sensitivity of the radar signal to soil moisture

The radar signal approximately follows a logarithmic law with soil moisture. Moreover, this logarithmic function represented approximately as a linear function for soil moisture between 10 and 35 vol. % (Figure II.6). When the soil moisture increases than about 35 vol. %, the radar signal stabilizes and starting to decrease with the increasing of the soil moisture. So that, the estimation of soil moisture is difficult after 35 vol. % (e.g. Baghdadi et al., 2007; Holah et al., 2005).

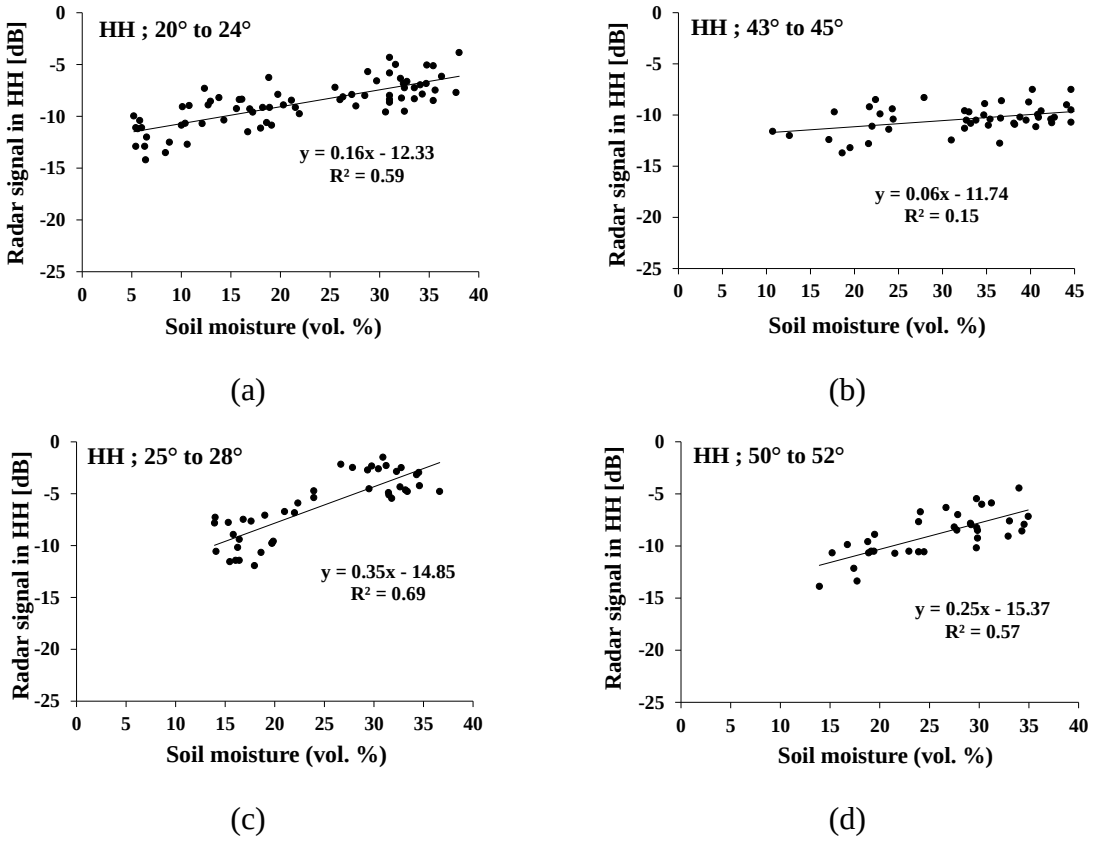


**Figure II.6.** Sensitivity of the radar signal in C and X bands to soil moisture. The *Hrms* values vary between 0.5 and 1.5 cm. (a): C-HH(20°-24°), (b): C-HH(43°-45°) (c): X-HH(25°-28°), (d): X-HH(50°-52° ) (Baghdadi and Zribi, 2016).

Numerous studies (Aubert et al., 2011a; Baghdadi and Zribi, 2016; Baghdadi et al., 2007; Choker et al., 2017) show the radar signal's sensitivity to soil moisture as a function of different radar parameters (incidence angle, polarization, wavelength). Over bare soil, the optimal radar signal configuration to get the better sensitivity to soil moisture consists of X-band (in comparison to L and C bands), HH polarization and a low incidence angle (Anguela et al., 2010; Aubert et al., 2011; Baghdadi and Zribi, 2016; Beaudoin et al., 1990; Toan, 1982;

Ulaby et al., 1986; Weisse et al., 2003). These radar's incidence angles are ranging from 15° to 35° (Beaudoin et al., 1990; Lievens et al., 2009; Ulaby et al., 1986).

The sensitivity of radar signal to soil moisture, in C-band it is approximately between 0.15 dB/vol.% and 0.3 dB/vol.% (Baghdadi et al., 2008; Le Hégarat-Mascle et al., 2002; Quesney et al., 2000; Srivastava et al., 2003). For the effect of wavelength, Aubert et al. (2011) showed that the sensitivity of the radar signal toward the soil moisture is twice high in X-band than in C-band (about 0.35 dB/vol. % in X-band and 0.15 dB/Vol. % in C-band). Narvekar et al. (2015) showed that the sensitivity to soil moisture in L-band is approximately the same as in C-band. Moreover, the sensitivity for all frequency decreases as the incidence angle increases (Baghdadi and Zribi, 2016; Baghdadi et al., 2008a) (Figure II.6).

## II.5 SAR data processing

Before processing the SAR images, the data are radiometrically calibrated, which allows the backscattering coefficient (σ°) to be extracted from the signal intensity of each pixel. This calibration enables to carry out multi-temporal analysis of different images (using either the same, or different sensors, but the same radar frequency, incidence angle and polarization). The pixel-by-pixel interpretation of SAR images are extremely difficult because of the presence of speckle noise. It is due to the coherent interference of waves reflected from many elementary scatterers. Due to these reasons, soil surface characteristics are always estimated over homogeneous sectors including several pixels, or at the scale of single fields (which helps to reduce the speckle effect). The mean backscattering coefficients are calculated from calibrated SAR images, by averaging the linear intensity values of all pixels within the field (or sub-field). The reduction in speckle noise and the improvement in the quality of backscattering estimations are thus highly dependent on the size of homogeneous units used (Joughin et al., 1993; Lee et al., 1994).

## II.6 Radar backscattering modeling and evaluation

The radar backscattered models have been the subject of many studies based on theoretical or experimental research. In general, there are several classes of models: empirical, semi-empirical and physical models. These models will be briefly discussed in chapter three.

### II.6.1 Case of bare soil

*II.6.1.1 Modeling of radar backscattering on bare soils*

The modeling of the radar backscattered signal was developed in order to link and analyze the radar signal's sensitivity to the physical parameters of the soil surface (roughness and water content in particular) as a function of SAR configurations (mainly radar wavelength, incidence angle and polarization) (Baghdadi and Zribi, 2016; Baghdadi et al., 2004, 2006a, 2011b, 2015, 2016a; Beckmann and Spizzichino, 1987; Fung et al., 1992; Rice, 1951; Ulaby et al., 1986).

The empirical models require calibration using in situ measurements and SAR observations acquired (Baghdadi et al., 2004, 2006a, 2011b, 2015, 2016a; Dubois et al., 1995; Oh, 2004; Oh et al., 1992, 1994, 2002). In addition, the range of validity of the empirical models is limited to the range of variations in the data used for model calibration.

In addition, the physical models are based on laws of the resolution of Maxwell's equations, with physical approximations limiting their areas of validity. The disadvantages of these models are the complexity of implementations and require many parameters in simulations. The development of these models have been the goal of several studies such as (Chen et al., 2003; Fung, 1994; Fung et al., 1992; Ulaby et al., 1986). In the IEM model (Fung et al., 1992), the discrepancy between SAR simulations and SAR measurements is mainly related to the description of surface roughness which is an important input to SAR backscattering models (Baghdadi et al., 2011b; Mattia et al., 2003; Verhoest et al., 2008). The surface roughness is described by three parameters: the standard deviation of the height (*Hrms*), the correlation length (*L*) and the shape of the correlation function (Fung et al., 1992). The correlation length is usually measured with an uncertainty which introduces an error on simulated backscattering coefficients (Baghdadi et al., 2000; Davidson et al., 2000; Le Toan et al., 1999; Lievens et al., 2011). A few studies proposed a semi-empirical calibration of SAR backscattering models in order to reduce the uncertainty on SAR simulations (Baghdadi et al., 2002b, 2004, 2006a, 2011a, 2011b, 2015; Rahman et al., 2007) . In Baghdadi et al. (2002b, 2004, 2006, 2011a, 2011b, 2015) the method consisted of replacing the measured *L* by a fitting parameter, so-called *Lopt*, which was found to be related to *Hrms* (*Lopt* increases with *Hrms*). *Lopt* is a function of *Hrms* (linear, exponential, or power calibration) which depends on SAR parameters (incidence angle, polarization and frequency). This calibration reduces IEM's input soil parameters (*Hrms* and *mv* instead of *Hrms*, *L* and *mv*). Rahman et al.

(2007) proposed a method for deriving *L* through the IEM. In this method, the radar signal is modeled as a function of only *Hrms* and *L*, and the contribution of soil moisture on backscattering coefficients is ignored (dry soil). Thus, *L* could be estimated by inverting the IEM.

#### *II.6.1.2 Estimation of soil parameters using radar backscattering on bare soils*

For bare soil, many studies have shown the potential of radar data to retrieve soil parameters (moisture and roughness) (Aubert et al., 2011; Baghdadi and Zribi, 2006; Baghdadi et al., 2002a, 2007, 2008a, 2012a; Le Hégarat-Mascle et al., 2002; Zribi et al., 2005b). The SAR signal increases with increasing soil moisture for values between 0 and 35% (Aubert et al., 2011a; Baghdadi et al., 2007; Gorrab et al., 2015a; Holah et al., 2005). Beyond this threshold, the backscattering coefficients tend to saturate and then decreases with increasing soil moisture (Holah et al., 2005). Most bare soil moisture estimation studies have used SAR data in X and C bands and the results show a precision on the estimation of soil moisture between 3 and 6 vol.% (Aubert et al., 2011; Baghdadi et al., 2012, 2016b; El Hajj et al., 2014; Paloscia et al., 2013; Srivastava et al., 2003, 2009; Zribi et al., 2011). Moreover, in C-band, the accuracy of the soil moisture estimates depends on the effect of surface roughness and of the sensor incidence angle. On the other hand, in X-band, the effect of roughness on the accuracy of the soil moisture estimation is negligible and the quality of estimates is slightly better with low incidence angle (RMSE < 1 vol.%) (Aubert et al., 2011a, 2013; Galarneau et al., 2001; Hégarat-Mascle, 2000; Quesney et al., 2000). Thus, the accuracy of the moisture estimates in X-band is twice as well as that obtained in C-band data (3 vol.% in the X-band compared with 6 vol.% in the C-band) (Baghdadi and Zribi, 2016).

Baghdadi et al. (2002a) analyzed the potential of synthetic aperture radar (SAR) data for monitoring roughness states over bare agricultural fields using one ERS image (23°) and two RADARSAT images (39° and 47°). The relationships between the backscattering coefficient, incidence angle, soil surface roughness and row direction have been examined in order to determine the best SAR configuration for such monitoring. The result showed a strong dependence of incidence angle on the discrimination between radar return over areas of different surface roughness. The influence of soil roughness on radar return is more sensitive at a high incidence angle (47°), over the influence of other soil parameters, making it possible to differ and map various surface roughness classes (smooth, medium and rough) over agricultural fields.

In addition, Baghdadi et al. (2012a) developed an approach to estimate soil surface parameters from C-band polarimetric SAR data in the case of bare agricultural soils. An inversion technique based on multi-layer perceptron (MLP) neural networks was introduced. The neural networks were trained and validated on a noisy simulated dataset generated from the Integral Equation Model (IEM) on a wide range of surface roughness and soil moisture. The performances of neural networks in retrieving soil moisture and surface roughness over bare soils were tested using or not *a priori* knowledge on soil moisture. The inversion approach was then validated using RADARSAT-2 images in polarimetric mode. The polarimetric parameter $\alpha_1$ (alpha angle that corresponds to the first eigenvector of coherency matrix) was used to discriminate two soil moisture classes (very wet soils, and dry to wet soils) and the anisotropy parameter A to separate two soil roughness's (smooth with $kHrms<1.0$ and rough with $kHrms\geq1.0$). The inversion errors obtained with the RADARSAT-2 images on the *mv* estimates is about 6.5 vol.% with a priori information on *mv* compared with 9.8 vol.% without a priori information on *mv*. The use of polarimetric parameters slightly improves the soil moisture estimates in comparison to the case without a priori information on *mv* (8.3 vol.% as compared to 9.8 vol.%). This is due to the weak dynamics of the polarimetric parameters (alpha angle, entropy, anisotropy) with the soil parameters for the C-band. Results show also that the estimation of soil surface roughness (*Hrms*) is possible with accuracy around 0.5 cm (RMSE). The estimation is better for *Hrms* lower than 2 cm. For higher *Hrms*, the NNs underestimate the surface roughness.

### II.6.2 Case of soil with vegetation cover

The presence of vegetation makes the inversion of the radar signal much more complicated because the vegetation not only attenuates the backscattered signal but also produces its own contribution. Thus, in the presence of vegetation, the total backscattered radar signal is the result of contributions from soil attenuated by the vegetation and the vegetation contribution. The possibility of estimating soil moisture in the presence of vegetation from SAR images has been widely studied using C-band radar data (De Roo et al., 2001; Gherboudj et al., 2011; He et al., 2014; Notarnicola et al., 2006; Prevot et al., 1993; Sikdar and Cumming, 2004; Wang et al., 2011; Yu and Zhao, 2011; Zribi et al., 2011). Conversely, very few studies have been conducted using X-band radar data (El Hajj et al., 2014; Kseneman et al., 2012; Kweon et al., 2012) or L-band (Paloscia et al., 2012; Wigneron et al., 1995).

The most used models to estimate soil moisture in the presence of vegetation are the Michigan Microwave Canopy Scattering model ″MIMICS″ (Ulaby et al., 1990) and the Water Cloud Model ″WCM″ (Attema and Ulaby, 1978). MIMICS is based on the theoretical principle of the first order radiative transfer model to simulate radar backscatter from soil and vegetation parameters. In MIMICS vegetation is described in detail (stem diameter and leaf slope, among others), which makes it possible to better quantify the contribution of vegetation to the total backscattered radar signal and thus a better estimation of soil moisture. However, MIMICS is complicated to use, and requires a large number of input parameters. For this reason, most studies have used the WC model because it is relatively simple and requires only few input variables (De Roo et al., 2001; Gherboudj et al., 2011; Kweon et al., 2012; Prevot et al., 1993; Sikdar and Cumming, 2004; Wang et al., 2011; Yang et al., 2012; Zribi et al., 2011).

In the WCM, the total backscattered radar signal is modeled as the sum of soil attenuated by vegetation and vegetation contribution. The contribution of vegetation (direct backscatter and attenuation) is calculated using mainly a single biophysical parameter (leaf area index, vegetation water content, NDVI, biomass, or vegetation height) representing the effect of vegetation. The soil contribution is calculated as a function of soil moisture and roughness using a radar backscattering model. Optical data are often required to reverse the radar signal using the WCM. Indeed, the optical data are complementary to the radar data, and their interest lies in their sensitivity to the physical vegetation parameters. In the WCM, the biophysical parameters allow to evaluate the vegetation contribution to the radar signal, and to then reverse the soil contribution in order to estimate soil moisture (Baghdadi et al., 2016b; El Hajj et al., 2014; Fieuzal et al., 2011; He et al., 2014; Hosseini and Saradjian, 2011; Notarnicola et al., 2006; Prakash et al., 2012).

The Water Cloud model (WCM) defines the backscattered radar signal in a linear scale ($\sigma^0_{tot}$) which is the sum of the contribution from the vegetation ($\sigma^0_{veg}$), the soil ($\sigma^0_{soil}$) attenuated by the vegetation ($T^2\ \sigma^0_{soil}$), and multiple soil-vegetation scatterings that are often neglected:

$$\sigma^0_{tot} = \sigma^0_{veg} + T^2\ \sigma^0_{soil} \quad (2.9)$$

$$\sigma^0_{veg} = A.V_1.\cos\theta\ (1 - T^2) \quad (2.10)$$

$$T^2 = \exp(-2.B.V_2.\sec\theta) \quad (2.11)$$

Where:

- V1 and V2 are vegetation descriptors (NDVI: Normalized Differential Vegetation Index, BIO: biomass, VWC: vegetation water content, HVE: vegetation height, LAI: foliar index, FAPAR: fraction of solar radiation absorbed, and FCOVER: canopy fraction)
- $\theta$ is the incidence angle
- A and B are WCM parameters dependent on vegetation parameters, and radar configurations
- *mv* is the volumetric moisture content of the soil.

The soil contribution $\sigma^0_{soil}$ that depends on the soil moisture and surface roughness with SAR instrumental parameters can be simulated using physical backscattering model (IEM) or empirical models (Oh, Dubois, Baghdadi) (Baghdadi et al., 2016b; Dubois et al., 1995; Oh, 2004; Oh et al., 1992, 1994, 2002).

Several studies have used the WCM to estimate soil moisture in presence of vegetation. The results showed a soil moisture precision between 2 and 8 vol.% (De Roo et al., 2001; El Hajj et al., 2014; Gherboudj et al., 2011; He et al., 2014; Notarnicola et al., 2006; Prevot et al., 1993; Sikdar and Cumming, 2004; Wang et al., 2011; Yang et al., 2012; Yu and Zhao, 2011; Zribi et al., 2011). Prevot et al. (1993) combined radar data in C and X bands to estimate the soil moisture of wheat plots (LAI of wheat between 0.1 and 8 $m^2/m^2$). The accuracy on the soil moisture estimation was 6.5 vol. %. Similar precision was obtained by Zribi et al. (2011) using ASAR (C band) images acquired on wheat plots (LAI between 0.01 and 3.7 $m^2/m^2$). Kweon et al. (2012) estimated soil moisture from soybean plots using X-band SAR data with an accuracy of 3 vol. % (VWC "water content" and LAI "leaf index" at 1.8 $kg/m^2$ and 4.5 $m^2/m^2$, respectively). He et al. (2014) combined radar data (C-HH and C-VV) and optical data to estimate soil moisture. The results showed an accuracy of about 3 vol.%. Gherboudj et al. (2011) combined "WC" and "Oh" models to estimate soil moisture with vegetation (wheat, peas, lentils, fallows, pasture and canola) from C-band radar data. Soil moisture was estimated with an accuracy of 6 vol.% for vegetation heights between 11 and 97 cm. Finally, De Roo et

al. (2001) used the MIMICS model in conjunction with the "Oh model" to estimate soil moisture in soybean plots (with VWC between 0.02 and 0.97 kg/m$^2$) from the C and L polarimetric data. Accuracy of soil moisture estimates was about 2 vol.%.

## II.7 Conclusion

Through the diversity of the radar backscattering models over bare soils, my first work is to evaluate the most commonly backscatter models using a wide dataset of SAR data and in situ measurements acquired over numerous agricultural sites in France, Italy, Germany, Belgium, Luxembourg, Canada and Tunisia. Thus, this study could be of a great importance for scientific community since it helps understanding backscatter models performance for a wide range of soil surface conditions, acquired for several study areas through the world by numerous SAR sensors. Never before have all these backscatter models been evaluated together in the same literature with such a wide dataset. This step is very important to find the model that produces good agreement between the radar data and the simulations in order to be used in the inverse mode later in this thesis.

# III. ***Chapter 3:*** *Evaluation of radar backscattering models*

## III.1 Introduction

The aim of this chapter is to evaluate the most popular backscattering SAR models (Oh, Dubois, IEM, IEM_B, and AIEM) by using a wide range of SAR data and in situ measurements. With the arrival of Sentinel-1A and -1B satellites that provide free high resolution SAR data with 6 days revisit time, several research teams work actually on developing methods for mapping soil moisture using these Sentinel-1 data. Most of methods for soil moisture mapping are based on backscatter models for soil moisture estimations. The objective of this part is to evaluate the most commonly backscatter models using a wide dataset of SAR data and in situ measurements acquired over numerous agricultural sites in France, Italy, Germany, Belgium, Luxembourg, Canada and Tunisia. Thus, this study could be of a great importance for scientific community since it help on understand backscatter models performance for wide range of soil surface conditions, acquired for several study areas through the world by numerous SAR sensors. Never before have been evaluated all these backscatter models together in the same literature with such a wide dataset. In addition, this study is the first that evaluates the backscatter models using L-, C- and X-bands together. A description of the study areas and different datasets used in this study is provided in Section 2. Section 3 the models are described. The results are shown in Section 4. Finally, Section 5 presents the conclusion.

## III.2 Dataset

### III.2.1 Study Areas

A wide range of datasets composed of AIRSAR, SIR-C, JERS-1, PALSAR-1, ESAR, ERS, RADARSAT, ASAR and TerraSAR-X acquisitions over numerous agricultural sites in France, Italy, Germany, Belgium, Luxembourg, Canada and Tunisia (Table III.1), have been used in this research work. In addition, in situ measurements of soil moisture and surface roughness were carried out simultaneously to SAR acquisitions over bare soil surfaces.

### III.2.2 Satellite Data

A large number of L-, C- and X-band images (approximately 1.25 GHz, 5.3 GHz and 9.6 GHz, respectively) were acquired between 1994 and 2014 with different incidence angles (between 18° and 57°) and in HH, VV and HV polarizations (Table III.1). The spatial resolution of SAR images is between 1 m and 30 m (Table III.1). Images were first

radiometrically calibrated to enable the extraction of the backscattering coefficients ($\sigma^0$). Then, the mean backscattering coefficients were computed from calibrated SAR images by linearly averaging the $\sigma^0$ values of all pixels within the plot.

### III.2.3 Field Data

Field measurements of soil moisture and surface roughness have been collected from bare plots selected over the study areas. Each plot is a homogeneous surface (similar soil type, moisture content and surface roughness) of around one hectare or more. In situ measurements of soil moisture (*mv*, in vol. %) were carried out for a soil layer of 5 cm or 10 cm in each reference plot by using both the gravimetric method or a calibrated TDR (time domain reflectometry) probe. For each bare soil reference field the average soil moisture (*mv*) of all samples was calculated. The soil moisture ranged between 2 vol. % and 47 vol. %.

Roughness measurements were carried out by using laser or needle profilometers (mainly 1 m and 2 m long, and with 1 cm and 2 cm sampling intervals); while for some in situ measurement campaigns, a meshboard technique was used. Several roughness profiles along and across the direction of tillage were acquired in each reference field. The standard deviation of surface heights (*Hrms*) and the correlation length (*L*) were calculated by using the mean of all experimental correlation functions. In our dataset, *Hrms* ranged from 0.2 cm to 9.6 cm and the *L* from 1.2 cm to 38.5 cm. The reference plots in the datasets were chosen with low density of stones.

A total of 2442 experimental data of soil moisture content and surface roughness were available, together with the corresponding values of backscattering coefficient, of which 1262 at HH polarization, 790 at VV polarization, and 390 at HV polarization (Table III.1).

| Site | SAR Sensor | Spatial Resolution | Freq | Year | Number of Data |
|---|---|---|---|---|---|
| **Orgeval (Fr)** (Zribi et al., 1997) | **SIR-C** | **30 m × 30 m** | **L** | **1994** | **HH: 1262 measurements 66 in L-band 766 in C-band 430 in X-band VV: 790 measurements 159 in L-band 411 in C-band 220 in X-band HV: 390 measurements 13 in L-band 313 in C-band 64 in X-band** |
| **Orgeval (Fr)** (Baghdadi et al., 2008a, 2013; Zribi et al., 1997) | **SIR-C, ERS, ASAR** | **30 m × 30 m** | **C** | **1994; 1995; 2008; 2009; 2010** | |
| **Orgeval (Fr)** (Baghdadi et al., 2008a) | **PALSAR-1** | **30 m × 30 m** | **L** | **2009** | |
| **Orgeval (Fr)** (Baghdadi et al., 2012b) | **TerraSAR-X** | **1 m × 1 m** | **X** | **2008, 2009, 2010** | |
| **Pays de Caux (Fr)** (Baghdadi et al., 2002a, 2004) | **ERS; RADARSAT** | **30 m × 30 m** | **C** | **1998; 1999** | |
| **Villamblain (Fr)** (Baghdadi et al., 2006a; Holah et al., 2005) **Villamblain (Fr)** (Baghdadi et al., 2011c, 2013) | **ASAR TerraSAR-X** | **30 m × 30 m** | **C**<br>**X** | **2003; 2004; 2006**<br>**2008; 2009** | |
| **Thau (Fr)** (Baghdadi et al., 2007) | **RADARSAT TerraSAR-X** | **30 m × 30 m 1 m × 1 m** | **C X** | **2010; 2011 2010** | |
| **Touch (Fr)** (Baghdadi et al., 2007; Holah et al., 2005) | **ERS-2; ASAR** | **30 m × 30 m** | **C** | **2004; 2006; 2007** | |
| **Mauzac (Fr)** (Baghdadi et al., 2011c) | **TerraSAR-X** | **1 m × 1 m** | **X** | **2009** | |
| **Garons (Fr)** (Baghdadi et al., 2011c) | **TerraSAR-X** | **1 m × 1 m** | **X** | **2009** | |
| **Kairouan (Tu)** (Zribi et al., 2014b) **Kairouan (Tu)** (Baghdadi et al., 2011c; Gorrab et al., 2015b; Zribi et al., 2014b) | **ASAR TerraSAR-X** | **30 m × 30 m** | **C**<br>**X** | **2012**<br>**2010; 2012; 2013; 2014** | |
| **Yzerons (Fr)** (Aubert et al., 2013) | **TerraSAR-X** | **1 m × 1 m** | **X** | **2009** | |
| **Versailles (Fr)** (Baghdadi et al., 2011c) | **TerraSAR-X** | **1 m × 1 m** | **X** | **2010** | |
| **Seysses (Fr)** (Baghdadi et al., | **TerraSAR-X** | **1 m × 1 m** | **X** | **2010** | |

| | | | | |
|---|---|---|---|---|
| 2011c) | | | | |
| **Chateauguay (Ca)** (Baghdadi et al., 2004) | **RADARSAT** | **30 m × 30 m** | **C** | **1999** |
| **Brochet (Ca)** (Baghdadi et al., 2004) | **RADARSAT** | **30 m × 30 m** | **C** | **1999** |
| **Alpilles (Fr)** (Baghdadi et al., 2004) | **ERS; RADARSAT** | **30 m × 30 m** | **C** | **1996; 1997** |
| **Sardaigne (It)** (Dong et al., 2013) | **ASAR; RADARSAT** | **30 m × 30 m** | **C** | **2008; 2009** |
| **Matera (It)** (Mattia et al., 1997) | **SIR-C** | **30 m × 30 m** | **L** | **1994** |
| **Alzette (Lu)** (Lievens et al., 2011; Rahman et al., 2007) | **PALSAR-1** | **30 m × 30 m** | **L** | **2008** |
| **Dijle (Be)** (Lievens et al., 2011) | **PALSAR-1** | **30 m × 30 m** | **L** | **2008; 2009** |
| **Zwalm (Be)** (Lievens et al., 2011) | **PALSAR-1** | **30 m × 30 m** | **L** | **2007** |
| **Demmin (Ge)** (Lievens et al., 2011) | **ESAR** | **2 m × 2 m** | **L** | **2006** |
| **Montespertoli (It)** (Baronti et al., 1995; Panciera et al., 2014) | **AIRSAR SIR-C JERS-1** | **30 m × 30 m** | **L** | **1991** |
| **Montespertoli (It)** (Macelloni et al., 1999) | | | **L; C** | **1994** |
| **Montespertoli (It)** (Paloscia et al., 1999) | | | **L** | **1994** |

**Table III.1.** Description of the dataset used in this study. "Fr": France, "It": Italy, "Ge": Germany, "Be": Belgium, "Lu": Luxembourg, "Ca": Canada, "Tu": Tunisia. The radiometric accuracy of SAR data is about 1 dB.

### III.2.4 Soil texture

Twenty one agricultural study sites were used. The texture compositions (Silt; Clay; Sand) are described below (Table III.2).

| Site | Texture Composition (Silt; Clay; Sand) |
|---|---|
| **Orgeval (Fr)** | **(78%; 17%; 5%)** |
| **Pays de Caux (Fr)** | **(70%, 13%, 17%)** |
| **Villamblain (Fr)** | **(60%,30%, 10% )** |
| **Thau (Fr)** | **(53%, 35%, 12%)** |
| **Touch (Fr)** | **(55%, 21%, 24%)** |

| | |
|---|---|
| **Mauzac (Fr)** | **(48%, 16%, 36%)** |
| **Garons (Fr)** | **(54%, 40%, 6% )** |
| **Kairouan (Tu)** | **(11%, 32%, 57% )** |
| **Yzerons (Fr)** | **(13%, 20%, 67% )** |
| **Versailles (Fr)** | **(58%, 24%, 18%)** |
| **Seysses (Fr)** | **(50%, 16%, 34%)** |
| **Chateauguay (Ca)** | **(43%, 37%, 20%)** |
| **Brochet (Ca)** | **(43%, 37%, 20%)** |
| **Alpilles (Fr)** | **(54%, 40%, 6%)** |
| **Sardaigne (It)** | **(23%, 30%, 47%)** |
| **Matera (It)** | **(59%; 14%; 27%)** |
| **Alzette (Lu)** | **(50%; 30%; 20%)** |
| **Dijle (Be)** | **(84%; 12%; 4%)** |
| **Zwalm (Be)** | **(72%; 13%; 15%)** |
| **Demmin (Ge)** | **(25%; 7%; 68%)** |
| **Montespertoli (It)** | **(40%; 20%; 40%)** |

**Table III.2.** Description of the Texture Composition dataset (Silt; Clay; Sand) used in this study. "Fr": France, "It": Italy, "Ge": Germany, "Be": Belgium, "Lu": Luxembourg, "Ca": Canada, "Tu": Tunisia.

## III.3 Description of the Backscattering Models

### III.3.1 The Semi-Empirical Dubois Model

Dubois et al. (1995) proposed a semi-empirical model for simulating the backscattering coefficients in HH and VV polarizations ($\sigma^0_{HH}$ and $\sigma^0_{VV}$) over bare soils. The expression of $\sigma^0_{HH}$ and $\sigma^0_{VV}$ depends on the incident angle (θ), the soil dielectric constant (ε, which is a function of the soil moisture content), the soil roughness defined by the standard deviation of

surface height (*Hrms*), and the radar wavelength ($\lambda = 2\pi/k$ where $k$ is the wave number). The model optimized for bare soils according to the validity domain defined by $kHrms \leq 2.5$, $mv \leq$ 35 vol. %, and $\theta \geq 30°$ is expressed as:

$$\begin{aligned}\sigma^0_{VV} &= 10^{-2.35}\left(\frac{\cos^3\theta}{\sin^3\theta}\right)10^{0.046\varepsilon\tan\theta}\left(k\,Hrms\sin\theta\right)^{1.1}\lambda^{0.7}\\ \sigma^0_{HH} &= 10^{-2.75}\left(\frac{\cos^{1.5}\theta}{\sin^5\theta}\right)10^{0.028\varepsilon\tan\theta}\left(k\,Hrms\sin\theta\right)^{1.4}\lambda^{0.7}\end{aligned} \quad (3.1)$$

where $\theta$ is expressed in radians and $\lambda$ in cm, and $\sigma^0_{HH}$ and $\sigma^0_{VV}$ are expressed in linear units.

### III.3.2 The Semi-Empirical Oh Model

Oh (2004) and Oh et al. (1992b, 1994, 2002) developed between 1992 and 2004 several versions of a semi empirical backscattering model. Basing on theoretical models, scatterometer measurements and airborne SAR observations, the Oh model is built over a wide variety of bare soil surfaces. The Oh model relates the co-polarized ratio $p$ ($=\sigma^0_{HH}/\sigma^0_{VV}$) and the cross-polarized ratio $q$ ($=\sigma^0_{HV}/\sigma^0_{VV}$) to incident angle ($\theta$), wave number ($k$), standard deviation of surface height (*Hrms*), correlation length ($L$), and soil moisture (*mv*) or dielectric constant ($\varepsilon_r$).

The initial version of the Oh model (Oh et al., 1992) is defined as:

$$p = \frac{\sigma^0_{HH}}{\sigma^0_{VV}} = \left[1 - \left(\frac{\theta}{90}\right)^{1/3\Gamma_0} . e^{-kHrms}\right]^2 \quad (3.2)$$

$$q = \frac{\sigma^0_{HV}}{\sigma^0_{VV}} = 0.23\sqrt{\Gamma_0}\left(1 - e^{-kHrms}\right) \quad (3.3)$$

where:

$$\Gamma_0 = \left| \frac{1-\sqrt{\varepsilon_r}}{1+\sqrt{\varepsilon_r}} \right|^2 \tag{3.4}$$

Oh et al. (1994) proposed a new expression for $q$ to incorporate the effect of the incidence angle:

$$q = \frac{\sigma^0_{HV}}{\sigma^0_{VV}} = 0.25\sqrt{\Gamma_0}\left(0.1+\sin^{0.9}\theta\right)\left(1-e^{-\left[1.4-1.6\Gamma_0\right]kHrms}\right) \tag{3.5}$$

Oh et al. (2002) again modified the expressions for $p$ and $q$, and the following expression for the cross-polarized backscatter coefficient was proposed:

$$p = \frac{\sigma^0_{HH}}{\sigma^0_{VV}} = 1-\left(\frac{\theta}{90}\right)^{0.35mv^{-0.65}} . e^{-0.4(kHrms)^{1.4}} \tag{3.6}$$

$$q = \frac{\sigma^0_{HV}}{\sigma^0_{VV}} = 0.1\left(\frac{Hrms}{L}+\sin 1.3\theta\right)^{1.2}\left(1-e^{-0.9(kHrms)^{0.8}}\right) \tag{3.7}$$

$$\sigma^0_{HV} = 0.11\, mv^{0.7}\cos^{2.2}\theta\left(1-e^{-0.32(kHrms)^{1.8}}\right) \tag{3.8}$$

Oh and Kay (1998) demonstrated that the measurement of the correlation length is not accurate and that the ratio $q$ is not sensitive to the roughness parameter (defined as $Hrms/L$). Thus, (Oh, 2004) proposed a new equation for $q$ that ignores the correlation length ($L$):

$$q = \frac{\sigma^0_{HV}}{\sigma^0_{VV}} = 0.095\left(0.13+\sin 1.5\theta\right)^{1.4}\left(1-e^{-1.3(kHrms)^{0.9}}\right) \tag{3.9}$$

The Oh model (Oh, 2004) is optimized for bare soils in the following validity domain: $0.13 \leq kHrms \leq 6.98$, $4 \leq mv$ (vol. %) $\leq 29.1$, and $10° \leq \theta \leq 70°$.

The estimation of soil moisture and surface roughness from Oh model requires two backscattering coefficients at least, with one co-polarized coefficient ($\sigma^0_{HH}$ or $\sigma^0_{VV}$) and one cross-polarized coefficient ($\sigma^0_{HV}$ or $\sigma^0_{VH}$). The availability of $\sigma^0_{VV}$ and $\sigma^0_{VH}$ allows using the ratio $q$ and $\sigma^0_{HV}$ in the inversion process of SAR data, while the ratio $p/q$, as well as $\sigma^0_{HV}$, is used in the case where SAR data are available in the both HH and HV polarizations.

### III.3.3 The Physical Integral Equation Model (IEM)

The Integral Equation IEM is a physical model (Fung, 1994), where the soil is characterized by the dielectric constant ($\varepsilon_r$), the standard deviation of surface height (*Hrms*), the form of the correlation function, and the correlation length (*L*). The IEM also takes into account the sensor parameters such as the incidence angle (θ), the polarization (*pq* with *p*,*q* = H or V), and the radar wave number ($k = 2\pi/\lambda$ where λ is the wavelength). The IEM has a validity domain that covers the range of roughness values that are commonly encountered for agricultural surfaces:

$$kHrms \le 3$$
$$\left((k\,Hrms\cos\theta)^2 \Big/ \sqrt{0.46kL}\right)\exp\left\{-\sqrt{0.92\,kL(1-\sin\theta)}\right\} < 0.25 \qquad (3.10)$$

Over bare soils in agricultural areas, the backscattering coefficient of the surface contribution is expressed at HH and VV polarizations as:

$$\begin{aligned}\sigma^0_{pp} = {} & \frac{k^2}{2}\left|f_{pp}\right|^2 e^{-4k^2 Hrms^2\cos^2\theta}\sum_{n=1}^{+\infty}\frac{(4k^2 Hrms^2\cos^2\theta)^n}{n!}W^{(n)}(2k\sin\theta,0) \\ & + \frac{k^2}{2}\mathrm{Re}(f_{pp}^{*}F_{pp})\,e^{-3k^2 Hrms^2\cos^2\theta}\sum_{n=1}^{+\infty}\frac{(4k^2 Hrms^2\cos^2\theta)^n}{n!}W^{(n)}(2k\sin\theta,0) \\ & + \frac{k^2}{8}\left|F_{pp}\right|^2 e^{-2k^2 Hrms^2\cos^2\theta}\sum_{n=1}^{+\infty}\frac{(k^2 Hrms^2\cos^2\theta)^n}{n!}W^{(n)}(2k\sin\theta,0)\end{aligned} \qquad (3.11)$$

At cross polarization, the backscattering coefficient is as follows:

$$\sigma_{hv}^{0} = \frac{k^2}{16\pi} e^{-2k^2 Hrms^2 \cos^2\theta} \sum_{n=1}^{+\infty} \sum_{m=1}^{+\infty} \frac{(k^2 Hrms^2 \cos^2\theta)^{n+m}}{n!m!}$$

$$\iint \left[ \left| F_{hv}(u,v) \right|^2 + F_{hv}(u,v) F_{hv}^{*}(-u,-v) \right] W^{(n)}(u - k\sin\theta, v) W^{(m)}(u + k\sin\theta, v)\, du\, dv \tag{3.12}$$

where:

$$f_{hh} = \frac{-2R_h}{\cos\theta}; \quad f_{vv} = \frac{2R_v}{\cos\theta} \tag{3.13}$$

$$R_h = \frac{\mu_r \cos\theta - \sqrt{\mu_r \varepsilon_r - \sin^2\theta}}{\mu_r \cos\theta + \sqrt{\mu_r \varepsilon_r - \sin^2\theta}}: \text{Fresnel coefficient at horizontal polarization} \tag{3.14}$$

$$R_v = \frac{\varepsilon_r \cos\theta - \sqrt{\mu_r \varepsilon_r - \sin^2\theta}}{\varepsilon_r \cos\theta + \sqrt{\mu_r \varepsilon_r - \sin^2\theta}}: \text{Fresnel coefficient at vertical polarization} \tag{3.15}$$

$$F_{hh} = 2\frac{\sin^2\theta}{\cos\theta} \left[ 4R_h - \left( 1 - \frac{1}{\varepsilon_r} \right) \left( 1 + R_h \right)^2 \right] \tag{3.16}$$

$$F_{vv} = 2\frac{\sin^2\theta}{\cos\theta} \left[ \left( 1 - \frac{\varepsilon_r \cos^2\theta}{\mu_r \varepsilon_r - \sin^2\theta} \right) \left( 1 - R_v \right)^2 + \left( 1 - \frac{1}{\varepsilon_r} \right) \left( 1 + R_v \right)^2 \right] \tag{3.17}$$

$$F_{hv}(u,v) = \frac{uv}{k\cos\theta} \left[ \frac{8R^2}{\sqrt{k^2 - u^2 - v^2}} + \frac{-2 + 6R^2 + \frac{(1+R)^2}{\varepsilon_r} + \varepsilon_r (1-R)^2}{\sqrt{\varepsilon_r k^2 - u^2 - v^2}} \right] \tag{3.18}$$

$$R = \frac{R_v - R_h}{2} \tag{3.19}$$

$\varepsilon_r$ : dielectric constant, obtained on the basis of volumetric water content (*mv*). In our study, Hallikainen empirical model is used (Hallikainen et al., 1985).

$\mu_r$ : relative permittivity.

Re: real part of the complex number.

$f_{pp}^*$: conjugate of the complex number $f_{pp}$.

$W^{(n)}$ is the Fourier transform of the *n*th power of the surface correlation $\rho(x, y)$ function:

$$W^{(n)}(a,b) = \frac{1}{2\pi}\iint \rho^n(x,y)e^{-i(ax+by)}dxdy \tag{3.20}$$

The distribution of $\rho(x, y)$ is exponential for low surface roughness values and Gaussian for high surface roughness values.

### III.3.4 IEM Modified by Baghdadi (IEM_B)

Several studies reported important discrepancies between backscattering coefficients simulated by IEM and those measured by SAR sensors (Baghdadi et al., 2002a; Boisvert et al., 1997; Gorrab et al., 2015b; Panciera et al., 2014; Rakotoarivony et al., 1996; Remond, 1997; Zribi et al., 1997). Baghdadi et al. (2002b) showed that the discrepancy between the observed and IEM simulated backscattering coefficients is mainly due to the correlation length parameter which is difficult to measure with a good accuracy. To reduce such incongruities between simulated and measured backscattering values, Baghdadi et al. (2006, 2011a, 2011c, 2015) proposed a semi-empirical calibration of the IEM backscattering, which consists of replacing the in situ measured correlation length by a fitting parameter (*Lopt*). *Lopt* depends on surface roughness conditions and SAR configurations (incidence angle,

polarization and radar wavelength). This calibration has been performed by using large experimental datasets and SAR configurations (incidence angles from 23° to 57°, and HH, HV, and VV polarizations), and it has been carried separately at X-band in (Baghdadi et al., 2011c), C-band in (Baghdadi et al., 2006a, 2011b) and L-band in (Baghdadi et al., 2015). The proposed calibration reduces the IEM's input soil parameters from three to two (*Hrms* and *mv* only, instead of *Hrms*, *L* and *mv*).

*Lopt* is computed at L-, C-, and X-bands using a Gaussian correlation function and it is described as follows:

$$\text{In X-band: } \begin{cases} Lopt(Hrms,\ \theta, HH) = 18.102e^{-1.891\ \theta}\ Hrms^{\ 0.7644e^{0.2005\ \theta}} \\ Lopt(Hrms,\ \theta, VV) = 18.075e^{-2.1715\ \theta}\ Hrms^{\ 1.2594e^{-0.8308\ \theta}} \end{cases} \quad (3.21)$$

$$\text{In C-band: } \begin{cases} Lopt(Hrms,\ \theta, HH) = 0.162 + 3.006\ (\sin 1.23\ \theta)^{-1.494}\ Hrms \\ Lopt(Hrms,\ \theta, HV) = 0.9157 + 1.2289\ (\sin 0.1543\ \theta)^{-0.3139}\ Hrms \\ Lopt(Hrms,\ \theta, VV) = 1.281 + 0.134\ (\sin 0.19\ \theta)^{-1.59}\ Hrms \end{cases} \quad (3.22)$$

$$\text{In L-band: } \begin{cases} Lop\ (Hrms,\ \theta, HH) = 2.6590\ \theta^{\ -1.4493} + 3.0484\ Hrms\ \theta^{\ -0.8044} \\ Lopt(Hrms,\ \theta, VV) = 5.8735\ \theta^{\ -1.0814} + 1.3015\ Hrms\ \theta^{\ -1.4498} \end{cases} \quad (3.23)$$

where θ is in radians; *Lopt* and *Hrms* are in centimeters. Several studies showed that the use of the fitting parameter *Lopt* allows more correct estimations of the radar backscattering coefficient (Baghdadi et al., 2015; Dong et al., 2013; Gorrab et al., 2015a).

### III.3.5 The Advanced Integral Equation Model

The Advanced Integral Equation Model (AIEM) (Chen et al., 2003) is the updated version of the Integral Equation Model (IEM) (Fung, 1994). In a comparison with the IEM, two improvements have been integrated into the AIEM: (1) the complete expressions for the Kirchhoff field coefficient and the complementary field coefficient based on the removal of the simplification assumption of the Green's function have been included in the AIEM (Chen et al., 2003) and (2) a continuous Fresnel reflection coefficient is obtained using a transition model (Wu et al., 2001). This update allows a more precise calculation of the simple scattering for a surface with a wide range of dielectric constant ( $\varepsilon_r$ ), large standard deviation

of heights *Hrms*, and various remote sensing configurations. The AIEM simulates the radar backscattering coefficients basing on the same parameters as the IEM.

## III.4 Results and Discussion

This section shows the evaluation results of the five radar backscattering models Dubois, Oh, IEM, IEM_B and AIEM using large datasets, characterized by various radar wavelength (L, C and X), wide range of incidence angles and large geographical distribution in regions with different climate conditions (humid, semi-arid and arid sites). The size of reference plots is at least of 2 ha. For each plot, SAR data was simulated through backscatter models using in situ measurements (*mv*, *Hrms* and *L*) averaged within that plot. Then, the simulated SAR signal were compared with the backscattering coefficients computed from calibrated SAR images by linearly averaging the $\sigma^0$ values of all pixels within the plot

### III.4.1 Evaluation of the Dubois Model

The evaluation of Dubois model was carried out for different scenarios using all data, per radar wavelength, and by range of soil moisture, *kHrms*, and incidence angle.

Using all data, the Dubois model slightly over-estimates the radar signal by about 1.0 dB in HH polarization and slightly under-estimates the radar signal by about 0.7 dB in VV polarization (Table III.3, Figures III.1 and III.2). RMSE is about 4.0 dB and 2.9 dB at HH and VV polarization, respectively (Table III.3). The analysis of the error according to each radar frequency band separately (L, C and X) shows an over-estimation in HH polarization, which is almost the same at L-, C- and X-bands (between 0.9 dB and 1.1 dB). In VV polarization, the Dubois model under-estimates the radar signal by about 1.8 dB and 0.4 dB for X and C bands, respectively. For L band, the Dubois model fits correctly the radar signal in VV because the difference between real data and simulations is about 0.2 dB. The RMSE in HH is the same as at X- and C-bands, and is about 4.1 dB and decreases to 3.0 dB at L-band. In VV polarization, the RMSE increases with the radar frequency (2.5 dB at L-band, 2.8 dB at C-band and 3.1 dB at X-band).

| Model | Statistics | All Data | L-Band | C-Band | X-Band | *kHrms* < 2.5 | *kHrms* > 2.5 | *mv* < 20 vol.% | *mv* > 20 vol. % | θ < 30° | θ > 30° |
|---|---|---|---|---|---|---|---|---|---|---|---|
| Dubois for HH pol. | Bias (dB) | −1.0 | −1.0 | −1.1 | −0.9 | +0.4 | −2.9 | −2.6 | +0.3 | −4.2 | +0.3 |
| | RMSE (dB) | 4.0 | 3.0 | 4.1 | 4.1 | 3.6 | 4.6 | 4.6 | 3.4 | 5.5 | 3.2 |
| Dubois for VV pol. | Bias (dB) | +0.7 | −0.2 | +0.4 | +1.8 | +1.2 | −0.2 | +0.5 | +1.0 | −0.6 | +1.5 |
| | RMSE (dB) | 2.9 | 2.5 | 2.8 | 3.1 | 3.0 | 2.5 | 2.8 | 3.0 | 2.9 | 2.9 |

**Table III.3.** Comparison between the Dubois model output and real data using the entire dataset, and by separating two intervals of *kHrms*, soil moisture (*mv*) and incidence angle (θ). Bias = real data − simulations.

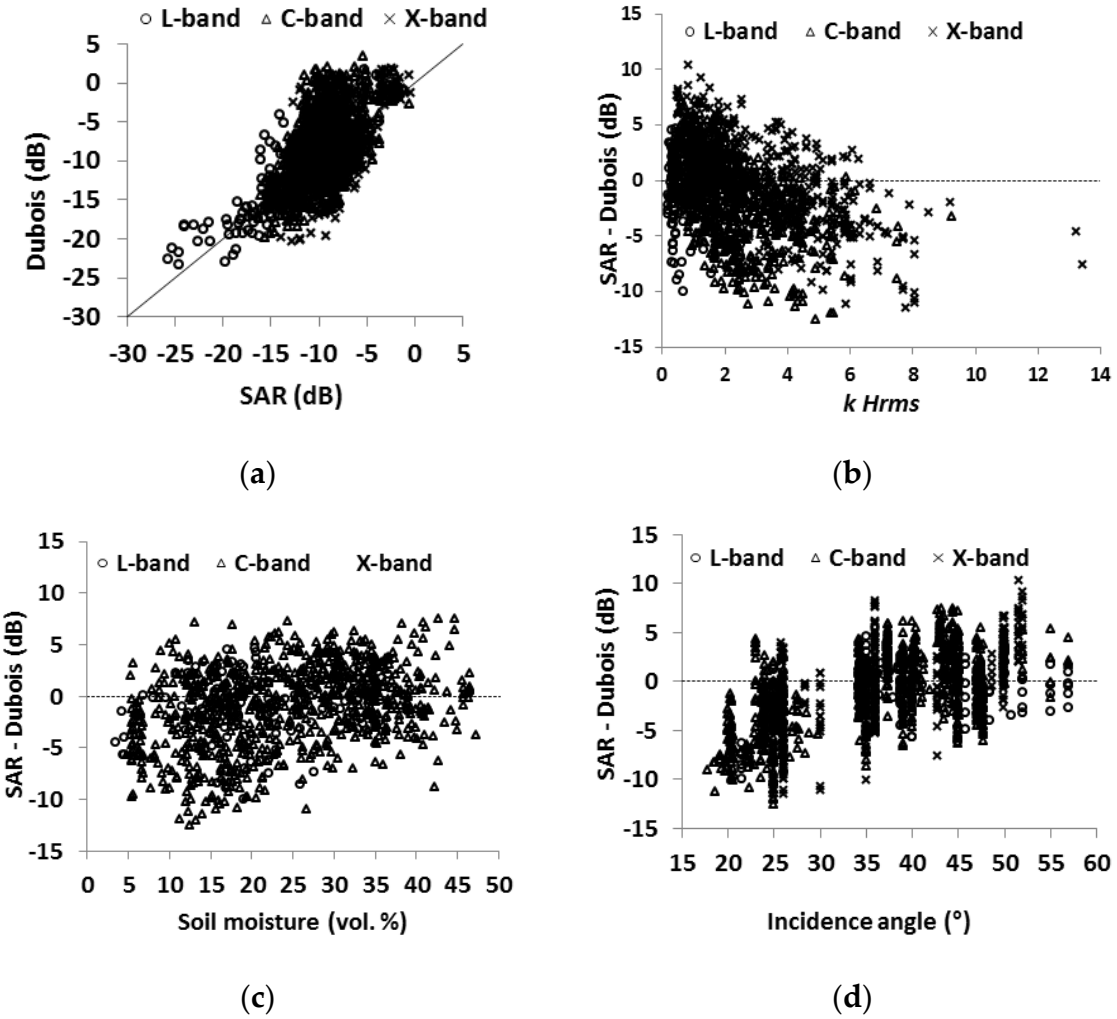


**Figure III.1.** Comparison between backscattering coefficient values obtained from SAR images and those estimated from the Dubois model at HH polarization. (a) Dubois model simulations vs. SAR data; (b) difference between SAR signal and the Dubois model vs. soil roughness (*kHrms*); (c) difference between SAR signal and the Dubois model vs. soil moisture (*mv*); (d) difference between SAR signal and Dubois model vs. incidence angle.

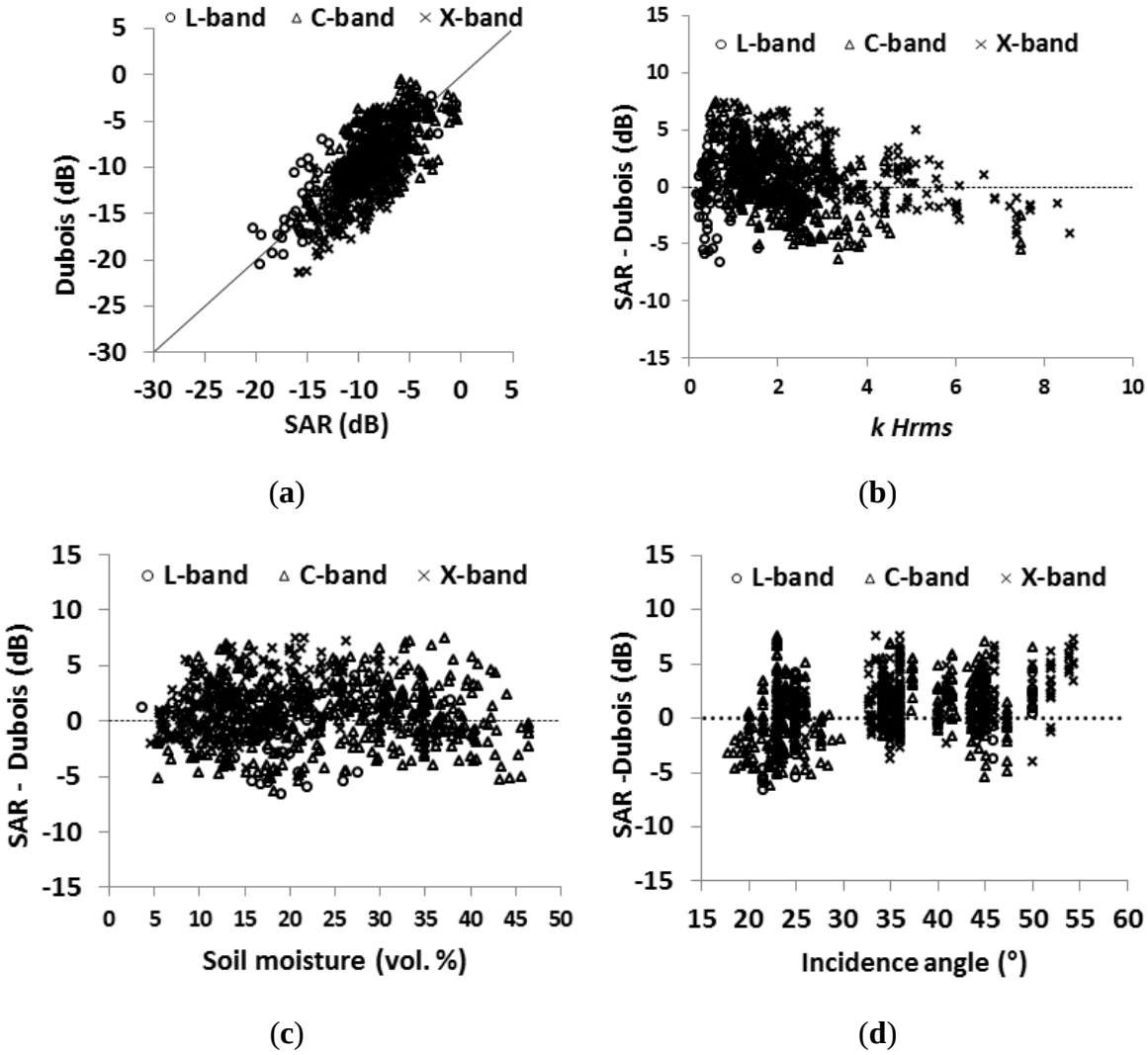


**Figure III.2.** Comparison between backscattering coefficient values obtained from SAR images and those estimated using the Dubois model at VV polarization. (a) Dubois model simulations vs. SAR data; (b) difference between SAR signal and the Dubois model vs. soil roughness (*kHrms*); (c) difference between SAR signal and the Dubois model vs. soil moisture (*mv*); (d) difference between SAR signal and Dubois model vs. incidence angle.

The analysis of the error of the Dubois model according to the validity domain was studied by range of surface roughness (*kHrms*), soil moisture (*mv*) and incidence angle (Table III.3). The Dubois model underestimates the radar signal for *kHrms* < 2.5 (validity domain of the Dubois model) by about 0.4 dB and 1.2 dB in HH and VV polarizations, respectively. In the case of *kHrms* < 2.5, the RMSE is about 3.6 and 3.0 dB for HH and VV polarizations, respectively. In addition, the Dubois model overestimates the radar signal for *kHrms* > 2.5 by about 2.9 dB in HH polarization with RMSE about 4.6 dB. In VV polarization, the Dubois model fits correctly the radar signal in the case of *kHrms* > 2.5 with a difference between real and simulated data of about 0.2 dB and a RMSE of 2.5 dB (Table III.3).

Moreover, the evaluation of the Dubois model was carried out by range of soil moisture (*mv*). Results show an overestimation in HH pol. by about 2.6 dB and a slightly underestimation in VV by about 0.5 dB with *mv*-values lower than 20 vol.% (RMSE = 4.6 and 2.8 dB at HH and VV, respectively) (Table III.3). Besides, the Dubois model correctly simulates the backscattering coefficient in HH pol. with a difference between real data and simulations about 0.3 dB and underestimates the radar signal in VV by about 1.0 dB with *mv*-values greater than 20 vol. %. In the case of *mv*-values greater than 20 vol. %, the RMSE is about 3.4 dB and 3.0 dB for HH and VV polarization respectively. Finally, the performance of Dubois model was studied according to ranges of incidence angle (Table III.3). For $\theta < 30°$ (outside the validity domain of the Dubois model), the Dubois model overestimates the radar signal by −4.2 dB in HH polarization (RMSE = 5.5 dB) and slightly underestimates the radar signal in VV polarization (real data − simulations = −0.6 dB) with a RMSE of 2.9 dB. At $\theta > 30°$, the Dubois model correctly simulates the backscattering coefficient in HH pol. with a difference between real data and model of 0.3 dB at HH polarization and underestimates the backscattering at VV pol. by about 1.5 dB (RMSE = 3.2 dB and 2.9 dB for HH and VV polarizations, respectively).

### III.4.2 Evaluation of the Oh Model

The Oh model versions developed in 1992, 1994, 2002 and 2004 were applied to our datasets. The evaluation of the different Oh model versions was carried out firstly using all data, successively for each radar wavelength (L, C and X bands), and finally by range of soil moisture, *kHrms* and incidence angle (Table III.4, Figures III.3–III.11).

Using the entire dataset, results showed that the different versions of Oh model correctly simulate the backscattering at both HH and VV polarizations with difference between real data and simulations varying between −0.9 and +0.4 dB at HH pol. and between (−1.3 dB and +0.4 dB) in VV pol. The RMSE values are approximately the same for all models and in both HH and VV polarizations, i.e., between 2.4 dB and 2.8 dB. The Oh 1992 model simulates slightly better the backscattering than the other versions (Table III.4). For HV polarization, the Oh 2002 model simulates correctly the backscattering with a difference between real and simulated data of about +0.7 dB, with RMSE equal to 2.9 dB.

| Model | Pol. | Statistics | All Data | L-Band | C-Band | X-Band | *kHrms* < 2.0 | *kHrms* > 2.0 | *mv* < 29.1 vol. % | *mv* > 29.1 vol. % |
|---|---|---|---|---|---|---|---|---|---|---|
| (Oh et al., 1992) | HH | Bias (dB) | +0.4 | +2.5 | +0.1 | 0.0 | +1.3 | −0.5 | −0.3 | +1.9 |
| | | RMSE (dB) | 2.6 | 3.7 | 2.4 | 2.5 | 2.9 | 2.3 | 2.3 | 3.1 |
| | VV | Bias (dB) | +0.1 | +2.1 | +0.4 | −1.2 | +1.0 | −0.7 | −0.4 | +1.5 |
| | | RMSE (dB) | 2.4 | 3.4 | 2.3 | 2.1 | 2.7 | 2.0 | 2.3 | 2.7 |
| (Oh et al., 1994) | HH | Bias (dB) | −0.9 | +1.3 | −1.2 | −1.2 | −0.05 | −1.7 | −1.6 | +0.5 |
| | | RMSE (dB) | 2.8 | 2.8 | 2.7 | 2.8 | 2.6 | 2.9 | 2.9 | 2.5 |
| | VV | Bias (dB) | −1.3 | +0.7 | −1.3 | −2.1 | −0.5 | −2.1 | −1.7 | −0.4 |
| | | RMSE (dB) | 2.6 | 2.6 | 2.6 | 2.7 | 2.4 | 2.9 | 2.8 | 2.2 |
| (Oh et al., 2002) | HH | Bias (dB) | −0.3 | +2.1 | −0.9 | −1.0 | +0.3 | −0.9 | −0.7 | +0.4 |
| | | RMSE (dB) | 2.7 | 3.2 | 2.7 | 2.8 | 2.7 | 2.6 | 2.7 | 2.5 |
| | HV | Bias (dB) | +0.7 | +1.5 | +1.0 | −0.9 | +1.8 | −0.7 | +0.5 | +0.8 |
| | | RMSE (dB) | 2.9 | 3.1 | 2.7 | 3.8 | 3.2 | 2.5 | 3.0 | 2.6 |
| | VV | Bias (dB) | −0.6 | +1.8 | −1.2 | +0.4 | −0.2 | −1.0 | −0.7 | −0.5 |
| | | RMSE (dB) | 2.5 | 2.9 | 2.7 | 2.0 | 2.5 | 2.6 | 2.6 | 2.5 |
| (Oh, 2004) | HH | Bias (dB) | −0.5 | +2.1 | −1.0 | −0.6 | 0.6 | +1.5 | −0.9 | +0.4 |
| | | RMSE (dB) | 2.6 | 3.3 | 2.7 | 2.3 | 2.6 | 2.6 | 2.7 | 2.6 |
| | VV | Bias (dB) | −1.1 | +1.4 | −1.5 | −1.4 | −0.2 | −2.0 | −1.3 | −0.8 |
| | | RMSE (dB) | 2.6 | 2.8 | 2.8 | 2.1 | 2.4 | 2.8 | 2.6 | 2.6 |

**Table III.4.** Comparison between real data and Oh models for all data and different ranges of *kHrms* and soil moisture (*mv*). Bias = real data − simulations.

In L-band, the different versions of the Oh model underestimate the backscattering at both HH and VV polarizations. This underestimation varies between 1.3 dB and 2.5 dB in HH polarization and between 0.7 dB and 2.1 dB in VV polarization (Table III.4). The RMSE is slightly higher in HH than in VV polarization (between 2.8 dB and 3.7 dB in HH and between 2.6 dB and 3.4 dB in VV). The Oh 1994 version better simulates the backscattering than other versions of Oh model, with an underestimation of the backscattering between 1.3 dB and 0.7 dB and RMSE of 2.8 and 2.6 dB for HH and VV polarizations, respectively. At HV polarization, the Oh model underestimates the backscattering by about 1.5 dB with RMSE equal to 3.1 dB.

In C-band, the Oh 1992 model correctly simulates the backscattering in both HH and VV polarizations with differences between real and simulated data of 0.1 dB and 0.4 dB at HH and VV polarizations, respectively (Table III.4). Besides, the RMSE is of 2.4 dB at HH and 2.3 dB at VV pol. Moreover, the other Oh versions overestimate the backscattering in both HH and VV polarizations (between 0.9 dB and 1.5 dB) with similar RMSE between 2.6 dB and 2.8 dB. At HV polarization, the Oh 2002 model slightly underestimates the backscattering by about 1.0 dB with a RMSE of 2.7 dB.

The analysis of results obtained in X-band shows that Oh model versions simulate the radar signal with difference between real data and simulations between 0.0 and −1.2 dB in HH and between +0.4 and −2.1 dB in VV (Table III.4, Figures III.3–III.11). The RMSE is between 2.3 and 2.8 dB in HH and between 2.0 and 2.7 dB in VV polarization. For HV polarization, the Oh model over-estimates the backscattering by about 0.9 dB with RMSE of 3.8 dB.

The analysis of the error was studied by selecting two ranges of surface roughness (*kHrms* < 2.0 and *kHrms* > 2.0) (Table III.4). This range is different from the general validity domain of the Oh model ($0.13 \leq kHrms \leq 6.98$) because it covers the entire dataset except only a few points. For *kHrms* < 2.0, the 1994, 2002 and 2004 Oh models simulate correctly the backscattering at both HH and VV polarizations with differences between real data and simulations between −0.5 and +0.6 dB and RMSE between 2.4 dB and 2.7 dB. The Oh 1992 model underestimates the backscattering by 1.3 dB and 1.0 dB at HH and VV polarizations, respectively (RMSE is 2.9 for HH pol. and 2.7 dB for VV pol.). For *kHrms* > 2.0, the 1992 and 2002 Oh versions simulate correctly backscattering at both HH and VV polarizations with difference between real and simulated data between −0.5 dB and −1.0 dB with RMSE between 2.3 and 2.6 dB. The 1994 Oh model over-estimates the backscattering at both HH and VV polarizations by about 1.7 dB and 2.1 dB, respectively (RMSE = 2.9 dB). The last version of the Oh model (Oh, 2004) underestimates the backscattering in HH polarization by about 1.5 dB (RMSE = 2.6 dB) and over-estimates it in VV polarization by about 2.0 dB (RMSE= 2.8 dB). At HV polarization, for *kHrms* < 2, the Oh 2002 model underestimates the backscattering in HV by 1.8 dB (RMSE = 2.5 dB). In addition, Oh model correctly fits the backscattering for *kHrms* > 2.0, with a difference between the real and simulated data of about −0.7 dB and RMSE of 2.5 dB.

Finally, the performance of the Oh model was studied according to its validity domain by selecting two intervals of soil moisture (*mv* < 29.1 and *mv* > 29.1 vol. %: validity domain of Oh model). For *mv* < 29.1 vol. %, the 1992 and 2002 Oh versions correctly simulate the backscattering coefficient at both HH and VV polarizations with a difference between real and simulated data varying between −0.3 dB and −0.7 dB. In addition, the 1994 and 2004 Oh models overestimate the backscattering at both HH and VV polarizations (Table III.4) with RMSE between 2.6 dB and 2.9 dB. In conclusion, for *mv* < 29.1 vol. %, the 1992 Oh model provides the best simulations. For *mv* > 29.1 vol. %, the 1994, 2002 and 2004 Oh models correctly simulate the backscattering with a difference between real and simulated data between −0.8 dB and +0.5 dB, while the 1992 Oh model underestimates the backscattering by

about 1.9 dB and 1.5 dB at HH and VV polarizations, respectively (RMSE = 3.1 dB for HH and 2.7 dB for VV). The RMSE values are approximately the same in the Oh 1994, 2002 and 2004 versions, and range between 2.2 dB and 2.6 dB. At HV polarization, the Oh model correctly simulates the backscattering for both range of *mv*-values, with RMSE of 3.0 dB for *mv* < 29.1 vol. % and RMSE of 2.6 dB for *mv* > 29.1 vol. %.

The validity domain of Oh model according to the incidence angle ($10° \leq \theta \leq 70°$) covers the entire dataset. Moreover, our results showed that the performance of the Oh model is not dependent on the incidence angle.

In conclusion, the Oh models simulate correctly the backscattering. Results showed that Oh 1992 version is slightly better than other model versions. The performance of Oh model seems to be better in C- and X-bands than L-band. Moreover, most versions of the Oh model correctly simulate the backscattering in most cases although outside its *mv* validity domain.

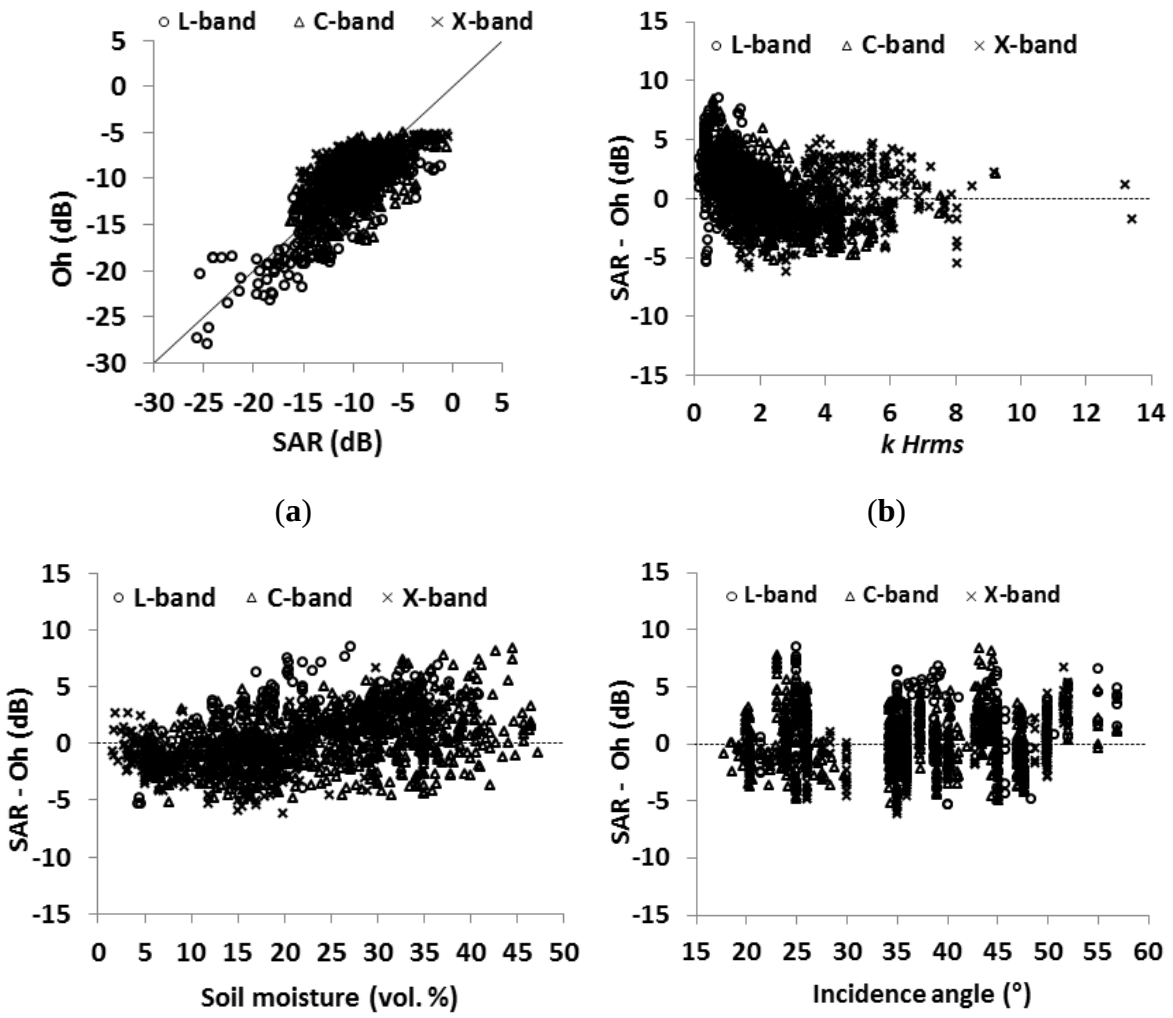


**Figure III.3.** Comparison between backscattering coefficients derived from SAR images and those estimated from the Oh 1992 model at HH polarization, (a) Oh model simulations vs. SAR data; (b) difference between SAR signal and Oh model results vs. soil roughness (*kHrms*); (c) difference between SAR signal and Oh model results vs. soil moisture (*mv*); (d) difference between SAR signal and Oh model results vs. incidence angle.

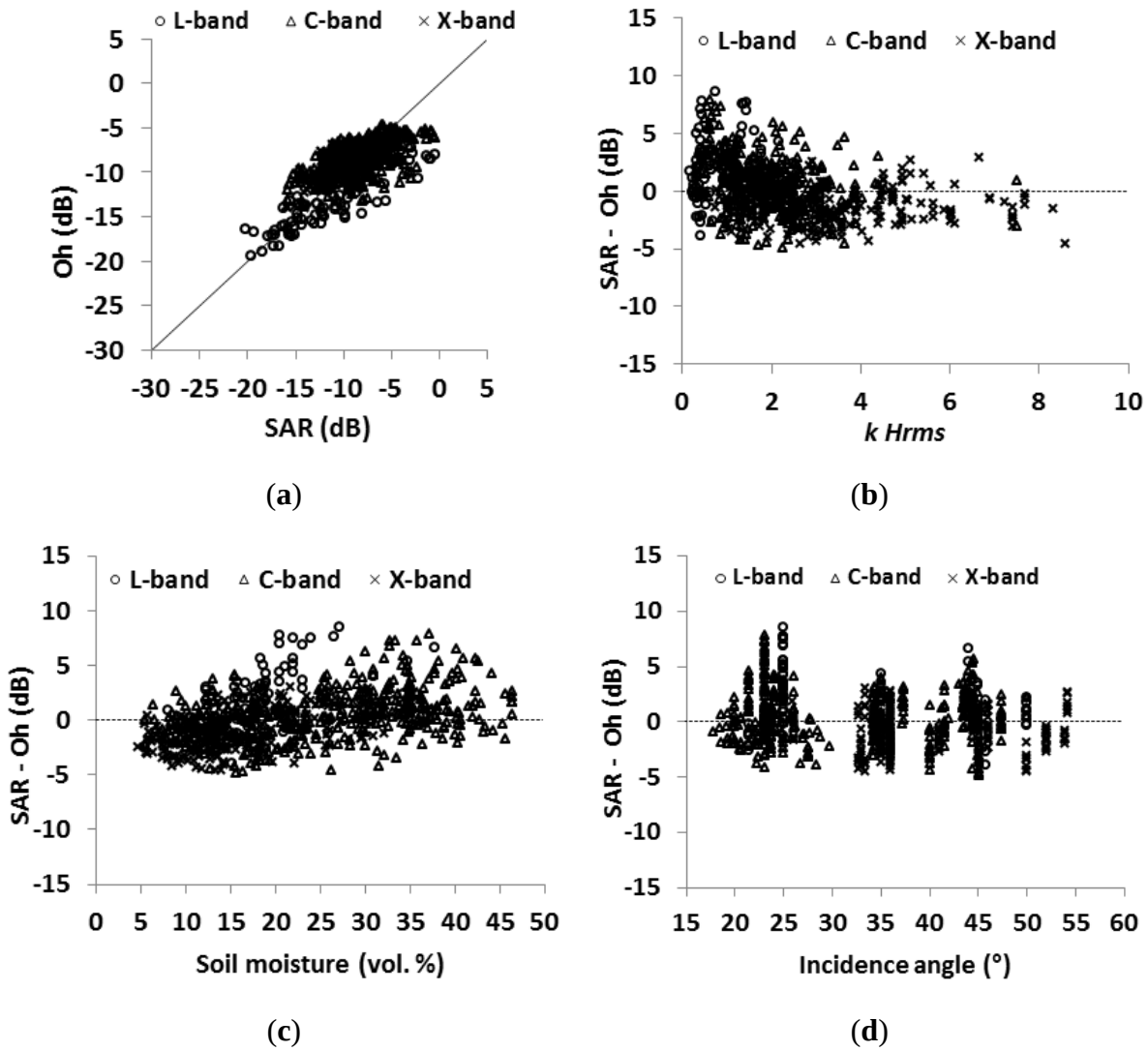


**Figure III.4.** Comparison between backscattering coefficients derived from SAR images and those estimated from the Oh 1992 model at VV polarization, (a) Oh simulations vs. SAR data; (b) difference between SAR signal and the Oh model vs. soil roughness (*kHrms*); (c) difference between SAR signal and Oh model results vs. soil moisture (*mv*); (d) difference between SAR signal and Oh model results vs. incidence angle.

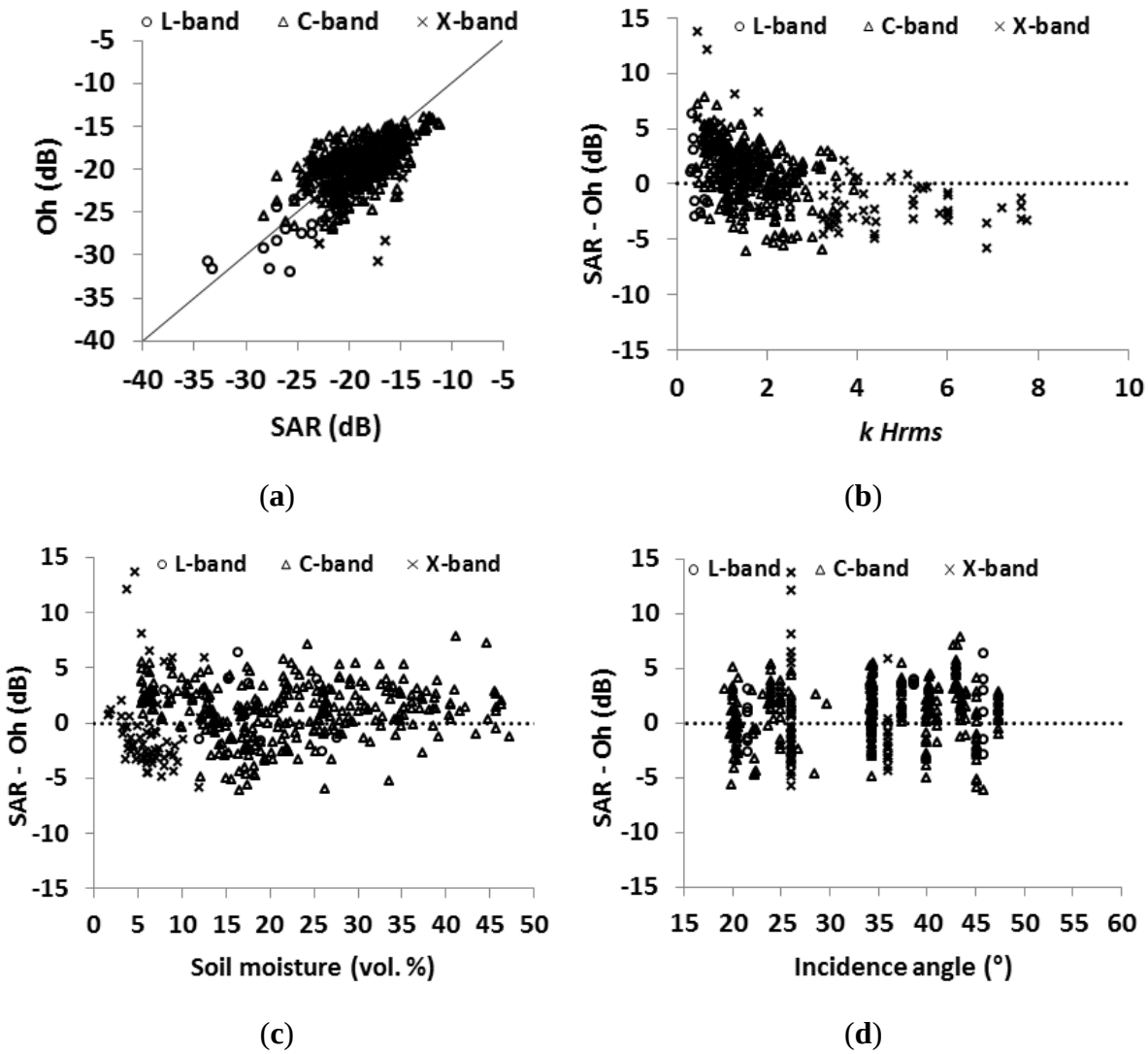


**Figure III.5.** Comparison between backscattering coefficients derived from SAR images and those estimated from the Oh 2002 model at HV polarization, (a) Oh simulations vs. SAR data; (b) difference between SAR signal and Oh model results vs. soil roughness (*kHrms*); (c) difference between SAR signal and Oh model results vs. soil moisture (*mv*); (d) difference between SAR signal and Oh model results vs. incidence angle.

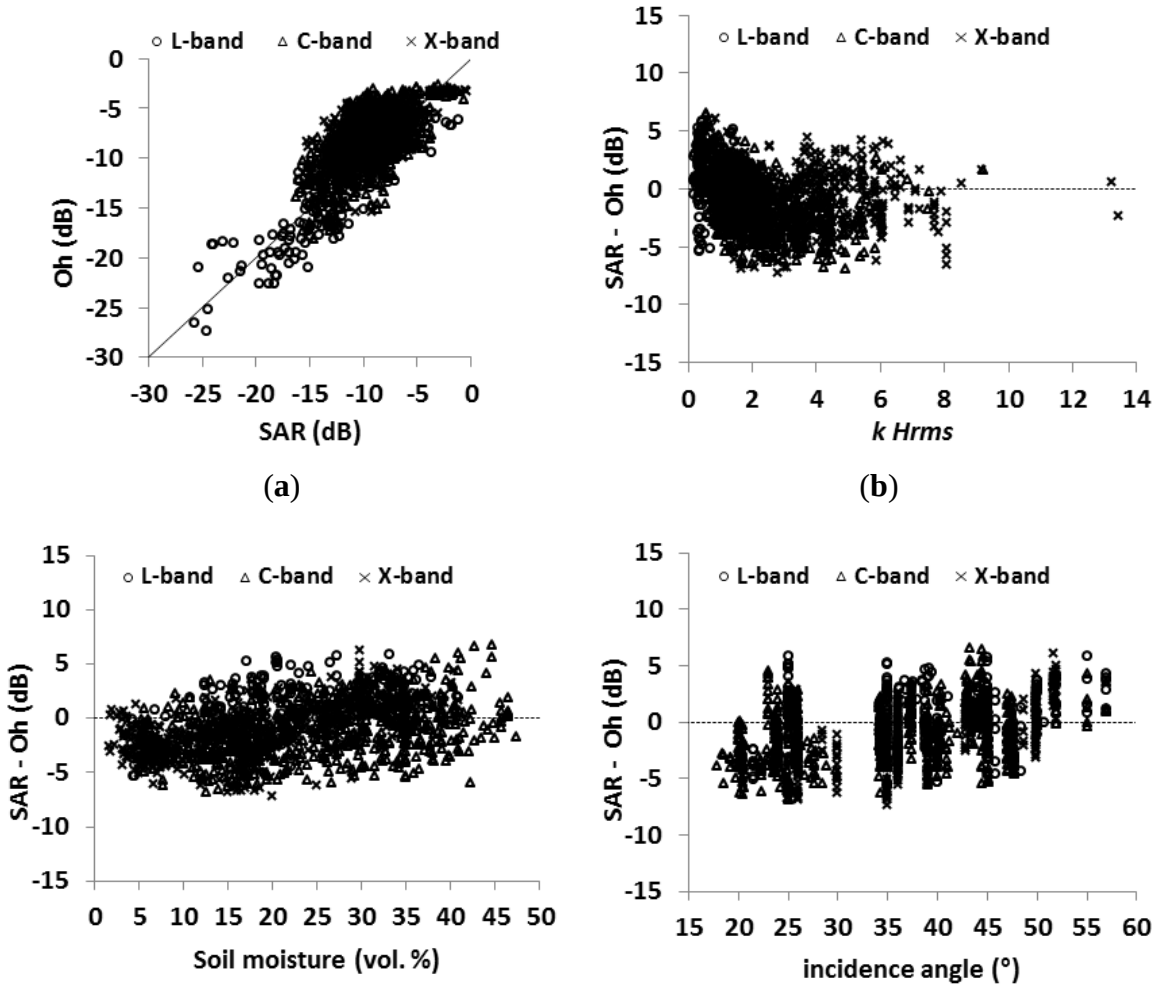


**Figure III.6.** Comparison between backscattering coefficients derived from SAR images and those estimated from the Oh 1994 model at HH polarization, (a) Oh model simulations vs. SAR data; (b) difference between SAR signal and Oh model results vs. soil roughness (*kHrms*); (c) difference between SAR signal and Oh model results vs. soil moisture (*mv*); (d) difference between SAR signal and Oh model results vs. incidence angle.

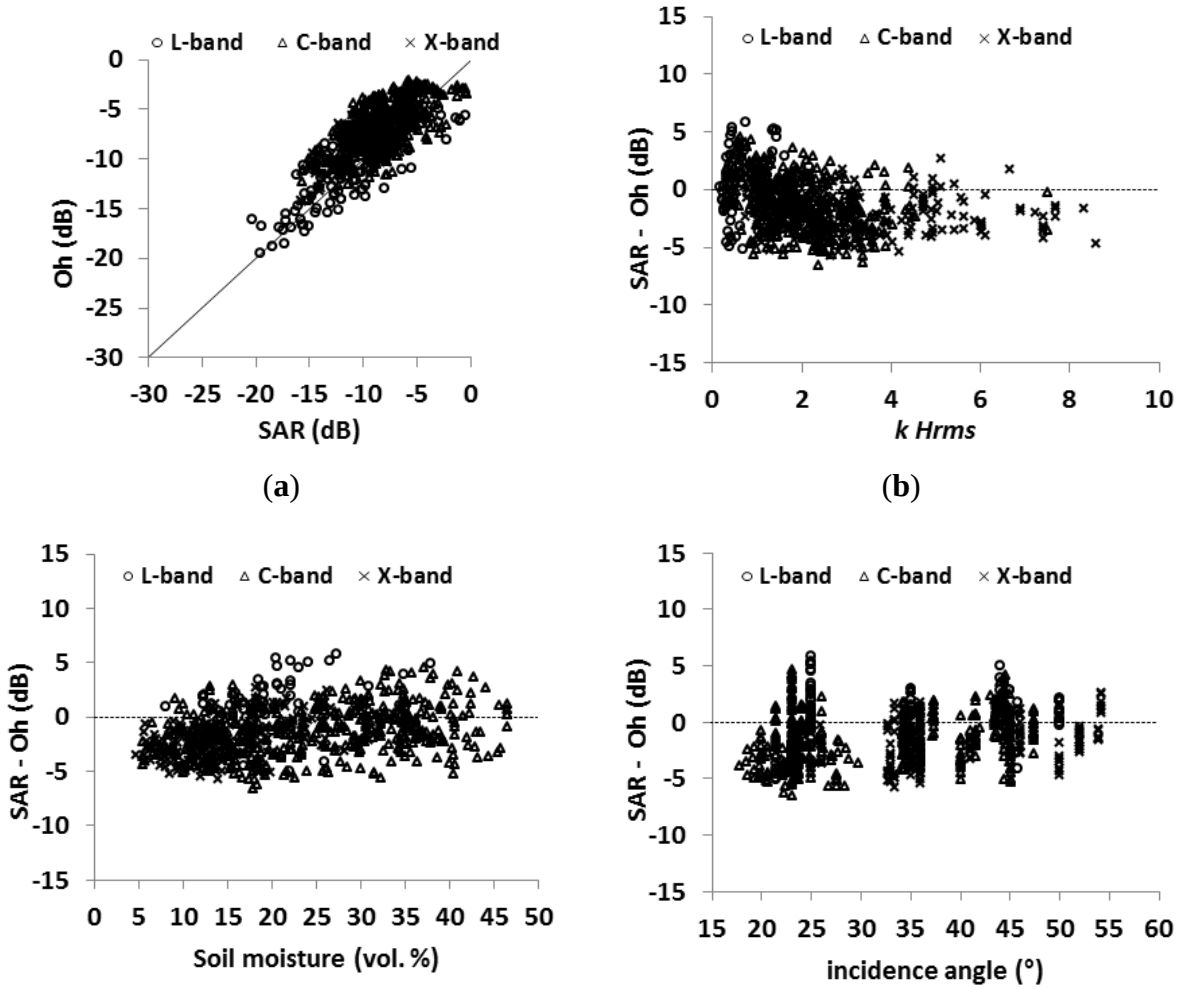


**Figure III.7.** Comparison between backscattering coefficients derived from SAR images and those estimated from the Oh 1994 model at VV polarization, (a) Oh simulations vs. SAR data; (b) difference between SAR signal and the Oh model vs. soil roughness (*kHrms*); (c) difference between SAR signal and Oh model results vs. soil moisture (*mv*); (d) difference between SAR signal and Oh model results vs. incidence angle.

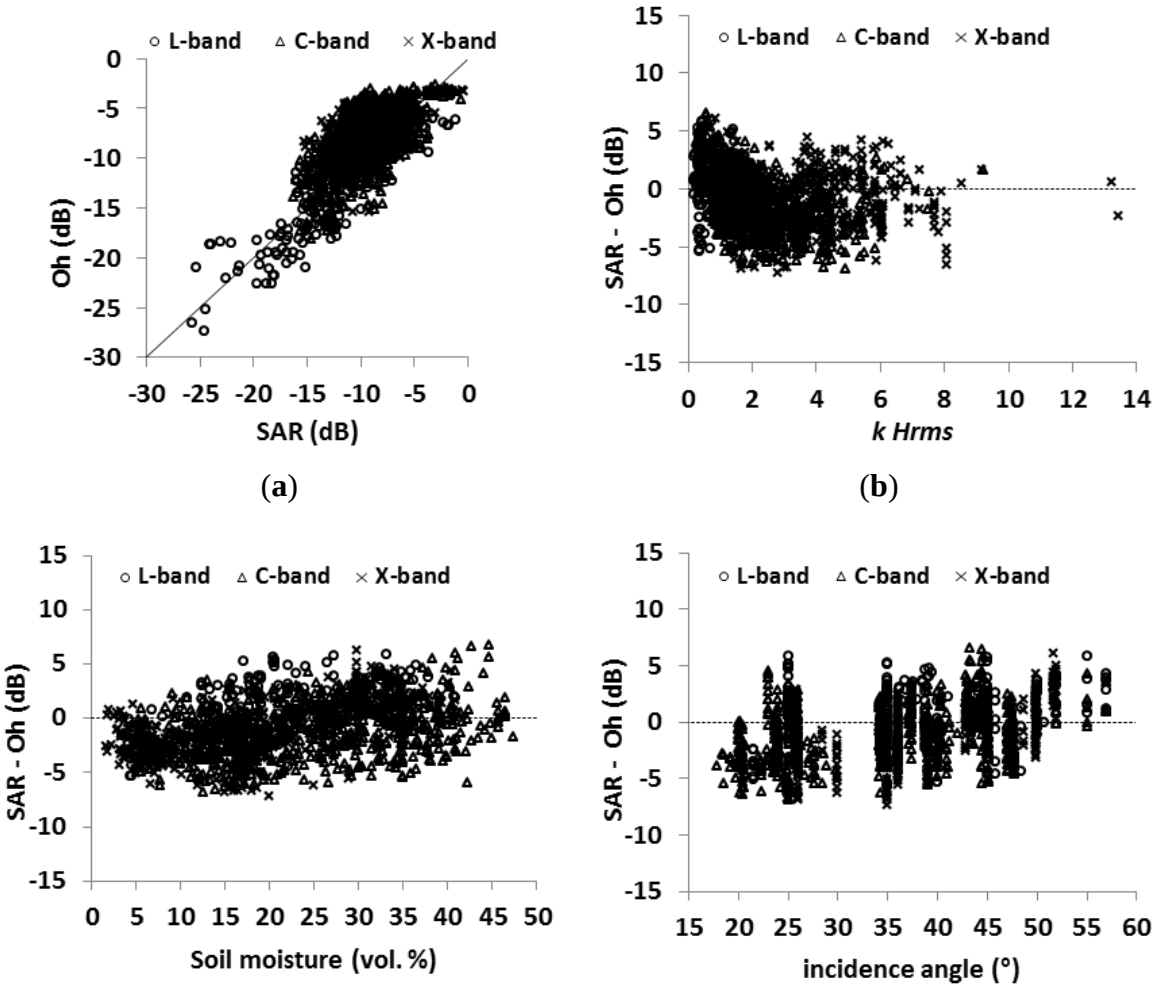


**Figure III.8.** Comparison between backscattering coefficients derived from SAR images and those estimated from the Oh 2002 model at HH polarization, (a) Oh model simulations vs. SAR data; (b) difference between SAR signal and Oh model results vs. soil roughness (*kHrms*); (c) difference between SAR signal and Oh model results vs. soil moisture (*mv*); (d) difference between SAR signal and Oh model results vs. incidence angle.

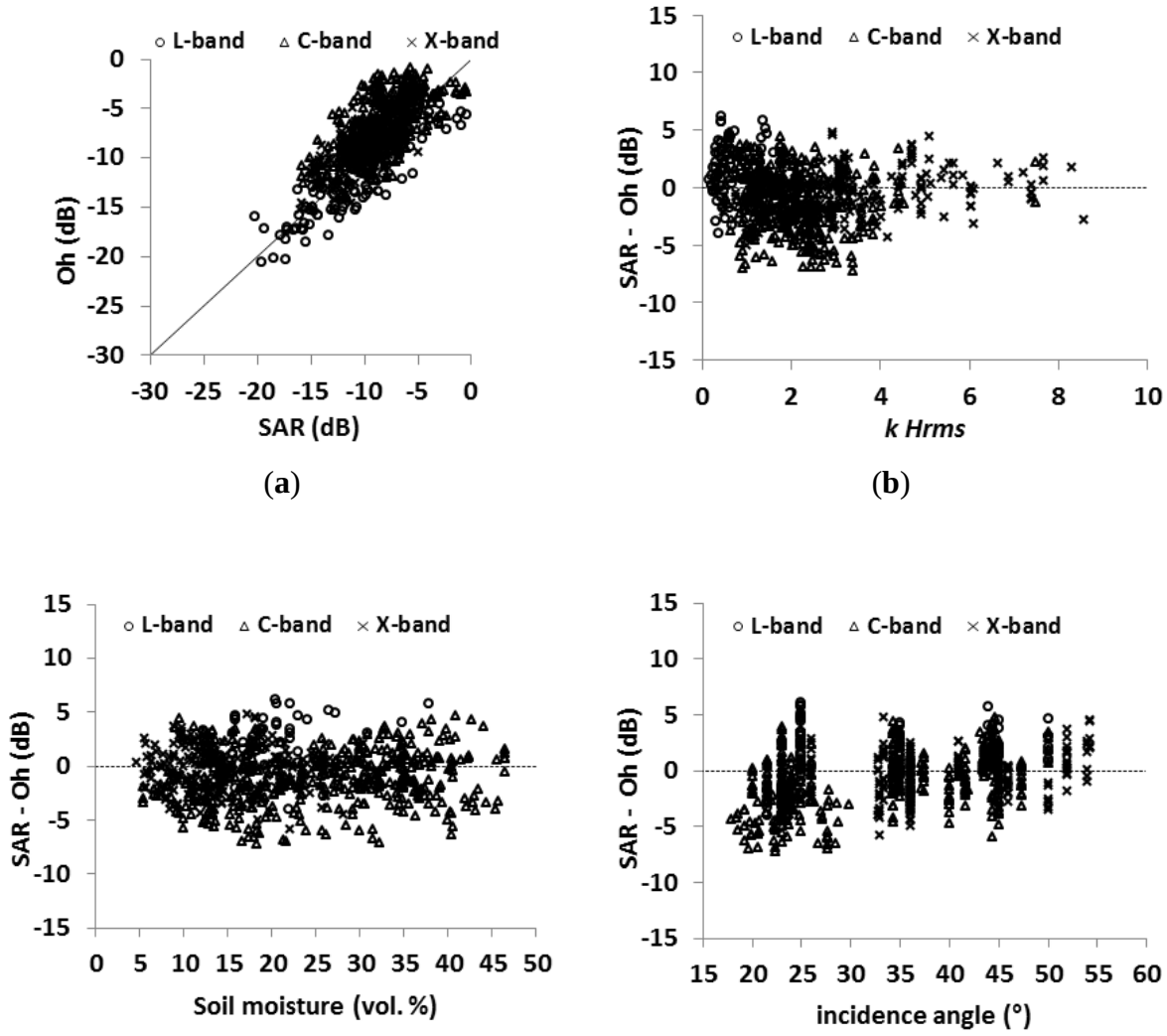


**Figure III.9.** Comparison between backscattering coefficients derived from SAR images and those estimated from the Oh 2002 model at VV polarization, (a) Oh simulations vs. SAR data; (b) difference between SAR signal and the Oh model vs. soil roughness (*kHrms*); (c) difference between SAR signal and Oh model results vs. soil moisture (*mv*); (d) difference between SAR signal and Oh model results vs. incidence angle.

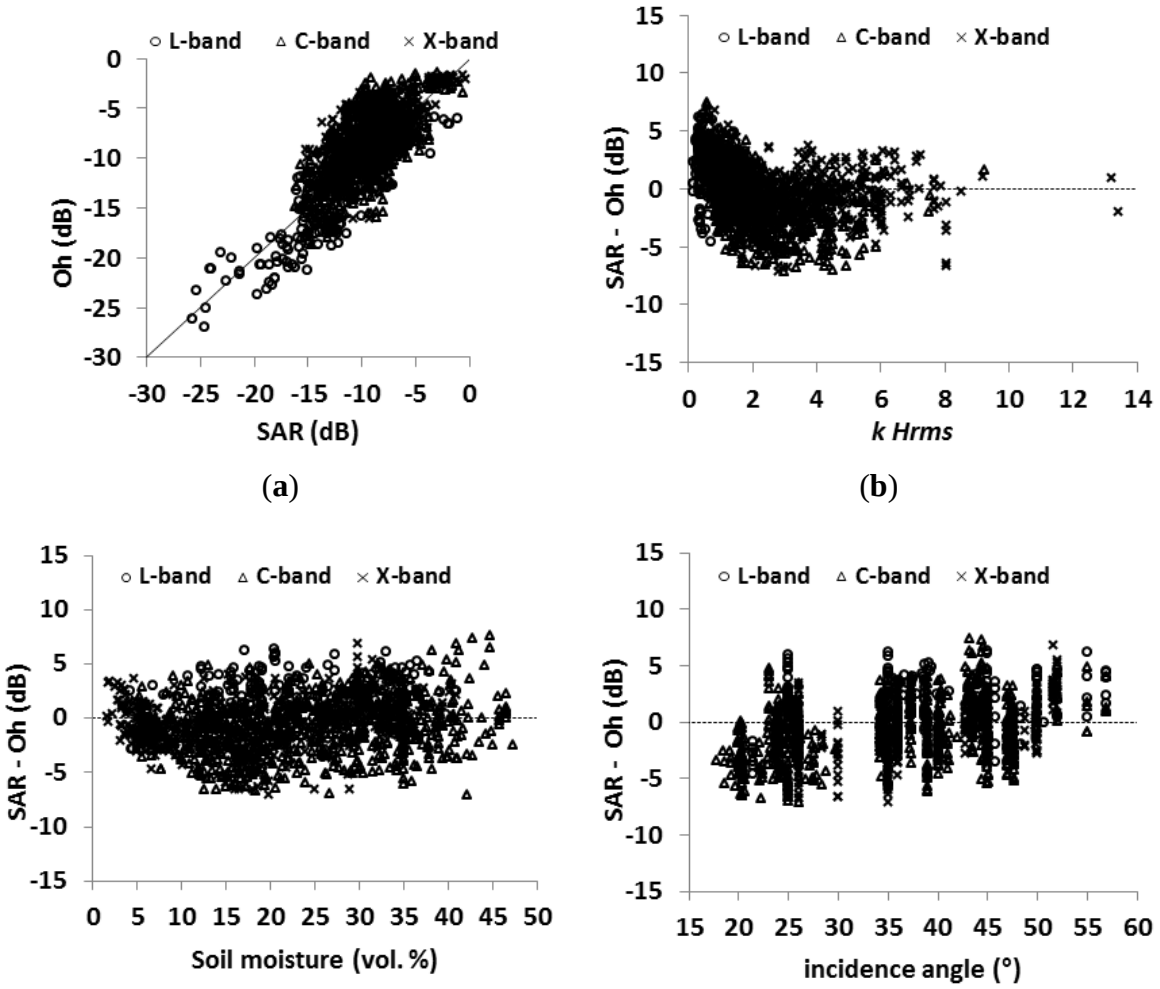


**Figure III.10.** Comparison between backscattering coefficients derived from SAR images and those estimated from the Oh 2004 model at HH polarization, (a) Oh model simulations vs. SAR data; (b) difference between SAR signal and Oh model results vs. soil roughness (*kHrms*); (c) difference between SAR signal and Oh model results vs. soil moisture (*mv*); (d) difference between SAR signal and Oh model results vs. incidence angle.

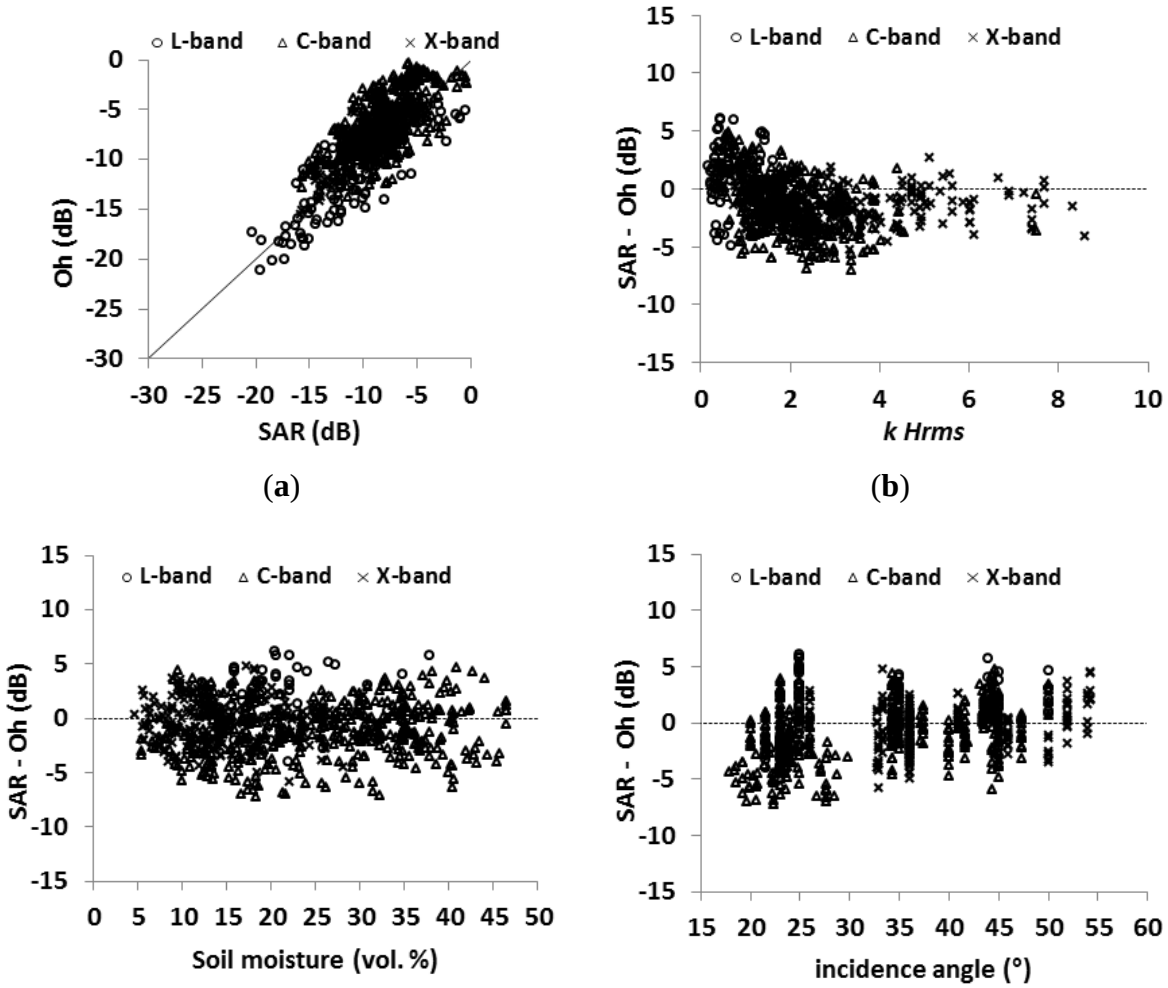


**Figure III.11.** Comparison between backscattering coefficients derived from SAR images and those estimated from the Oh 2004 model at VV polarization, (a) Oh simulations vs. SAR data; (b) difference between SAR signal and the Oh model vs. soil roughness (*kHrms*); (c) difference between SAR signal and Oh model results vs. soil moisture (*mv*); (d) difference between SAR signal and Oh model results vs. incidence angle.

### III.4.3 Evaluation of the IEM

The IEM was tested on our dataset using both a Gaussian correlation function (GCF) and an exponential correlation function (ECF). The evaluation of the IEM was carried out firstly using the entire dataset, later on for each radar wavelength (L-, C- and X-bands) and finally according to the validity domain of the IEM (Equation 3.10).

Using all data, the IEM simulates the backscattering in HH polarization with an RMSE of 10.5 dB and 5.6 dB for GCF and ECF, respectively (Table III.5). At VV polarization, the RMSE is 9.2 dB for GCF and 6.5 dB for ECF. At HV polarization, the RMSE is higher than 30.0 dB for both GCF and ECF. Some points show a large discrepancy between the real data and the IEM simulations performed using both ECF and GCF (Figures III.12–III.17). In case of the ECF (Figures III.15–III.17), these points are mainly outside the IEM validity domain (Equation 3.10). In case of GCF (Figures III.12–III.14), the huge error is due to the high sensitivity of the IEM to roughness parameters (*Hrms* and *L*). Using the GCF, the IEM underestimates the backscattering coefficients for data with low *Hrms* values ($kHrms < 3$), high *L* values ($L > 4$ cm) and with high incidence angle ($\theta > 35°$). Using the ECF, the sensitivity of backscattering to the roughness parameters is much lower (Figures III.15–III.17). (Altese et al., 1996), Zribi et al. (1997, 2005a) and (Callens et al., 2006) showed that in agricultural areas, the ECF usually provides better agreement to real data than the GCF.

The results obtained in L-band show that the IEM simulates the backscattering in HH pol. using both GCF and ECF with differences between real data and model simulations ranges between −0.9 dB and +0.6 dB, with an RMSE of 3.6 dB for GCF and 2.9 dB for ECF (Table III.5). At VV polarization, the IEM overestimates the backscattering by about 2.5 dB and 1.3 dB for GCF and ECF, respectively (RMSE of 5.0 dB for GCF and 3.5 dB for ECF). At HV polarization, the IEM simulates the backscattering using GCF with RMSE of 14.5 dB using GCF, and lower RMSE (6.8 dB) using ECF.

According to the results observed in C-band, the IEM simulates the backscattering using GCF with RMSE of 11.2 dB and 8.6 dB for HH and VV polarizations, respectively (Table III.5). The RMSE is lower with ECF than GCF about 4.1 dB for HH and 4.9 dB for VV polarizations. At HV polarization, the RMSE is higher than 25.0 dB using both GCF and ECF.

The results obtained in X-band show that the IEM simulates the backscattering with higher RMSE than L- and C-bands, the RMSE in HH pol. being about 10.6 dB for GCF and 8.3 dB for ECF. At VV polarization, the RMSE is 11.3 dB for GCF and 9.4 dB for ECF. At HV polarization, the IEM simulates the backscattering with high RMSE which is larger than 54.0 dB using both GCF and ECF.

| Model | Pol. | Statistics | All Data | L-Band | C-Band | X-Band | Inside the Validity Domain | Outside the Validity Domain |
|---|---|---|---|---|---|---|---|---|
| IEM using GCF | HH | Bias (dB) | +0.8 | −0.9 | +0.7 | +1.5 | +2.6 | −1.8 |
| | | RMSE (dB) | 10.5 | 3.6 | 11.2 | 10.6 | 12.4 | 6.7 |
| | HV | Bias (dB) | +17.2 | +5.2 | +11.8 | +46.3 | +18.0 | +14.1 |
| | | RMSE (dB) | 38.4 | 14.5 | 26.7 | 74.0 | 28.5 | 50.1 |
| | VV | Bias (dB) | +0.4 | −2.5 | +0.7 | +3.5 | +1.2 | −0.9 |
| | | RMSE (dB) | 9.2 | 5.0 | 8.6 | 11.3 | 11.5 | 3.1 |
| IEM using ECF | HH | Bias (dB) | +0.8 | +0.6 | −1.0 | +4.2 | −1.2 | +3.8 |
| | | RMSE (dB) | 5.6 | 2.9 | 4.1 | 8.3 | 3.2 | 7.8 |
| | HV | Bias (dB) | −15.8 | +1.2 | −19.9 | 0.0 | −15.8 | −17.1 |
| | | RMSE (dB) | 31.4 | 6.8 | 25.1 | 54.4 | 20.1 | 44.3 |
| | VV | Bias (dB) | +2.2 | −1.3 | +0.5 | +6.7 | −0.9 | +7.1 |
| | | RMSE (dB) | 6.5 | 3.5 | 4.9 | 9.4 | 3.7 | 9.4 |
| IEM_B with Lopt using GCF | HH | Bias (dB) | −0.3 | −0.1 | −0.6 | +0.3 | | |
| | | RMSE (dB) | 2.0 | 2.3 | 2.1 | 1.8 | | |
| | HV | Bias (dB) | | | −1.3 | | | |
| | | RMSE (dB) | | | 3.1 | | | |
| | VV | Bias (dB) | +0.1 | +0.2 | 0 | +0.3 | | |
| | | RMSE (dB) | 1.9 | 2.3 | 1.9 | 1.8 | | |
| AIEM using GCF | HH | Bias (dB) | +2.3 | −3.2 | +2.9 | +3.1 | | |
| | | RMSE (dB) | 12.2 | 5.4 | 13.4 | 11.7 | | |
| | VV | Bias (dB) | 0.0 | −4.1 | +0.5 | +0.5 | | |
| | | RMSE (dB) | 10.8 | 5.9 | 11.4 | 11.0 | | |
| AIEM using ECF | HH | Bias (dB) | −2.3 | −3.0 | −3.6 | +0.2 | | |
| | | RMSE (dB) | 4.4 | 4.4 | 4.6 | 4.2 | | |
| | VV | Bias (dB) | −1.8 | −2.4 | −2.3 | -0.7 | | |
| | | RMSE (dB) | 3.8 | 4.4 | 3.8 | 3.7 | | |

**Table III.5.** Comparison between real data and IEM versions (original IEM model, IEM_B and AIEM) using both GCF and ECF. (1) all data; (2) for different SAR wavelength; (3) according to the validity domain of IEM. Bias = real data − model simulations.

The analysis of the error was also studied according to the validity domain of the IEM (Equation (3.10)). Inside the validity domain, the RMSE is larger than 11.5 dB for both HH and VV polarizations using GCF. Better results were obtained using ECF, where the IEM correctly simulates the backscattering at both HH and VV polarizations with differences between real and simulated data between −1.2 dB and −0.9 dB with RMSE of 3.2 dB at HH and 3.7 dB at VV polarizations, using data concerning the IEM validity domain. Outside the IEM validity domain, the IEM simulates the backscattering with RMSE of 6.7 dB for HH and 3.1 dB for VV using GCF; whereas RMSE is 7.8 dB for HH and 9.4 dB for VV polarization

using ECF. At HV polarizations, model simulations show large differences from real data for both GCF and ECF for points inside or outside the validity domain of the IEM (in this case, RMSE is larger than 20 dB). Errors observed on IEM simulations were also studied as a function of the difference between *Lopt* and the measured correlation length (*L*). Results show that the IEM using GCF gives poor simulations mainly when the measured correlation length was over-estimated (*L* > *Lopt*). In this case, the IEM strongly under-estimates the SAR backscatter. In addition, the performance of the IEM was also analyzed using ECF according to the difference between *Lopt* and *L*. Results show the same performance of the IEM whatever the difference between *Lopt* and *L*.

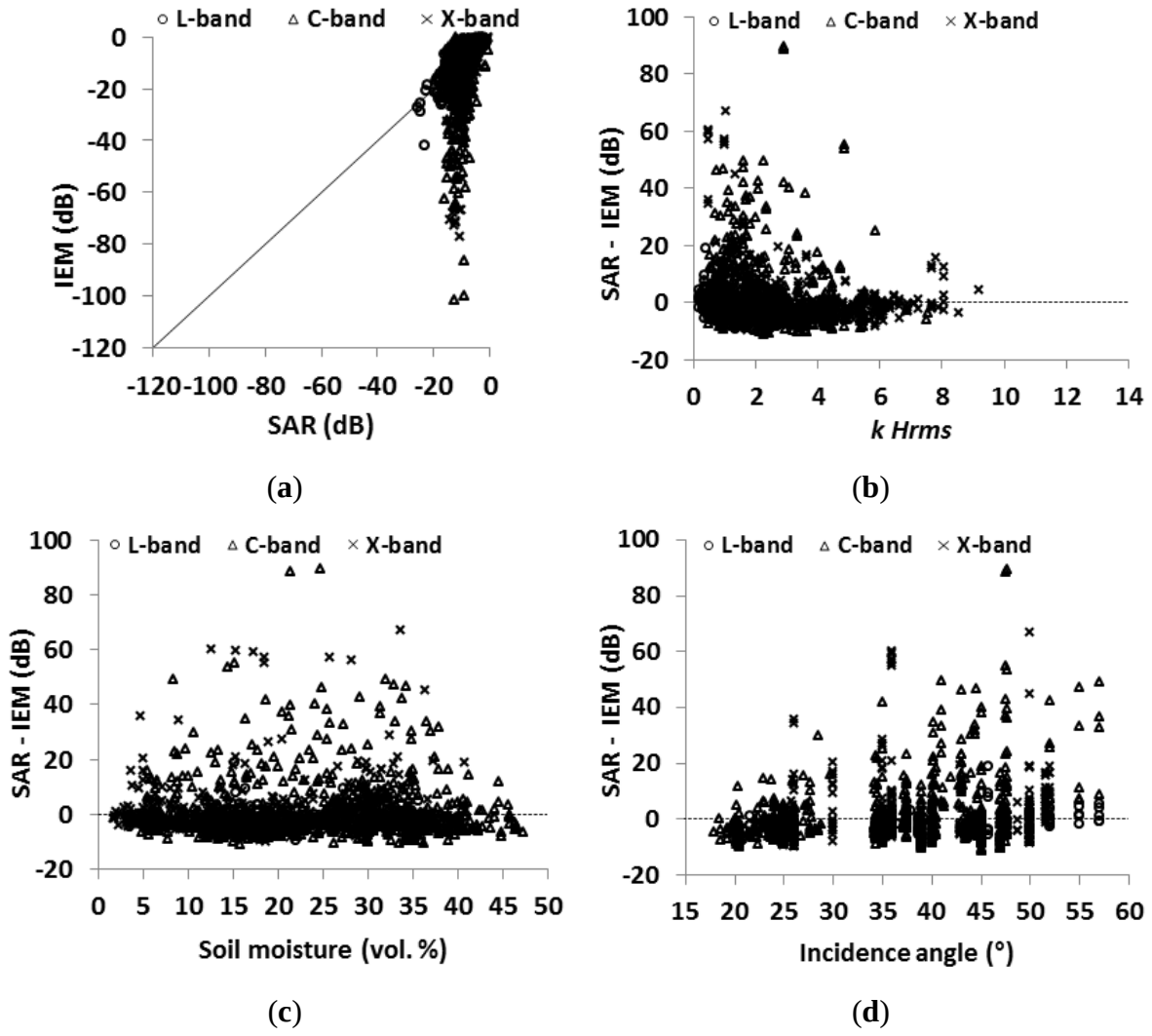


**Figure III.12.** Comparison between backscattering coefficients derived from SAR images and those estimated from IEM at HH polarization using GCF. (a) IEM simulations vs. SAR data; (b) difference between SAR signal and IEM vs. soil roughness (*kHrms*); (c) difference between SAR signal and IEM vs. soil moisture (*mv*); (d) difference between SAR signal and IEM vs. incidence angle.

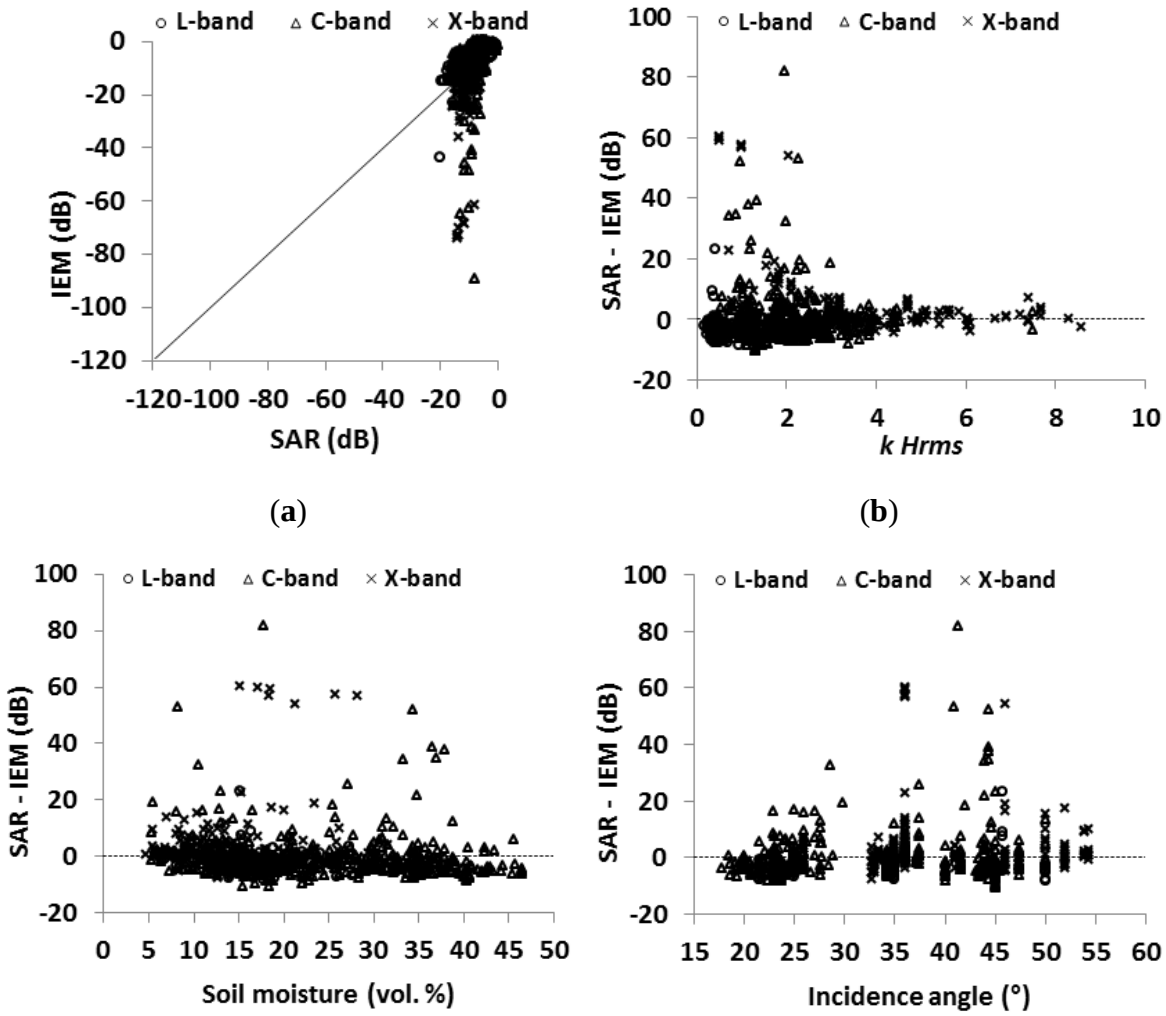


**Figure III.13.** Comparison between backscattering coefficients derived from SAR images and those estimated from IEM at VV polarization using GCF. (a) IEM simulations vs. SAR data; (b) difference between SAR signal and IEM vs. soil roughness (*kHrms*); (c) difference between SAR signal and IEM vs. soil moisture (*mv*); (d) difference between SAR signal and IEM vs. incidence angle.

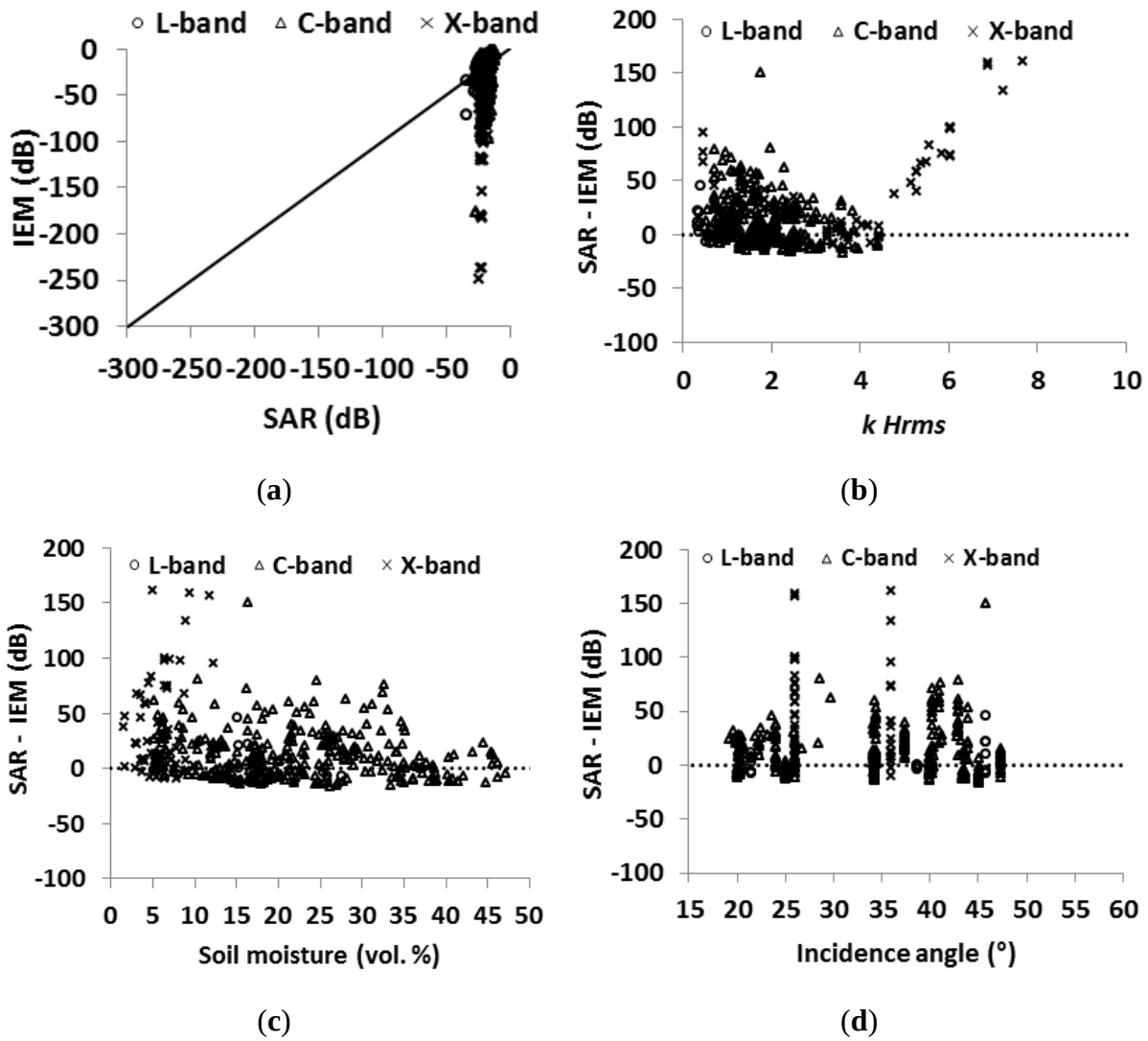


**Figure III.14.** Comparison between backscattering coefficients derived from SAR images and those estimated from IEM at HV polarization using GCF. (a) IEM simulations vs. SAR data; (b) difference between SAR signal and IEM vs. soil roughness (*kHrms*); (c) difference between SAR signal and IEM vs. soil moisture (*mv*); (d) difference between SAR signal and IEM vs. incidence angle.

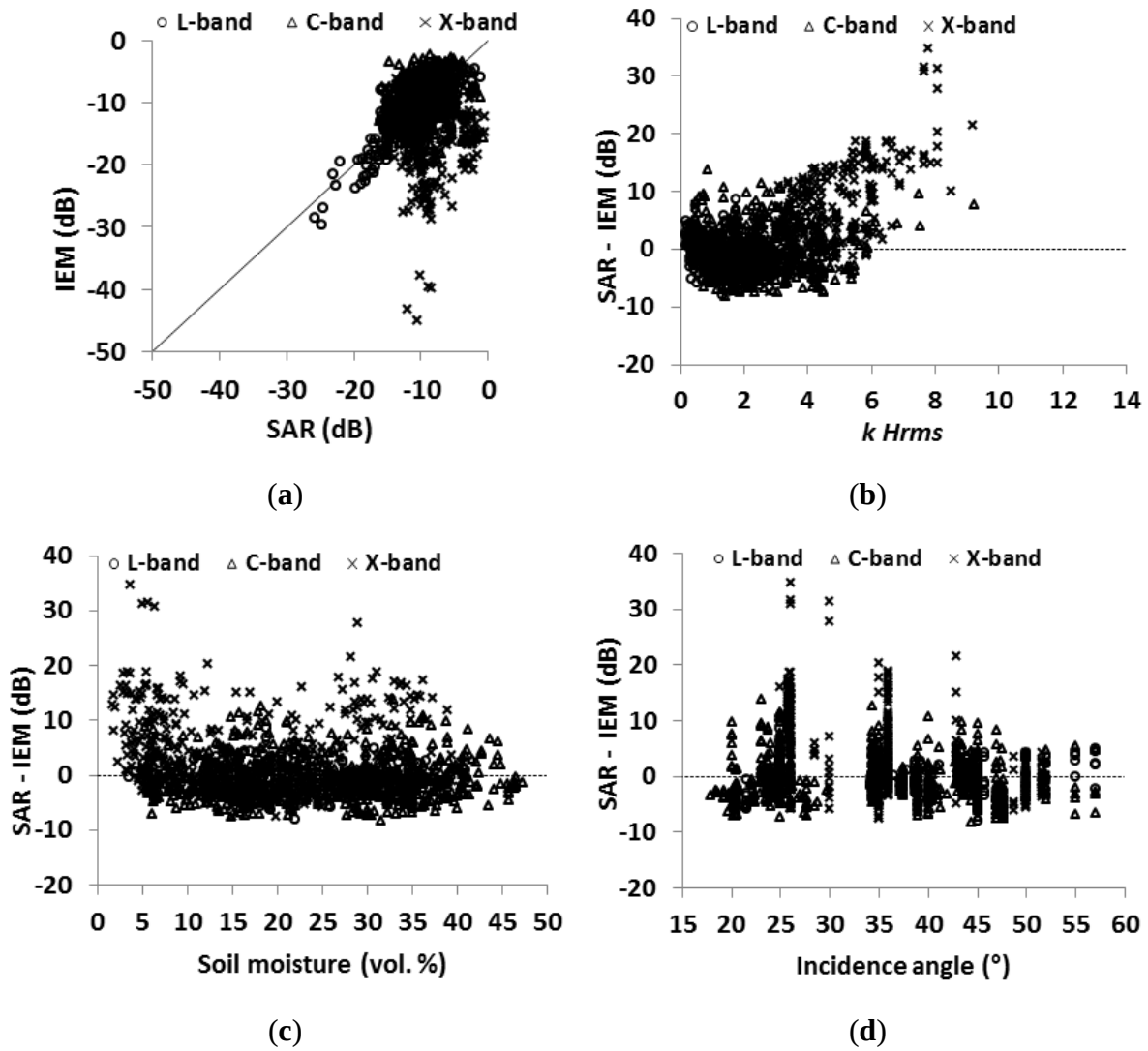


**Figure III.15.** Comparison between backscattering coefficients derived from SAR images and those estimated from IEM at HH polarization using ECF. (a) IEM simulations vs. SAR data; (b) difference between SAR signal and IEM vs. soil roughness (*kHrms*); (c) difference between SAR signal and IEM vs. soil moisture (*mv*); (d) difference between SAR signal and IEM vs. incidence angle.

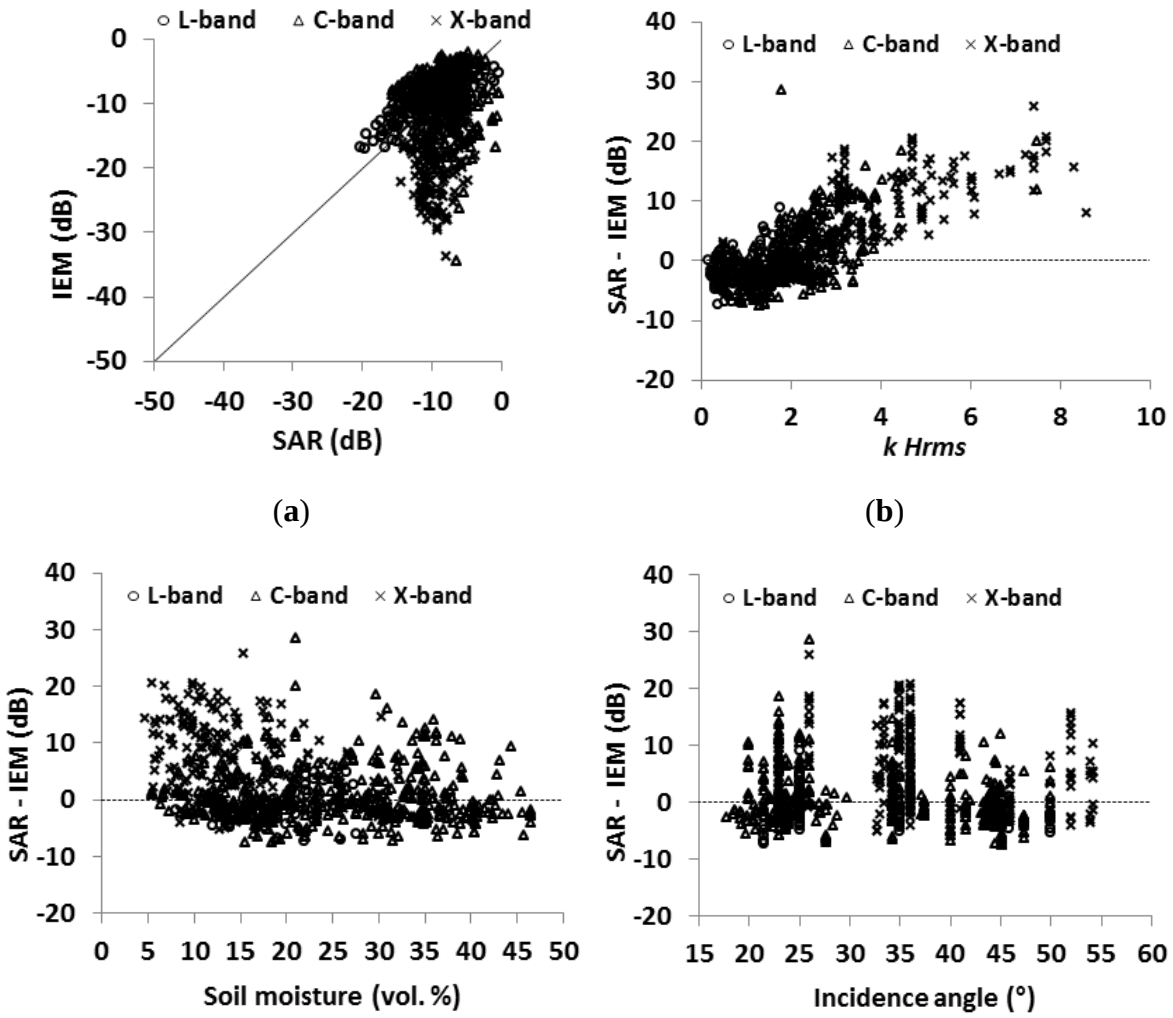


**Figure III.16.** Comparison between backscattering coefficients derived from SAR images and those estimated from IEM at VV polarization using ECF. (a) IEM simulations vs. SAR data; (b) difference between SAR signal and IEM vs. soil roughness (*kHrms*); (c) difference between SAR signal and IEM vs. soil moisture (*mv*); (d) difference between SAR signal and IEM vs. incidence angle.

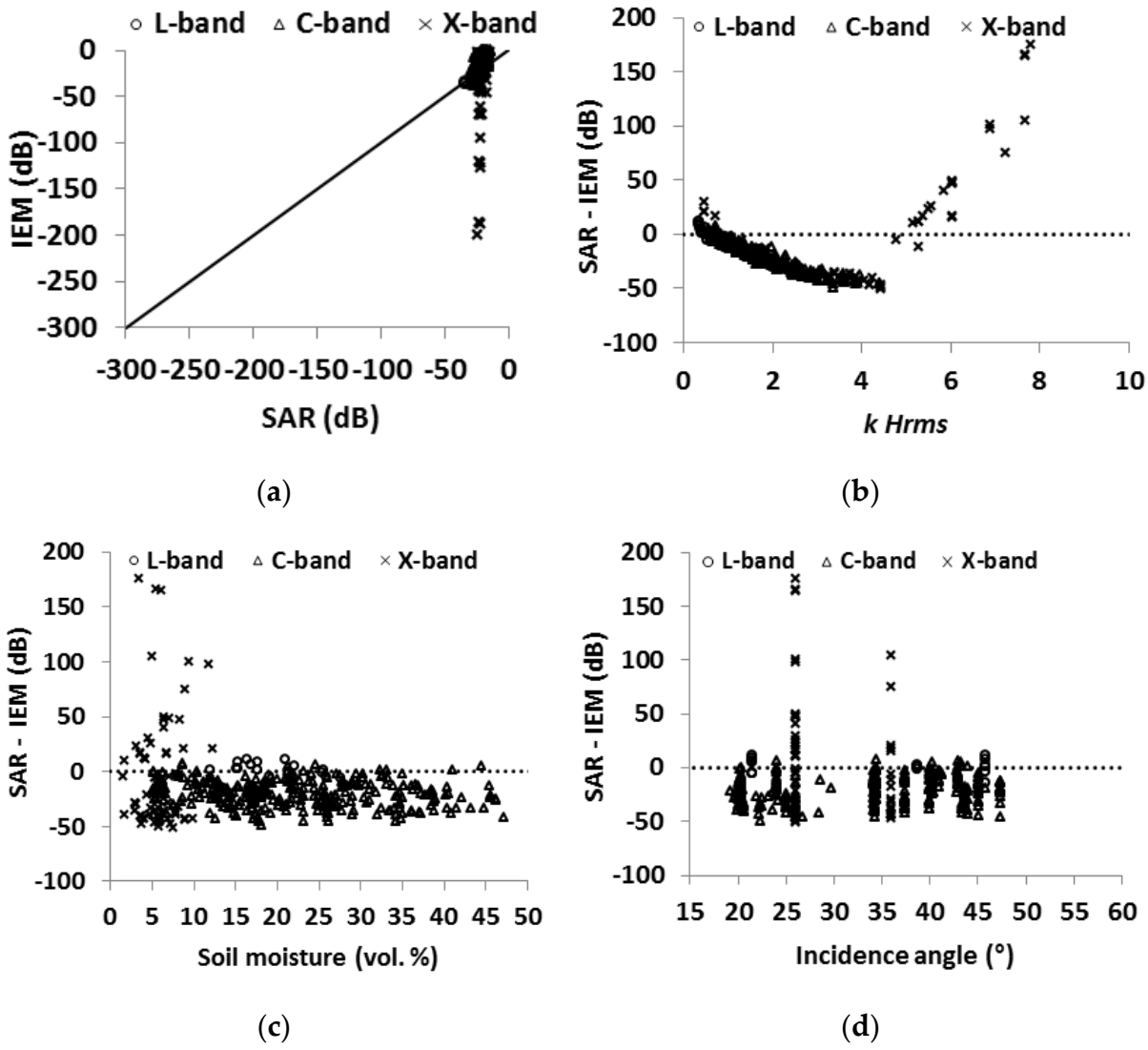


**Figure III.17.** Comparison between backscattering coefficients derived from SAR images and those estimated from IEM at HV polarization using ECF. (a) IEM simulations vs. SAR data; (b) difference between SAR signal and IEM vs. soil roughness (*kHrms*); (c) difference between SAR signal and IEM vs. soil moisture (*mv*); (d) difference between SAR signal and IEM vs. incidence angle.

As a conclusion, we could say that the IEM better simulates the backscattering in L-band than in C- and X-bands. Moreover, the results show a better fitting with real data using ECF instead than GCF, which agrees with the validity domain of the IEM.

### III.4.4 Evaluation of IEM Modified by Baghdadi (IEM_B)

The IEM_B was also tested on our dataset. This model version was run using GCF (Figures III.18–III.20). In comparison to the original IEM, results show that the RMSE was significantly lower. Using the entire dataset, the IEM_B correctly simulates the backscattering at both HH and VV polarizations showing low differences between real data and model simulations (−0.3 dB for HH and +0.1 dB for VV) with approximately similar RMSE of about 2.0 dB (Table III.5). Moreover, the evaluation of the IEM_B was tested separately for each SAR band. Results show that the IEM_B correctly simulates the backscattering in comparison to the original model for all bands and in both HH and VV polarizations with a difference between real data and model simulations lower than 1.0 dB and with approximately similar RMSE between 1.8 and 2.3 dB (Table III.5). At HV polarization, the IEM_B slightly over-estimates the backscattering by about 1.3 dB with RMSE of 3.1 dB, (the IEM_B was run only at C-band). Moreover, results show that the IEM_B simulations in both HH and VV pol., are slightly better in X- and C-bands than in L-band. The analysis of the difference between IEM_B simulations and SAR data versus the difference between *Lopt* and the measured correlation length (*L*) shows that IEM_B simulates well SAR data whatever the value of the difference between *Lopt* and *L*.

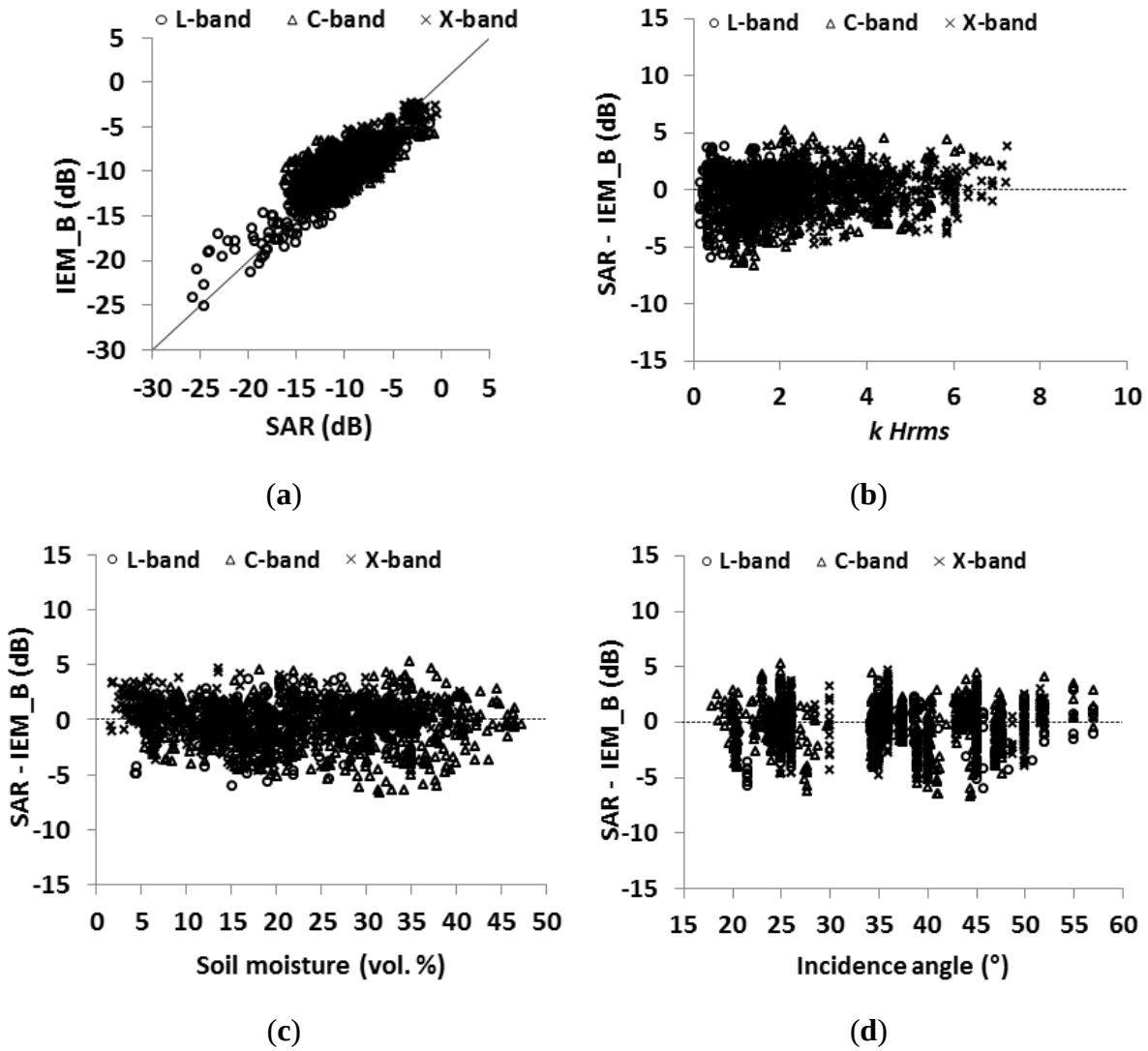


**Figure III.18.** Comparison between backscattering coefficients derived from SAR images and those estimated from IEM_B at HH polarization using GCF. (a) IEM_B simulations vs. SAR data; (b) difference between SAR signal and IEM_B vs. soil roughness (*kHrms*); (c) difference between SAR signal and IEM_B vs. soil moisture (*mv*); (d) difference between SAR signal and IEM_B vs. incidence angle.

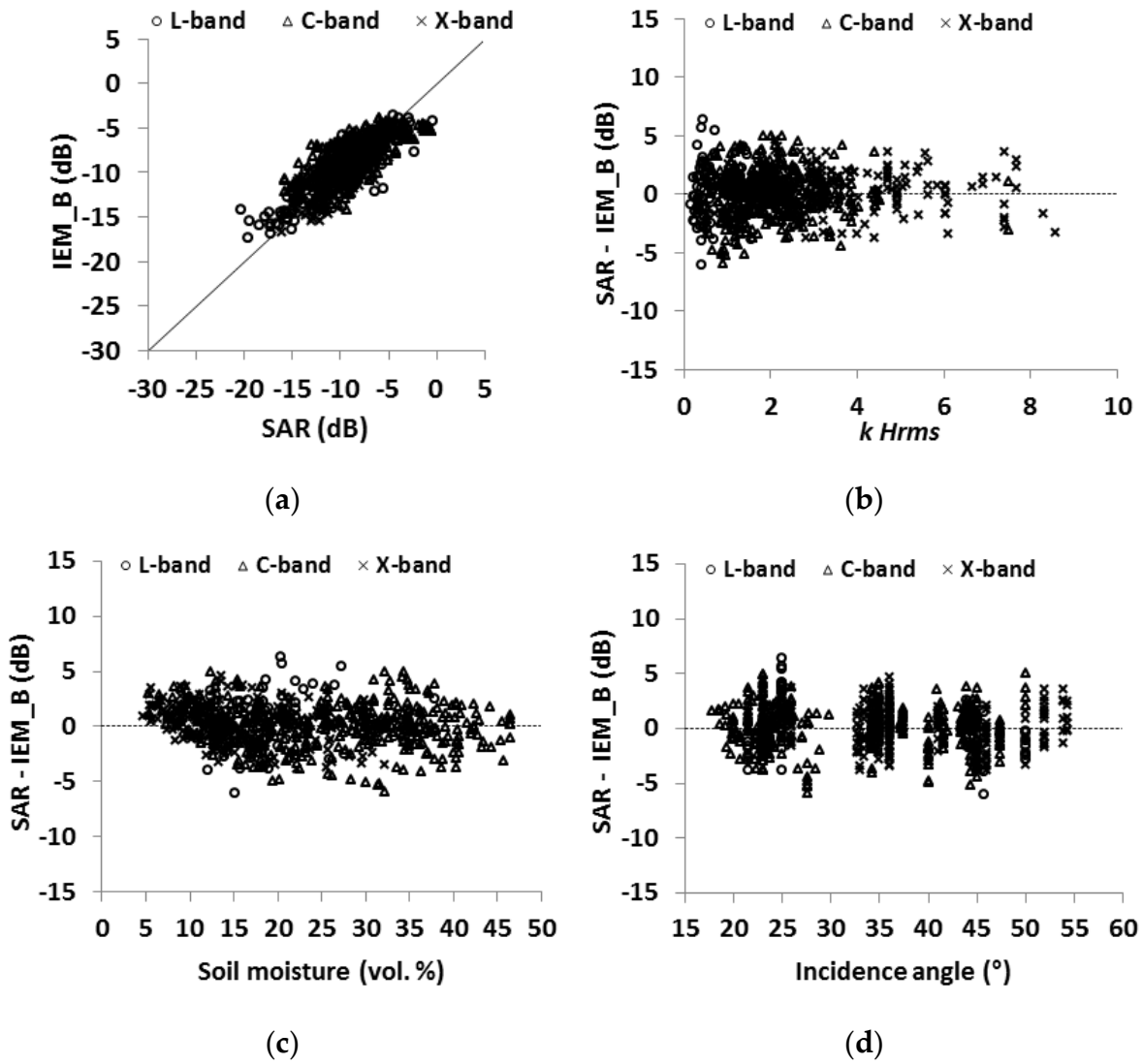


**Figure III.19.** Comparison between backscattering coefficients derived from SAR images and those estimated from IEM_B at VV polarization using GCF. (a) IEM_B simulations vs. SAR data; (b) difference between SAR signal and IEM_B vs. soil roughness (*kHrms*); (c) difference between SAR signal and IEM_B vs. soil moisture (*mv*); (d) difference between SAR signal and IEM_B vs. incidence angle.

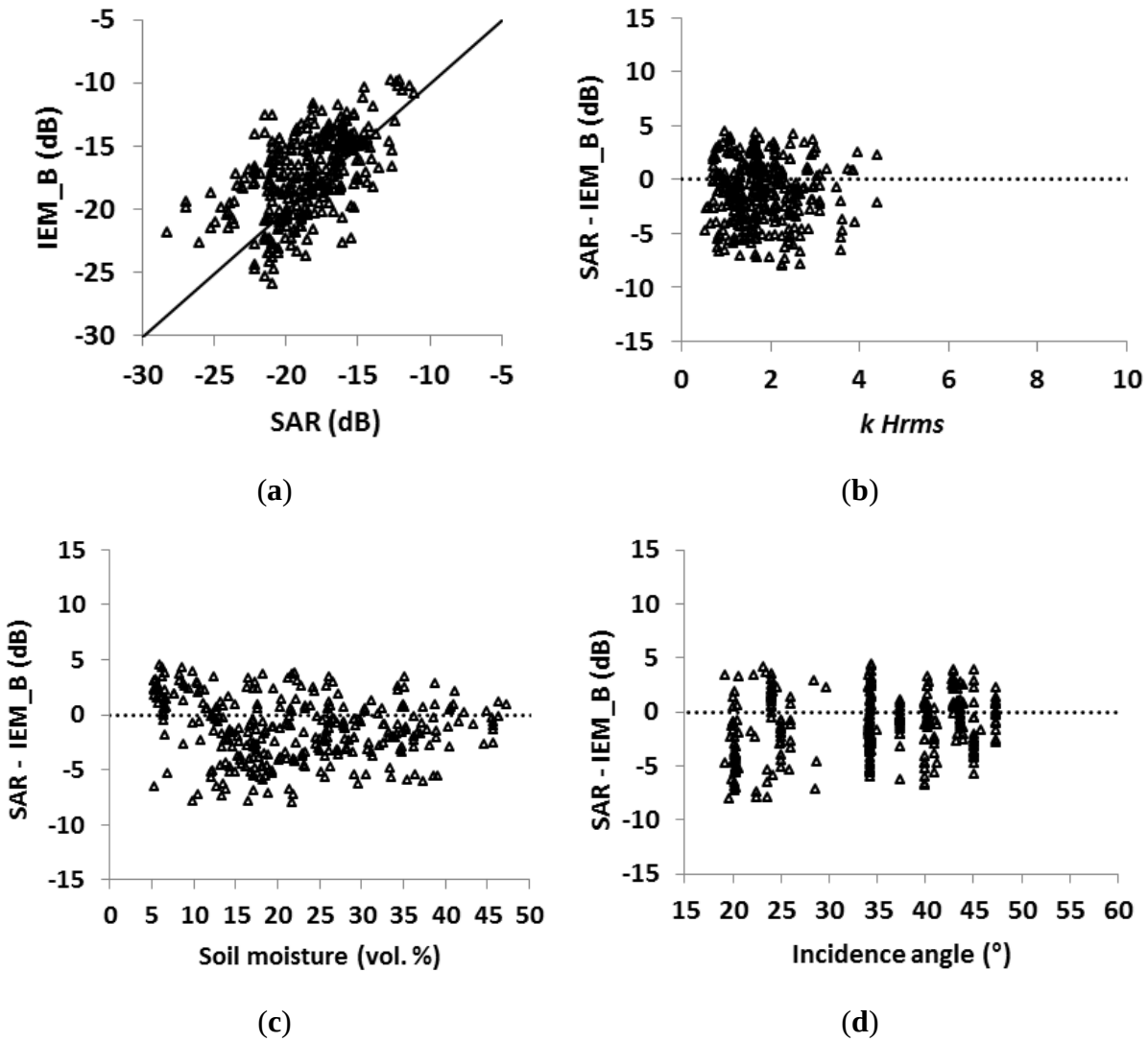


(**a**) (**b**)

(**c**) (**d**)

**Figure III.20.** Comparison between backscattering coefficients derived from SAR images and those estimated from IEM_B in C-band at HV polarization using GCF. (a) IEM_B simulations vs. SAR data; (b) difference between SAR signal and IEM_B vs. soil roughness (*kHrms*); (c) difference between SAR signal and IEM_B vs. soil moisture (*mv*); (d) difference between SAR signal and IEM_B vs. incidence angle.

### III.4.5 Evaluation of the Advanced Integral Equation Model (AIEM)

The AIEM was tested on our dataset at HH and VV polarizations using both GCF and ECF. For all data, the AIEM simulates the backscattering at HH and VV polarizations using GCF with RMSE larger than 10 dB (Table III.5, Figures III.21 and III.22). Moreover, results show better agreements of the AIEM with real data using ECF (Figures III.23 and III.24). Indeed, the AIEM tends to overestimates the backscattering by about 2.3 dB at HH and 1.8 dB at VV (RMSE is 4.4 dB for HH and 3.8 dB for VV). Using the ECF, Figures III.23 and III.24 show high overestimations of the backscattering for low values of surface roughness (*kHrms* < 4)

and for incidence angles higher than 35°. Moreover, Figures III.23 and III.24 show high underestimation of the radar signal (using ECF) in both HH and VV polarizations for points with high surface roughness (*kHrms* > 6), low *mv*-values (*mv* < 5 vol. %, and with low incidence angles (θ < 20°). Figures III.21 and III.22 show that some points show high discrepancies between the real data and the AIEM simulations using GCF. Due to the high sensitivity to surface roughness of the AIEM using GCF, these points correspond mainly to surface with *kHrms* < 3, *L* > 4 cm and θ > 35°.

The performance of the AIEM was also evaluated for each SAR wavelength. Results show that in L-band the AIEM simulates the backscattering with RMSE of about 5.0 dB at both HH and VV polarizations using the GCF. In C and X-bands, the AIEM using GCF simulates the backscattering with RMSE higher than in L-band (RMSE > 11 dB). Moreover, AIEM better simulates better the backscattering in using GCF than ECF for all wavelength (RMSE about 4 dB).

In conclusions, the AIEM is able to better simulate better the backscattering than the original IEM only using the ECF with better results in X-band than in C- and L-bands.

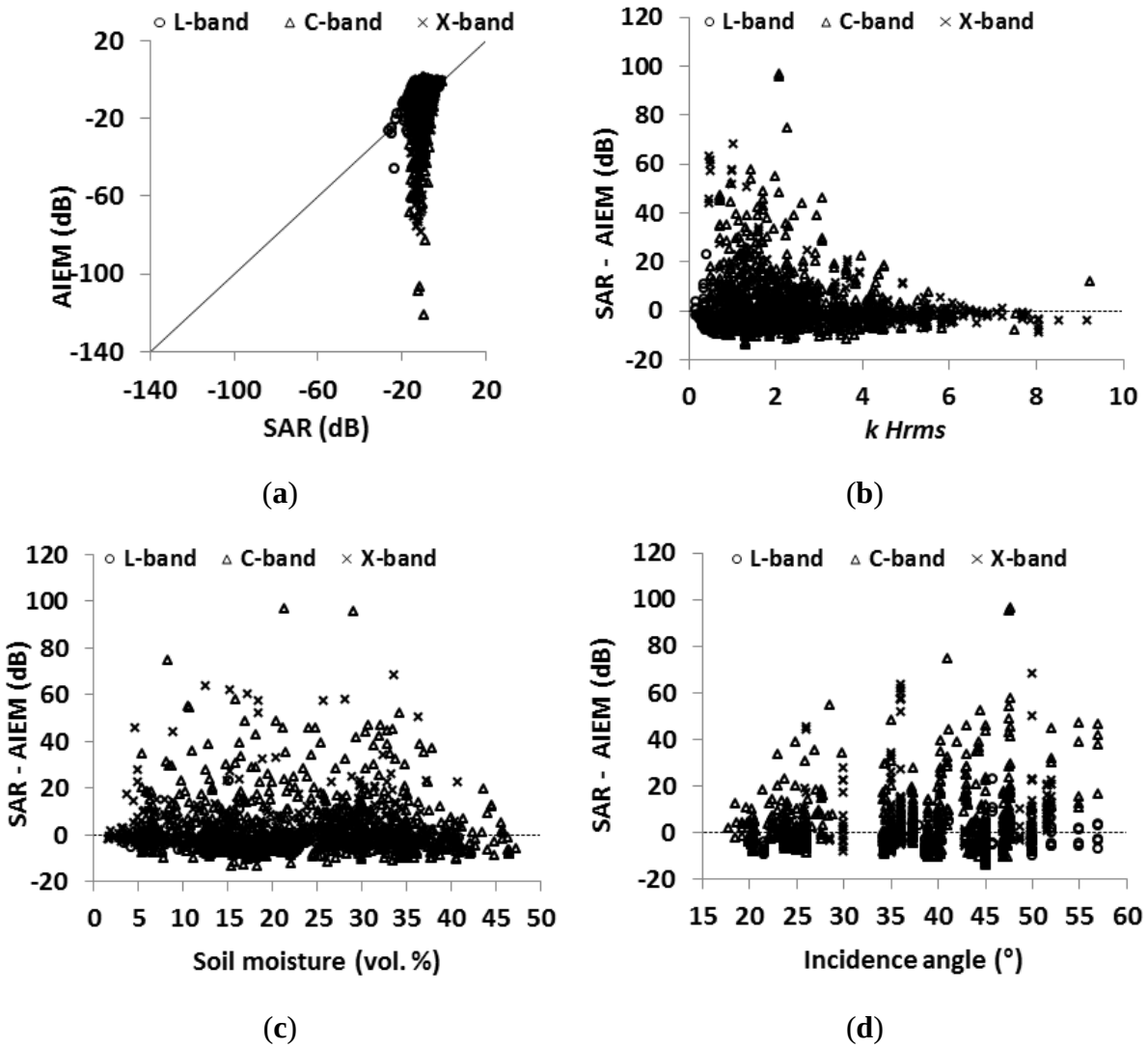


(**a**) (**b**)

(**c**) (**d**)

**Figure III.21.** Comparison between backscattering coefficients derived from SAR images and those estimated from AIEM at HH polarization using GCF. (a) AIEM simulations vs. SAR data; (b) difference between SAR signal and AIEM vs. soil roughness (*kHrms*); (c) difference between SAR signal and AIEM vs. soil moisture (*mv*); (d) difference between SAR signal and AIEM vs. incidence angle.

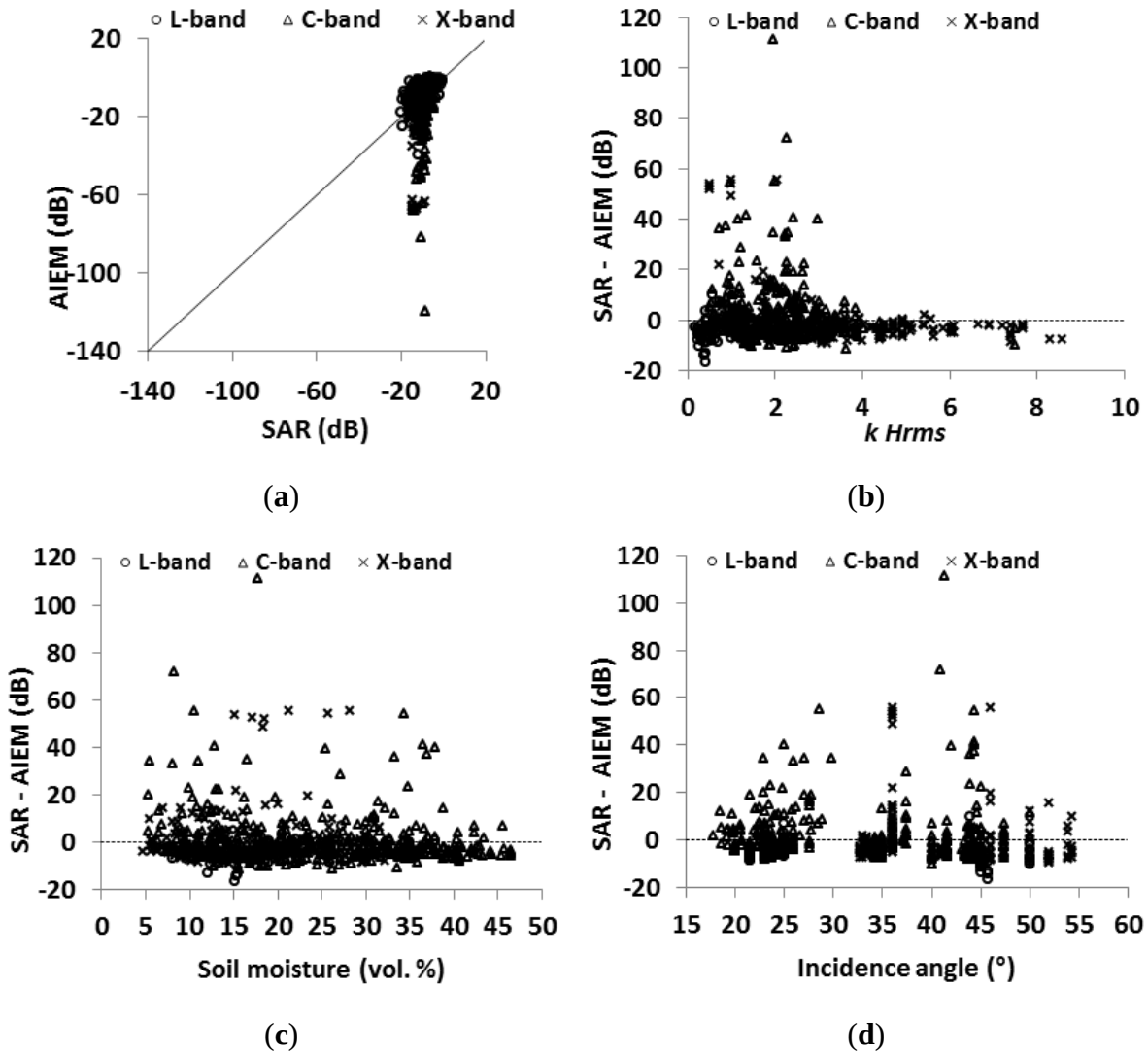


**Figure III.22.** Comparison between backscattering coefficients derived from SAR images and those estimated from AIEM at VV polarization using GCF. (a) AIEM simulations vs. SAR data; (b) difference between SAR signal and AIEM vs. soil roughness (*kHrms*); (c) difference between SAR signal and AIEM vs. soil moisture (*mv*); (d) difference between SAR signal and AIEM vs. incidence angle.

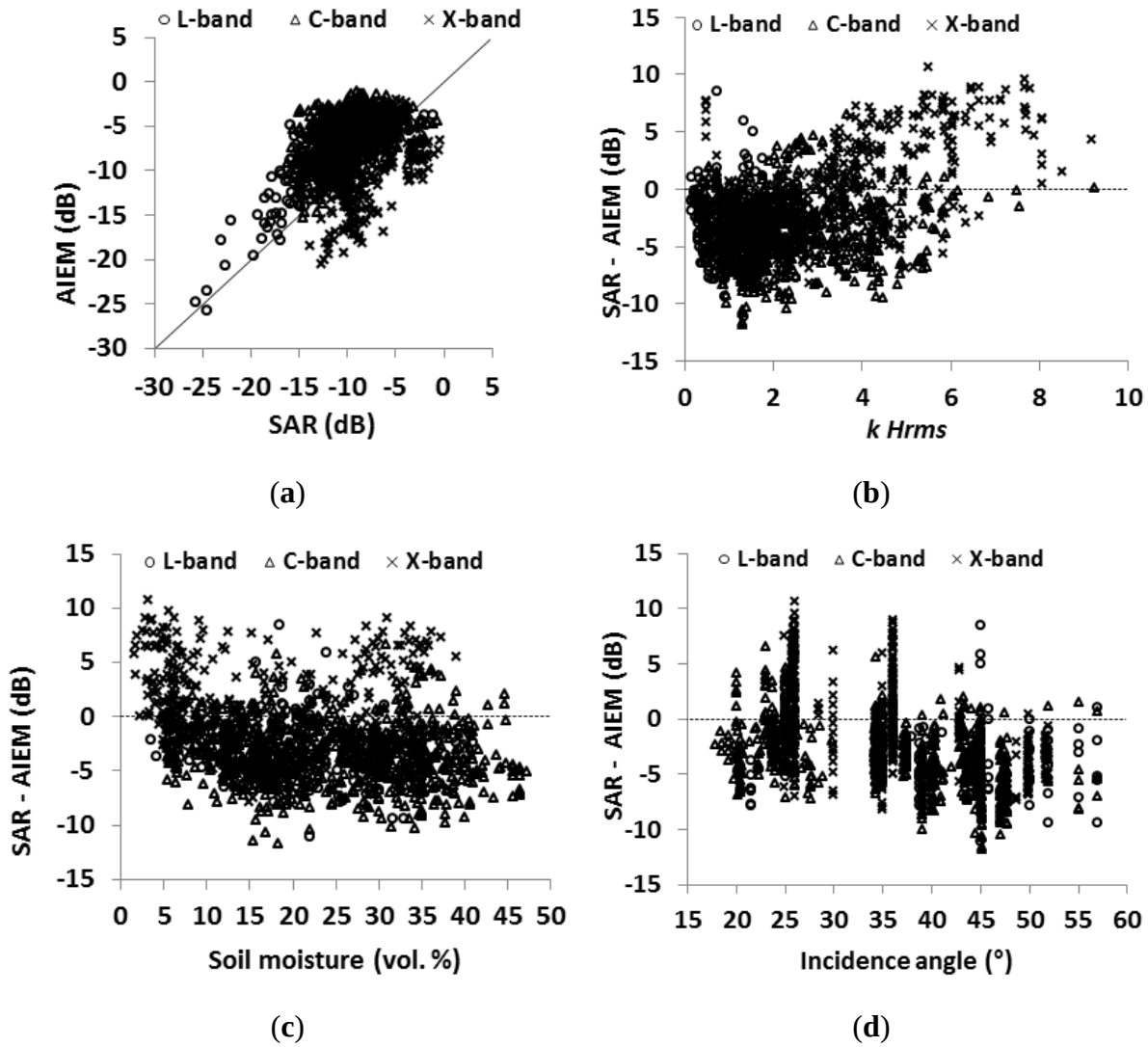


**Figure III.23**. Comparison between backscattering coefficients derived from SAR images and those estimated from AIEM at HH polarization using ECF. (a) AIEM simulations vs. SAR data; (b) difference between SAR signal and AIEM vs. soil roughness (*kHrms*); (c) difference between SAR signal and AIEM vs. soil moisture (*mv*); (d) difference between SAR signal and AIEM vs. incidence angle.

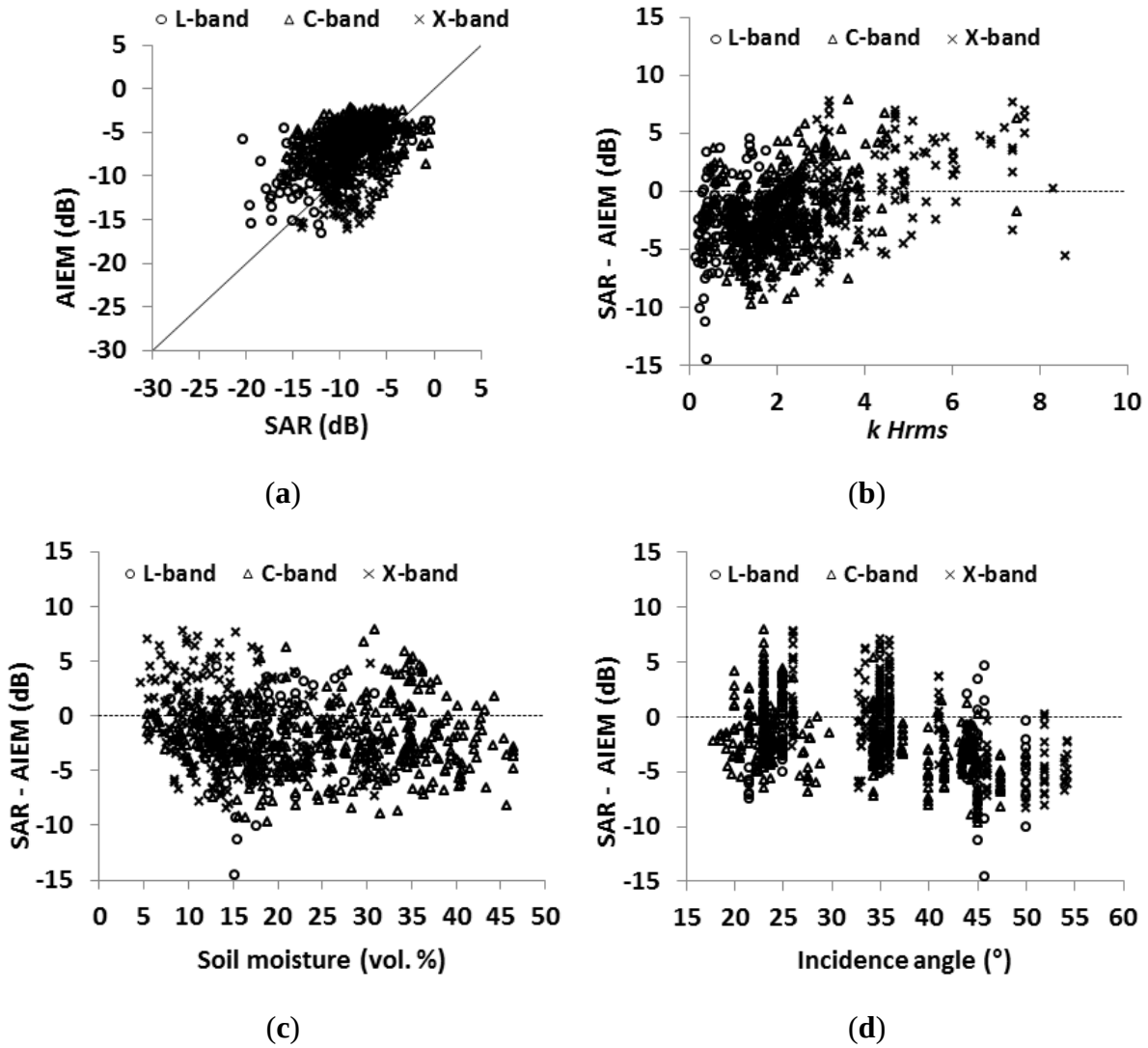


**Figure III.24.** Comparison between radar backscattering coefficients calculated from SAR images and those estimated from AIEM for VV polarization using ECF. (a) AIEM simulations vs. SAR data; (b) difference between SAR signal and AIEM vs. soil roughness (*kHrms*); (c) difference between SAR signal and AIEM vs. soil moisture (*mv*); (d) difference between SAR signal and AIEM vs. incidence angle.

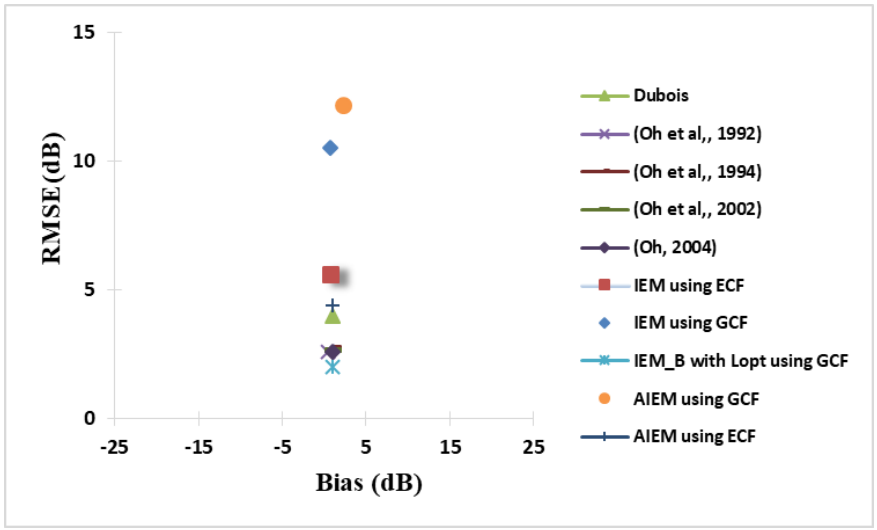


(a)

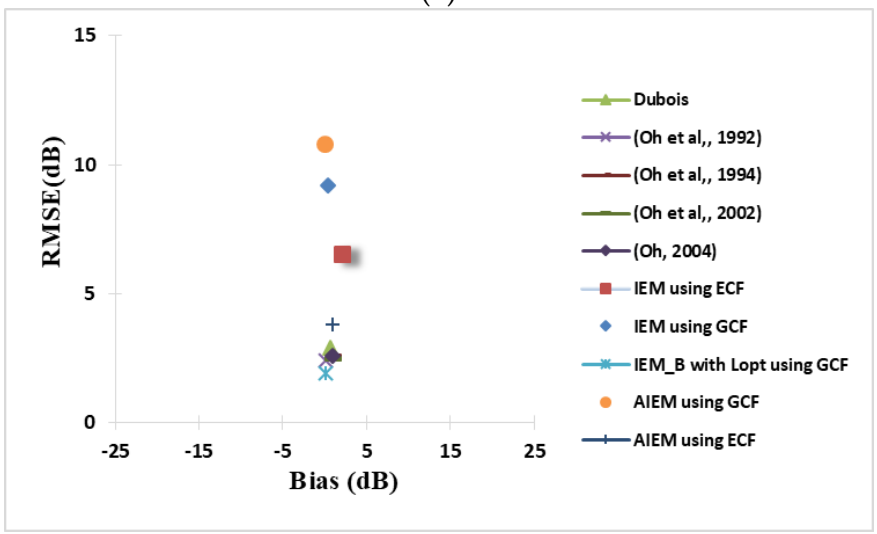


(b)

**Figure III.25.** For each Model (IEM, Dubois, Oh, IEM_B and AIEM), result of the comparison (RMSE versus Bias). (a) for HH polarization; (b) for VV Polarization.

## III.5 Conclusions

Physical (IEM, IEM_B and AIEM) and semi-empirical (Oh and Dubois) backscattering models were tested using a wide dataset composed by large intervals of surface conditions (*mv* between 2 vol. % and 47 vol. %, *Hrms* between 0.2 cm and 9.6 cm and *kHrms* from 0.2 and 13.4), the dataset was acquired over bare soils in various agricultural study sites (France, Italy, Germany, Belgium, Luxembourg, Canada and Tunisia) characterized by large variety of climatological conditions and using SAR sensors in L-, C- and X-bands with incidence angle between 18° and 57°.

Results (Figure III.25) show that the IEM modified by Baghdadi (IEM_B used the empirical correlation length instead of measured correlation length) provides the most accurate SAR simulations (bias lower than 1.0 dB and RMSE lower than 2.0 dB) with slightly better performance in X-band (RMSE = 1.8 dB) than in L- and C-bands (RMSE between 1.9 and 2.3 dB). At HV polarization, the IEM_B was only run at C-band. Results show that the RMSE strongly decreases from values higher than 25.1 dB, using the original IEM, to 3.1 dB, using IEM_B. In contrast, high RMSE were found using both IEM and AIEM using Gaussian correlation function (RMSE higher than 9.2 dB) for both HH and VV polarizations because of the high sensitivity of the Gaussian correlation function to roughness parameters, mainly for $kHrms < 3$ and $L > 4$ cm. Moreover, results show better simulations of measured backscattering coefficients for both IEM and AIEM using exponential correlation function (RMSE > 5.6 dB for IEM and RMSE > 3.8 dB for AIEM) at HH and VV polarizations. At HV polarization, IEM results show very high errors (RMSE larger than 30.0 dB using both Gaussian correlation function and exponential correlation function). The AIEM better simulates the backscattering than the original IEM only using the exponential correlation function with slightly better results in X-band than in C- and L-bands. In contrast, the IEM simulates better the backscattering in L- band than C- and X-bands (Table III.5).

Using the empirical models, all the Oh model versions show good agreements (RMSE < 3.0 dB) with measured backscattering with slightly better performance of the Oh 1992 version (bias less than 1.0 dB and RMSE less than 2.6 dB) at both HH and VV polarizations. The Oh model provides better results than Dubois model which simulates the backscattering in HH with RMSE of 4.0 dB, and slightly better simulations for VV with RMSE of 2.9 dB. At HV polarization, the Oh 2002 version correctly simulates the backscattering with difference between real and simulated data of about +0.7 dB and RMSE of 2.9 dB. The performance of

the Oh 1992 version in HH and VV polarizations is better in C- and X-bands (bias between −1.2 and +0.4 dB with RMSE < 2.5 dB) than in L-band (bias > +2.0 with RMSE > 3.0 dB).

It should be mentioned that the use of different in situ sampling methods and SAR acquisition techniques may also contribute to the modelling errors. Indeed, the datasets comprises both airborne and space-borne acquisitions, which may cause scaling effects. In addition, in situ data have been collected using different techniques, both regarding soil moisture (gravimetric and TDR, sometimes at different sampling depths) and roughness (different profile length and sampling intervals, and post-processing methods).

This study evaluated the robustness of the most used backscattering models by means of statistical indices (Bias and RMSE). These statistical indices should guide in choosing the appropriate model for backscattering coefficients simulation. As it has been shown in the present study, the IEM modified by Baghdadi (IEM_B) was the most accurate model among the others. Thus, it is preferred to use the IEM_B in the inversion procedure of SAR backscattering coefficient in order to more accurately estimate soil moisture and roughness parameters.

# *IV. **Chapter 4:** A New Empirical Model for Radar Scattering from Bare Soil Surfaces*

## IV.1 Introduction

Soil moisture content plays an important role in meteorology, hydrology, agronomy, agriculture, and risk assessment. This soil parameter can be estimated using synthetic aperture radar (SAR). Today, it is possible to obtain SAR data for global areas at high spatial and temporal resolutions with free and open access Sentinel-1 satellites (6 days with the two Sentinel-1 satellites, at 10 m spatial resolution).

The retrieval of soil moisture content and surface roughness requires the use of radar backscatter models capable of correctly modeling the radar signal for a wide range of soil parameter values. This estimation from imaging radar data implies the use of backscattering electromagnetic models, which can be physical, semi-empirical or empirical.

This estimation from imaging radar data implicates the use of backscattering electromagnetic models (Physical, empirical or semi-empirical. The physical models such as Integral Equation Model (IEM), Small Perturbation Model (SPM), Geometrical Optic Model (GOM) and Physical Optic Model (POM) that based on physical approximations corresponding to a range of surface conditions (soil moisture and surface roughness) provide site-independent relationships but have limited validity depending upon the soil roughness. Moreover, the semi-empirical or empirical models are often valid only for specific soil conditions and needs calibration on other soil conditions. Users preferred the empirical models because of their facility in implementation and inversion (Chai et al., 2015; Gherboudj et al., 2011; Kirimi et al., 2016; Le Hégarat-Mascle et al., 2002; Rao et al., 2013; Zribi and Dechambre, 2003; Zribi et al., 2011).

Popular semi-empirical models developed over bare soils as Oh model (Oh, 2004; Oh et al., 1992, 1994, 2002) and Dubois model (Dubois et al., 1995). The Oh model uses the ratios of the measured backscatter coefficients HH/VV and HV/VV to estimate volumetric soil moisture (mv) and surface roughness (Hrms), while the Dubois model links the backscatter coefficients in HH and VV polarizations to the soil's dielectric constant and surface roughness. Numerous studies evaluated several semi-empirical models, but these models showed conflict in the results obtained. Some studies show good agreement between measured backscatter coefficients and those predicted by the models, while others have found great discrepancies between them (Baghdadi and Zribi, 2006; Baghdadi et al., 2011c; Le Hégarat-Mascle et al., 2002; Wang et al., 2014, 1997; Zribi and Dechambre, 2003; Zribi et al.,

2011). The discrepancy between simulations and measurements often reaches several decibels, making soil parameter estimates not useful.

The goal of this chapter is to produce a new robust, empirical, radar backscattering model. The simple formulations of Dubois model that directly relates the radar signal to soil (dielectric constant and soil roughness) and SAR parameters (incidence angle, polarization and radar wavelength) lead us to select the formulations of Dubois model as basic of the new model. The formulations of Oh model was not used because only the co-polarized ratio p and cross-polarized ratio q are available.

First, the performance of the Dubois model is analyzed using a large dataset acquired at several worldwide study sites by numerous SAR sensors. The dataset consists of SAR data (multi-angular and multi-frequency) and measurements of soil moisture and surface roughness over bare soils. Then, the different terms of Dubois equations that describe the dependence between the SAR signal and both sensor and soil parameters have been validated or modified to improve the modelling of the radar signal. Ultimately, a new semi-empirical backscattering model has been developed for radar scattering in the HH, VV, and HV polarization from bare soil surfaces.

A description of the dataset is presented in section 2, section 3 describes and analyzes the potential and the limitations of the Dubois model in radar signal simulations over bare soils. In section 4, the new model is described and its performance is evaluated for different available SAR data (L-, C- and X-bands, incidence angles between 20° and 45°). Conclusions are presented in section 5.

## IV.2 Dataset description

A wide experimental dataset was used, consisting of SAR images and ground measurements of soil moisture content and roughness collected over bare soils at several agricultural study sites (Chapter III, Table III.1). SAR images were acquired by various airborne and spaceborne sensors (AIRSAR, SIR-C, JERS-1, PALSAR-1, ESAR, ERS, RADARSAT, ASAR, TerraSAR-X). The radar data were available in L-, C- and X-bands (approximately 1.25 GHz, 5.3 GHz and 9.6 GHz, respectively); with incidence angles between 18° and 57°; and in HH, VV and HV polarizations. For several reference plots, the mean backscatter coefficients have been obtained from radiometrically and geometrically calibrated SAR images by averaging backscatter coefficient values for each plot for all pixels within the plot.

A total of 1569 experimental data acquisitions with radar signal, soil moisture content and roughness were available for HH polarization, 930 for VV polarization, and 605 for HV polarization. This dataset is approximately the same as descripted in chapter III, section III.2.

## IV.3 Validation and analysis of the Dubois model

### IV.3.1 Description of Dubois model

A complete description of Dubois model is done in chapter III, section III.3.1.

### IV.3.2 Comparison between simulated and real data

The Dubois model overestimates the radar signal by 0.7 dB in HH polarization and underestimates the radar signal by 0.9 dB in VV polarization for all data combined (Table IV.1). The results show that the overestimation in HH is of the same order for L-, C- and X-bands (between 0.6 dB and 0.8 dB). For the L-band, a slight overestimation of approximately 0.2 dB of SAR data is observed in VV polarization. Also in VV polarization, Dubois model based simulations underestimate the SAR data in C- and X-bands by approximately 0.7 dB and 2.0 dB, respectively.

The rms error (RMSE) is approximately 3.8 dB and 2.8 dB in HH and VV, respectively (Table IV.1). Analysis of the RMSE according to the radar frequency band (L, C and X separately) shows in HH an increase of the RMSE with the radar frequency (2.9 dB in L-band, 3.7 dB in C-band, and 4.1 dB in X-band). In VV polarization, the quality of Dubois simulations (RMSE) is similar for L- and C-bands but is less accurate in X-band (2.3 dB in L-band, 2.6 dB in C-band, and 3.2 dB in X-band).

| | **Dubois for HH** | | **Dubois for VV** | |
|---|---|---|---|---|
| | **Bias (dB)** | **RMSE (dB)** | **Bias (dB)** | **RMSE (dB)** |
| *For all data* | -0.7 | 3.8 | +0.9 | 2.8 |
| *L-band* | -0.8 | 2.9 | -0.2 | 2.3 |
| *C-band* | -0.6 | 3.7 | +0.7 | 2.6 |
| *X-band* | -0.7 | 4.1 | +2.0 | 3.2 |
| *kHrms < 2.5* | +0.4 | 3.4 | +1.3 | 2.9 |
| *kHrms > 2.5* | -2.7 | 4.5 | -0.1 | 2.5 |
| *mv < 20 vol.%* | -2.0 | 4.3 | +0.9 | 2.8 |
| *mv > 20 vol. %* | +0.5 | 3.2 | +0.9 | 2.8 |
| $\theta < 30°$ | -4.1 | 5.4 | -0.6 | 2.9 |
| $\theta > 30°$ | +0.6 | 3.0 | +1.5 | 2.7 |

**Table IV.1.** Comparison between the Dubois model and real data for all data and by range of *kHrms*, soil moisture (*mv*) and incidence angle (θ). Bias = real data – model.

In addition, the agreement between Dubois model simulations and SAR data is analyzed according to soil roughness, moisture content and incidence angle (Figures IV.1 and IV.2). The results indicate a slight underestimation of the radar signal by the Dubois model in the case of *kHrms* lower than 2.5 (Dubois validation domain) for both HH and VV polarizations (Figures IV.1b, IV.2b; Table IV.1). For surfaces with a roughness *kHrms* greater than 2.5, an overestimation of the radar signal is obtained with the Dubois model in HH while the model works correctly in VV (Figures IV.1b, IV.2b; Table IV.1). Higher under- and overestimations are observed in HH than they are in VV (reach approximately 10 dB in HH).

Analysis of the error as a function of soil moisture (*mv*) shows that for both VV-polarized data, whatever the *mv*-values, and HH-polarized data with *mv*-values higher than 20 vol.%, the observed bias between real and simulated data is small (Figures IV.1c and IV.2c; Table IV.1). However, a strong overestimation of the radar signal is observed by the Dubois model in HH for *mv*-values lower than 20 vol.% (-2.0 dB, Table IV.1).

Finally, the discrepancy between SAR and the model is larger in HH for incidence angles lower than 30° (outside of the Dubois validity domain) than for incidence angles higher than 30° (Table IV.1). The Dubois model strongly overestimates the radar signal in HH for incidence angles lower than 30° but agrees closely with the measured data for incidence angles higher than 30° (Figures IV.1d, IV.2d; Table IV.1). In VV polarization, the Dubois model slightly overestimates the radar signal for incidence angles lower than 30° and underestimates the signal for incidence angles higher than 30° by +1.5 dB (Figures IV.1d and, IV.2d; Table IV.1).

In conclusion, the Dubois model simulates VV better than it does HH (RMSE=2.8 and 3.8 dB, respectively). The disagreements observed between the Dubois model and measured data are not limited to data that are outside the optimal application domain of the Dubois model.

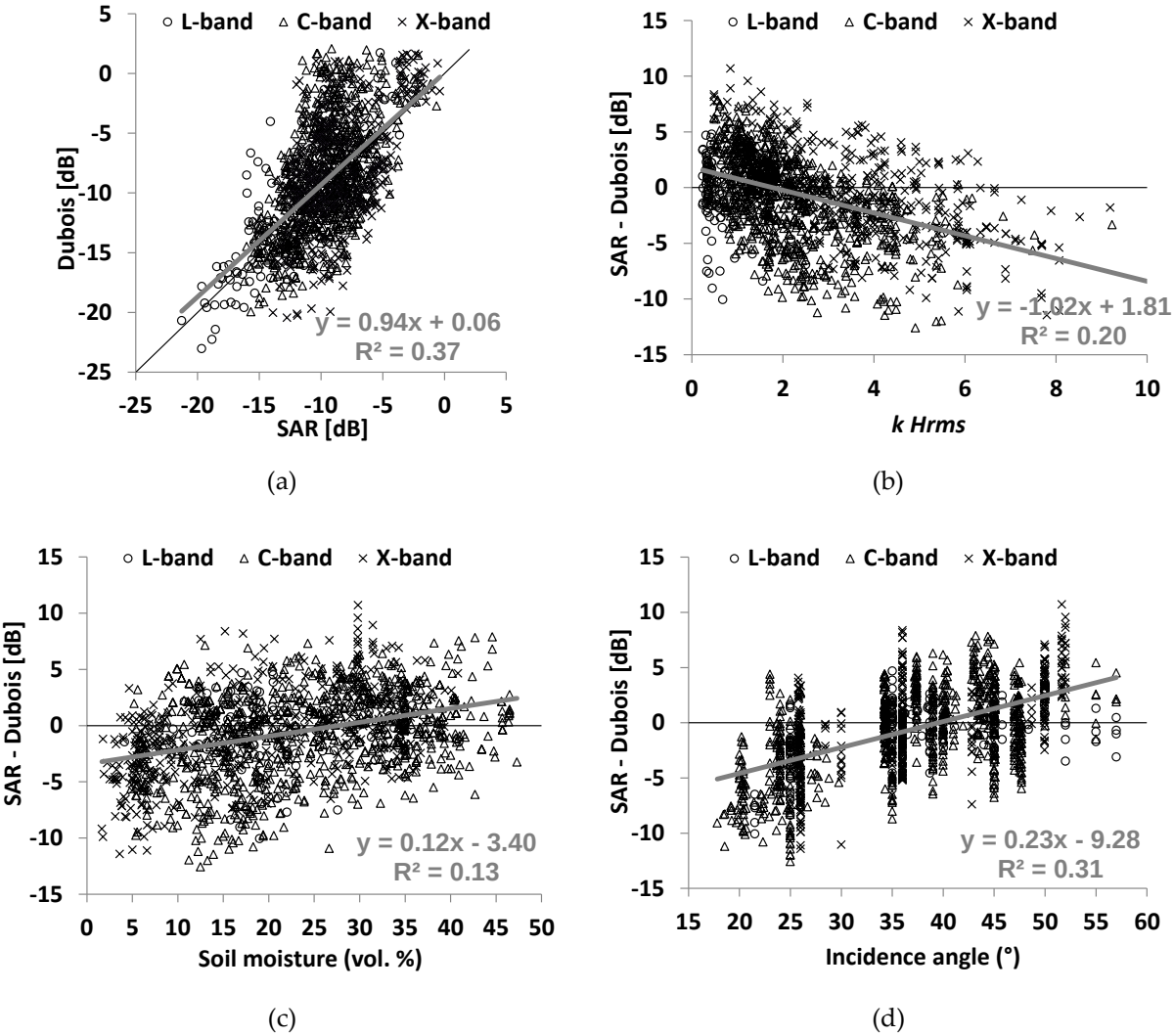


**Figure IV.1.** For HH polarization, (a) comparison between radar backscattering coefficients calculated from SAR images and estimated from the Dubois model, (b) difference between the SAR signal and the Dubois model relative to soil roughness (*kHrms*), (c) difference between the SAR signal and the Dubois model relative to soil moisture (*mv*), (d) difference between the SAR signal and the Dubois model relative to incidence angle. The best regression model is ploted in gray.

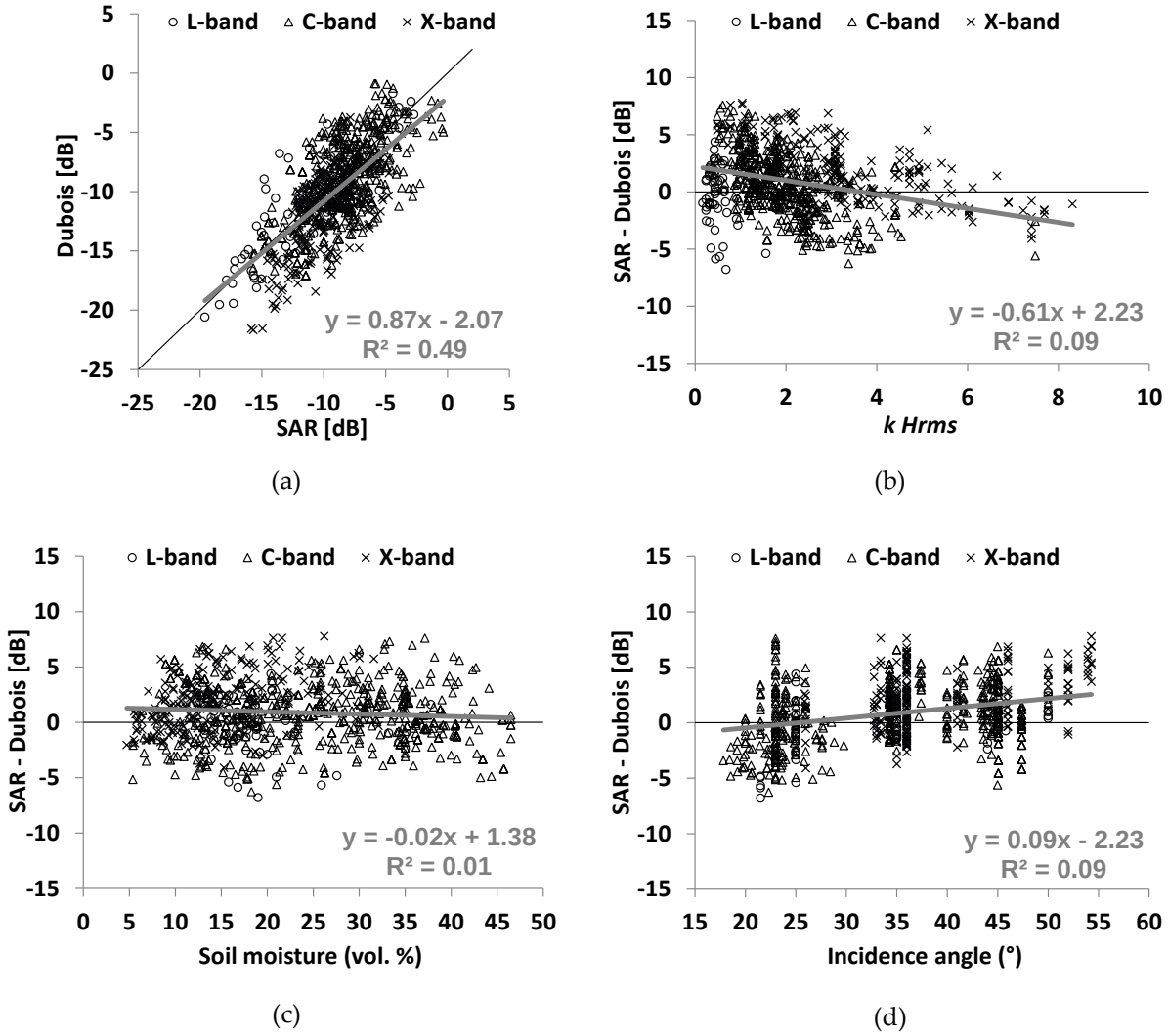


**Figure IV.2.** For VV polarization, (a) comparison between radar backscattering coefficients calculated from SAR images and estimated from the Dubois model, (b) difference between the SAR signal and the Dubois model relative to soil roughness (*kHrms*), (c) difference between the SAR signal and the Dubois model relative to soil moisture (*mv*), (d) difference between the SAR signal and the Dubois model relative to incidence angle. The best regression model is ploted in gray.

## IV.4 New empirical model

### IV.4.1 Methodology

The disagreement observed between measured radar signal and simulated data by empirical model (Dubois and Oh) encouraged us to develop a new empirical backscattering model using SAR observations and soil in situ measurements. The simple formulations of Dubois model that directly relates the radar signal to soil (dielectric constant and soil roughness) and SAR parameters (incidence angle, polarization and radar wavelength) lead us to select the

formulations of Dubois model as basic of the new model. The formulations of Oh model was not used because only the co-polarized ratio p and cross-polarized ratio q are available.

The new model is based on the Dubois model and uses the dependency observed between the SAR signal and soil parameters according to results obtained in various studies. For bare soils, the backscattering coefficient depends on soil parameters (roughness and moisture) and SAR instrumental parameters (incidence angle, polarization and wavelength). For bare soils, the radar signal in pq polarization (p and q = H or V, with HV=VH) can be expressed as the product of three components:

$$\sigma^{\circ}_{pq} = f_{pq}(\theta)\, g_{pq}(mv, \theta)\, \Gamma_{pq}(kHrms, \theta) \qquad (4.1)$$

The radar backscatter coefficient is related to the incidence angle (θ) by the relation $f_{pq}(\theta) = \alpha(cos\,\theta)^{\beta}$ (Baghdadi et al., 2001; Beauchemin et al., 1995; Ulaby et al., 1982). This relationship describes the decrease of σ° with the incidence angle (decrease higher for low angles than for high angles).

The second term represents the relationship between the radar backscatter coefficient and soil moisture (*mv)*. The results obtained in several investigations show that, for bare soils, the radar signal (σ°) in decibels linearly increases with soil moisture (*mv*) when *mv* is in the range between approximately 5 and 35 vol.% (Baghdadi et al., 2006b, 2008a; Le Hégarat-Mascle et al., 2002; Zribi et al., 2011). In linear scale $g_{pq}(mv, \theta)$ can be written as $\delta\, 10^{\gamma\, mv}$. The sensitivity of the radar signal to the soil moisture γ depends on θ. Higher sensitivity is observed for low than for high incidence angles (Aubert et al., 2011a; Baghdadi et al., 2008b). To include this dependence on incidence angle, the soil moisture value is multiplied with the term $cotan(\theta)$. Thus, $g_{pq}(mv, \theta)$ can be written as $\delta\, 10^{\gamma\, cotan(\theta)\, mv}$.

The last term $\Gamma_{pq}(kHrms, \theta)$ represents the behaviour of σ° with soil roughness. An exponential or logarithmic function is often used to express the radar signal (in dB) in terms of surface roughness (Baghdadi et al., 2006b; Sahebi et al., 2002; Srivastava et al., 2003; Zribi and Dechambre, 2003). For a logarithmic behaviour of σ°(dB) with *k Hrms*, $\Gamma_{pq}$ in linear scale can be written as $\mu(kHrms)^{\xi}$. Baghdadi et al. (2002a) showed that at high incidence angles, radar return is highly sensitive to surface roughness and shows much larger dynamics

than at a low incidence angle. In addition, the term $sin(\theta)$ is intended to include this dependence with the incidence angle: $\Gamma_{pq=}\mu(kHrms)^{\xi\ sin(\theta)}$.

Finally, the relationship between the radar backscattering coefficient ($\sigma°$) and the soil parameters (soil moisture and surface roughness) for bare soil surfaces can be written by equation (4.2):

$$\sigma_{pq}^{\circ} = \delta(cos\,\theta)^{\beta}\ 10^{\gamma\ cotan(\theta)\ mv}\ (kHrms)^{\xi\ sin(\theta)} \tag{4.2}$$

The coefficients δ, β, γ, and ξ are then estimated for each radar polarization using the method of least squares by minimizing the sum of squares of the differences between the measured and modelled radar signal. The error in the modelling of radar backscatter coefficients by the new backscattering model was assessed for each polarization using a 5-fold cross-validation to validate the predictive performance of the new model. To do the 5-fold cross-validation, the dataset was first randomly divided into 5 equal size subsets. Next, 4 of the subsets are used to train the new model and one was retained to validate its predictive performance. The cross-validation process was then repeated 5 times, with each of the 5 sub-datasets used exactly once as the validation data. The final validation result combines the 5 validation results. The advantage of this method over repeated random sub-sampling is that all observations are used for both training and validation, and each observation is used for validation exactly once.

The fitting of various coefficients parameter in the equation (4.2) was done using all dataset (fitting errors are about 2 dB for all polarizations). This fitting allows writing σ° as a function of the rms surface height (*Hrms*) and incidence angle (θ), by equations (4.3), (4.4) and (4.5):

$$\sigma_{HH}^{\circ} = 10^{-1.287}(cos\,\theta)^{1.227}\ 10^{0.009\ cotan(\theta)\ mv}\ (kHrms)^{0.86\ sin(\theta)}, \tag{4.3}$$

$$\sigma_{VV}^{\circ} = 10^{-1.138}(cos\,\theta)^{1.528}\ 10^{0.008\ cotan(\theta)\ mv}\ (kHrms)^{0.71\ sin(\theta)} \tag{4.4}$$

$$\sigma_{HV}^{\circ} = 10^{-2.325}(cos\,\theta)^{-0.01}\ 10^{0.011\ cotan(\theta)\ mv}\ (kHrms)^{0.44\ sin(\theta)}, \tag{4.5}$$

where θ is expressed in radians and *mv* is in vol.%. Equations (4.3), (4.4), and (4.5) show that the sensitivity (γ) of the radar signal to the soil moisture in decibel scale is 0.25 dB/vol.% in HH polarization, 0.22 dB/vol.% in VV polarization and 0.30 dB/vol.% in HV polarization for an incidence angle of 20°. This sensitivity decreases to 0.09 dB/vol.% in HH, 0.08 dB/vol.% in VV and 0.11 dB/vol.% for an incidence angle of 45°. As for the signal's sensitivity to soil roughness, it is of the same order of magnitude in HH and VV and twice as large than that of the HV signal. The few data in HV polarization may explain the higher sensitivity observed in HV than in HH and VV. Indeed, several studies showed very near sensitivity of radar signal to soil moisture in HV, HH and VV polarizations.

The availability of a backscatter model for the cross polarization component is required because most spaceborne SAR acquisitions are made with one co-polarization and one cross-polarization in case of dual-polarization mode.

### IV.4.2 Comparison between Dubois model and new model

In comparison between Dubois model (Equation 3.1) and the new model (Equation 4.2), several terms have been changed, simplified or removed:

- In the new model, the first term that describes the relationship between the radar backscatter coefficient and the incidence angle (θ) which describes the decrease of σ° with the incidence angle was simplified using the function $f_{pq}(\theta) = \alpha(cos\,\theta)^{\beta}$. In Dubois model, the relation between the radar backscatter signal and the incidence angle (θ) is more complex (Equation 4.6).
- The second term which describes the relationship between the radar backscatter coefficient and soil moisture (*mv)* was modified. First, the dielectric constant was changed into the volumetric soil moisture. Second, the dependence between the sensitivity of the radar signal to the incidence angle (θ) described by *tan(θ)* in Dubois model was corrected into *cotan(θ)* in the new model. Indeed, higher sensitivity is observed for low than for high incidence angles. To include this dependence on incidence angle, the soil moisture value is multiplied with the term $cotan(\theta)$. Thus, $g_{pq}(mv, \theta)$ can be written as $\delta\, 10^{\gamma\, cotan(\theta)\, mv}$.
- In the new model, the term $\Gamma_{pq}(kHrms, \theta)$ represents the behaviour of σ° with soil roughness. For a logarithmic behaviour of σ°(dB) with *k Hrms*, $\Gamma_{pq}$ in linear scale can be written as $\mu(kHrms)^{\xi}$. At high incidence angles, radar return is highly sensitive to

surface roughness and shows much larger dynamics than at a low incidence angle. Thus, the term $sin(\theta)$ is intended to include this dependence with the incidence angle: $\Gamma_{pq=}\mu(kHrms)^{\xi\, sin(\theta)}$.

- Finally the dependence of the radar signal on the radar wavelength described in Dubois model by $(\lambda)^c$ (Equation 4.6) does not seem validated using our in situ dataset. Thus, this term has been removed in the new model.

### IV.4.3 Results and discussion

*IV.4.3.1 Performance of the new model*

Results show that the new model provides more accurate results. The biases and the RMSE decrease for both HH and VV polarizations. The RMSE decreases from 3.8 dB to 2.0 dB for HH and from 2.8 dB to 1.9 dB for VV (Table IV.2). In addition, the high over- or underestimations of radar backscattering coefficients observed with the Dubois model according to soil moisture, surface roughness and radar incidence angle are clearly eliminated with the new model (Figures IV.3 and IV.4).

| | **Dubois for HH and VV** | | **New model** | |
|---|---|---|---|---|
| | **Bias (dB)** | **RMSE (dB)** | **Bias (dB)** | **RMSE (dB)** |
| **HH for all data** | -0.7 | 3.8 | 0.4 | 2.0 |
| **VV for all data** | +0.9 | 2.8 | 0.0 | 1.9 |
| **HV for all data** | - | - | 0.0 | 2.1 |
| **HH, L-band** | -0.8 | 2.9 | -0.1 | 2.3 |
| **HH, C-band** | -0.6 | 3.7 | +0.3 | 1.9 |
| **HH, X-band** | -0.7 | 4.1 | 0.7 | 1.9 |
| **VV, L-band** | -0.2 | 2.3 | -0.1 | 2.7 |
| **VV, C-band** | +0.7 | 2.6 | +0.1 | 1.9 |
| **VV, X-band** | +2.0 | 3.2 | -0.4 | 1.8 |
| **HV, L-band** | - | - | -1.3 | 1.6 |
| **HV, C-band** | - | - | +0.2 | 2.2 |
| **HV, X-band** | - | - | -1.3 | 1.9 |

**Table IV.2.** Comparison between the results obtained with the Dubois model and those obtained with the new model. Bias = real – model.

Analysis of the new model's performance for each radar wavelength separately (L-, C- and X-bands) shows that the most significant improvement is observed in X-band with an RMSE that decreases from 4.1 dB to 1.9 dB in HH and from 3.2 dB to 1.8 dB in VV. In L-band, the performance of the new model is not better than that of the Dubois model because the RMSE decreases slightly with the new model of 3.0 dB to 2.3 dB in HH and remains similar in VV (RMSE = 2.3 dB with the Dubois model and 2.7 dB with the new model). The improvement

is also important for the C-band with an RMSE that decreases from 3.7 dB to 1.9 dB in HH and from 2.6 dB to 1.9 dB in VV. With respect to bias, the results show that it decreases with the new model for all radar wavelengths. In addition, the new model does not show bias according the range of soil moisture, surface roughness, and radar incidence angle.

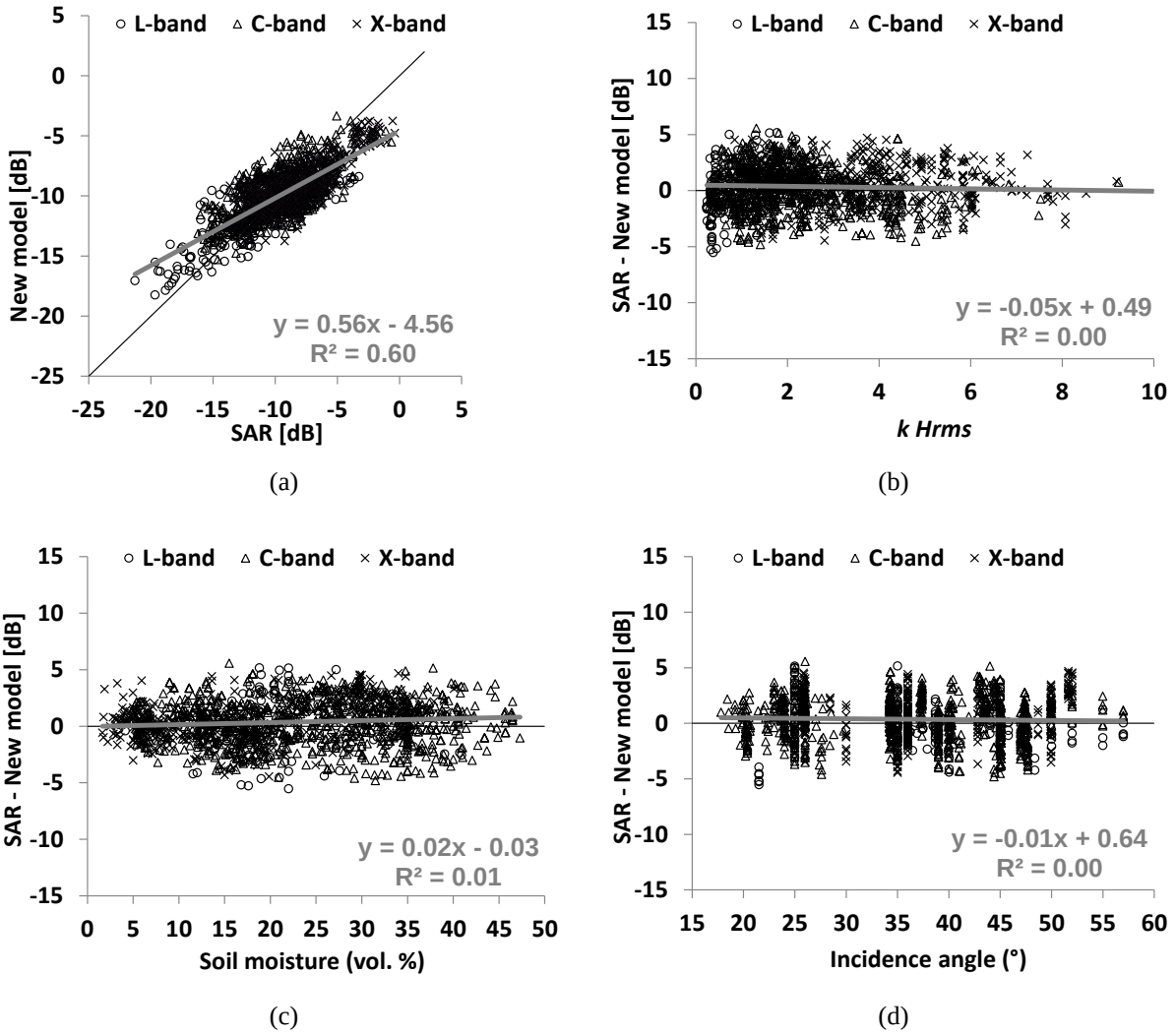


**Figure IV.3.** (a) Comparison between $\sigma^{\circ}$ modelled in the new model and $\sigma^{\circ}$ measured (for all SAR bands) for HH polarization, (b) difference between SAR and the new model as a function of surface roughness (*kHrms*), (c) difference between SAR and the new model as a function of soil moisture (*mv*), (d) difference between SAR and the new model as a function of incidence angle. The best regression model is ploted in gray.

The comparison between the new model simulations in HV polarization (Equation 4.5) and the real data (SAR data) shows an RMSE of 2.1 dB (Table IV.2) (1.6 dB in L-band, 2.2 dB in C-band, and 1.9 dB in X-band). The bias ($\sigma^{\circ}$SAR - model) is -1.3 dB in L-band, 0.2 dB in C-band, and -1.3 dB in X-band. Figure IV.5 shows also that the new model correctly simulates

the radar backscatter coefficient in HV for all ranges of soil moisture, surface roughness and radar incidence angle.

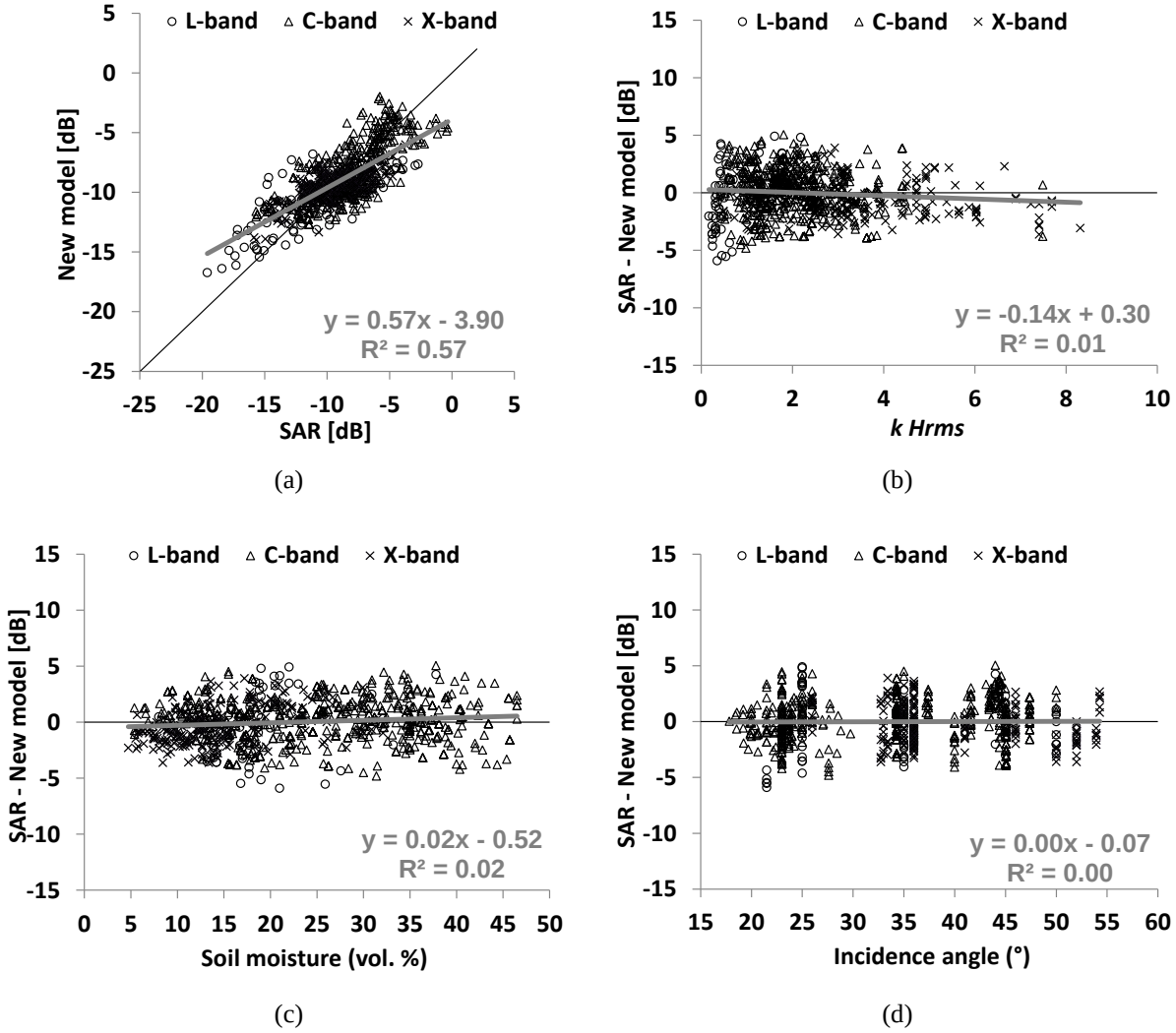


**Figure IV.4.** (a) Comparison between $\sigma^{\circ}$ in the new model and $\sigma^{\circ}$ measured (for all SAR bands) for VV polarization, (b) difference between SAR and the new model as a function of surface roughness (*kHrms*), (c) difference between SAR and the new model as a function of soil moisture (*mv*), (d) difference between SAR and the new model as a function of incidence angle. The best regression model is ploted in gray.

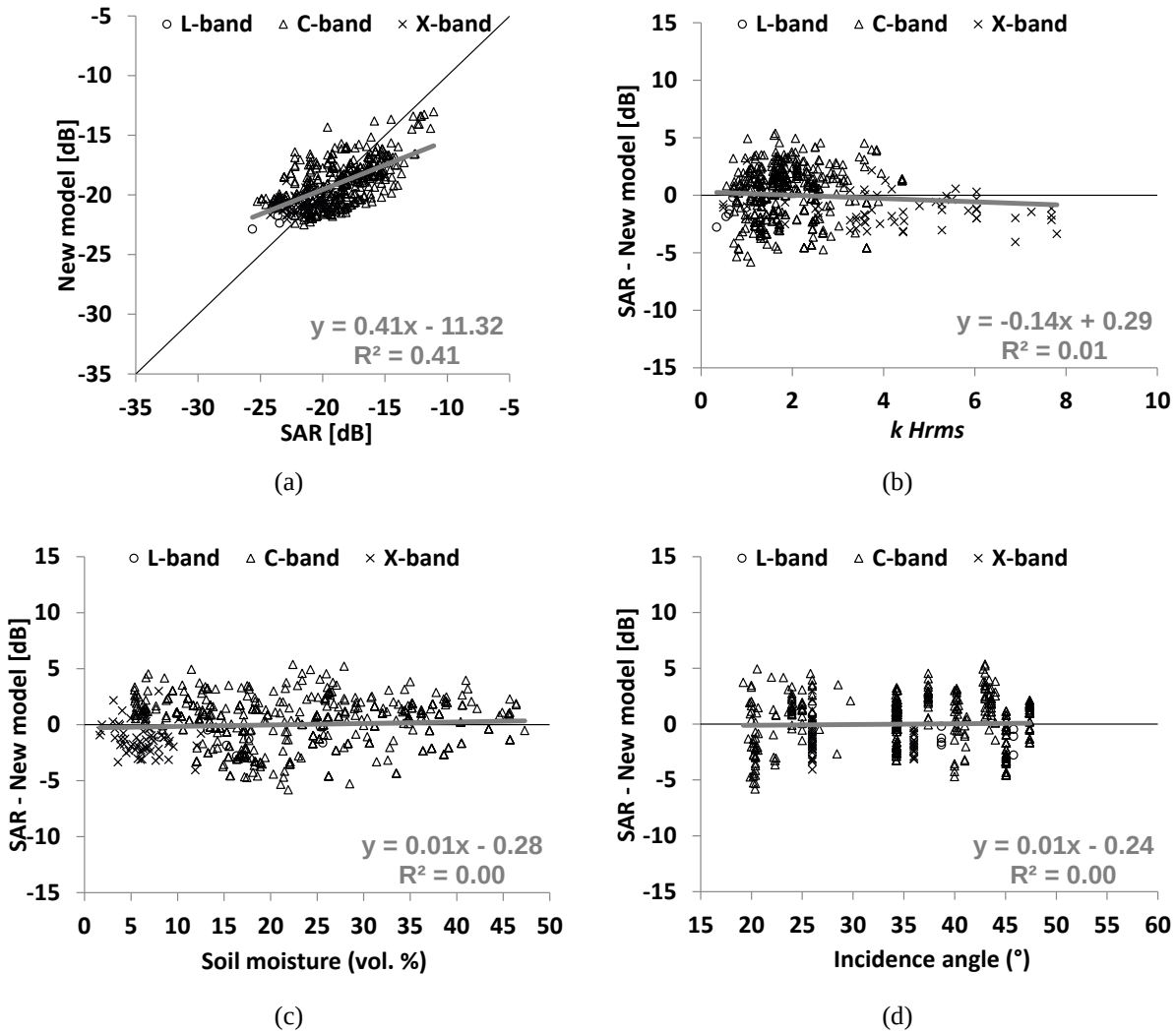


**Figure IV.5.** (a) Comparison between $\sigma^{\circ}$ in the new model and $\sigma^{\circ}$ measured (for all SAR bands) for HV polarization, (b) difference between SAR and the new model as a function of *kHrms*, (c) difference between SAR and the new model as a function of *mv*, (d) difference between SAR and the new model as a function of incidence angle. The best regression model is ploted in gray.

*IV.4.3.2 Behaviour of the new model*

The physical behaviour of the new radar backscatter model was studied in function of incidence angle (θ), soil moisture (*mv*) and surface roughness (*kHrms*).

Figure IV.6 shows that the radar signal is strongly sensitive to surface roughness, especially for small values of *kHrms*. In addition, this sensitivity increases with the incidence angle. Concerning the influence of polarization, the new model shows, as do many theories and experimental studies, that a given soil roughness leads to slightly higher signal dynamics with the soil moisture in HH than in VV polarization (Figure IV.6). The radar signal σ° increases with *kHrms*. This increase is higher for either low *kHrms* values or high θ-values than it is for either high *kHrms* values or low θ-values. For θ=45°, $\sigma^\circ$ increases approximately 8 dB in HH and 6.5 dB in VV when *kHrms* increases from 0.1 to 2 compared with only 3 dB when *kHrms* increases from 2 to 6 (for both HH and VV). This dynamic of $\sigma^\circ$ is only half for θ=25° in comparison to that for θ=45°. In HV, the dynamic of $\sigma^\circ$ to *kHrms* is half that observed for HH and VV.

The behaviour of $\sigma^\circ$ according to soil moisture shows a larger increase of σ° with *mv* for low incidence angles than for high incidence angles. Figure IV.6 shows that $\sigma^\circ_{HH}$ and $\sigma^\circ_{VV}$ increase approximately 6 dB for θ=25° compared with only 3 dB for θ=45° when *mv* increases from 5 to 35 vol.%. In HV, the signal increases approximately 7.5 dB for θ=25° and 3.5 dB for θ=45° when *mv* increases from 5 to 35 vol.%.

As mentioned in Dubois et al. (Dubois et al., 1995), the ratio $\sigma^\circ_{HH}/\sigma^\circ_{VV}$ should increase with *kHrms* and remain less than 1. The new model shows that this condition is satisfied when 20°< θ <45°, *kHrms* < 6 and *mv* < 35 vol.%.

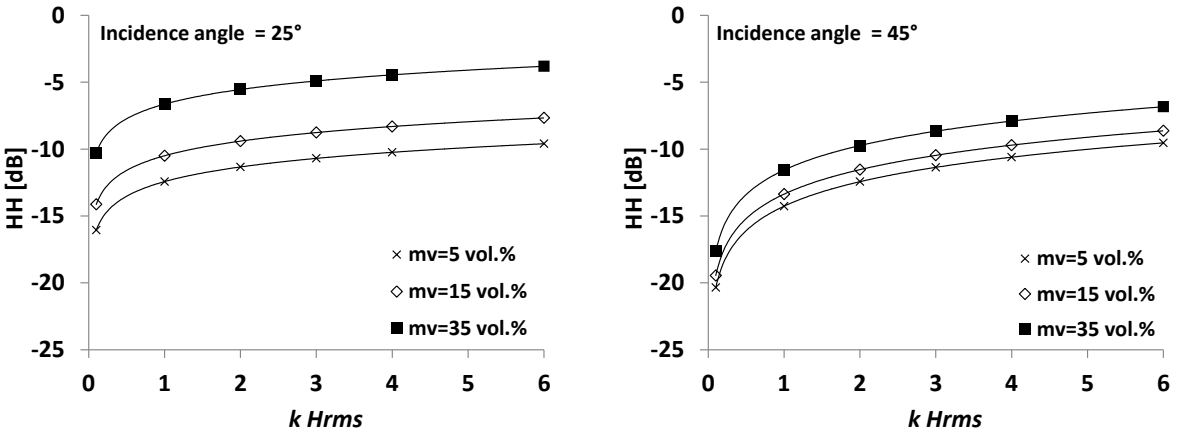


(a)




(b)

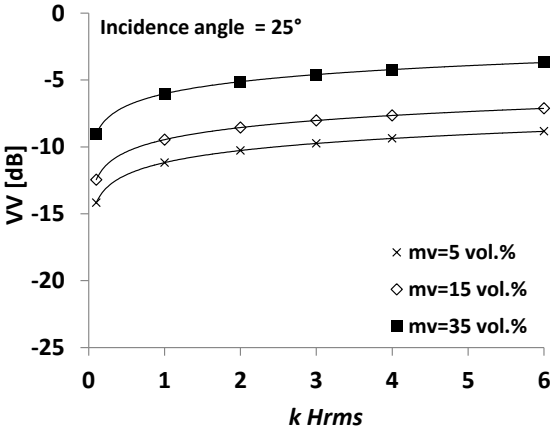


(c)

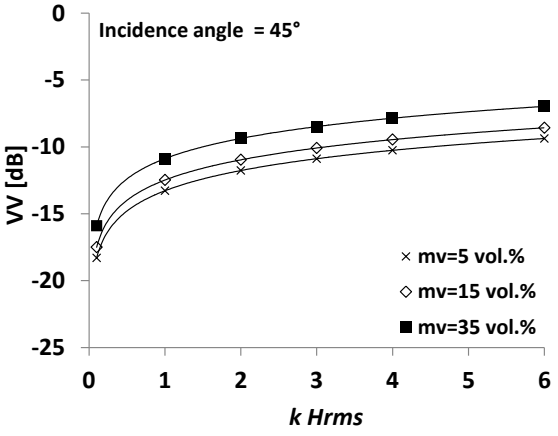


(d)

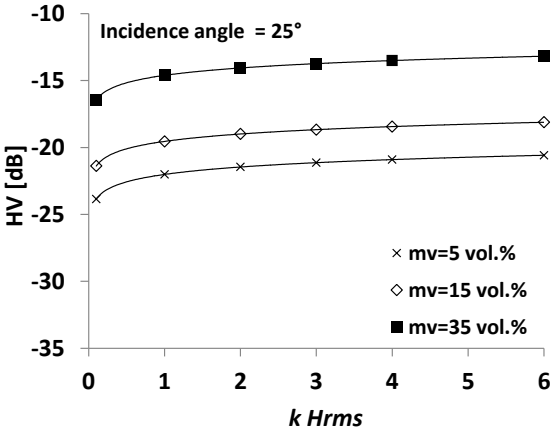


(e)

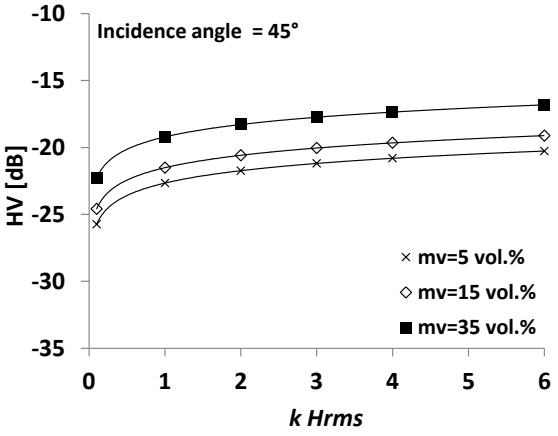


(f)

**Figure IV.6**. Behavior of the new model as a function of incidence angle, surface roughness (*k Hrms*) and soil moisture (*mv*) in HH, VV and HV polarizations.

## IV.5 Conclusion

This investigations objective is to propose a new empirical model for radar backscatter from bare soil surfaces. The new model is based on the formulation made in the Dubois model where the radar signal in HH and VV polarizations is described according to radar wavelength, incidence angle, soil moisture and roughness. This new model is based on the formulation made in the Dubois model. A large dataset was used, composed of ground measurements and SAR images over bare agricultural soils.

Results show that the new model provides improved results in comparison to the Dubois model (in the case of HH and VV). Biases and RMSE have decreased for both HH and VV polarizations. In addition, the high over- or under-estimations observed with the Dubois model for some ranges of soil moisture, surface roughness and radar incidence angle were clearly eliminated with the new model. Analysis of the new model's performance for each radar wavelength separately (L, C and X) shows that in the L-band, the performance of the new model was similar to that of the Dubois model (may be due to the few data used in L-band). The model shows significant improvement in C- and X-bands (RMSE approximately 1.9 dB with the new model and between 2.6 and 4.1 dB with the Dubois model).

Based on the same equation as that used for HH and VV, a radar signal in HV polarization was also proposed. Finally, the new empirical model proposed in the present study would allow more accurate soil moisture estimates using the new Sentinel-1A and -1B SAR data.

# *V. **Chapter 5:** Estimation of soil roughness using neural networks from sentinel-1 SAR data*

## V.1 Introduction

Soil surface characteristics (mainly soil moisture and surface roughness) play a key role in different hydrological processes (floods, runoff, evapotranspiration, infiltration, soil erosion, and imbalances in the water and carbon cycles). Surface roughness has a role in trapping water at the surface and reducing flow velocity, which increases infiltration and in turn reduces downstream runoff. The roughness scales observed by a radar sensor have a strong dependence on the frequency and radar incidence (Ogilvy and Ogilvy, 1991).

Radar data were used since a long time for estimating and mapping the surface soil parameters (mainly soil moisture and roughness) of bare soils. Soil moisture and surface roughness can be estimated from SAR images by using physical or statistical models (Baghdadi and Zribi, 2016; Baghdadi et al., 2002c, 2012a; Merzouki et al., 2011; Rahman et al., 2008). The best known physical model is the Integral Equation Model (IEM) (Fung, 1994; Fung et al., 1992). This model simulates the radar backscattering coefficients from SAR and soil parameters (radar wavelength, polarization, incidence angle, surface roughness and soil moisture 'dielectric constant'). The validity domain of IEM in C-band covers the range of roughness values that are commonly encountered for bare agricultural surfaces ($k\,Hrms \leq 3$, where *Hrms* is the root mean square surface height and k the radar wave number $\approx 1.12$ cm−1 for a frequency in C-band of 5.4 GHz as Sentinel-1 SAR). Most *Hrms* values of agricultural bare soils range from 0.5 to 4 cm (Baghdadi et al., 2012a).

The discrepancies observed between the IEM and the SAR data had encouraged Baghdadi et al., (2004, 2006a, 2011a, 2015) to propose an empirical calibration of IEM model. Moreover, Baghdadi et al. (2016a) proposed an new empirical model based on Dubois model that make the estimation of soil moisture and surface roughness possible in an easy way. Actually, physical, empirical and semi-empirical models were developed to invert the radar signal in order to monitor the soil parameters (moisture and roughness).

Baghdadi et al., (2002a) investigated the potential of the first generation of SAR data (ERS-2 and RADARSAT-1) for monitoring roughness states over bare agricultural fields. Results indicate that high incidence angles (about 45°) are more suitable to discriminate various roughness classes (smooth, medium and rough) over bare agricultural fields. An algorithm based on an experimental exponential relationship between the radar backscattering coefficient and the surface roughness (root mean square surface height, *Hrms*) independently

of the soil moisture was used. Next, Baghdadi et al. (2012) developed an approach to estimate soil moisture and surface roughness from C-band polarimetric RADARSAT-2 data based on neural networks (NNs). Results showed that the accuracy on the soil roughness estimates was about 0.5 cm using polarimetric data. The estimation is better for *Hrms*-values lower than 2 cm than for *Hrms*-values higher than 2 cm. For higher *Hrms*, the NNs under-estimate the surface roughness. Moreover, Zribi and Dechambre (2002) proposed an approach based on the use of two SAR images acquired at two different incidence angles, one image with a weak incidence (~20°) and one image with a strong incidence (~40°) for estimating both soil moisture and surface roughness. The surface roughness defined by $Zs=Hrms/L$ ($L$ is the correlation length) is estimated with an RMSE of 0.08 cm for *Zs*-values between 0.075 and 0.75 cm.

The aim of this part is to develop an approach to estimate the soil surface roughness from C-band Sentinel-1 SAR data in the case of bare agricultural soils. This approach is an inversion technique based on Multi-Layer Perceptron (MLP) neural networks. The training of the neural networks is performed using synthetic dataset simulated by the Integral equation model calibrated by Baghdadi (Baghdadi et al., 2004, 2006a, 2011b, 2015) and the new proposed model by Baghdadi modified Dubois (Baghdadi et al., 2016a) on a wide range of surface roughness and soil moisture. The inversion approach was then validated in using Sentinel-1 datasets (one in France and one in Tunisia) composed on Sentinel 1 images and in-situ measurements. This work is done in order to evaluate the potential of Sentinel-1 SAR sensors for retrieving soil roughness. Section 2 presents a review of datasets. A presentation of the methodology developed in order to estimate the soil roughness is done is section 3. The results and discussions are presented in section 4, and finally, the main conclusion is presented in section 5.

## V.2 Dataset

### V.2.1 Synthetic dataset

The Integral Equation Model calibrated by Baghdadi et al., (2004, 2006a, 2011a, 2015) 'IEM_B' and the modified Dubois Model (Baghdadi et al., 2016a) are used to generate the reference datasets for the inversion of SAR data by the neural networks (NN) technique. The IEM modified by Baghdadi and the new semi-empirical modified Dubois model are able to reproduce the radar signal at VV, HH and VH from SAR parameters (incidence angle and radar wavelength) and soil surface characteristics (soil moisture and surface roughness). The

standard mode of Sentinel-1 corresponds only to acquisitions in both VV and VH polarizations. For this reason, only VV and VH polarizations will be used in this chapter.

A synthetic dataset combining a wide range of soil parameters (soil roughness "*Hrms*" and soil moisture "*mv*") and corresponding backscattering coefficients was generated from the calibrated IEM and the modified Dubois in order to evaluate the performance of the NN technique. 18 soil roughness values (*Hrms* between 0.35 and 3.8 cm with a step of 0.2 cm), 20 soil moisture values (*mv* between 2 vol.%. and 40 vol.%.with a step of 2 vol.%), 25 radar incidence angles (θ between 20°and 45° with a step of 1°) are considered. In order to make the IEM simulations more realistic, the SAR measurement error which includes both calibration errors and measurements precision errors is added to the simulated backscattering coefficients. Realistic values of measurements errors are 0.75 for VV and 1dB for VH (Schwerdt et al., 2017).To better simulate an experimental dataset, the synthetic dataset is then obtained by adding a zero mean Gaussian random noise with a standard deviation of ±0.75 and ±1 dB to the simulated backscattering coefficients VV and VH (in dB scale), respectively. In order to obtain a statistically significant dataset, 250 noise samples are generated for each couple of *mv* and *Hrms*. A total of 1350000 elements (C-band VV and VH) are also obtained to produce the synthetic dataset.

The noisy synthetic datasets are then divided into two equal datasets one of which is used for training the NNs, the remaining is being used for the validation of the NNs.

### V.2.2 Real dataset

An experimental dataset is used in this study, consisting of Sentinel-1 images as well as ground measurements of soil moisture and surface roughness collected over two agricultural study sites: one in France and one in Tunisia (Figure V.1, Table V.1). Sentinel-1 images (C-band, radar wavelength about 6 cm) were acquired with incidence angles between 37° and 41°, and in VV and HV polarizations.

#### *V.2.2.1 Study sites*

The French study site is the Versailles plain. It is located west of Paris and covers about 221 km² (48°46′ –48°56′ N; 1°50′–2°07′ E, Figure V.1) (Vaudour et al., 2014). This agricultural peri-urban site is characterized by a semi-oceanic climate with an average rainfall of 570 mm/year and an average annual temperature of 11.3°C (INRA meteorological station of

Thiverval-Grignon, 1986-2016). Rainfed annual crop systems cover 99 km² and develop over two embedded plateaus, the gentle slopes at their edges and the valleys at their bottom. The main crop rotations in the area involve winter wheat, winter rapeseed, winter and spring barley and maize on occasion (Vaudour et al., 2015). Conventional tillage practices are used: ploughing in November-December, followed by chisel in March then seedbed preparation for spring cereals (spring barley in March, maize in April). The main cultivated soils according to the FAO classification (World Reference Base (WRB) (Vaudour et al., 2014) are haplic or glossic luvisols deriving from loessic material over the plateaus, calcaric cambisols deriving from limestones and/or colluvic material and/or chalk along slopes and stagnic colluvic cambisols in the valley bottoms. The topsoil texture is dominated by silt loam (silt > 50%) with extreme textural classes varying from sandy loam to silty clay. Clay content is comprised between 14 and 32% (22% in median).

The Tunisian site is situated in the Kairouan plain (9°23′−10°17′E, 35°1′−35°55′N) in central Tunisia (Figure V.1b). The climate in this region is semi-arid, with an average annual rainfall of approximately 300 mm/year, characterized by a rainy season lasting from October to May, with the two rainiest months being October and March (Gorrab et al., 2015a). As known, in the case of semi-arid areas, the rainfall patterns in this area are highly variable in time and space. The mean temperature in Kairouan City is 19.2 °C (minimum of 10.7 °C in January and maximum of 28.6 °C in August). The mean annual potential evapotranspiration (Penman) is close to 1600 mm. The landscape is mainly flat, and the vegetation is dominated by agricultural production (cereals, olive groves, fruit trees, market gardens and bare soils). Soil texture measurements showed a clay percentage between 2.4% and 53.1% and sand percentage between 4.4% and 84.3% (Gorrab et al., 2015a). The soil roughness was assumed isotropic. So, the row direction is not considered.

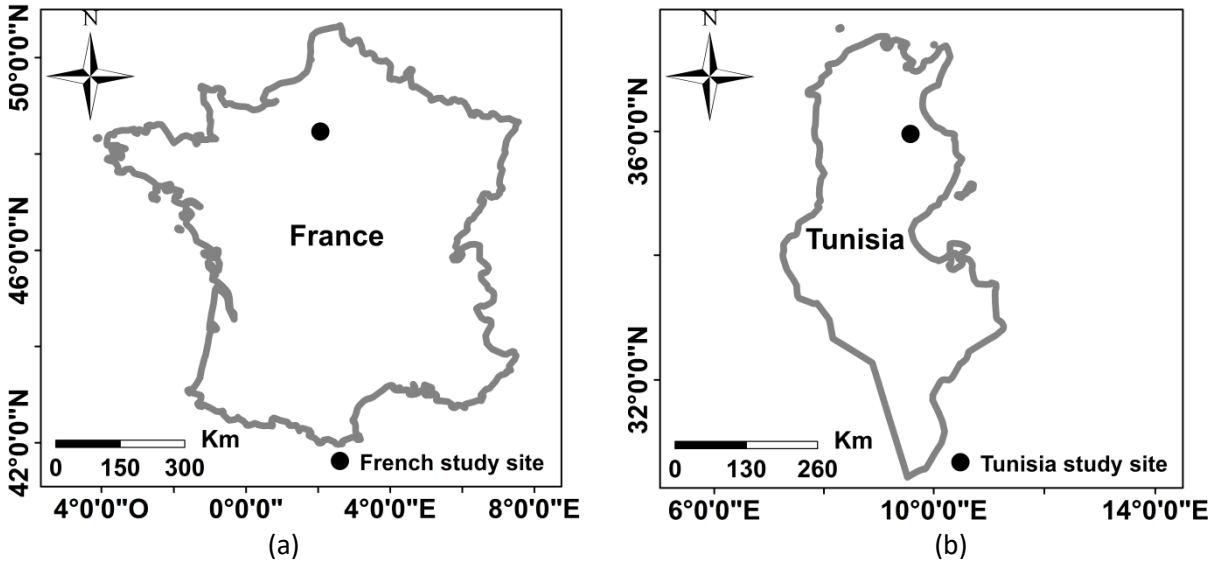


**Figure V.1.** Location of the two study sites, (a): location of Versailles in France. (b): location of Kairouan in Tunisia.

*V.2.2.2. SAR Satellite images*

Four Sentinel-1 images were acquired in March and April 2017 (Table V.1) over the French study site. In addition, 7 Sentinel-1 images acquired over the Kairouan plain between 2015 and 2017 are used in this study. All Sentinel-1 images acquired with a spatial resolution of 10 m and in VV and VH polarizations are radiometrically calibrated in order to convert the digital number to radar backscattering coefficients.

| Site | SAR sensor | Incidence angle (°) | Dates (dd/mm/yyyy) | Number of data |
|---|---|---|---|---|
| **French site** | Sentinel-1 | ~37° | 15/03/2017 ; 27/03/2017<br>02/04/2017 ; 08/04/2017 | 24 measurements |
| **Tunisian site** | Sentinel-1 | ~39° to 41° | 18/12/2015 ; 04/02/2016<br>03/04/2016 ; 04/04/2016<br>23/12/2016 ; 05/01/2017<br>09/02/2017 | 85 measurements |

**Table V.1.** Description of the real dataset used in this study for validating the inversion approach.

*V.2.2.3 In situ measurements*

Simultaneously with the Sentinel-1 acquisitions, in situ measurements of soil moisture and surface roughness were collected on several reference bare plots of a few hectares. Soil moisture was determined gravimetrically at each reference plot of the French site in using soil samples collected between 0 and 8 cm depth (one measure by plot). For the Tunisian site, between 20 and 30 volumetric soil moisture measurements (*mv*) were performed in the first top 5 cm using calibrated TDR (Time Domain Reflectometry) probes. The mean volumetric soil moisture was then calculated for each reference plot and each date. The soil moisture on the reference plots ranged between 11.5 et 25.1 vol.% for the French site and between 4.6 and 41.7 vol.% for the Tunisia site.

The soil roughness measurements made in Tunisia on the reference plots use 1 m long pin profiler with a resolution of 2 cm. Ten roughness profiles (five parallel and five perpendicular to the tillage row direction) were made in each reference field using a 1 m long needle-profilometer and a sampling interval of 2 cm. From these roughness profiles, the root mean square surface height (*Hrms*) were then calculated for each reference plot using the mean of all autocorrelation functions acquired for each reference plot. All data bases are described in (Bousbih et al., 2017). For the French site, soil roughness was estimated with a fully automatic photogrammetric method (Gilliot et al., 2017). The rms surface height ranged between 0.56 cm and 4.55 cm for the reference plots in the Tunisian site and between 0.41 cm and 2.90 cm for the reference plots in the French site.

Finally, each element of our real dataset corresponds to in situ measurements (*mv* and *Hrms*) and Sentinel-1 information (mean of radar backscattered coefficients in VV and VH, and radar incidence angle). The mean of radar backscattered coefficients was calculated by averaging for each reference plot the values of all pixels within the reference plot.

## V.3 Methodology for estimating soil moisture

### V.3.1 Neural Networks

In this study, surface roughness was estimated by means of multi-layer perceptron (MLP) neural networks. The Levenberg-Marquardt optimization algorithm (Marquardt, 1963) was used to train the Neural Networks. The Neural Networks (NN) architecture is created from three layers: input, hidden, and output. The NNs have two dimensional input vectors when using one polarization (VV or VH) which are the backscattered signal and the incidence

angle. Using two polarizations (VV and VH), the NNs have three dimensional input vectors which are the two backscattered signals (VV and VH) and the incidence angle. In order to estimate only *mv* or *Hrms*, the output vector contains only the soil moisture (*mv*) or the soil surface roughness (*Hrms*). When the estimation concern both *Hmrs* and *mv*, the two dimensional output vector contains both soil moisture and surface roughness. The numbers of neurons associated with the hidden layer was determined by training the Neural Networks using different numbers of neurons. 20 hidden neurons provided accurate estimates of reference parameters (Baghdadi et al., 2012a; Chai et al., 2009). To develop a neural network, it is necessary to train the network with training synthetic dataset composed of input and output vectors. Training is accomplished to minimize the mean square error between the predicted Neural Networks outputs and the reference values. All transfer functions were tested in the Neural Networks which give different results. Best results are shown by the Purlin and Tansig transfer functions for the estimation of soil moisture and Logsig for the estimation of the surface roughness.

### V.3.2 Methodological overview

An approach based on neural networks is chosen to estimate the soil roughness from Sentinel-1 images (SAR data) over bare agricultural soils at very high spatial resolution ″VHSR″ (plot scale or on a finer scale). Two networks are applied one after the other, the first to estimate soil moisture and the second to estimate soil roughness. Three SAR configurations corresponding to the standard acquisition mode of Sentinel-1 with image acquisitions in both VV and VH polarizations are tested: VV alone, VH alone, VV and VH together. In order to improve the soil parameters estimates, a priori knowledge about soil moisture *mv* is introduced. Baghdadi et al. (2012a) showed that the use of a priori knowledge on the soil moisture (dry to slightly wet or very wet information) improves the soil moisture estimates. The priori information on *mv* is provided in using meteorological data (precipitations, temperature) and terrain knowledge. Indeed, it is easily to define from the weather forecasts (precipitation and temperature) if the soil is either dry to slightly wet (no precipitation for many days before SAR acquisition) or very wet (heavy rainfall preceding SAR acquisition). The integration of a priori information constrains the range of possible soil moisture parameter values estimated and thus leads to a better estimation of the soil moisture.

Three neural networks are developed for the estimation of *mv*, with and without a *priori* information on the soil moisture state:

- Case 1: No *a priori* information is available on the soil moisture state. In this case *mv* will be estimated between 2 and 40 vol.%.

- Case 2: *A priori* information is available on *mv*. The soil is supposed to be dry to slightly wet according to expertise based mainly on meteorological data (precipitations, temperature). Soil moisture values are assumed to range from 2 to 25 vol.%.

- Case 3: *A priori* information is available on *mv*. The soil is supposed to be very wet according to expertise based on meteorological data. *mv*-values are assumed to vary between 25 and 40 vol.%.

The three NNs use the backscattering coefficient in each SAR configuration (VV polarization alone, VH polarization alone, VV and VH polarizations together) and the incidence angle as input. The output is only the soil moisture *mv*. An overlapping of 10 vol.% on *mv* was used on the training datasets of the two networks in the cases of a priori information on the soil moisture *mv*. So that, in the case of dry to slightly wet soils, the *mv*-values used for the training ranged from 2 to 30 vol.%. In the case of very wet soils, the *mv*-values used for the training ranged from 20 to 40 vol.%.

Next, the soil roughness could be estimated at a fine spatial scale (plot or sub-plot scale) using the soil moisture estimated by the first network. The standard acquisition mode of Sentinel-1 corresponds to acquisitions in both VV and VH polarizations. The Neural Networks used to estimate the soil roughness use the backscattering coefficient in VV alone, VH alone, VV and VH together and the incidence angle and the estimated soil moisture as input. The output is the soil surface roughness. The validation of these NNs will be made using the soil moisture estimated without and with a priori information on *mv*.

## V.4 Results and discussion

The different neural networks are tested for the evaluation of the precision on soil roughness estimates using synthetic (built from IEM model and Baghdadi model) and real datasets.

### V.4.1 Synthetic dataset

In this first approach, the estimation of soil roughness (*Hrms*) requires the use of an estimate of the soil moisture (*mv*). First, we will discuss the performance of networks developed for the estimation of *mv*. Then, network built for estimating *Hrms* is analyzed.

#### *V.4.1.1 Estimation of mv*

##### *V.4.1.1.1 Using the IEM model*

In order to estimate the soil moisture *mv*, three radar configurations will be tested: VV alone, VH alone, VV and VH together.

###### *V.4.1.1.1.1 Use of VV polarization alone*

First the results are discussed in using the synthetic dataset simulated from the Integral Equation Model (IEM). In the case of VV polarization and *mv* between 2 and 40 vol.%, the RMSE on the *mv* estimates is of 4.89 vol.% for *mv* between 2 and 25 vol.% and 6.64 vol.% for *mv* between 25 and 40 vol.%. An overestimation of +2.40 vol.% on *mv* is observed for *mv* between 2 and 25 vol.%, and an underestimation of -3.84 vol.% is obtained for *mv* between 25 and 40 vol.%. For the entire range of *mv*, between 2 and 40%, the RMSE on *mv* is of 5.66 vol.% (Figure V.2a).

In the case where the NNs were trained using a priori information on *mv* with dry to slightly wet soil conditions (training with *mv* between 2 and 30 vol.% and validation using *mv* between 2 and 25 vol.%), results show that the introduction of a priori information on *mv* improves the *mv* estimates. The RMSE on *mv* estimates decreases from 4.89 vol.% without a priori information on *mv* to 3.58 vol.% in the case of a priori information on *mv*. In addition, the difference between estimated and measured *mv* is also reduced from 2.40 vol.% to 1.06 vol.% (Figure V.2b).

In addition, the use of a priori information on *mv* in the case of very wet soil conditions also improves the *mv* estimates. The RMSE on *mv* estimates decreases from 6.64 vol.% without a priori information on *mv* to 5.04 vol.% in the case of a priori information on *mv*. In addition, the difference between estimated and measured *mv* is also reduced from -3.84 vol.% to -2.29 vol.% (Figure V.2c).

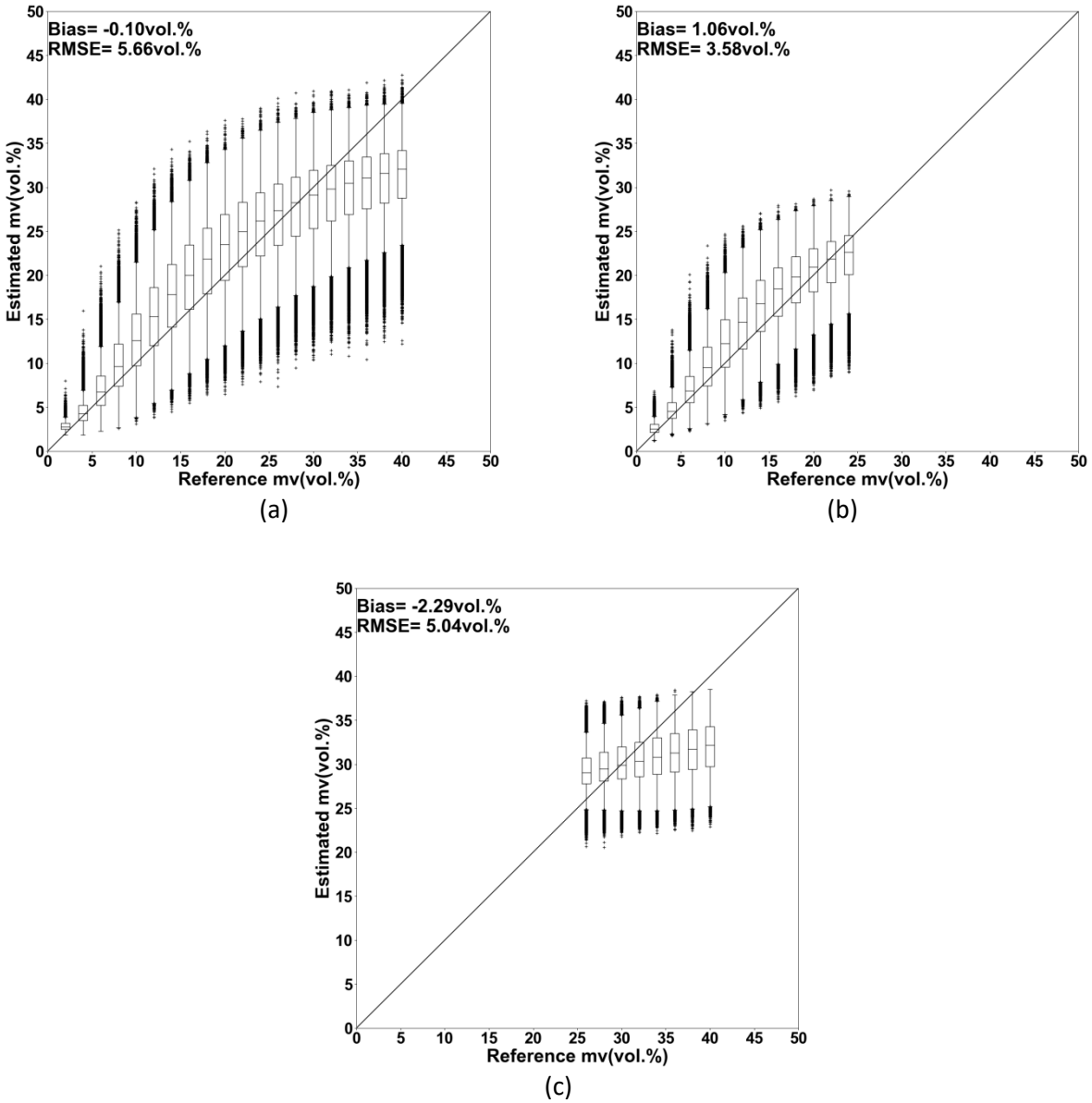


**Figure V.2.** Box plots of *mv* estimates retrieved from the synthetic dataset generated using IEM. Neural networks were trained and validated using VV polarization alone. (a): no a priori information on *mv*; (b): with a prior information on *mv* and dry to slightly wet soil conditions; (c): with a prior information on *mv* and very wet soil condition.

First the performance of the inversion algorithm was analyzed according to *Hrms* and incidence angle "θ" (Figure V.3) in the case without a priori on *mv* is used. For VV, results show that the bias (estimated *mv* - measured *mv*) and the RMSE are strongly dependent on *Hrms* (Figures V.3a and V.3b). The RMSE on *mv* in the case of inversion without a priori information on *mv* increases from 4.40 vol.% for *Hrms*=0.5 cm to 7.0 vol.% for *Hrms* = 3.8 cm for *mv* between 2 and 25 vol.% (dry to slightly wet soils). In very wet soil conditions, the RMSE on *mv* decreases from 11.5 vol.% for *Hrms*=0.5 cm to 4.0 vol.% for *Hrms* = 3.8 cm. The high RMSE values of in the case of dry to slightly wet conditions and high *Hrms*-values

are due to an overestimation of *mv* (bias increases from -3.0 to +5.0 vol.% for *Hrms* between 0.5 and 3.8 cm). Similarly, the high RMSE values in the case of very wet conditions and low *Hrms*-values are due to an underestimation of *mv* (bias decreases from -11.0 to -1.5 vol.% for *Hrms* between 0.5 and 3.8 cm). In addition, results show that the RMSE on *mv* slightly depends on θ in the case of no a priori information on *mv* (Figures V.3c and V.3d). The RMSE on *mv* is between 4.2 vol.% (for θ=20°) and 5.0 vol.% (for θ between 25° and 45°) for dry to slightly wet soil conditions and between 6.0 and 7.0 vol.% for very wet soils. The overestimation of *mv* in dry to slightly conditions is approximately +2.5 vol.% for θ between 20° and 45°. For very wet soil conditions, the underestimation of *mv* is approximately -4.0 vol.% for θ between 20° and 45°.

In the case of a priori information on *mv* with dry to slightly wet soil conditions, the RMSE on *mv* estimates varies between 2.2 and 5.0 vol.% for all *mv* and *Hrms* values of the validation synthetic dataset (case of dry to slightly wet conditions). The bias reduction varies between -3.0 vol. % (low *Hrms*) and +3.0 vol.% (high *Hrms*). In addition, RMSE and bias on *mv* estimates are slightly dependent on the incidence angle.

In the case of a priori information on *mv* with very wet soil conditions, the RMSE on *mv* estimates varies between 4.3 and 7.0 vol.% for all *mv* and *Hrms* values of the validation synthetic dataset in the case of very wet conditions. The highest RMSE-values correspond to low *Hrms*-values. The bias is also well reduced mainly for low *Hrms*-values from -6.0 vol.% to –1.0 vol.% for *Hrms*-values of 3.8 cm. The analysis of the RMSE and the bias shows relatively close values according to the incidence angle. The RMSE is about 5.00 vol.% for incidence angle between 20° and 45° and the bias is about -2.5 vol.% for incidence angle between 20° and 45° (Figures V.3c and V.3d).

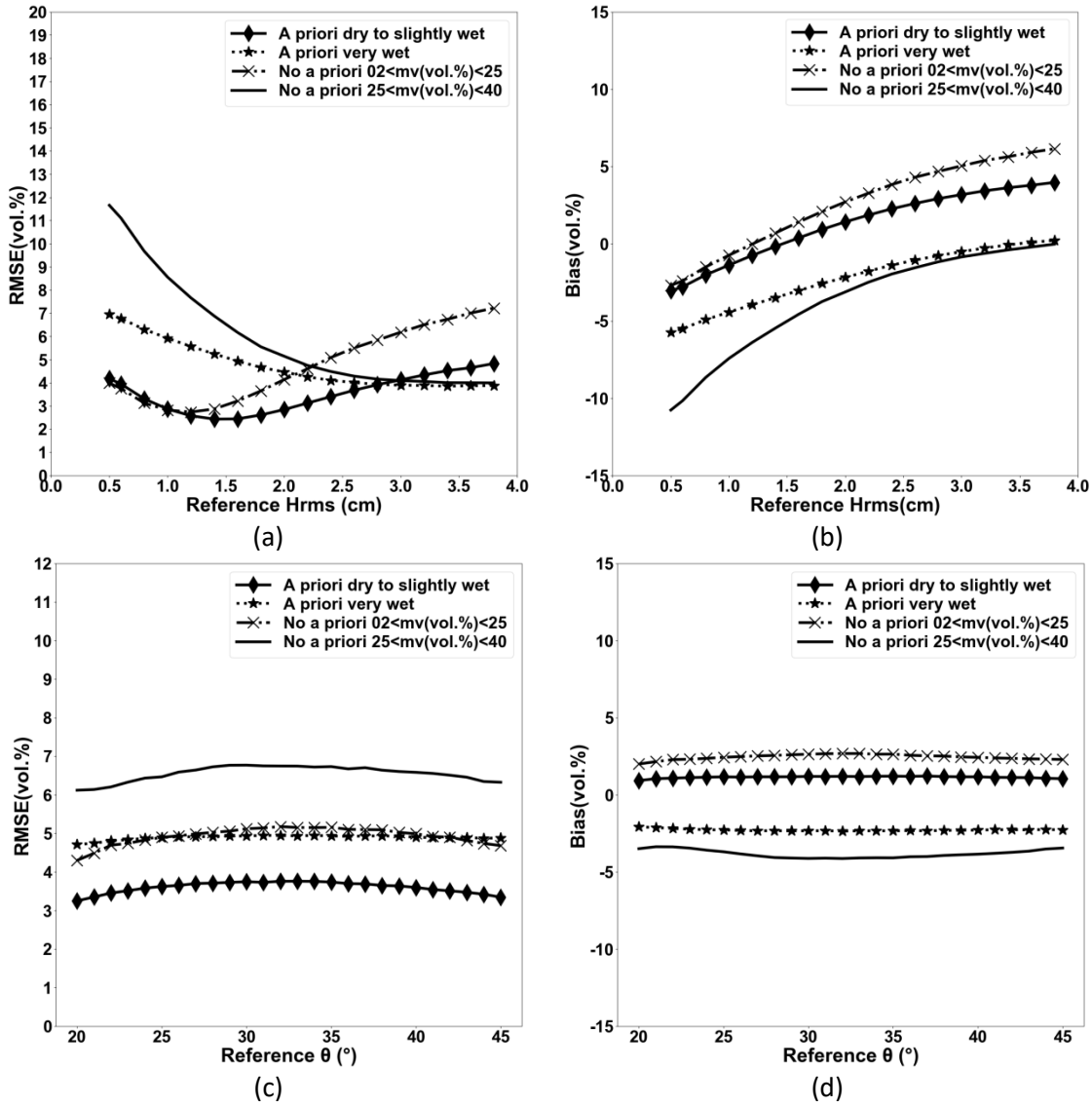


**Figure V.3.** Accuracy on the *mv* estimates (RMSE and bias "=estimated – measured") retrieved from the synthetic dataset in VV polarization using IEM. Three NNs are tested: without a priori information on *mv* (case 1), with a priori information on *mv* with dry to slightly wet soil conditions (case 2), with a priori information on *mv* with very wet conditions (case 3).

*V.4.1.1.1.2 Use of VH polarization alone*

In the case of VH polarization and *mv* between 2 and 40 vol.%, the RMSE on the *mv* estimates is of 5.27 vol.% for *mv* between 2 and 25 vol.% and 8.27 vol.% for *mv* between 25 and 40 vol.%. An overestimation of 2.94 vol.% on *mv* is observed for *mv* between 2 and 25 vol.%, and an underestimation of -4.64 vol.% is obtained for *mv* between 25 and 40 vol.%. Moreover, the RMSE for all the range of *mv* between 2 and 40% is 6.63 vol.% (Figure V.4a).

The RMSE on *mv* estimates decreases from 5.27 vol.% without a priori information on *mv* to 4.16 vol.% in the case of a priori information on *mv* for dry to slightly wet soil conditions. Also, the difference between estimated and measured *mv* is well reduced (approximately by a factor of 2) from 2.94 vol.% to 1.23 vol.% (Figure V.4b).

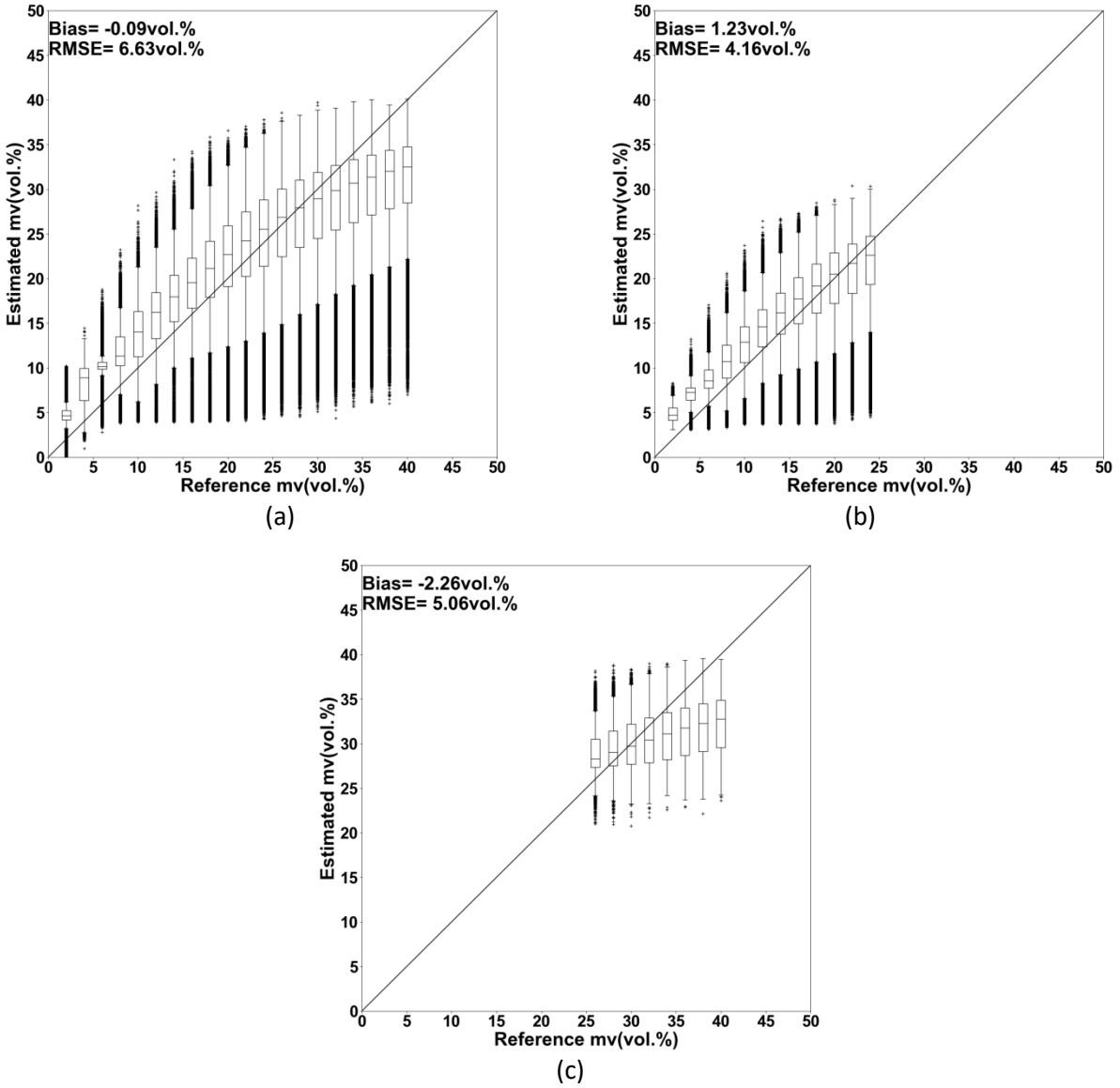


**Figure V.4.** Box plots of *mv* estimates retrieved from the synthetic dataset generated using IEM. Neural networks were trained and validated using VH polarization alone. (a): no a priori information on *mv*; (b): with a prior information on *mv* and dry to slightly wet soil conditions; (c): with a prior information on *mv* and very wet soil condition.

Results also show that the use of a priori information on *mv* in the case of very wet soil conditions improves slightly the *mv* estimates. The RMSE on *mv* estimates decreases from

8.27 vol.% without a priori information on *mv* to 5.06 vol.% in the case of a priori information on *mv*. In addition, the difference between estimated and measured *mv* is also well reduced from -4.64 vol.% to -2.26 vol.% (Figure V.4c).

First the performance of the inversion algorithm was analyzed according to *Hrms* and incidence angle "θ" in the case without a priori on *mv* is used. For VH polarization alone (Figure V.5), the performance analysis of the inversion algorithm shows that the bias (estimated *mv* - measured *mv*) and the RMSE on *mv* are strongly dependent on *Hrms* (Figures V.5a and V.5b). The RMSE on *mv* in the case of inversion without a priori information on *mv* increases from 6.60 vol.% for *Hrms*=0.5 cm to 7.0 vol.% for *Hrms* = 3.8 cm for *mv* between 2 and 25 vol.% (dry to slightly wet soils). In very wet soil conditions, the RMSE on *mv* decreases from 19.0 vol.% for *Hrms*=0.5 cm to 4.0 vol.% for *Hrms* = 3.8 cm. The high RMSE values of in the case of very wet conditions and low *Hrms*-values are due to an underestimation of *mv* (bias increases from -19.0 to 0.0 vol.% for *Hrms* between 0.5 and 3.8 cm). Similarly, the high RMSE values in the case of dry to slightly wet conditions and low *Hrms*-values are due to an overestimation of *mv* (bias increases from -6.0 to 6.0 vol.% for *Hrms* between 0.5 and 3.8 cm). Moreover, results show that the RMSE on *mv* slightly depends on θ in the case of no a priori information on *mv* (Figures V.5c and V.5d). The RMSE slightly decreases from 5.70 vol.% for θ=20° to 4.8 vol.% for θ = 45° in the case of dry to slightly wet soil conditions. It also slightly decreases from 8.5 vol.% for θ=20° to 7.5 vol.%(for θ = 45° for very wet soils. The overestimation of *mv* in dry to slightly conditions is approximately +3.0 vol.% for θ between 20° and 45°. For very wet soil conditions, the underestimation of *mv* is approximately about 5.0 vol.% for θ between 20° and 45°.

In the case of a priori information on *mv* with dry to slightly wet soil conditions, the quality of the estimation is also well improved when the accuracy on *mv* estimates is analyzed according to *Hrms* and θ (Figure V.5). The RMSE on *mv* estimates varies between 3.0 and 7.5 vol.% for all *mv* and *Hrms* values of the validation synthetic dataset (case of dry to slightly wet conditions). The bias reduction varies between -6.0 vol. % for low *Hrms*-values and +4.0 vol.% for high *Hrms*-values. In addition, RMSE and bias on *mv* estimates are slightly dependent on the incidence angle.

In the case of a priori information on *mv* with very wet soil conditions, the RMSE on *mv* estimates varies between 3.0 and 7.0 vol.% for all *mv* and *Hrms* values of the validation

synthetic dataset (case of very wet conditions). The highest RMSE-values correspond to low *Hrms*-values. The bias is also well reduced mainly for low *Hrms*-values from -6.0 vol.% for *Hrms*-values of 0.5 cm to –1.0 vol.% for *Hrms*-values of 3.8 cm. The analysis of the RMSE and the bias shows relatively close values according to the incidence angle. The RMSE is about 5.00 vol.% for incidence angle between 20° and 45° and the bias is about -2.5 vol.% for incidence angle between 20° and 45° (Figures V.5c and V.5d).

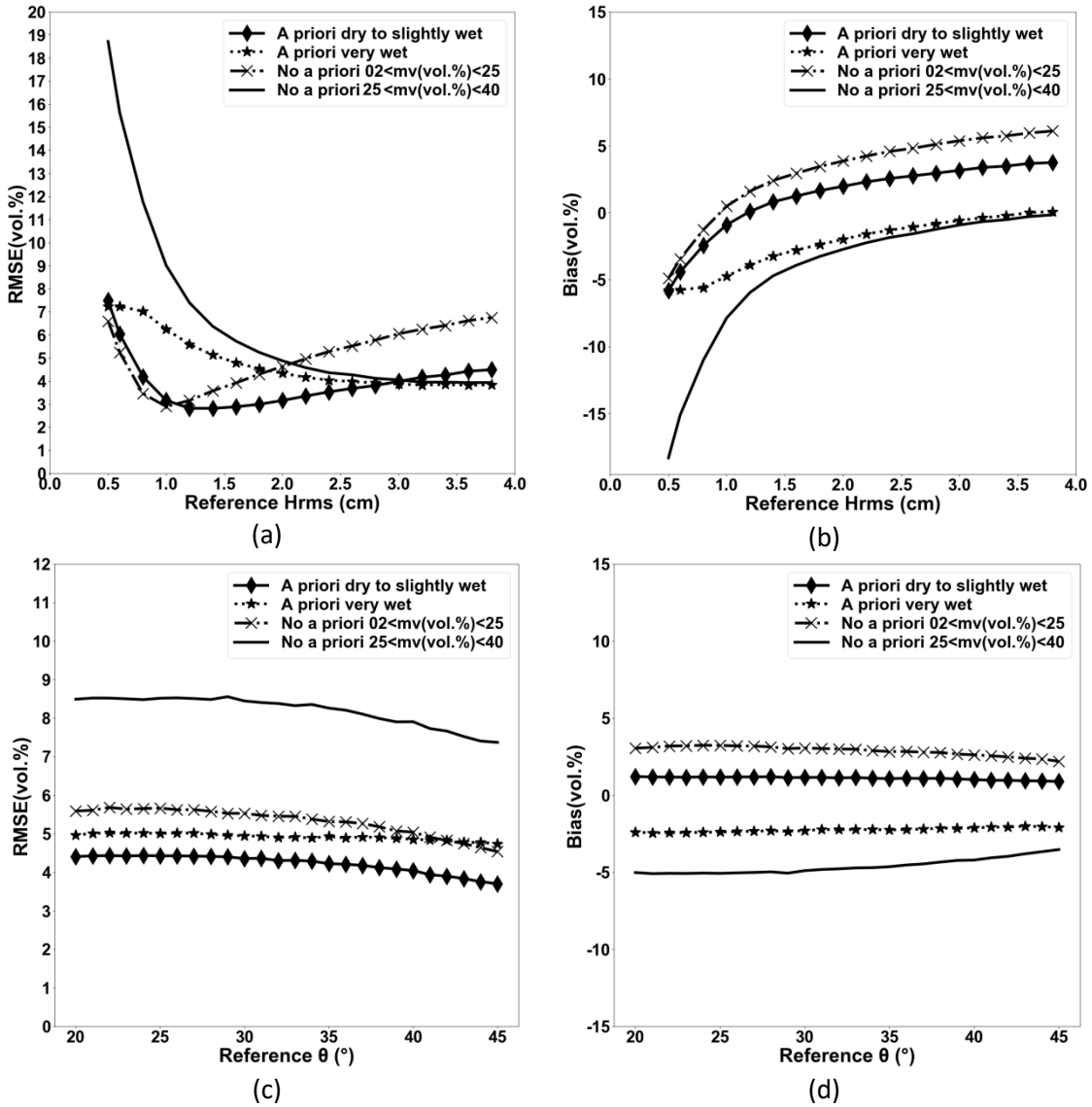


**Figure V.5.** Accuracy on the *mv* estimates (RMSE and Bias "=estimated – measured") retrieved from the synthetic dataset in VH polarization using IEM. Three NNs are tested: without a priori information on *mv* (case 1), with a priori information on *mv* with dry to slightly wet soil conditions (case 2), with a priori information on *mv* with very wet conditions (case 3).

*V.4.1.1.1.3 Use of VV and VH polarizations together*

In the case of VV and VH polarizations together and *mv* between 2 and 40 vol.%, the RMSE on the *mv* estimates is of 4.33 vol.% for *mv* between 2 and 25 vol.% and 6.27 vol.% for *mv* between 25 and 40 vol.%. An overestimation of +2.vol.% on *mv* is observed for *mv* between 2 and 25 vol.%, and an underestimation of -3.23 vol.% is obtained for *mv* between 25 and 40 vol.%. For the entire range of *mv*, between 2 and 40%, the RMSE on *mv* is of 5.19 vol.% (Figure V.6a).

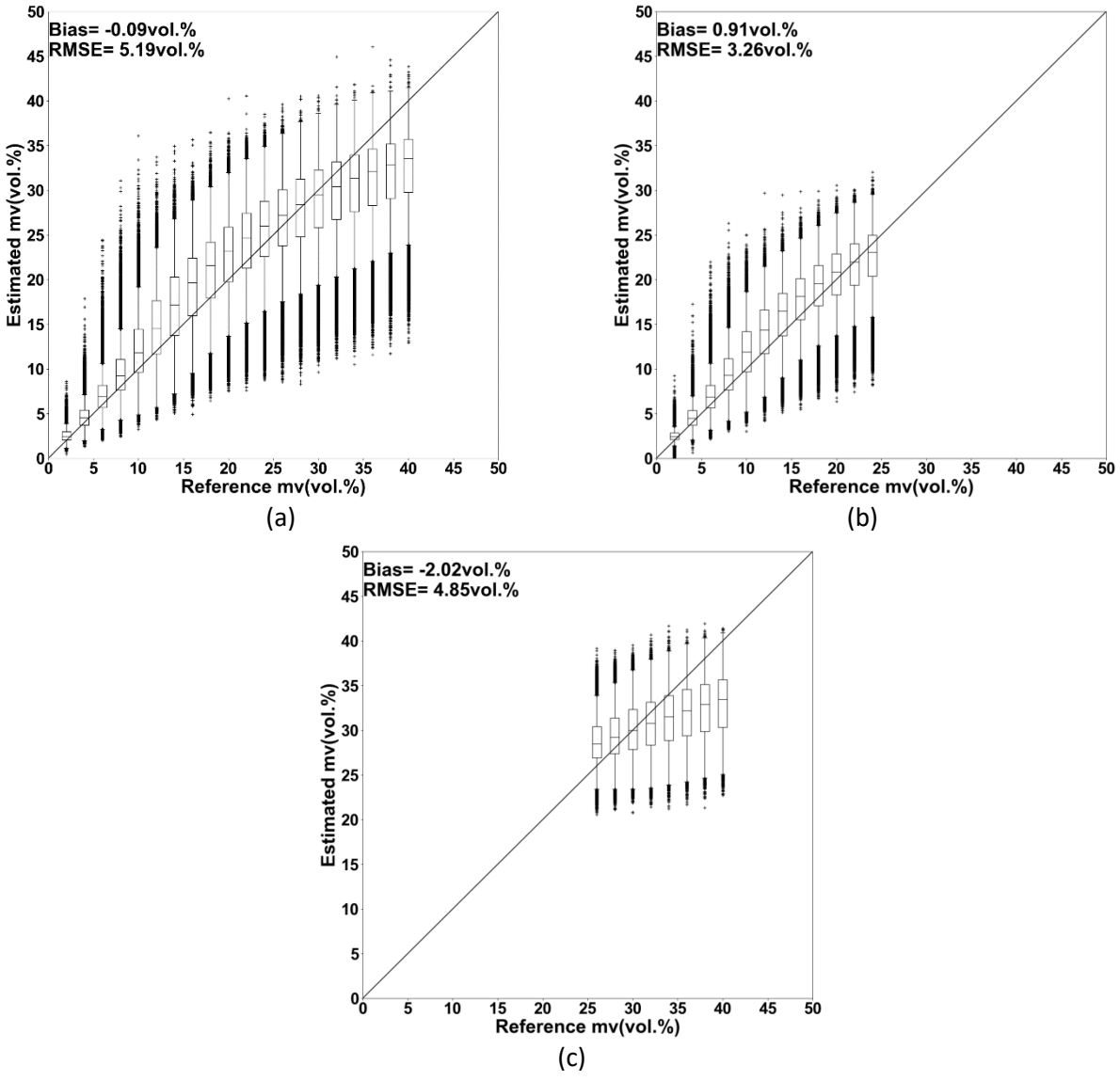


**Figure V.6.** Box plots of *mv* estimates retrieved from the synthetic dataset generated using IEM. Neural networks were trained and validated using VV and VH polarization together. (a): no a priori information on *mv*; (b): with a prior information on mv and dry to slightly wet soil conditions; (c): with a prior information on *mv* and very wet soil condition.

With a priori information on *mv* with dry to slightly soil conditions, the RMSE on *mv* estimates decreases from 4.33 vol.% without a priori information on *mv* to 3.26 vol.% in the case of a priori information on *mv*. In addition, the difference between estimated and measured *mv* is also reduced from +2.00 vol.% to +0.91 vol.% (Figure V.6b).

The use of a priori information on *mv* in the case of very wet soil conditions improves the estimation of *mv*. The RMSE on *mv* estimates decreases from 6.27 vol.% without a priori information on *mv* to 4.85 vol.% in the case of a priori information on *mv*. Also, the difference between estimated and measured *mv* is reduced from -3.23 vol.% to -2.02 vol.% (Figure V.6c).

First the performance of the inversion algorithm was analyzed according to *Hrms* and incidence angle "θ" in the case without a priori on *mv* is used (Figure V.7). Results show that the RMSE on *mv* in the case of inversion without a priori information on *mv* increases from 4.80 vol.% for *Hrms*=0.5 cm to 7.0 vol.% for *Hrms* = 3.8 cm in dry to slightly wet soil conditions (*mv* between 2 and 25 vol.%) (Figures V.7a and V.7b). In very wet soil conditions, the RMSE on *mv* decreases from 12.50 vol.% for *Hrms*=0.5 cm to 4.0 vol.% for *Hrms* = 3.8 cm. The high RMSE values in the case of very wet conditions and low *Hrms*-values are due to an underestimation of *mv* (bias increases from -5.0 to +5.0 vol.% for *Hrms* between 0.5 and 3.8 cm). Similarly, the high RMSE values in the case of dry to slightly wet conditions and low *Hrms*-values are due to an overestimation of *mv* (bias increases from –12.0 to 0.0 vol.% for *Hrms* between 0.5 and 3.8 cm). Moreover, results show that the RMSE on *mv* slightly depends on θ in the case of no a priori information on *mv* in the inversion process in the case of VV and VH polarizations together (Figures V.7c and V.7d). The RMSE is approximately about 6.0 vol.% for θ between 20° and 45° for dry to slightly wet soil conditions and about 4.50 vol.% for θ between 20° and 45° for very wet soils. The overestimation of *mv* in dry to slightly conditions is approximately +2.0 vol.% for θ between 20° and 45°. For very wet soil conditions, the underestimation of *mv* is approximately about -3.0 vol.% for θ between 20° and 45°.

With a priori information on *mv* with dry to slightly soil conditions, the estimation quality is also well improved when the accuracy on *mv* estimates is analyzed according to *Hrms* and θ (Figures V.7). The RMSE on *mv* estimates varies between 2.0 and 5.0 vol.% for all *mv* and

*Hrms* values of the validation synthetic dataset (case of dry to slightly wet conditions). The bias reduction varies between -4.0 vol. % (low *Hrms*) and +4.0 vol.% (high *Hrms*). Finally, RMSE and bias on *mv* estimates are slightly dependent on the incidence angle. The RMSE is about 3.00 vol. % for incidence angle between 20° and 45° and the bias is about -2.50 vol. % for incidence angle between 20° and 45°.

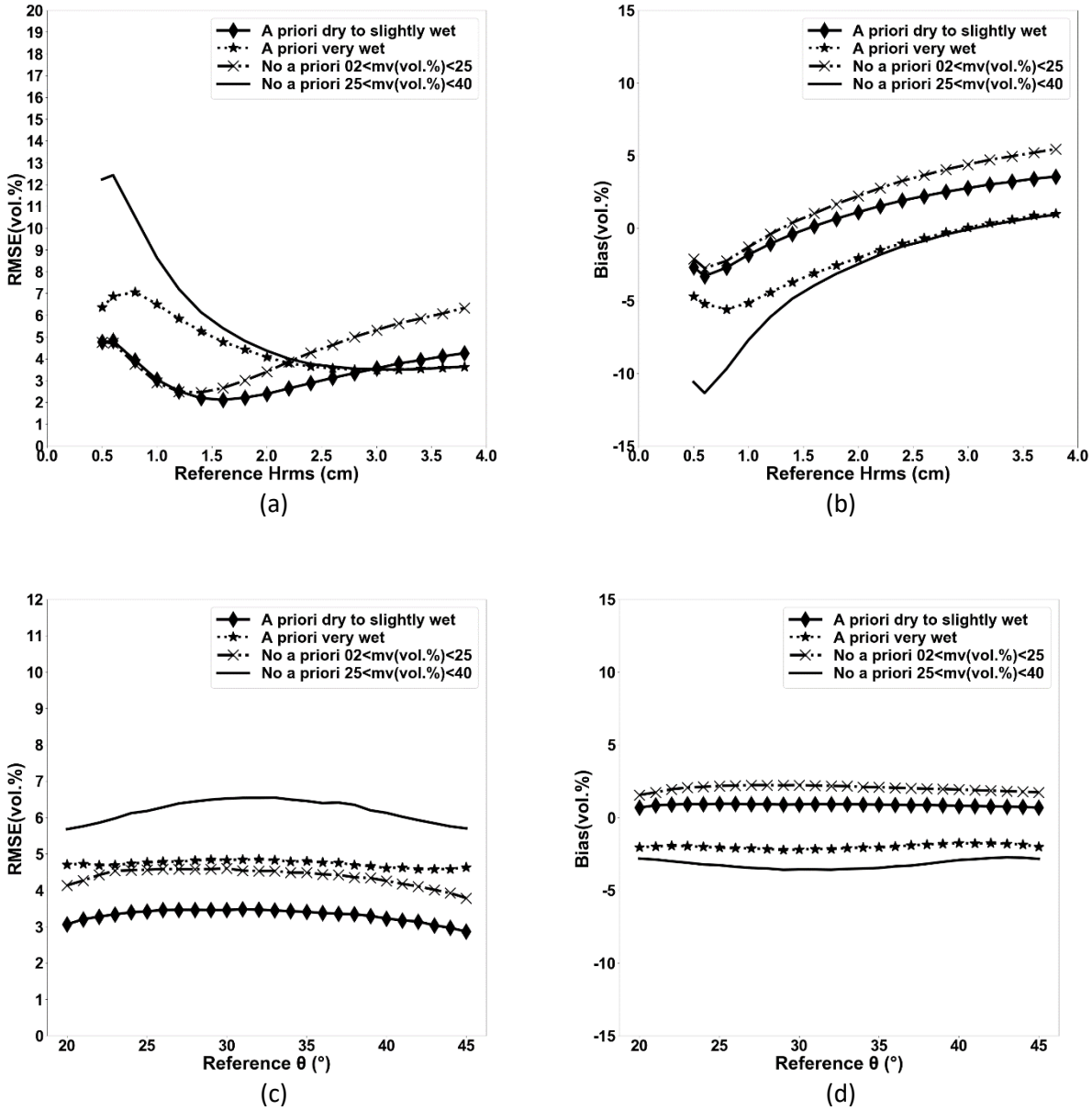


**Figure V.7.** Accuracy on the *mv* estimates (RMSE and Bias "=estimated – measured") retrieved from the synthetic dataset in VV and VH polarizations together using IEM. Three NNs are tested: without a priori information on *mv* (case 1), with a priori information on *mv* with dry to slightly wet soil conditions (case 2), with a priori information on *mv* with very wet conditions (case 3).

With a priori information on *mv* with very wet soil conditions, the RMSE on *mv* estimates varies between 3.0 and 7.0 vol.% for all *mv* and *Hrms* values of the validation synthetic dataset in the case of very wet conditions. The highest RMSE-values correspond approximately to low *Hrms*-values. The bias is also well reduced mainly for low *Hrms*-values from -6.0 vol.% for *Hrms*-values of 0.5 cm to +1.0 vol.% for *Hrms*-values of 3.8 cm. According to the incidence angle, the RMSE and the bias shows relatively close values. The RMSE is about 4.9 vol.% for incidence angle between 20° and 45° and the bias is about -2.0 vol.% for incidence angle between 20° and 45° (Figures V.7c and V.7d).

*V.4.1.1.2 Using Baghdadi model*

Three radar configurations will be tested in order to analyze the accuracy on *mv* estimates: VV alone, VH alone, VV and VH together.

*V.4.1.1.2.1 Use of VV polarization alone*

In the case of no a priori information on *mv*, the RMSE on the *mv* estimates is of 7.03 vol.% for *mv* between 2 and 25 vol.% and 8.43 vol.% for *mv* between 25 and 40 vol.%. An overestimation of +3.39 vol.% on *mv* is observed for *mv* between 2 and 25 vol.%, and an underestimation of -5.09 vol.% is obtained for *mv* between 25 and 40 vol.%. For the entire range of *mv*, between 2 and 40%, the RMSE on *mv* is of 7.62 vol.% (Figure V.8a).

Results show that the introducing of a priori information on *mv* improves the *mv* estimates. The RMSE on *mv* estimates decreases from 7.03 vol.% without a priori information on *mv* to 5.88 vol.% in the case of a priori information on *mv* for dry to slightly wet soil conditions. In addition, the difference between estimated and measured *mv* is also reduced from +3.39 vol.% to +1.64 vol.% (Figure V.8b).The use of a priori information on *mv* in the case of very wet soil conditions improves the *mv* estimates. The RMSE on *mv* estimates decreases from 8.43 vol.% without a priori information on *mv* to 4.79 vol.% in the case of a priori information on *mv*. In addition, the difference between estimated and measured *mv* is also well reduced from -5.09 vol.% to -1.52 vol.% (Figure V.8c).

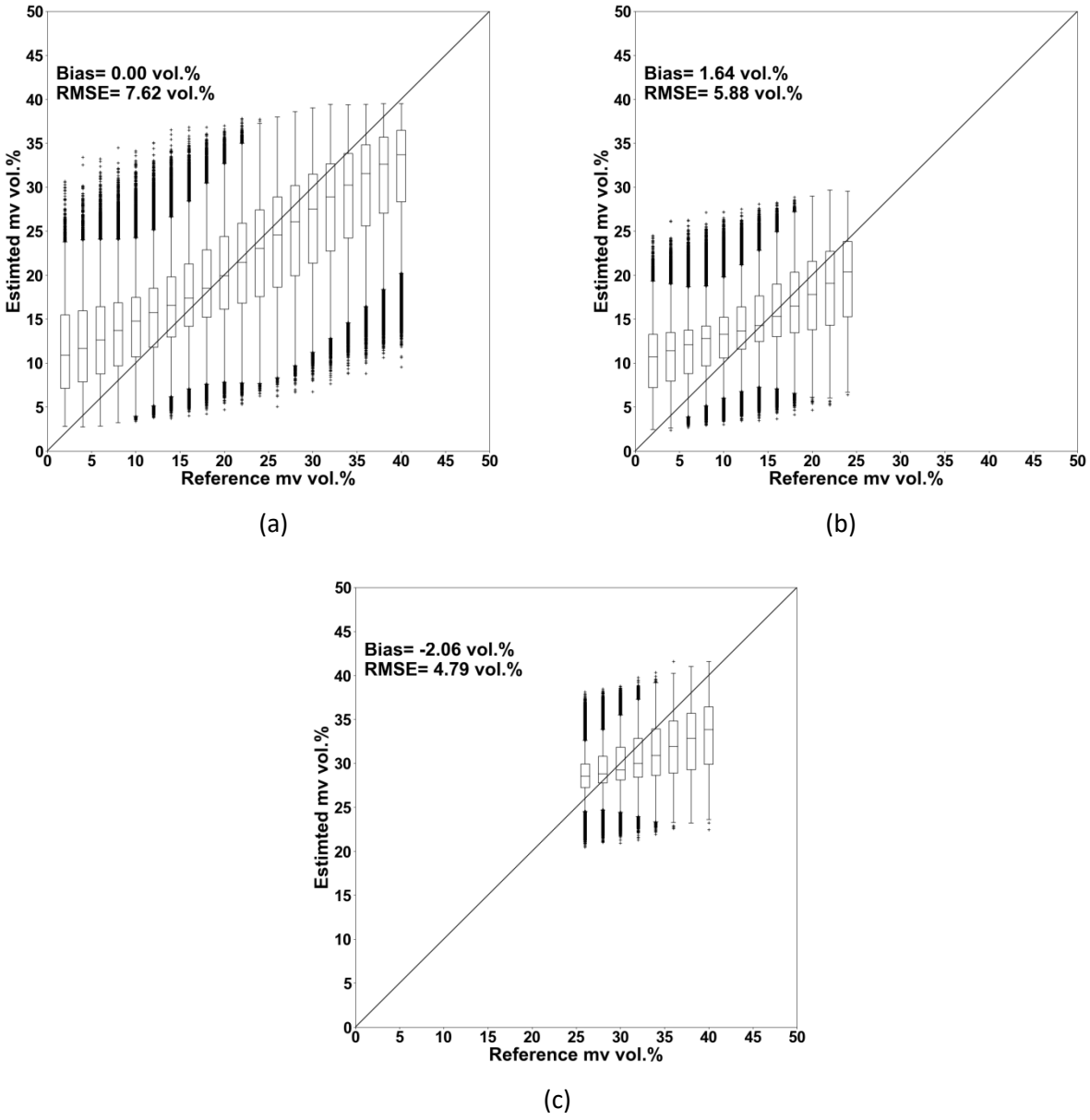


**Figure V.8.** Box plots of *mv* estimates retrieved from the synthetic dataset generated using Baghdadi model. Neural networks were trained and validated using VV polarization alone. (a): no a priori information on *mv*; (b): with a prior information on *mv* and dry to slightly wet soil conditions (*mv* between 2 and 25 vol.%); (c): with a prior information on *mv* and very wet soil condition (*mv* between 25 and 40 vol.%).

The performance of the algorithm was also analyzed according to *Hrms* and the incidence angle "θ" (Figure V.9). Results show that the bias (estimated *mv* - measured *mv*) and the RMSE are strongly dependent on *Hrms* and θ. According to *Hrms*, the RMSE on *mv* in the case of inversion without a priori information on *mv* increases from 6.0 vol.% for *Hrms*=0.5 cm to 10.0 vol.% for *Hrms* = 3.8 cm in the case of dry to slightly wet soils. In very wet soil conditions, the RMSE on *mv* decreases from 14.5 vol.% for *Hrms*=0.5 cm to 4.0 vol.% for

*Hrms* = 3.8 cm. The high RMSE values of in the case of dry to slightly wet conditions and high *Hrms*-values are due to an overestimation of *mv* (bias increases from -2.5 to +8.0 vol.% for *Hrms* between 0.5 and 3.8 cm). Similarly, the high RMSE values in the case of very wet conditions and low *Hrms*-values are due to an underestimation of *mv* (bias about -13.0 for *Hrms*=0.5cm).

According to the incidence angle "θ", results show that the RMSE on *mv* is strongly dependent on θ in the case of no a priori information on *mv* (Figures V.9c and V.9d). The RMSE increases from 4.0 vol.% (for θ=20°) to 9.0 vol.% (for θ= 45°) for dry to slightly wet soils and increases from 4.0 (for θ=20°) to 11.0 vol.% (for θ=45°) for very wet soil conditions. In the case of dry to slightly wet conditions with high incidence angle values, the high RMSE values are due to an overestimation of *mv* (bias increases from +1.0 to +5.5 vol.% for θ between 20° and 45°). Similarly, the high RMSE values in the case of very wet conditions and high incidence angle values are due to an underestimation of *mv* (bias decreases from -1.5 to -9.0 vol.% for θ between 20° and 45°).

The RMSE on *mv* estimates varies slightly with *Hrms* in the case of a priori information on *mv* for dry to slightly wet soils (between 6.0 and 7.1 vol.%) (Figure V.9).In addition, RMSE and bias on *mv* estimates are also dependent on the incidence angle "θ". The RMSE increases from 4.0 vol. % for θ=20° to 7.0 vol. % for θ=45°. The overestimation of *mv* increases from +1.0 to +2.5 vol.% for θ between 20° and 45°.

Figure V.9 shows that the RMSE on mv estimates is well reduced in the case of a priori information on *mv* for very wet soil conditions (it varies between 4.0 and 7.0 vol.%). The highest RMSE-values correspond to low *Hrms*-values. The underestimation of *mv* is well reduced mainly for low *Hrms*-values from -13.0 vol.% without a priori information on *mv* to -6.0 vol.% with a prior information *on mv* (case of very wet conditions). In addition, the analysis of the RMSE on *mv* estimates shows that the RMSE is well reduced mainly for high incidence angles (θ=45°) from 11.0 vol.% without a priori information on *mv* to 5.1 vol.% with a priori information on *mv*. Moreover, the underestimation on *mv* is well decreased from -9.0 vol.% .% without a priori information on *mv* to -2.5 vol.% with *a* priori information on *mv* (case of very wet conditions and θ=45°).

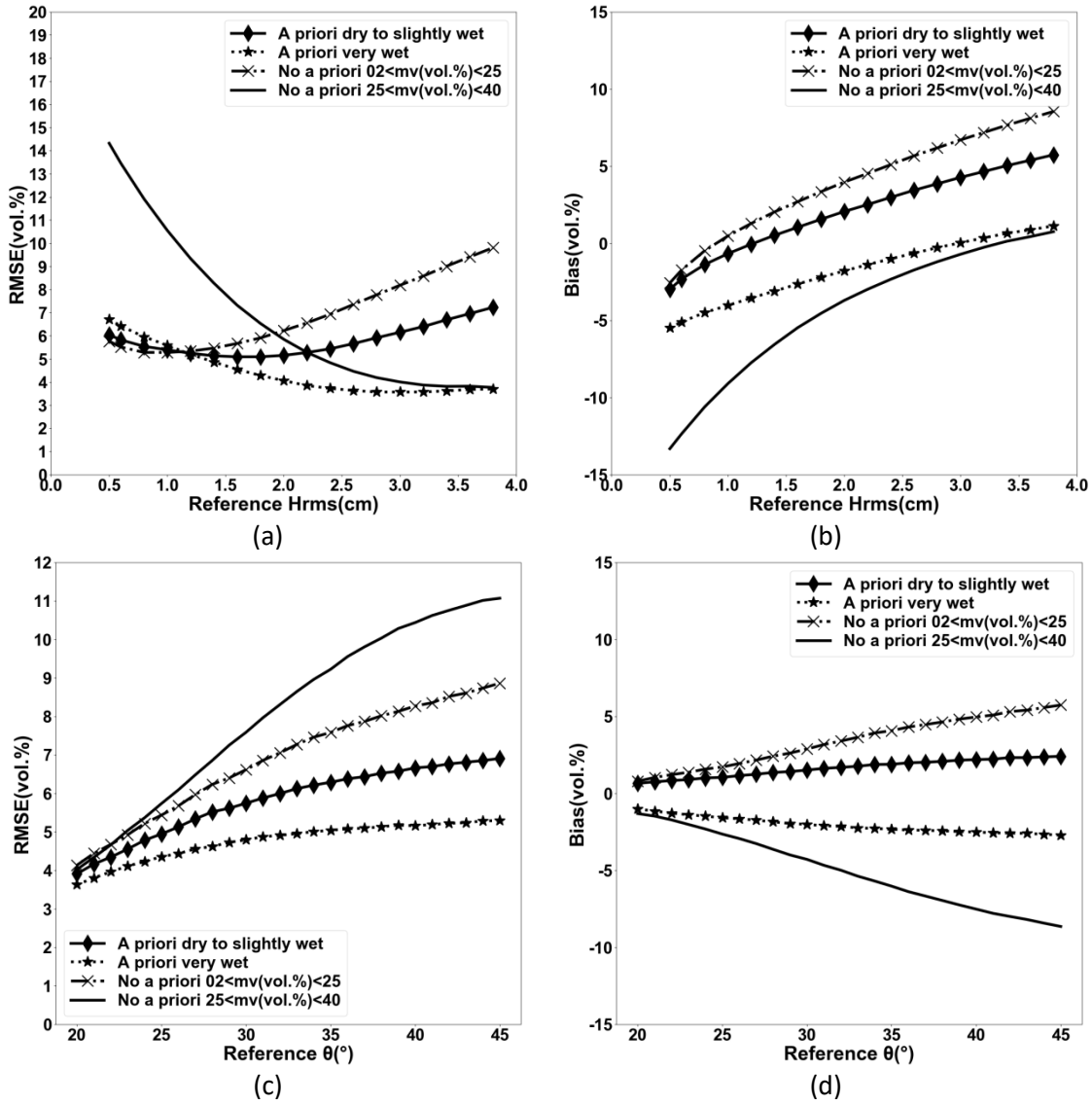


**Figure V.9.** Accuracy on the *mv* estimates (RMSE and bias "=estimated – measured") retrieved from the synthetic dataset in VV polarization using Baghdadi model. Three NNs are tested: without a priori information on *mv* (case 1), with a priori information on *mv* with dry to slightly wet soil conditions (case 2), with a priori information on *mv* with very wet conditions (case 3).

*V.4.1.1.2.2 Use of VH polarization alone*

In using VH alone, the RMSE on *mv* is of 6.05 vol.% in the case of no a priori information on *mv* (Figure V.10a). For *mv* between 2 and 25 vol.%, the RMSE on *mv* is of 5.91 vol.%. It is of 6.25 vol.% for *mv* between 25 and 40 vol.%. An overestimation of +2.08 vol.% on *mv* is observed for *mv* between 2 and 25 vol.%, and an underestimation of -3.15 vol.% is obtained for *mv* between 25 and 40 vol.%.

Results show that the introduction of a priori information on *mv* improves the *mv* estimates. The RMSE on *mv* estimates decreases from 5.91 vol.% without a priori information on *mv* to 5.15 vol.% in the case of a priori information on *mv* for dry to slightly wet soils. For very wet soils, the RMSE on *mv* estimates decreases from 6.27 vol.% without a priori information on *mv* to 4.34 vol.% in the case of a priori information on *mv*. In addition, the difference between estimated and measured *mv* is also reduced from +2.08 vol.% to +1.19 vol.% for dry to slightly soils (Figure V.10b) and from -3.15 vol.% to -1.62 vol.% for very wet soils (Figure V.10b).

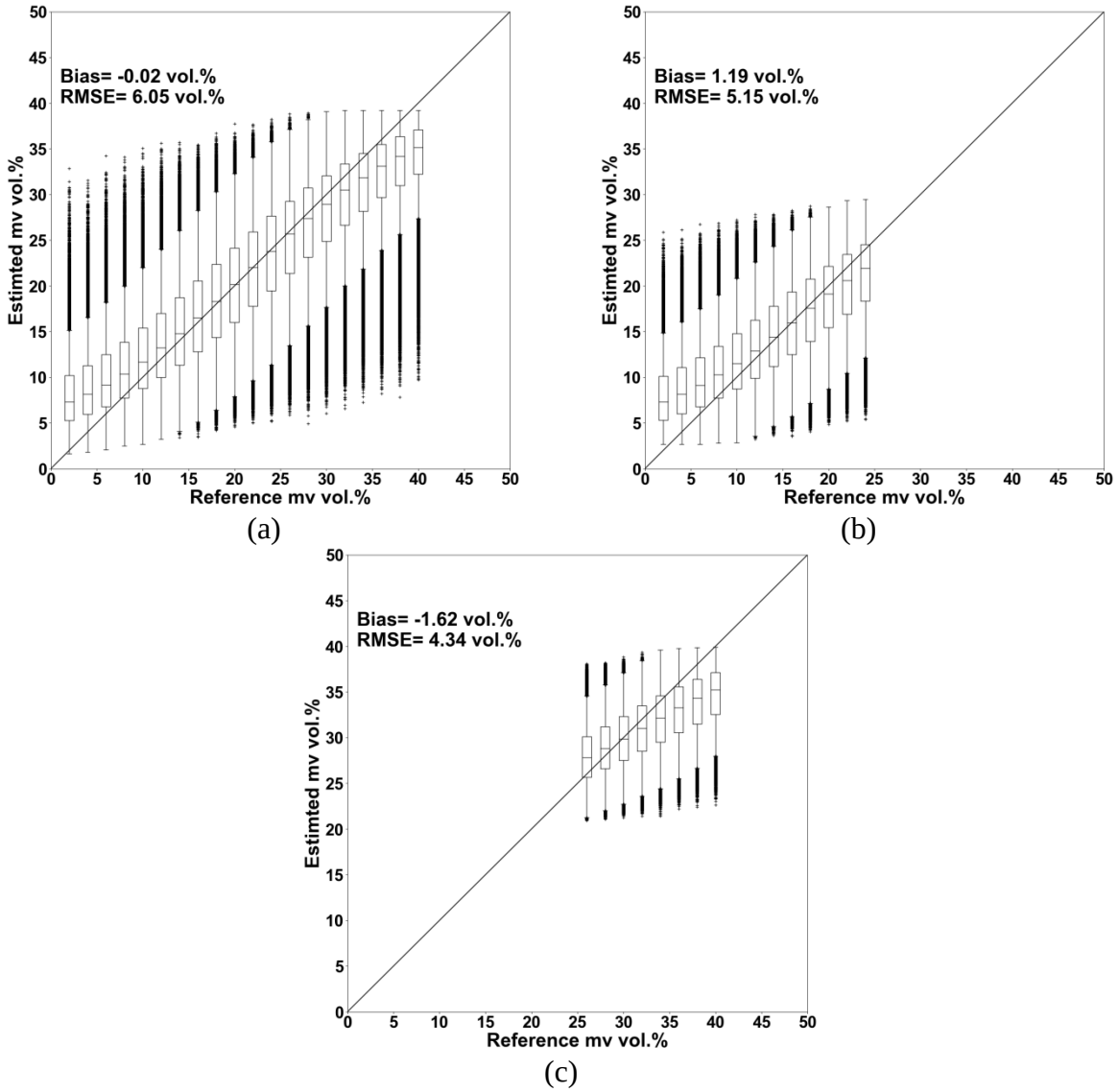


**Figure V.10.** Box plots of *mv* estimates retrieved from the synthetic dataset generated using Baghdadi model. Neural networks were trained and validated using VH polarization alone. (a): no a priori information on *mv*; (b): with a prior information on *mv* and dry to slightly wet soil conditions (*mv* between 2 and 25 vol.%); (c): with a prior information on *mv* and very wet soil condition (*mv* between 25 and 40 vol.%).

The analysis of the accuracy on *mv* estimates shows that the bias (estimated *mv* - measured *mv*) and the RMSE are strongly dependent on both *Hrms* and incidence angle θ" (Figure V.11). According to *Hrms*, The RMSE on *mv* in the case of inversion without a priori information on *mv* increases from 5.50 vol.% for *Hrms*=0.5 cm to 7.50 vol.% for *Hrms* = 3.8 cm for *mv* between 2 and 25 vol.% (dry to slightly wet soils). In very wet soil conditions, the RMSE on *mv* decreases from 10.0 vol.% for *Hrms*=0.5 cm to 4.5 vol.% for *Hrms* = 3.8 cm. The high RMSE values of in the case of dry to slightly wet conditions and high *Hrms*-values are due to an overestimation of *mv* (bias about +6.0 vol.% for *Hrms*=3.8 cm). Similarly, the high RMSE values in the case of very wet soils and low *Hrms*-values are due to an underestimation of *mv* (bias about -7.0 vol.% for *Hrms*=0.5 cm).

In the case of a priori information on *mv*, the RMSE on *mv* estimates varies between 5.5 and 6.0 vol.% for dry to slightly wet soil conditions and between 6.0 and 8.0 vol.% for very wet soils (FigureV.11).

According to the incidence angle θ, results show that the RMSE on *mv* is strongly dependent on θ (Figures V.11c and V.11d). In the case of no a priori information on *mv*, the RMSE increases from 3.5 vol.% for θ=20° to 7.9 vol.% for θ= 45° for dry to slightly wet soils and increases from 3.3 for θ=20° to 9.0 vol.% for θ= 45° for very wet soils. In the case of a priori information on *mv*, the RMSE increases from 3.25 vol. % for θ=20° to 6.5 vol. % for θ=45° for dry to slightly wet soils. For a priori information on *mv* and very wet soils, the RMSE on *mv* estimates is well reduced for high incidence angles (θ=45°) from 9.0 vol.% without a prior information on *mv* to 5.0 vol.% with a prior information on *mv*. In using a priori information on *mv*, the bias is slightly dependent on θ (between +1.0 and +2.5 vol.% for θ between 20° and 45° in the case of dry to slightly wet soils and between -1.0 and -2.5 vol.% for θ between 20° and 45° in the case of very wet soils).

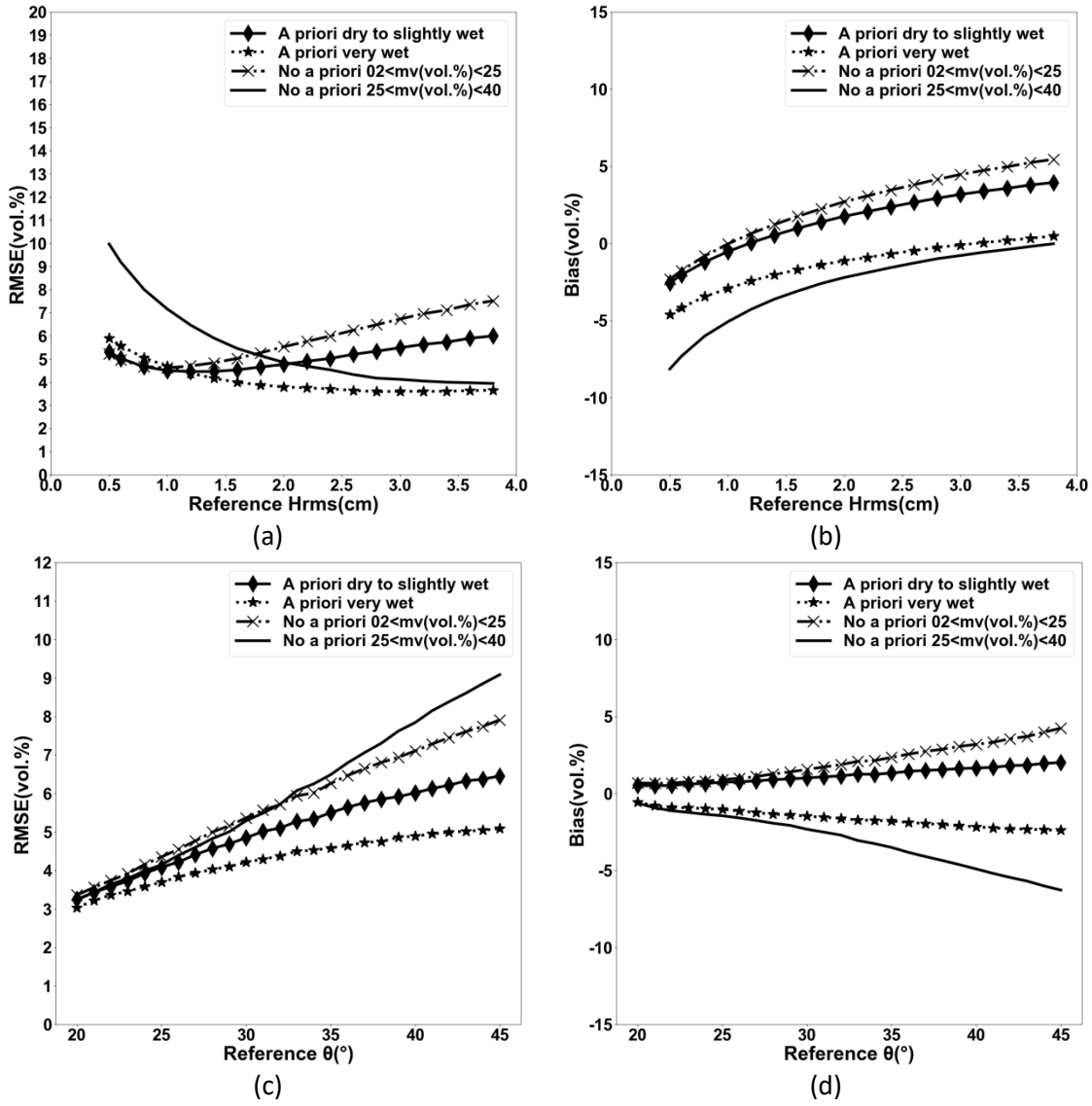


**Figure V.11**. Accuracy on the *mv* estimates (RMSE and bias "=estimated – measured") retrieved from the synthetic dataset in VH polarization using Baghdadi model. Three NNs are tested: without a priori information on *mv* (case 1), with a priori information on *mv* with dry to slightly wet soil conditions (case 2), with a priori information on *mv* with very wet conditions (case 3).

*V.4.1.1.2.3 Use of VV and VH polarizations together*

In using VV and VH polarizations together without a priori information on *mv*, the RMSE on the *mv* estimates is of 5.68 vol.% for *mv* between 2 and 25 vol.% and 6.14 vol.% for *mv* between 25 and 40 vol.%. An overestimation of +1.98 vol.% on *mv* is observed for *mv* between 2 and 25 vol.%, and an underestimation of -2.94 vol.% is obtained for mv between 25 and 40 vol.%. For *mv* between 2 and 40 vol.%, the RMSE on *mv* is of 5.87 vol.% (Figure V.12a).

The introduction of a priori information on *mv* in the case of dry to slightly wet soil conditions improves the *mv* estimates. The RMSE decreases from 5.68 vol.% without a priori information on *mv* to 4.97 vol.% in the case of a priori information on *mv*. In addition, the difference between estimated and measured *mv* is also reduced from +1.98 vol.% to +1.11 vol.% (Figure V.12c). The RMSE on mv estimates in the case of very wet soil conditions decreases from 6.14 vol.% without a priori information on *mv* to 4.24 vol.% in the case of a priori information on *mv*. In addition, the difference between estimated and measured *mv* is also well reduced from -2.94 vol.% to -1.52 vol.% (Figure V.12c).

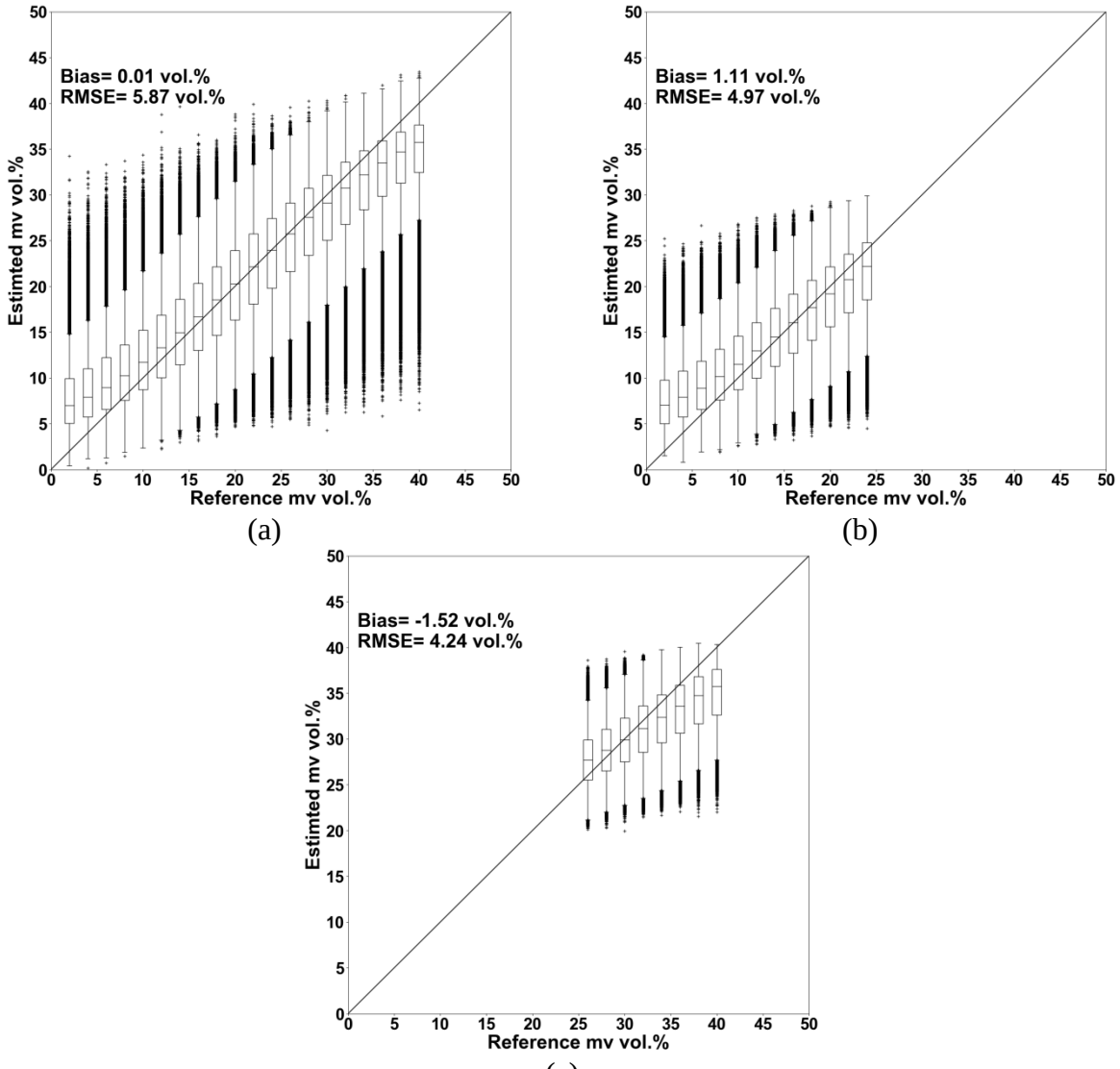


**Figure V.12**. Box plots of mv estimates retrieved from the synthetic dataset generated using Baghdadi model. Neural networks were trained and validated using VV and VH polarization together. (a): no a priori information on *mv*; (b): with a prior information on *mv* and dry to slightly wet soil conditions (*mv* between 2 and 25 vol.%); (c): with a prior information on *mv* and very wet soil condition (*mv* between 25 and 40 vol.%).

The analysis of the accuracy on *mv* estimates according to *Hrms* shows similar results than in the case of VV alone. The RMSE on *mv* in the case of inversion without a priori information on *mv* increases from 5.0 vol.% for *Hrms*=0.5 cm to 7.0 vol.% for *Hrms* = 3.8 cm for dry to slightly wet soils and decreases from 10.0 vol.% for *Hrms*=0.5 cm to 4.0 vol.% for *Hrms* = 3.8 cm for very wet soil conditions (Figure V.13).

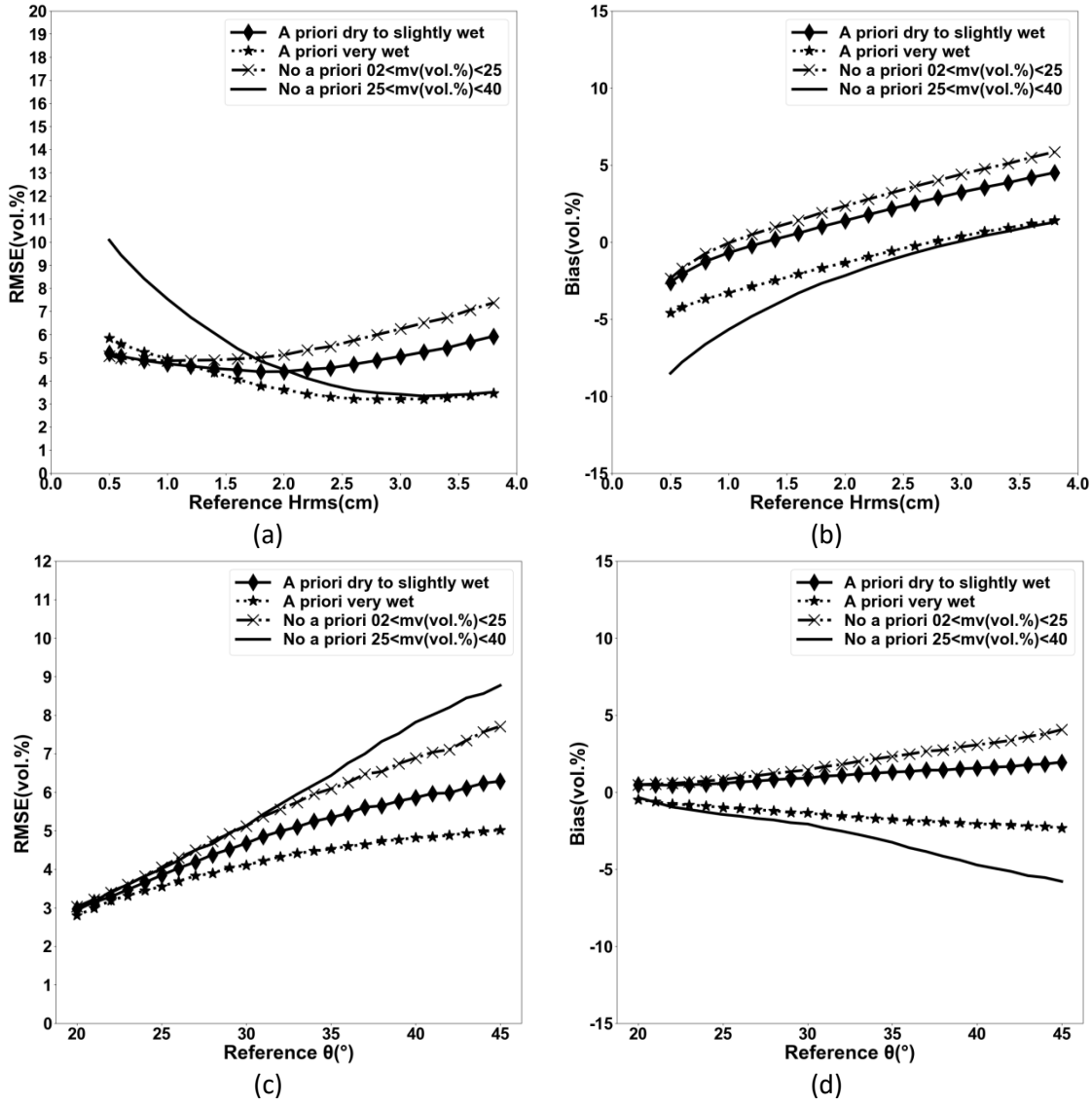


**Figure V.13.** Accuracy on the *mv* estimates (RMSE and bias "=estimated – measured") retrieved from the synthetic dataset generated from Baghdadi model. VV and VH are used together. Three NNs are tested: without a priori information on *mv* (case 1), with a priori information on *mv* with dry to slightly wet soil conditions (case 2), with a priori information on *mv* with very wet conditions (case 3).

Figure V.13b shows that the bias on *mv* estimates increases when *Hrms* increases. According to the incidence angle "θ", results show that the RMSE on *mv* is strongly dependent on θ in

the case of no a priori information on *mv* (Figures V.13c and V.13d). The RMSE increases from 3.0 vol.% for θ=20° to 8.0 vol.% for θ= 45° for dry to slightly wet soil conditions and increases from 3.0 for θ=20° to 9.0 vol.% for θ= 45° for very wet soils.

In the case of a priori information on *mv*, the RMSE on *mv* shows slight dependence with *Hrms* and the incidence angle (Figures V.13a and V.13c).

#### *V.4.1.1.3 Conclusion*

Using the two models (IEM and Baghdadi), the use of a priori information on *mv* strongly improves the estimation of *mv*. With IEM, better results are obtained with VV polarization. The use of VV and VH together provides similar performances than those obtained with VV alone. For the range of surface roughness the most encountered in agricultural environments with *Hrms* between 1 and 2 cm, results show that the RMSE on *mv* in VV polarization varies between 3.0 and 6.0 vol.%. The difference between estimated and real *mv* varies between -1.0 and +1.0 vol.% in the case of dry to slightly wet soils. An underestimation of *mv* from -4.5 to -2.5 vol.% in the case of very wet soils is observed for *Hrms* between 1 and 2 cm.

The use of Baghdadi model shows slightly better results when VV and VH are used together (RMSE about 5.9 vol.% with VV alone, 5.2 vol.% with VH alone and 4.9 vol.% with VV and VH together). For surface roughness between 1 and 2 cm, the RMSE on *mv* varies between 3.9 and 5.5 vol.%. The difference between estimated and real *mv* varies between -0.5 and +2.0 vol.% in the case of dry to slightly wet soils. An underestimation of *mv* from -4.0 to -1.3 vol.% is observed in the case of very wet soils are observed for *Hrms* between 1 and 2 cm.

In a comparison between the two models with *Hrms* ranged between 1 and 2 cm, Baghdadi model shows slightly better results than IEM model mainly with VH polarization alone and with VV and VH polarizations together. Using the IEM model, results show slightly better results for *Hrms* between 1 and 2 cm with VV than with VH alone or with VV and VH polarizations together.

### *V.4.1.2 Estimation of Hrms*

The estimation of the soil roughness (*Hrms*) is carried out after a first step which consisted to estimate *mv*. Indeed, the neural network (NN) which should estimate *Hrms* needs an estimate of *mv*. The two conditions on the soil moisture state are considered in input to the NN: no a priori information on *mv*, a priori information on *mv* (dry to slightly wet soil conditions or

very wet soils). As input to the network, these are the *mv* estimated by the previous networks built to estimate *mv* which are used. In addition to these cases corresponding to operational conditions for estimating soil roughness, the configuration where the input *mv* to the network corresponds to exact *mv* without estimation error (those that are in the validation dataset) is also tested.

According to the results obtained on the estimation of the soil moisture *mv*, results showed that the IEM model shows better performance in using VV polarization in comparison to VH alone or to the use of VV and VH together. Baghdadi model provides better results in using VV and VH polarizations together in comparison to VV alone or to the use of VH alone. Therefore, in the case of surface roughness (*Hrms)* estimation, only the results obtained from the IEM model corresponding to VV alone and results obtained from Baghdadi model corresponding to VV and VH polarizations together are presented briefly. Other results corresponding to VH alone, VV and VH polarizations together for data generated from the IEM model and corresponding to the use of VV alone and VH alone for data generated from Baghdadi model are presented in Annex 1 and Annex 2, respectively.

#### *V.4.1.2.1 Using IEM model*

Figure 1V.8 shows the results for estimating the soil roughness using the synthetic dataset generated from the IEM model with VV polarization alone. Better estimates of *Hrms* are obtained when the *mv* used at the input of the NN corresponds to the exact *mv* (RMSE=0.72 cm). The results obtained using the *mv* estimated without and with a priori information on *mv* are with a higher RMSE, respectively 1.01 cm and 0.94 cm. This shows that the use of *mv* estimates with an accuracy of about 5 vol.% is not sufficient to accurately estimate the soil roughness in C-band and VV polarization. In addition, figure V.14 shows an overestimation of *Hrms* for low *Hrms*-values and an underestimation of *Hrms* for *Hrms* higher than 2 cm.

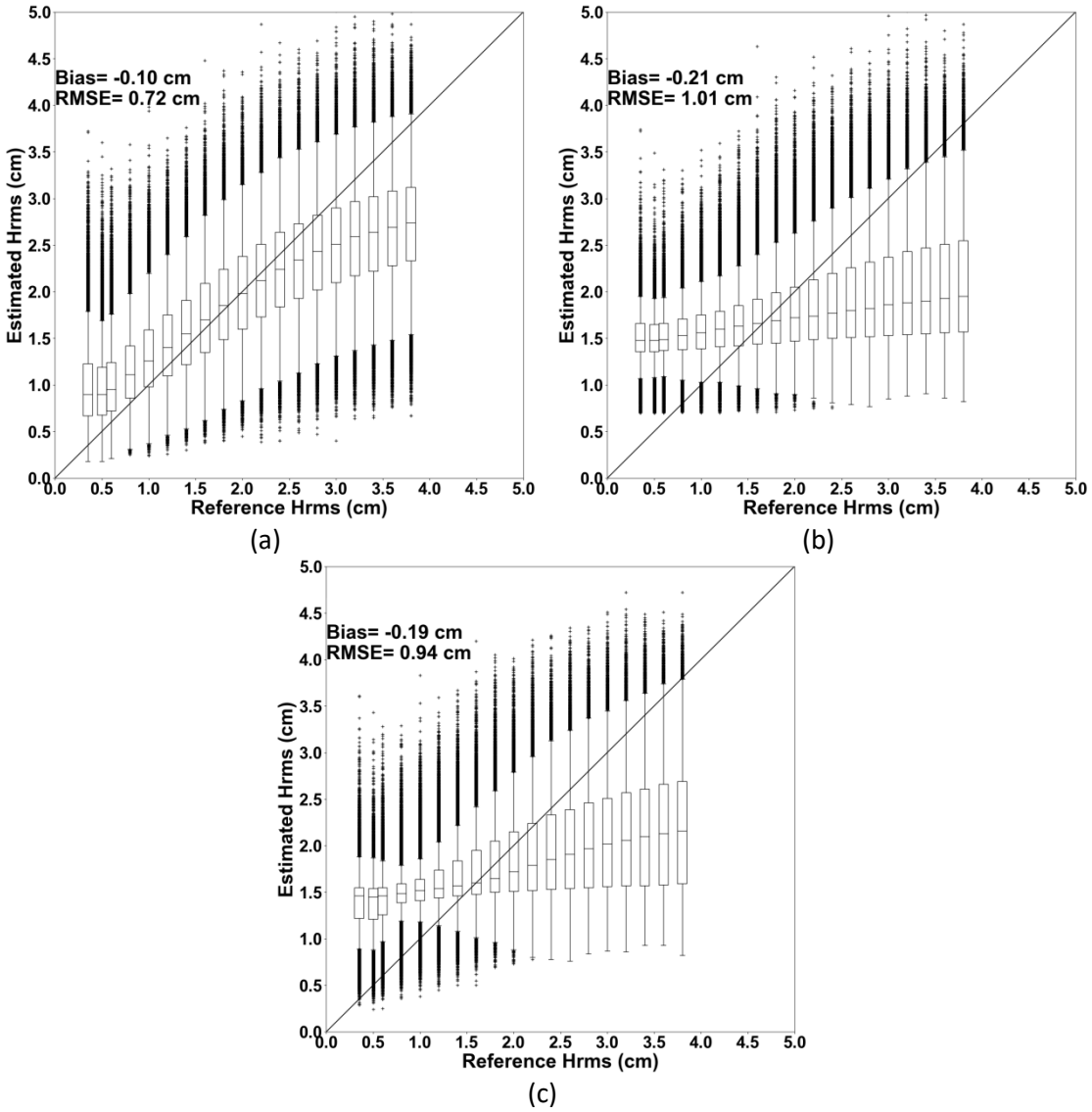


**Figure V.14.** Box plots of *Hrms* (cm) retrieved from the synthetic dataset generated from the IEM model in using VV polarization. (a) the input *mv* to the NN corresponds to exact *mv* (those that are in the validation dataset without estimation error), (b) the input *mv* to the NN corresponds to *mv* estimated by the NN built for estimating *mv* without a priori information on *mv*, (c) the input *mv* to the NN corresponds to *mv* estimated by the NN built for estimating *mv* with a priori information on *mv*.

The performance of the neural network is also studied as a function of *mv* and the incidence angle (θ) only when the *mv* in input to the NN corresponds to the exact *mv* (without estimation error) (Figure V.15). The RMSE on *Hrms* decreases from 0.84 cm for *mv*=2 vol.% to 0.70 cm for *mv* higher than 15 vol.%. In addition, the RMSE on *Hrms* decreases when the incidence angle increases (Figure V.15a). The RMSE on *Hrms* shows values between 0.92 cm for θ=20° and 0.65 cm for θ=45° (Figure V.15b). This is due to the sensitivity of radar signal to θ, much stronger for high values of *Hrms* than for low values of *Hrms* (Baghdadi et al.,

2002a).The difference between estimated and exact *Hrms* very low dependence on reference *mv* and the incidence angle (Figure V.15c and V.15d).

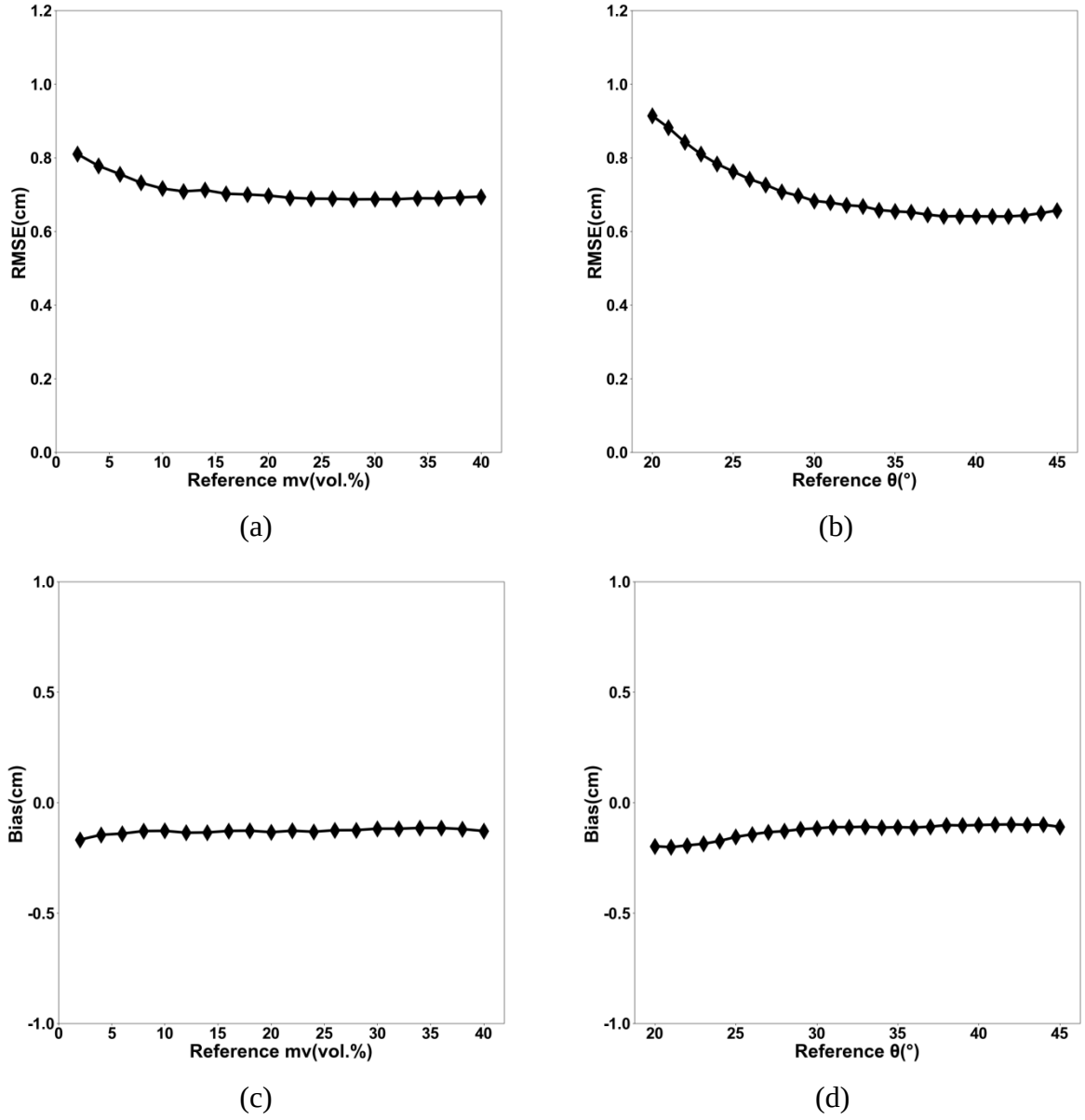


**Figure V.15**. Accuracy on the *Hrms* estimates (RMSE and Bias) as a function of the soil moisture and the incidence angle for VV polarization using the synthetic data generated from the IEM model (*mv* in input corresponds to exact *mv*, without estimation error).

*V.4.1.2.2 Using Baghdadi model*

Results corresponding to the use of synthetic dataset generated from Baghdadi model in VV and VH polarizations together are shown in Figure V.16. Better estimations are observed for *Hrms* when the *mv* used at the input of the NN corresponds to the exact *mv* (RMSE=0.60 cm).

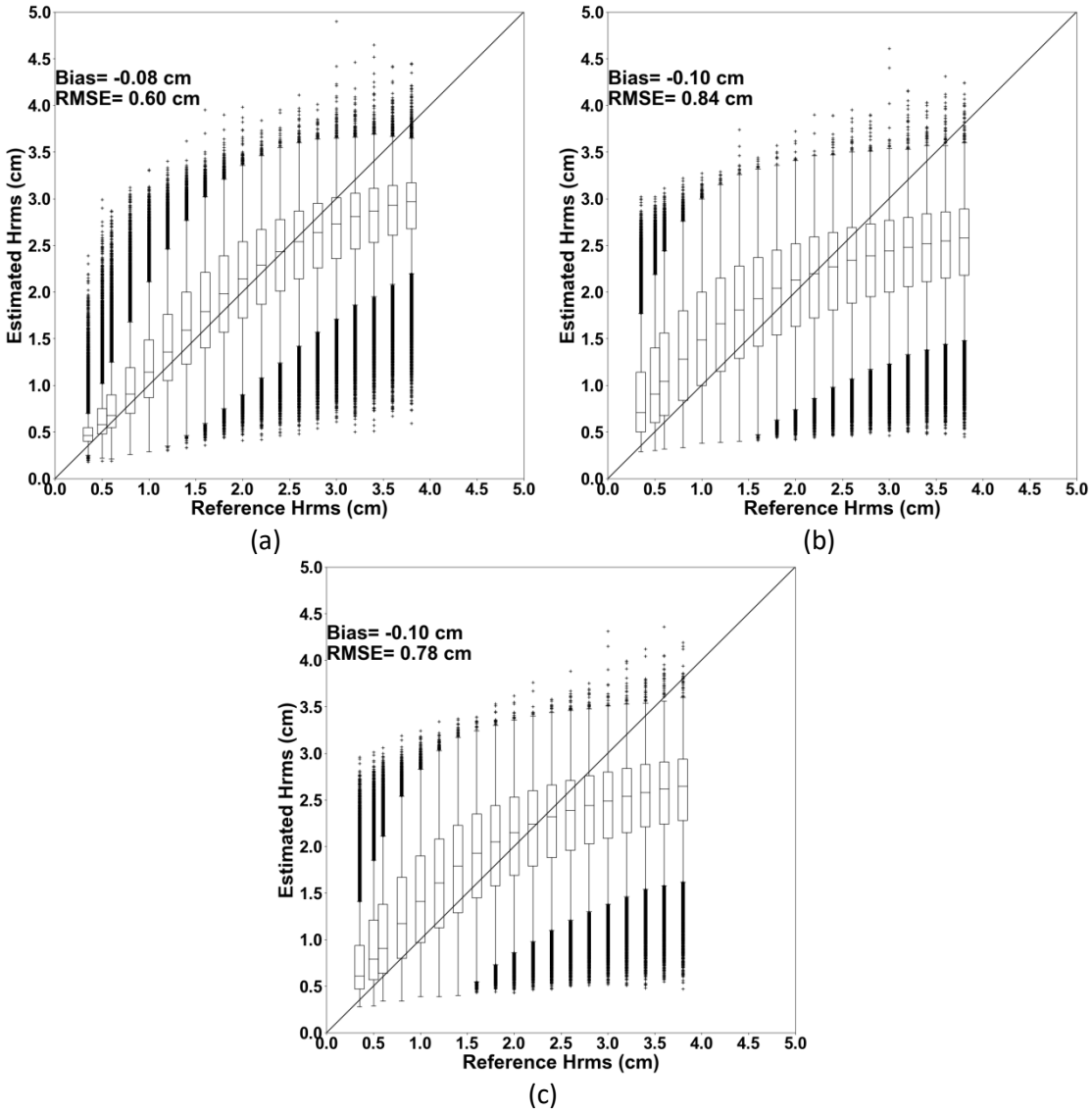


**Figure V.16.** Box plots of *Hrms* retrieved from the synthetic dataset generated from Baghdadi model in using VV and VH polarizations together. (a) the input *mv* to the NN corresponds to real *mv* (those that are in the validation dataset), (b) the input *mv* to the NN corresponds to *mv* estimated by the NN built for estimating *mv* without a priori information on *mv* (with estimation error), (c) the input *mv* to the NN corresponds to *mv* estimated by the NN built for estimating *mv* with a priori information on *mv* (with estimation error).

The results obtained using the *mv* estimated without or with a priori information on *mv* show higher RMSE with respectively 0.84 cm and 0.78 cm. This shows that the use of *mv* estimates with an accuracy of about 5 vol.% is not sufficient to accurately estimate the soil roughness in C-band and VV polarization. In addition, figure V.20 shows an overestimation of *Hrms* for low *Hrms*-values and an underestimation of *Hrms* for *Hrms* higher than 2 cm when the *mv* used in the NN is estimated without or with a priori information on *mv* (Figure V.16b and Figure V.16c).

The performance of the neural network is also studied as a function of *mv* and θ only when the *mv* in input to the NN corresponds to the exact *mv* (without estimation error) (Figure V.17). The RMSE on *Hrms* is about 0.6 cm for all *mv* between 2 and 40 vol.%. In addition, the RMSE on *Hrms* decreases when the incidence angle increases. The RMSE on *Hrms* shows values between 0.78 cm for θ=20° and 0.50 cm for θ=45°. In addition, The difference between estimated and exact *Hrms* very low dependence on reference *mv* and the incidence angle (Figure V.17c and V.17d).

The comparison between Figure V.14 (using IEM) and Figure V.16 (using Baghdadi model) shows that the estimation of *Hrms* seems better in using the Baghdadi model.

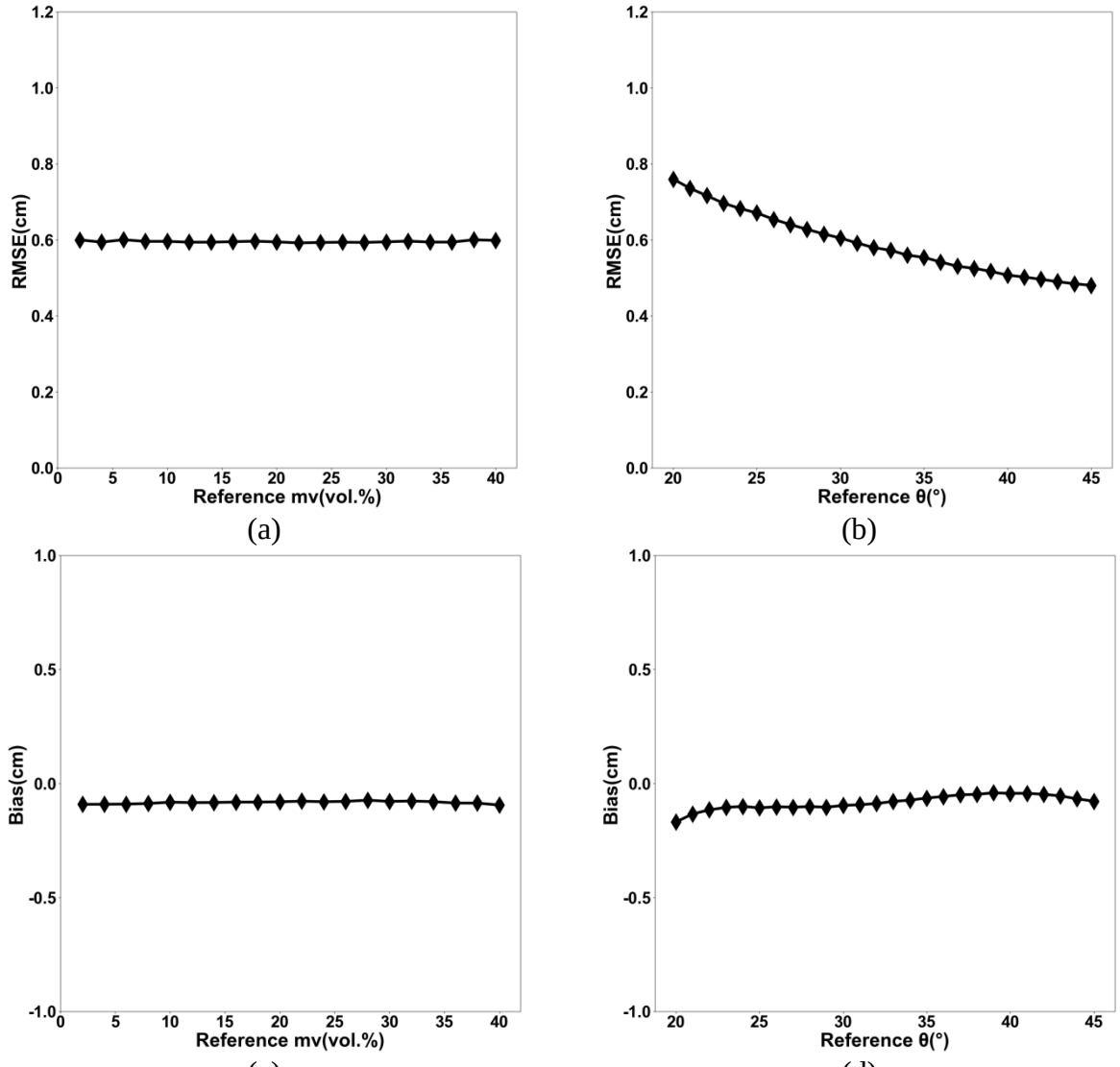


**Figure V.17.** Accuracy on the *Hrms* estimates (RMSE and Bias) as a function of the soil moisture and the incidence angle for VV and VH polarizations together using the synthetic data generated from Baghdadi model (*mv* in input corresponds to exact *mv*, without estimation error).

### V.4.2 Real dataset

The NNs built for estimating *mv* and *Hrms* are then analyzed using the real Sentinel-1 dataset.

#### *V.4.2.1 Estimation of soil moisture (mv)*

##### *V.4.2.1.1 Using the IEM model*

For VV polarization alone and using the IEM model, the results obtained for the estimation of *mv* are shown in Figure V.18. Results show that the introduction of a priori information on *mv* provides better accuracy on the *mv* estimates than the case without a priori information on *mv* (RMSE=6.00 vol.% with a priori information on *mv* and RMSE=7.25 vol.% without a priori on *mv*).

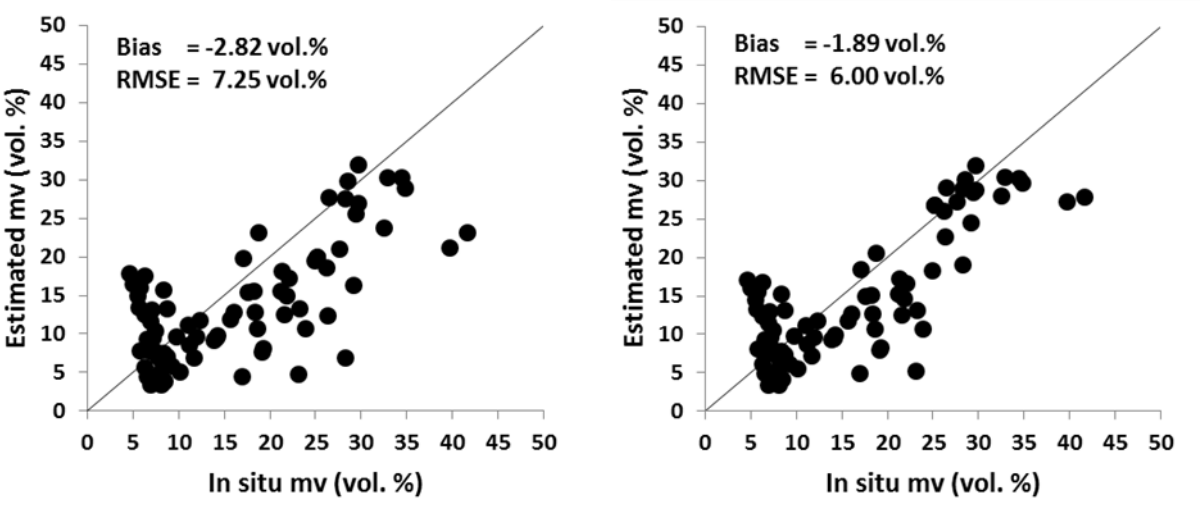


(a) (b)

**Figure V.18.** Retrieved *mv* versus in situ measurements in using the IEM model. (a): using VV without a priori information on *mv*; (b): using VV with a priori information on *mv*. Each point corresponds to one reference plot.

For VH polarization alone, the results obtained for the estimation of *mv* are shown in Figure V.19. Better resulys are obtained when a priori information on *mv* is used (RMSE=5.63vol.% with a priori on *mv* and RMSE=7.52 vol.% without a priori on *mv*). In the case of VV and VH polarizations together, the results obtained for the estimation of *mv* are shown in Figure V.20. The use of introduction of a priori information on *mv* provides better accuracy on the *mv* estimates than the case without a priori information on *mv* (RMSE=5.79 vol.% with a priori on *mv* and RMSE=7.46 vol.% without a priori on *mv*).

The analysis of the difference between the estimated and measured *mv* shows that the strong underestimates of the *mv* corresponds to low *Hrms*-values (*Hrms*<2 cm) and the strong overestimates corresponds to high *Hrms*-values (*Hrms*>2 cm).

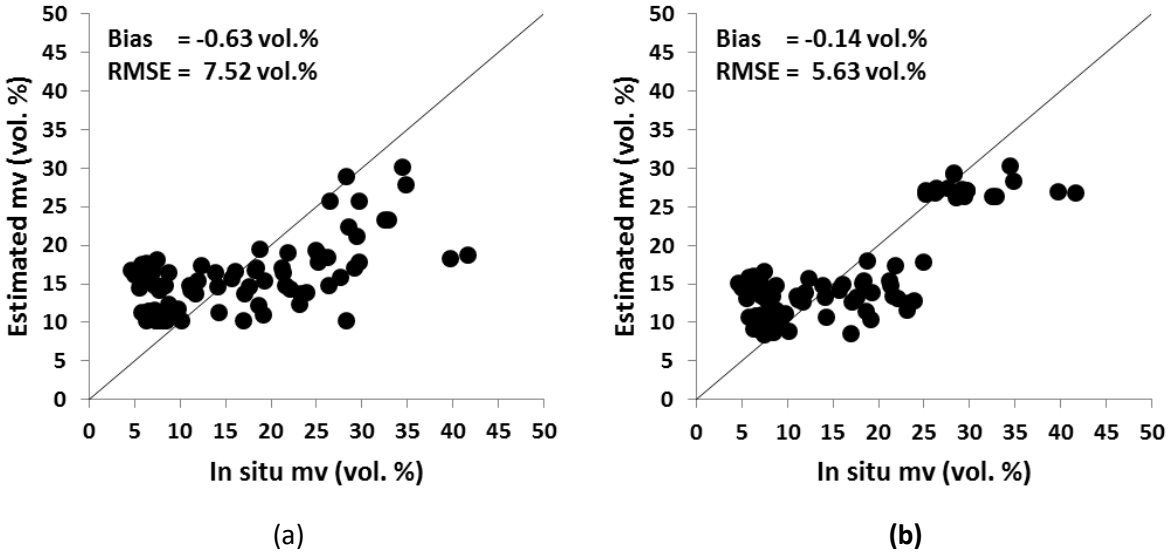


(a) **(b)**

**Figure V.19.** Retrieved *mv* versus in situ measurements in using the IEM model. (a): using VH without a priori information on *mv*; (b): using VH with a priori information on *mv*. Each point corresponds to one reference plot.

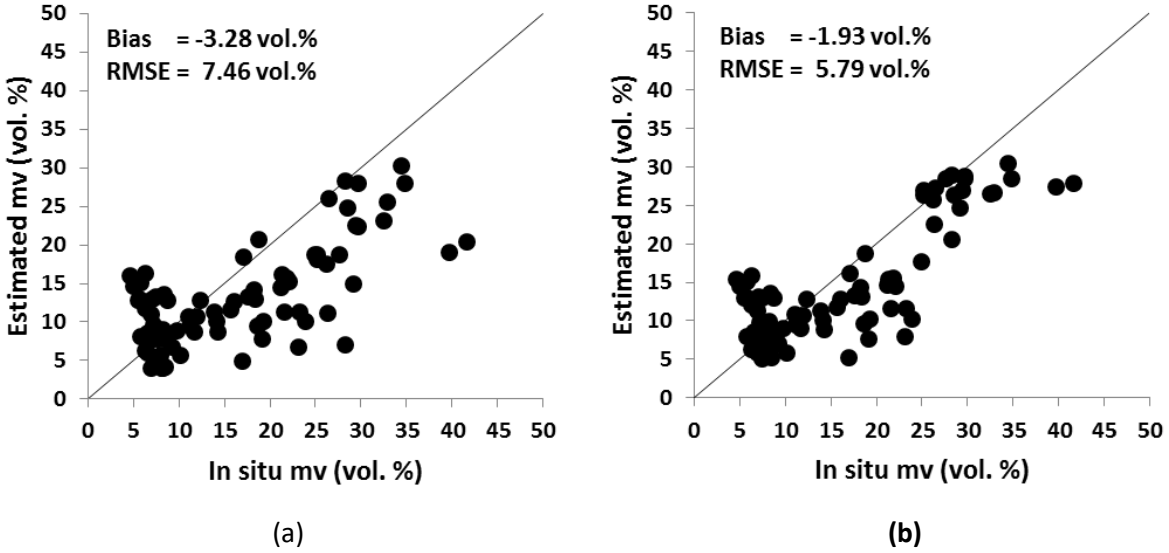


(a) **(b)**

**Figure V.20.** Retrieved *mv* versus in situ measurements in using the IEM model. (a): using VV and VH together without a priori information on *mv*; (b): using VV and VH together with a priori information on *mv*. Each point corresponds to one reference plot.

*V.4.2.1.2 Using Baghdadi model*

Using Baghdadi model for VV polarization alone, the results obtained for the estimation of *mv* are shown in Figure V.21. Results show that the introduction of a priori information on *mv* provides better accuracy on the *mv* estimates than the case without a priori information on *mv* (RMSE=5.58 vol.% with a priori on *mv* and RMSE=7.00 vol.% without a priori on *mv*).

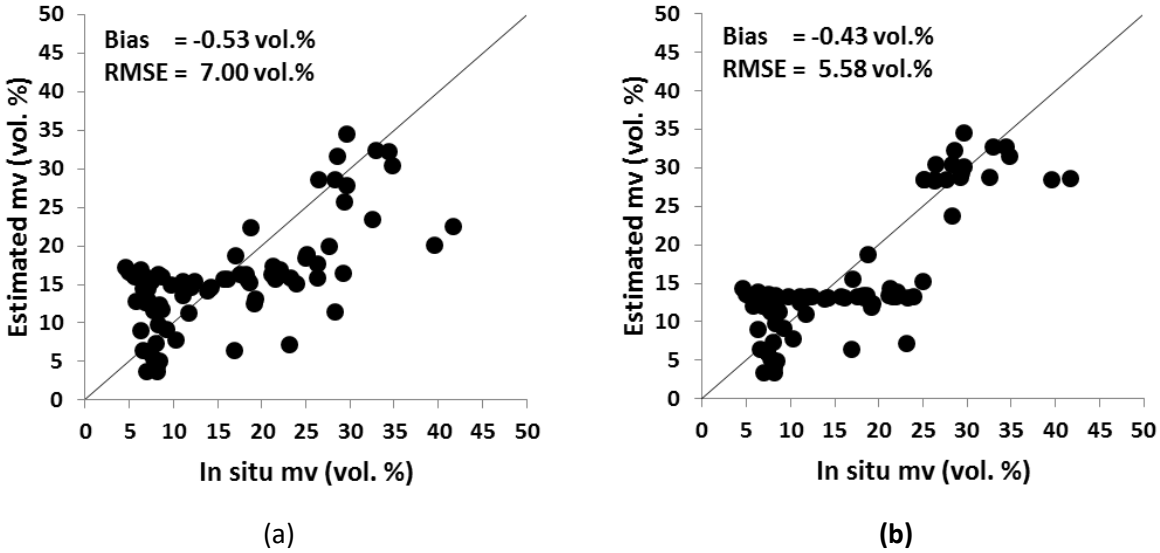


**Figure V.21.** Retrieved *mv* versus in situ measurements in using Baghdadi model. (a): using VV without a priori information on *mv*; (b): using VV with a priori information on *mv*. Each point corresponds to one reference plot.

Figure V.22 shows the results obtained for the estimation of *mv* in the case of VH polarization alone. Better results are obtained when a priori information on *mv* is used (RMSE=6.45 vol.% with a priori on *mv* and RMSE=7.97 vol.% without a priori on *mv*). Figure V.23 shows the results obtained for the estimation of *mv* in the case of VV and VH polarizations together. An RMSE of 6.67 vol.% is obtained with the introduction of a priori information on *mv* and an RMSE of 8.25 vol.% in the case without a priori information on *mv*.

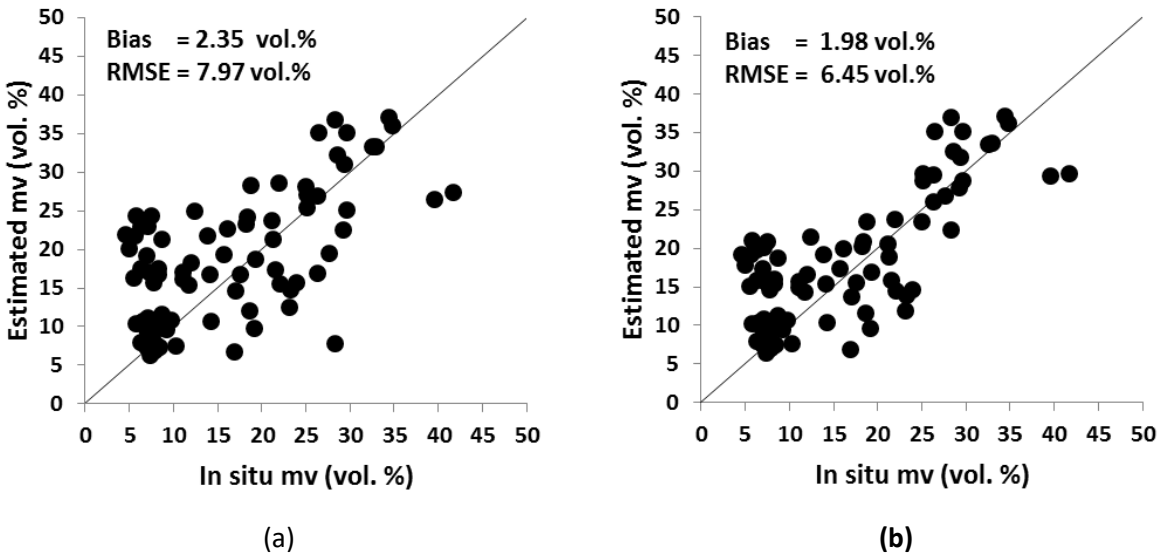


(a) **(b)**

**Figure V.22.** Retrieved *mv* versus in situ measurements in using Baghdadi model. (a): using VH without a priori information on *mv*; (b): using VH with a priori information on *mv*. Each point corresponds to one reference plot.

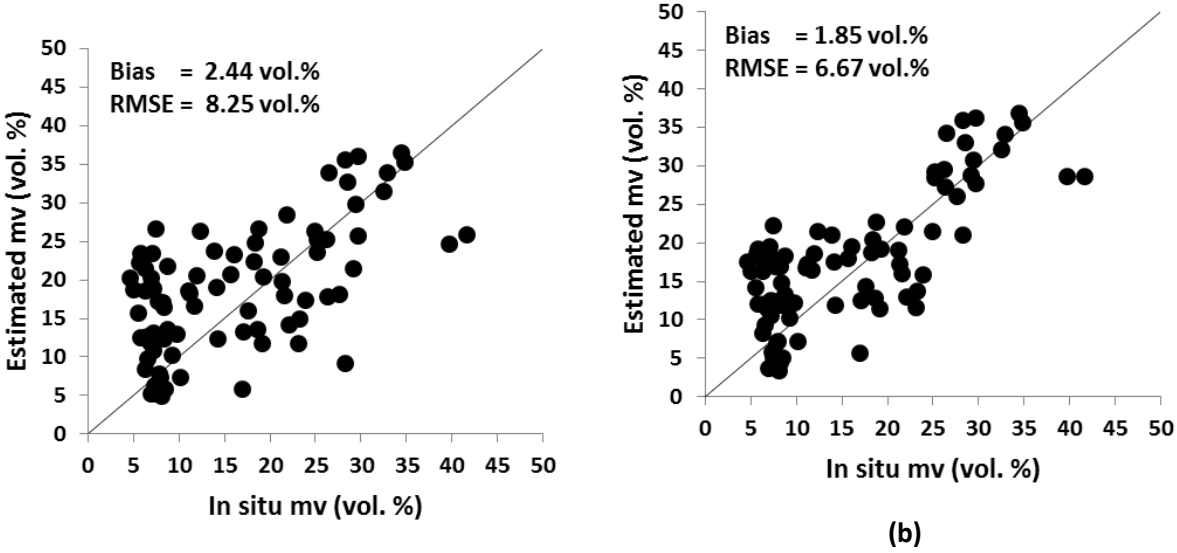


(a) **(b)**

**Figure V.23.** Retrieved *mv* versus in situ measurements in using Baghdadi model. (a): using VV and VH together without a priori information on *mv*; (b): using VV and VH together with a priori information on *mv*. Each point corresponds to one reference plot.

### *V.4.2.2 Estimation of surface roughness (Hrms)*

The results of the estimation of *Hrms* are done in using two inversion configurations:

- At the input of the network for the estimation of *Hrms*, the *mv* used corresponds to *mv* estimated at plot scale (using the mean radar signal calculated by averaging for each reference plot the values of all pixels within the reference plot).

- At the input of the network for the estimation of *Hrms*, the *mv* used corresponds to *mv* estimated at the scale of the study site (using the mean radar signal calculated by averaging the values of all bare soil pixels within the study site). This second approach assumes that the soil moisture is of the same order for all bare agricultural plots located in the area under consideration (no irrigation activities and similar soil composition). The use of *mv* estimated at the scale of the study site in the estimation technique of *Hrms* could be relevant only when the study site is not irrigated. Indeed, if the SAR images are acquired during the dry season with irrigation activities on the study site, the use of an average soil moisture estimated at the scale of the study site (average *mv* calculated on all the bare soil agricultural plots) will lead to a strong overestimation of *Hrms* since the *mv* used for irrigated plots in the neural network for estimating *Hrms* will most probably be underestimated.

For these two configurations *a priori* information on *mv* is used in the network for estimating *mv*.

#### *V.4.2.2.1 Using the IEM model*

In the case of VV polarization alone, results show that the accuracy on the estimates of *Hrms* is similar in using the *mv* estimated at the study site scale (a few tens of km²) and in using the *mv* estimated at the plot scale. The RMSE is of 0.98 cm when the *mv* used correspond to *mv* estimated at the scale of the study site and of 0.81 cm when the *mv* is estimated at the plot scale (Figure V.24). Figure V.25 shows the result using VH alone. The accuracy on the estimates of *Hrms* is mostly the same in using the *mv* estimated at the study site scale (RMSE = 0.82cm) and in using the *mv* estimated at the plot scale (RMSE=0.74 cm). In the case of VV and VH used together, results show that the accuracy on the estimates of *Hrms* is better in using the *mv* estimated at the plot scale (RMSE = 0.81 cm ) than in using the *mv* estimated at the study site scale (RMSE =1.31 cm) (Figure V.26).

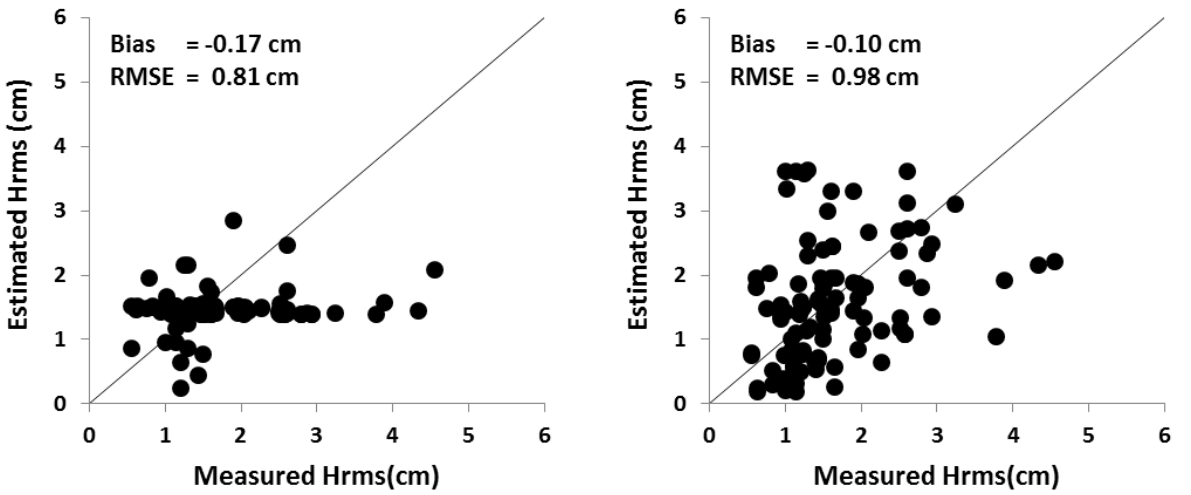


(a) (b)

**Figure V.24.** Retrieved *Hrms* versus measured measurements in VV polarization alone using the NN trained with synthetic data simulated from IEM model. (a): the *mv* used at the input of the network corresponds to *mv* estimated at plot scale; (b): the *mv* used at the input of the network corresponds to *mv* estimated at the scale of the study site.

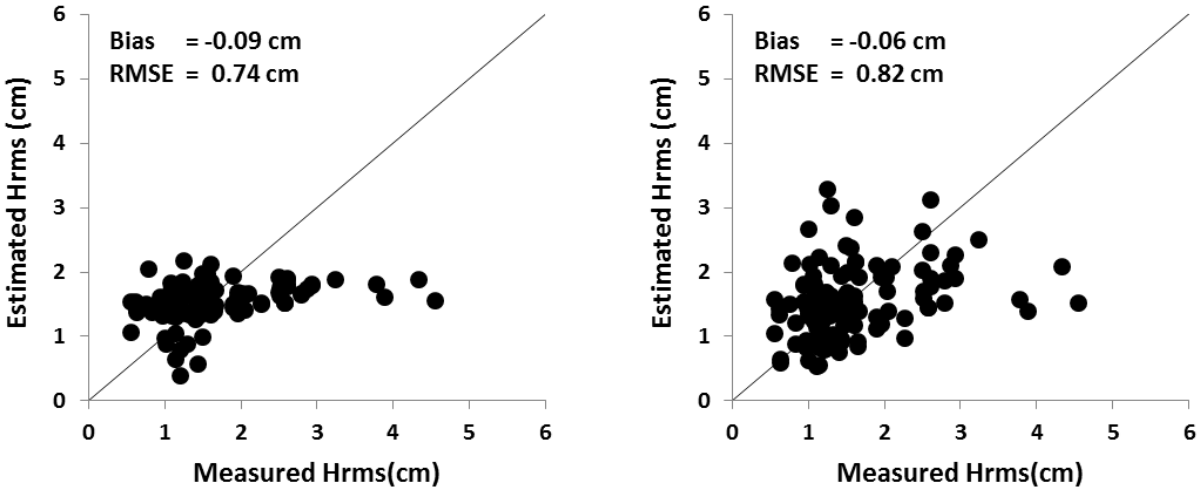


(a) (b)

**Figure V.25.** Retrieved *Hrms* versus measured measurements in VH polarization alone using the NN trained with synthetic data simulated from IEM model. (a): the *mv* used at the input of the network corresponds to *mv* estimated at plot scale; (b): the *mv* used at the input of the network corresponds to *mv* estimated at the scale of the study site.

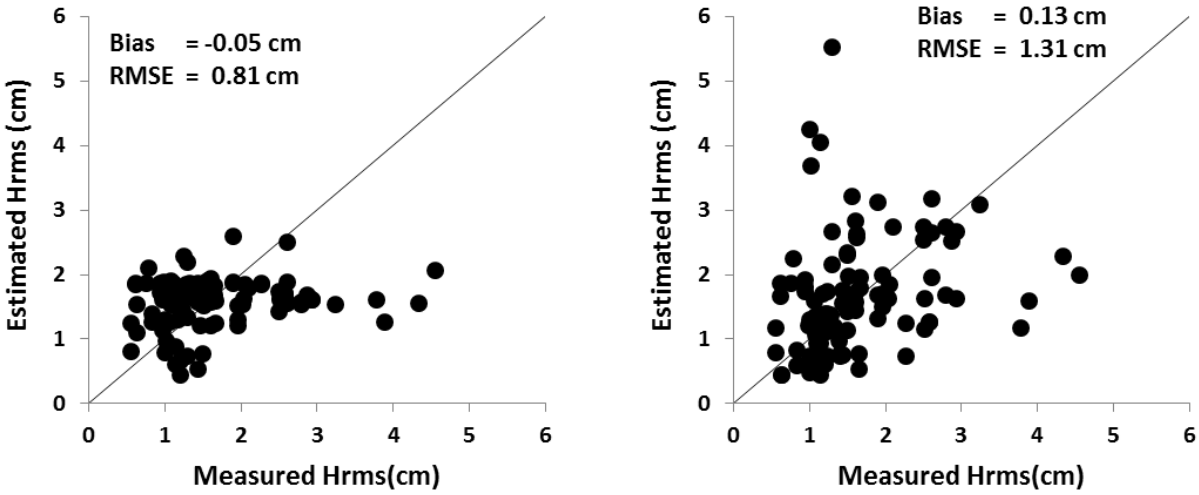


(a) (b)

**Figure V.26.** Retrieved *Hrms* versus measured measurements in VV and VH polarizations together using the NN trained with synthetic data simulated from IEM model. (a): the *mv* used at the input of the network corresponds to *mv* estimated at plot scale; (b): the *mv* used at the input of the network corresponds to *mv* estimated at the scale of the study site.

*V.4.2.2.2 Using Baghdadi model*

With VV polarization alone, the accuracy on the estimates of *Hrms* is mostly the same in using the *mv* estimated at the study site scale and in using the *mv* estimated at the plot scale with RMSE of 1.04 cm and 0.95 cm, respectively (Figure V.27). Figure V.28 shows the result according to VH polarization alone. The precision on the estimates of *Hrms* is similar in using the *mv* estimated at the study site scale is approximately the same as in using the *mv* estimated at the plot scale (RMSE of 0.92 cm and of 0.84 cm, respectively). Figure V.29 shows that the estimation of *Hrms* using VV and VH together is carried out with a precision about 1.0 cm for the two inversion configurations.

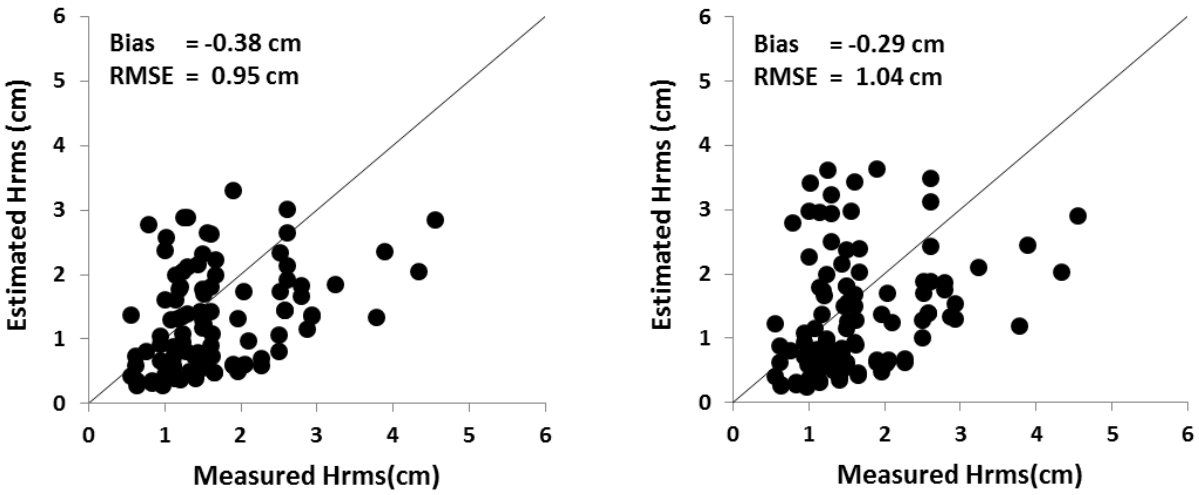


(a) (b)

**Figure V.27.** Retrieved *Hrms* versus measured measurements in VV polarization alone using the NN trained with synthetic data simulated from Baghdadi model. (a): the *mv* used at the input of the network corresponds to *mv* estimated at plot scale; (b): the *mv* used at the input of the network corresponds to *mv* estimated at the scale of the study site.

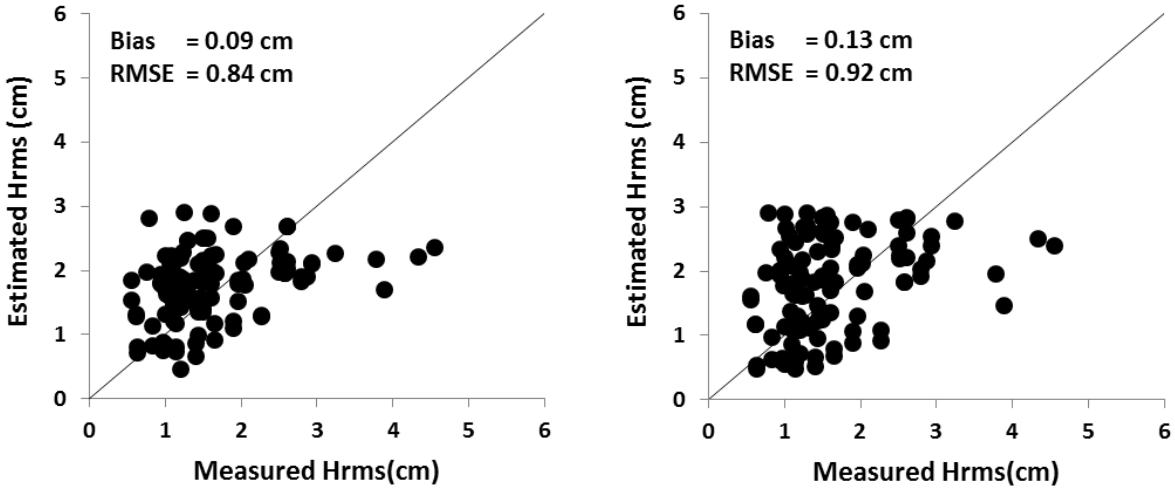


(a) (b)

**Figure V.28.** Retrieved *Hrms* versus measured measurements in VH polarization alone using the NN trained with synthetic data simulated from Baghdadi model. (a): the *mv* used at the input of the network corresponds to *mv* estimated at plot scale; (b): the *mv* used at the input of the network corresponds to *mv* estimated at the scale of the study site.

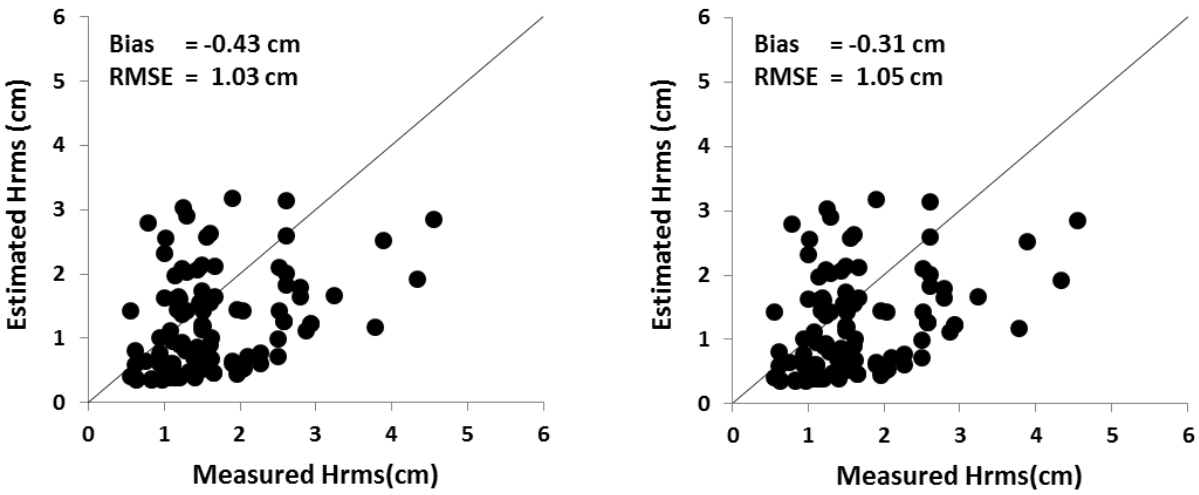


(a) (b)

**Figure V.29.** Retrieved *Hrms* versus measured measurements in VV and VH polarizations together using the NN trained with synthetic data simulated from Baghdadi model. (a): the *mv* used at the input of the network corresponds to *mv* estimated at plot scale; (b): the *mv* used at the input of the network corresponds to *mv* estimated at the scale of the study site.

*V.4.2.2.3 Discussion*

Results obtained in using the NN built with a priori information on *mv* show estimates of *Hrms* with an RMSE higher than 0.7 cm. This accuracy on *Hrms* obtained shows that the use of *mv* estimates with an accuracy of about 6 vol.% is not sufficient to accurately estimate the soil roughness in C-band. From the real dataset, results show that the accuracy on *Hrms* estimates in using the *mv* estimated at the study site scale is similar to that in using the *mv* estimated at the plot scale. The use of *mv* estimated at the scale of the study site is possible only when the study site is not irrigated. In addition, results are similar using the neural networks trained with data simulated from IEM model and Baghdadi model.

This first study on the potential of Sentinel-1 data for estimating the soil roughness shows that the development of an automatic and generalizable inversion procedure of the C-band radar signal does not allow a pertinent estimation of the soil roughness. The accuracy on soil roughness estimates obtained in this study cannot satisfy the requirements of operational users of soil roughness products (in particular to modelers) because the need is at least three roughness classes: smooth (sowing), medium (small plowing) and rough (large plowing).

Only methods based on the use of experimental relationships, which are often difficult to apply to sites other than those for which they were developed and are generally valid only for specific soil conditions, allows the mapping of three roughness classes (Baghdadi et al., 2002a). Indeed, different experimental studies have revealed that the sensitivity of the radar

signal to surface roughness (i.e. the slope of the regression lines) can be highly variable from one site to another. In addition, the experimental relationships between the radar signal and *Hrms* are established for a given incidence angle and a range of soil moisture. The soil composition could be also different from one site to another. All these reasons explain why the experimental relationships are not generalizable.

### V.4.3 Estimation of *Hrms* and *mv* both at very high spatial resolution "VHSR"

In this second approach, soil roughness *Hrms* estimates are analyzed when the output of the neural network is both soil moisture and surface roughness at the same time. In this configuration, both VV and VH polarizations are used as input of the neural networks. The transfer function that are used in the Neural Networks for this configuration is Logsig.

Three neural networks are analyzed corresponding to the three cases of soil moisture conditions with and without a *priori* information on the soil moisture state:

- Case 1: No *a priori* information on the soil moisture state is available. In this case *mv* will be estimated between 2 and 40 vol.%.
- Case 2: *A priori* information is available on *mv*. The soil is supposed to be dry to slightly wet according to expertise based mainly on meteorological data (precipitations, temperature). Soil moisture values are assumed to range from 2 to 25 vol.%.
- Case 3: *A priori* information is available on *mv*. The soil is supposed to be very wet according to expertise based on meteorological data. *mv*-values are assumed to vary between 25 and 40 vol.%.

The three NNs use the backscattering coefficients in VV and VH polarizations and the incidence angle as input. The NN outputs are the soil moisture *mv* and the surface roughness *Hrms.* An overlapping of 10 vol.% on *mv* was used on the training datasets of the two networks in the case of a priori information on the soil moisture *mv*. So that, in the case of dry to slightly wet soils, the *mv*-values used for the training is ranged from 2 to 30 vol.%. In the case of very wet soils, the *mv*-values used for the training is ranged from 20 to 40 vol.%.

The different neural networks are tested for the evaluation of the precision on soil roughness and moisture estimates using synthetic and real datasets.

*V.4.3.1 Synthetic dataset*

First, we will discuss the performance of networks for the estimation of *mv*. Then, the performance of the same networks for estimating *Hrms* is analyzed.

*V.4.3.1.1 Estimation of mv*

*V.4.3.1.1.1 Using the IEM model*

In the case of no a priori information on *mv*, the RMSE on the *mv* estimates is of 4.55 vol.% for *mv* between 2 and 25 vol.% and 6.37 vol.% for *mv* between 25 and 40 vol.%, with an overestimation of +2.14 vol.% and an underestimation of -3.22 vol.% on *mv* respectively for each *mv* range. For the entire range of *mv*, between 2 and 40%, the RMSE on *mv* is of 5.35 vol.% (Figure V.30a).

In the case where the NNs were trained using a priori information on *mv* with dry to slightly wet soil condition, the RMSE on *mv* estimates decreases from 4.55 vol.% without a priori information on *mv* to 3.40 vol.% in the case of a priori information on *mv*. In addition, the difference between estimated and measured *mv* is also reduced from +2.14 vol.% to +1.01 vol.% (Figure V.30b).

In addition, the use of a priori information on *mv* in the case of very wet soil conditions also improves the *mv* estimates. The RMSE on *mv* estimates decreases from 6.37 vol.% without a priori information on *mv* to 4.89 vol.% in the case of a priori information on *mv*. Also, the difference between estimated and measured *mv* is reduced from -3.23 vol.% to -1.96 vol.% (Figure V.30c).

The performance of the inversion algorithm was analyzed according to *Hrms* and incidence angle "θ" (Figure V.31). Results show that the bias (estimated *mv* - measured *mv*) and the RMSE are strongly dependent on *Hrms*. The RMSE on *mv* in the case of inversion without a priori information on *mv* increases from 4.10 vol.% for *Hrms*=0.5 cm to 6.50 vol.% for *Hrms* = 3.8 cm for *mv* between 2 and 25 vol.% (bias increases from -8.8 to +1.2 vol.% for *Hrms* between 0.5 and 3.8 cm). In very wet soil conditions, the RMSE on *mv* decreases from 11.00 vol.% for *Hrms*=0.5 cm to 4.1 vol.% for *Hrms* = 3.8 cm (bias increases from –1.2 to 5.1 vol.% for *Hrms* between 0.5 and 3.8 cm). Moreover, results show that the RMSE on *mv* slightly depends on θThe RMSE on *mv* estimates is about 5 vol.% for θ between 20° and 45° for dry to slightly wet soil conditions ( overestimation of *mv* of +2.0 vol.%) and about 6

vol.% for θ between 20° and 45° for very wet soils in the case of no a priori information on *mv* ( underestimation of *mv* of about -3.0 vol.%) (Figures V.31c and V.31d).

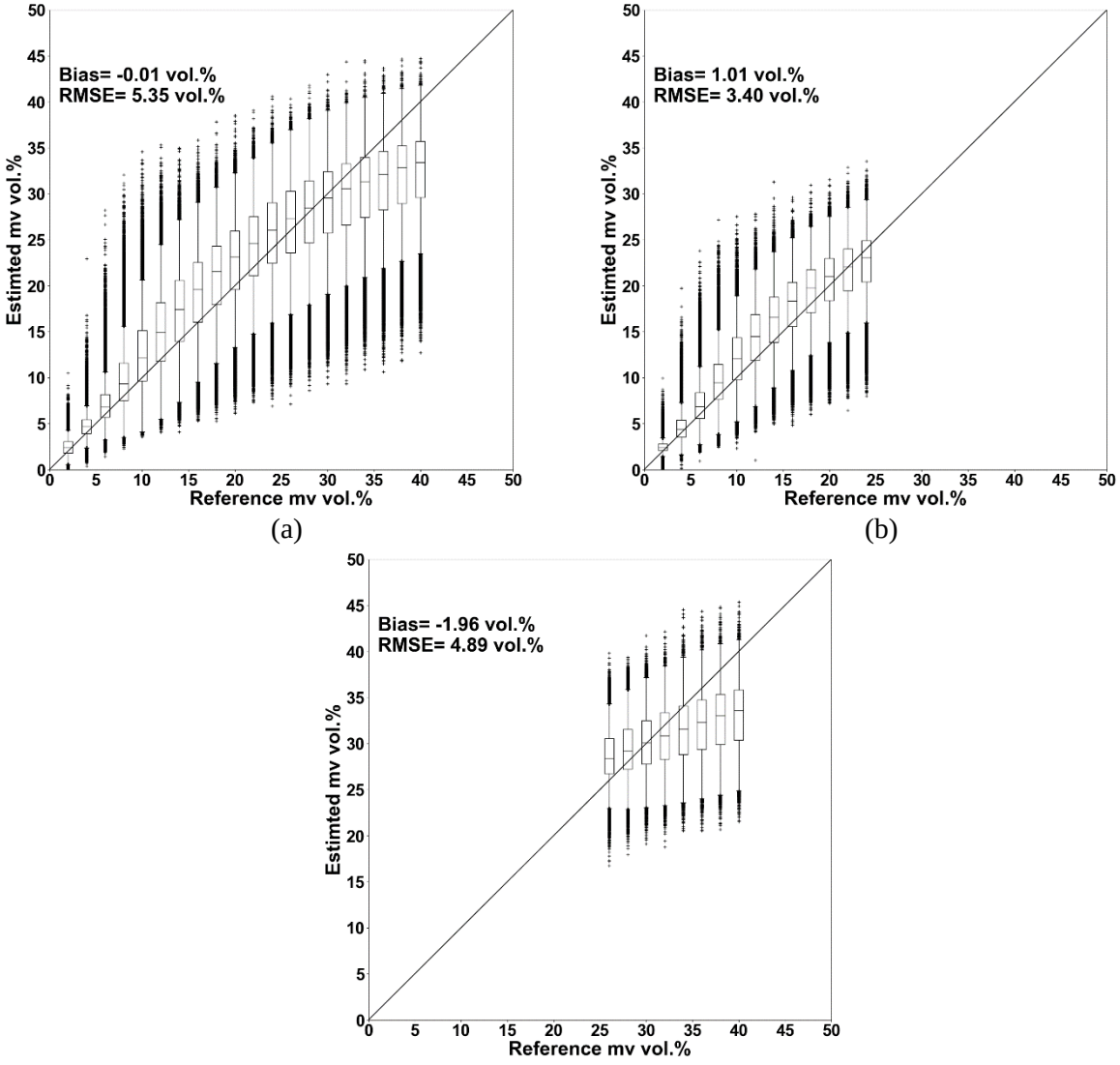


**Figure V.30.** Box plots of *mv* estimates retrieved from the synthetic dataset generated using IEM. Neural networks were trained and validated using VV and VH polarizations. The NNs outputs are *Hrms* and *mv* together. (a): no a priori information on *mv*; (b): with a prior information on *mv* and dry to slightly wet soil condition; (c): with a prior information on *mv* and very wet soil condition.

In the case of a priori information on *mv*, the RMSE on *mv* estimates varies between 4.0 and 4.5 vol.% for all *mv* and *Hrms* values of the validation synthetic dataset for dry to slightly wet soil conditions (Figures V.31). With the use of a priori information on *mv*, the bias reduction varies between -1.0 vol. % (low *Hrms*) and +4.0 vol.% (high *Hrms*). In addition, RMSE and bias on *mv* estimates are slightly dependent on the incidence angle. The RMSE is about 3 vol.

% and the bias is about +1.2 vol. % for incidence angles between 20° and 45°. For very wet soil conditions, the RMSE on *mv* estimates varies in the case of a priori information on *mv* between 4.1 and 7.0 vol.% for all *mv* and *Hrms* values of the validation synthetic dataset. The highest RMSE-values correspond approximately to low *Hrms*-values. The bias is also well reduced mainly for low *Hrms*-values (-4.0 vol.% for *Hrms*-values of 0.5 cm).

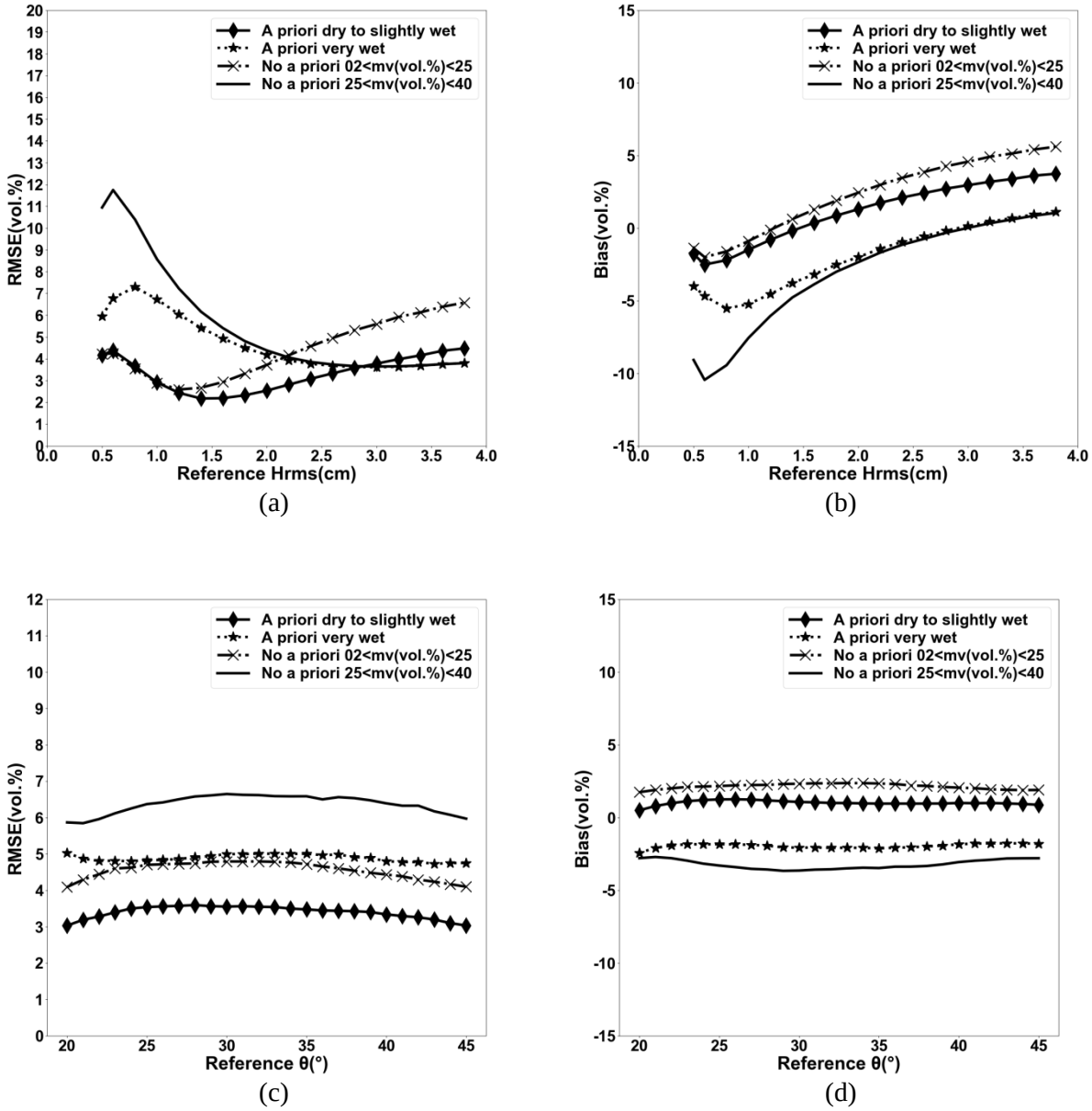


**Figure V.31.** Accuracy on the *mv* estimates (RMSE and bias "=estimated – measured") retrieved from the synthetic dataset generated from IEM. VV and VH are the inputs of the NNs. The NNs outputs are *Hrms* and *mv* together. Three NNs are tested: without a priori information on *mv*, with a priori information on *mv* with dry to slightly wet soil conditions, with a priori information on *mv* with very wet conditions.

*V.4.3.1.1.2 Using Baghdadi model*

The results show that the introducing of a priori information on *mv* in the case of dry to slightly wet soil conditions improves the *mv* estimates. The RMSE on *mv* estimates decreases from 5.67 vol.% without a priori information on *mv* to 4.97 vol.% in the case of a priori information on *mv*. In addition, the difference between estimated and measured *mv* is also reduced from +1.96 vol.% to +1.1 vol.% (Figure V.32). The RMSE on *mv* estimates in the case of very wet soil conditions decreases from 6.14 vol.% without a priori information on *mv* to 4.24 vol.% in the case of a priori information on *mv*. In addition, the difference between estimated and measured *mv* is also well reduced from -2.9 vol.% to -1.5 vol.% (Figure V.32).

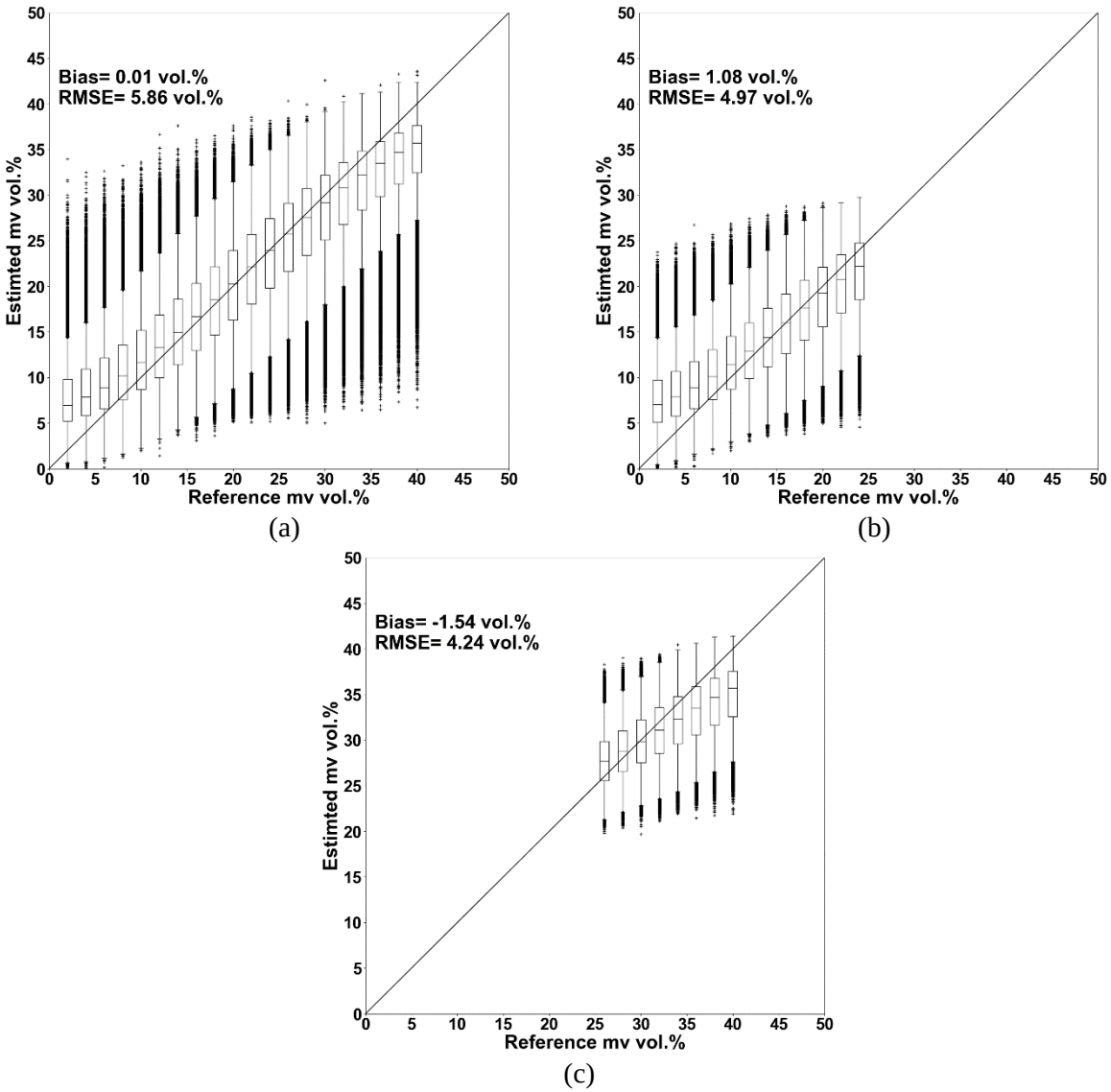


**Figure V.32.** Box plots of *mv* estimates retrieved from the synthetic dataset generated using Baghdadi model. Neural networks were trained and validated using VV and VH polarizations. The NNs outputs are *Hrms* and *mv* together. (a): no a priori information on *mv*; (b): with a prior information on *mv* and dry to slightly wet soil conditions; (c): with a prior information on *mv* and very wet soil condition.

The analysis according to *Hrms* and incidence angle "θ" show that the bias (estimated *mv* - measured *mv*) and the RMSE are strongly dependent on *Hrms* and incidence angle "θ" (Figure V.33). In the case of a priori information on *mv*, the RMSE on *mv* estimates varies between 5.1 and 6.0 vol.% for all *mv* and *Hrms* values considered in this study for dry to slightly wet soil conditions. In comparison to the case where no a prior information on *mv* is used, the use of a priori information shows that the bias reduction varies between -2.5 vol. % (low *Hrms*) and +4.0 vol.% (high *Hrms*). Finally, RMSE and bias on *mv* estimates are slightly dependent on the incidence angle "θ". The RMSE increases from 3.0 vol. % (for θ=20°) to 6.1 vol. % (for θ=45°). The bias on *mv* is approximately about +1.0 vol. % for "θ" between 20° and 45°. In addition, Figure V.33 shows that the RMSE on *mv* estimates is well reduced in the case of a priori information on *mv* for very wet soil conditions (between 4.0 and 6.0 vol.%). The highest RMSE values correspond to low *Hrms*-values. The underestimation of *mv* is well reduced mainly for low *Hrms*-values from -8.80 vol.% without a priori information on *mv* to -4.5 vol.% with a prior information on *mv* for very wet soils. In addition, the analysis of the RMSE on *mv* estimates shows that the RMSE is well reduced mainly for high incidence angles (θ=45°) from 9.00 vol.% without a priori information on *mv* to 5.00 vol.% with a priori information on *mv*.

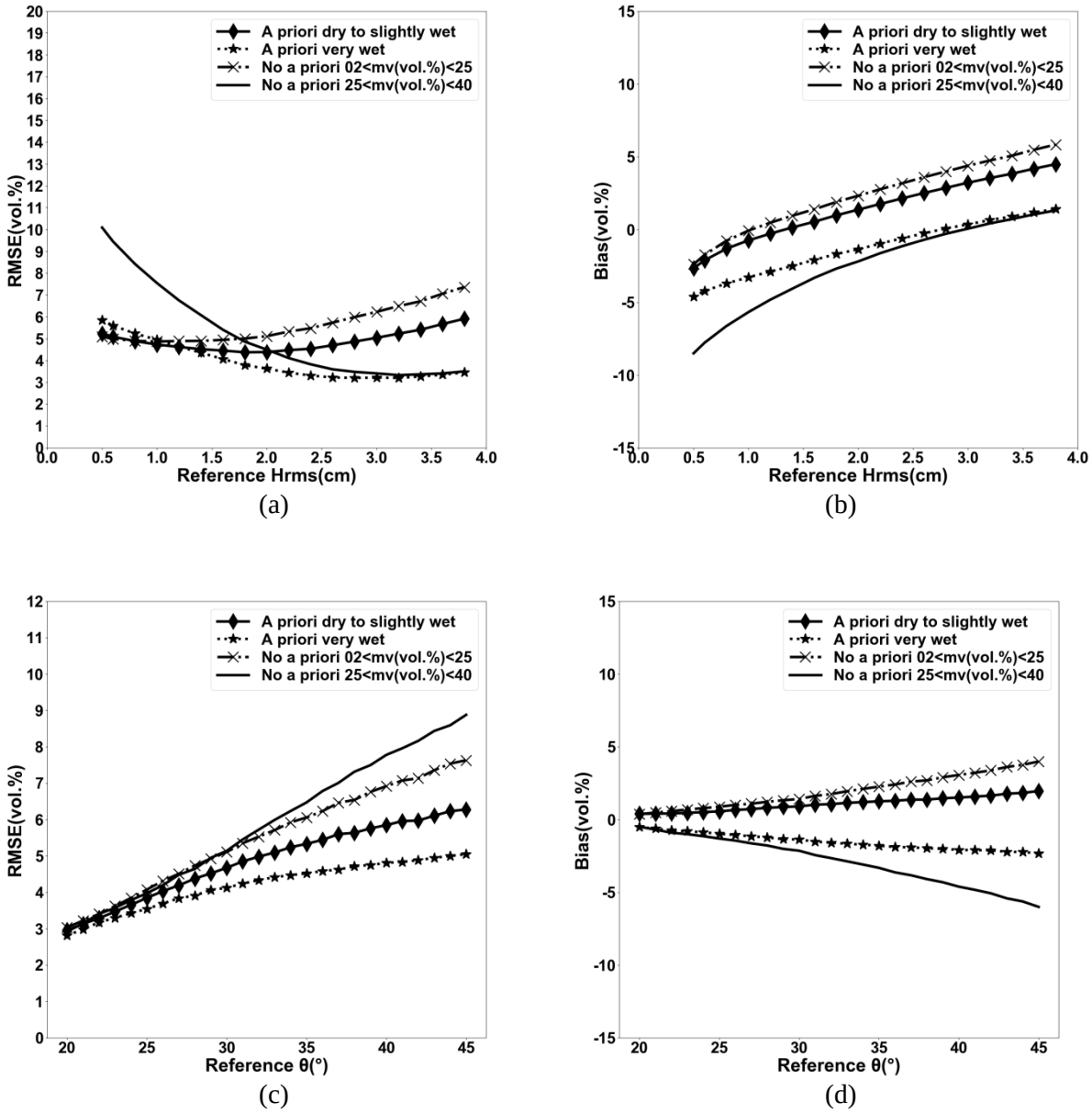


**Figure V.33.** Accuracy on the *mv* estimates (RMSE and bias "=estimated – measured") retrieved from the synthetic dataset generated from Baghdadi model. VV and VH are the inputs of the NNs. The NNs outputs are *Hrms* and *mv* together. Three NNs are tested: without a priori information on *mv*, with a priori information on *mv* with dry to slightly wet soil conditions, with a priori information on *mv* with very wet conditions.

*V.4.3.1.1.3 Discussion*

The comparison between results obtained with IEM and Baghdadi model shows similar performances in the estimation of soil moisture.

Using IEM and Baghdadi model, the use of a priori information on *mv* strongly improves the estimation of *mv*. For *Hrms* between 1 and 2 cm (the range of surface roughness the most

encountered in agricultural environments) results show that the RMSE on *mv* varies between 3.0 and 6.0 vol.% using the IEM model and between 3.9 and 5.5 vol.% using Baghdadi model. The difference between estimated and real *mv* in the case of dry to slightly wet soils varies between -1.0 and +1.0 vol.% using IEM model and between -0.5 and +2.0 vol.% using Baghdadi model. For very wet soils and *Hrms* between 1 and 2 cm, an underestimation of *mv* is observed using both IEM and Baghdadi model, from -5.0 to -2.5 vol.% and from -4.0 to -1.3 vol.%, respectively.

#### *V.4.3.1.2 Estimation of soil roughness "Hrms"*

##### *V.4.3.1.2.1 Using the IEM model*

Figure V.34 shows the results for estimating the soil roughness using the synthetic dataset generated from the IEM model with VV and VH polarizations in input to neural networks. The RMSE is 0.96 cm in the case of no a priori information on *mv*. Similar RMSE is obtained for dry to slightly wet conditions about 0.98 cm when a priori information on *mv* is used. Lower RMSE is obtained with a priori information on *mv* in the case of very wet soils (RMSE=0.65 cm).

In addition Figure V.34 shows an overestimation of *Hrms* for *Hrms* lower than 2 cm and an underestimation of *Hrms* for *Hrms* higher than 2 cm.

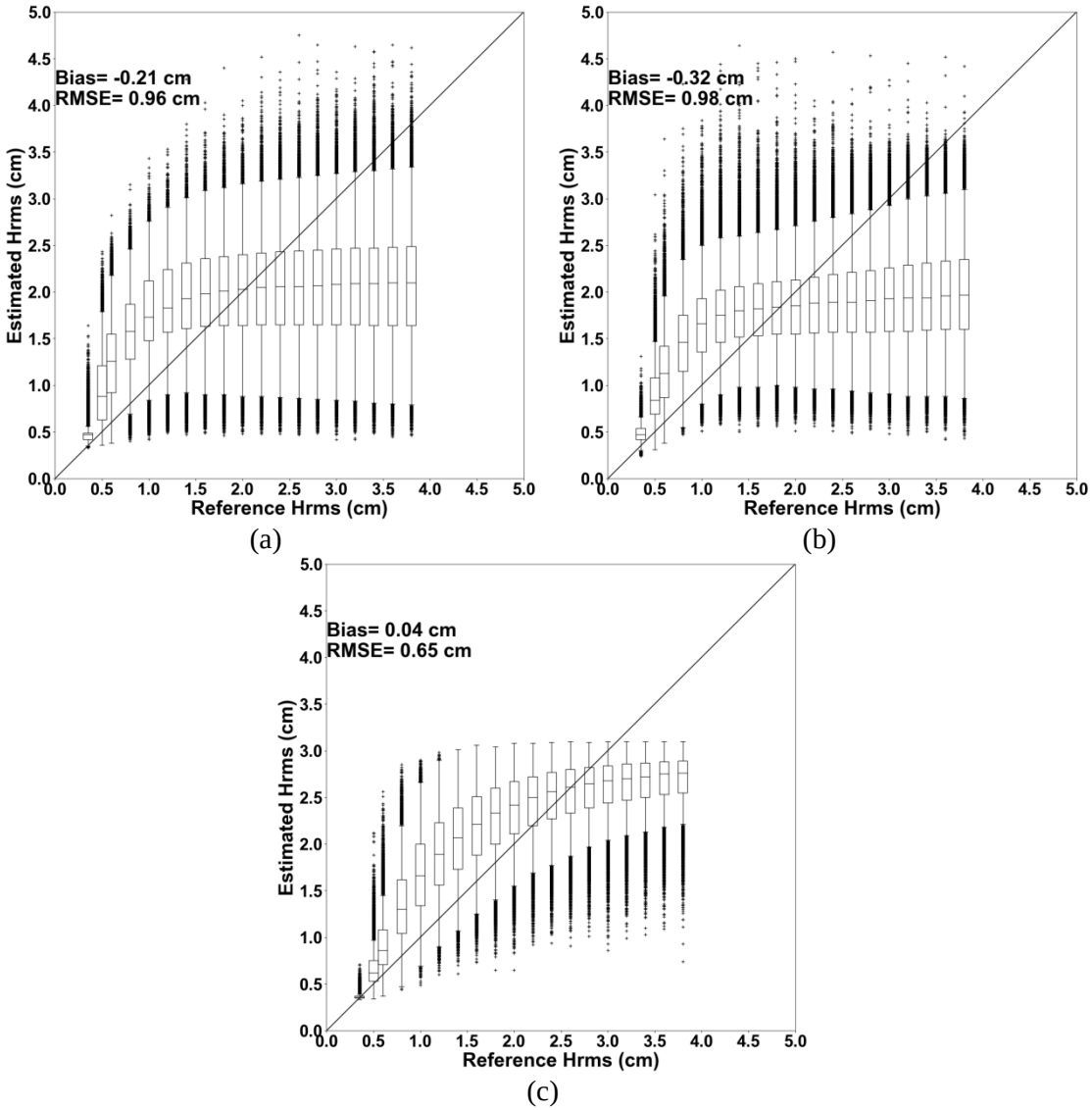


**Figure V.34.** Box plots of *Hrms* (cm) retrieved from the synthetic dataset generated from the IEM model in using VV and VH polarizations together. (a): without a priori information on *mv*, (b): with a priori information on *mv* and dry to slightly wet soils, (c): with a priori information on *mv* and very wet soils.

#### *V.4.3.1.2.2 Using Baghdadi model*

Results show that the RMSE on *Hrms* estimates without a priori information on *mv* or with a priori information on *mv* for dry to slightly wet soils are similar (0.87 and 0.86 cm, respectively) (Figure V.35). In the case of very wet soil conditions, the RMSE obtained using a priori information on *mv* is about 0.74 cm (Figure V.35).

In addition Figure V.35 shows an overestimation of *Hrms* for *Hrms* lower than 2 cm and an underestimation of *Hrms* for *Hrms* higher than 2 cm.

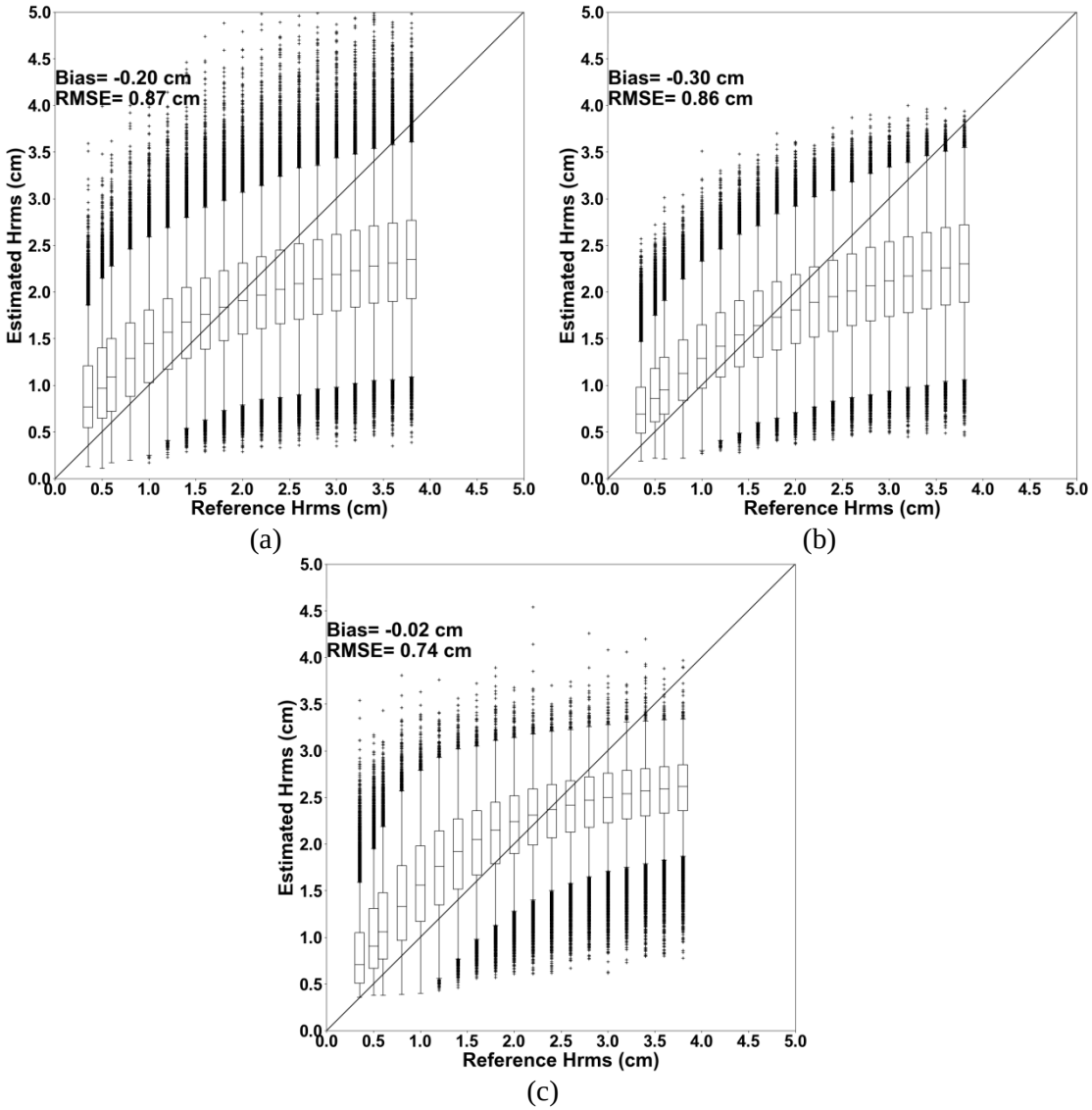


**Figure V.35**. Box plots of *Hrms* (cm) retrieved from the synthetic dataset generated from Baghdadi model in using VV and VH polarizations together. (a): without a priori information on *mv*, (b): with a priori information on *mv* and dry to slightly wet soils, (c): with a priori information on *mv* and very wet soils.

*V.4.3.1.2.3 Discussion*

The comparison between results obtained with IEM and Baghdadi model shows slightly better estimation of soil roughness in using Baghdadi model. Both models show an overestimation of *Hrms* for *Hrms* lower than 2 cm and an underestimation of *Hrms* for *Hrms* higher than 2 cm. Howewer, these over- and under-estimations are lower with Baghdadi model than with IEM model.

*V.4.3.2 Real dataset*

The NNs built for estimating *mv* and *Hrms* are then analyzed using the real Sentinel-1 dataset. VV and VH are the inputs of NNs.

*V.4.3.2.1 Estimation of soil moisture (mv)*

*V.4.3.2.1.1 Using the IEM model*

Using the IEM model, the results obtained for the estimation of *mv* are shown in Figure V.36. Results show that the introduction of a priori information on *mv* provides better accuracy on the *mv* estimates than the case without a priori information on *mv* (RMSE=5.83 vol.% with a priori information on *mv* and RMSE=7.25 vol.% without a priori on *mv*).

The analysis of the difference between the estimated and measured *mv* shows that the strong underestimates of the *mv* corresponds to low *Hrms*-values (*Hrms*<2 cm) and the strong overestimates corresponds to high *Hrms*-values (*Hrms*>2 cm).

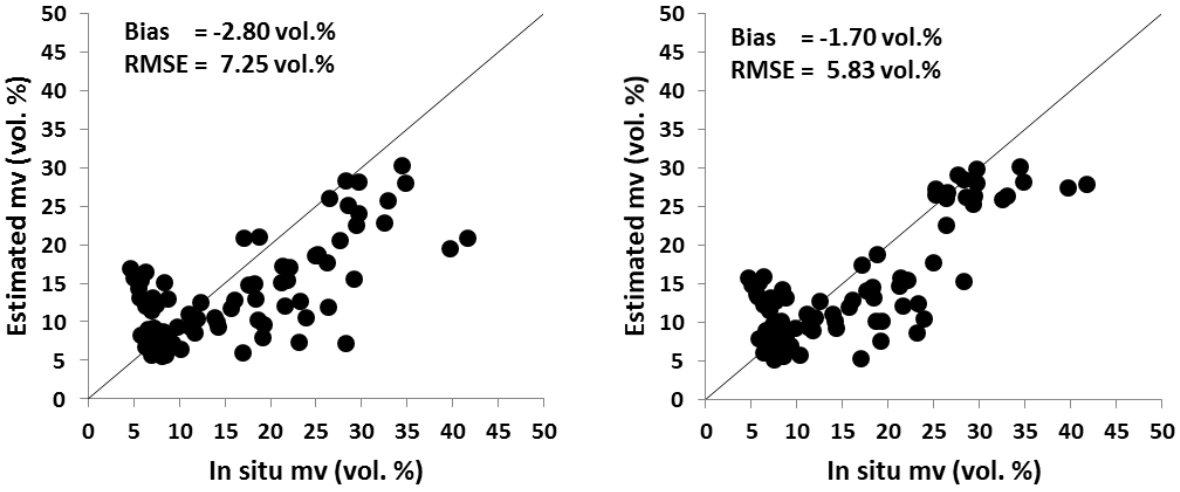


(a) (b)

**Figure V.36.** Retrieved *mv* versus in situ measurements in using the IEM model. VV and VH are used in input to neural networks. *Hrms* and *mv* are the outputs. (a): without a priori information on *mv*; (b): with a priori information on *mv*. Each point corresponds to one reference plot.

*V.4.3.2.1.2 Using Baghdadi model*

Figure V.37 shows the results obtained for the estimation of *mv* using Baghdadi model. An RMSE of 6.62 vol.% is obtained with the introduction of a priori information on *mv* and an RMSE of 8.30 vol.% in the case without a priori information on *mv*.

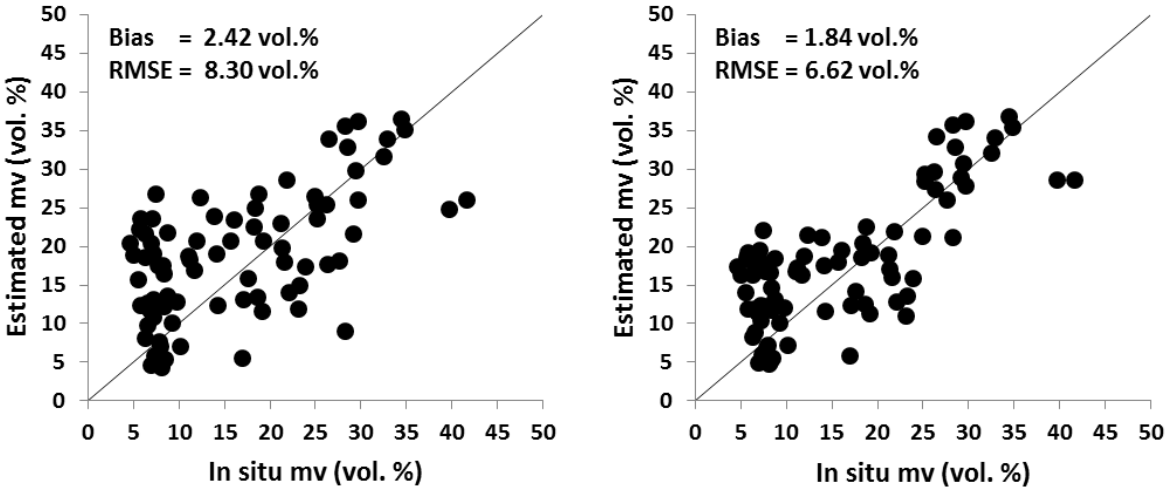


(a) (b)

**Figure V.37.** Retrieved *mv* versus in situ measurements in using Baghdadi model. VV and VH are used in input to neural networks. *Hrms* and *mv* are the outputs. (a): without a priori information on *mv*; (b): with a priori information on *mv*. Each point corresponds to one reference plot.

*V.4.3.2.2 Estimation of surface roughness (Hrms)*

*V.4.3.2.2.1 Using the IEM model*

Results show that the RMSE on *Hrms* estimates is 0.84 cm in the case of without a priori information on *mv*. In the case with a priori information on *mv*, the RMSE is of 0.75 cm (Figure V.38).

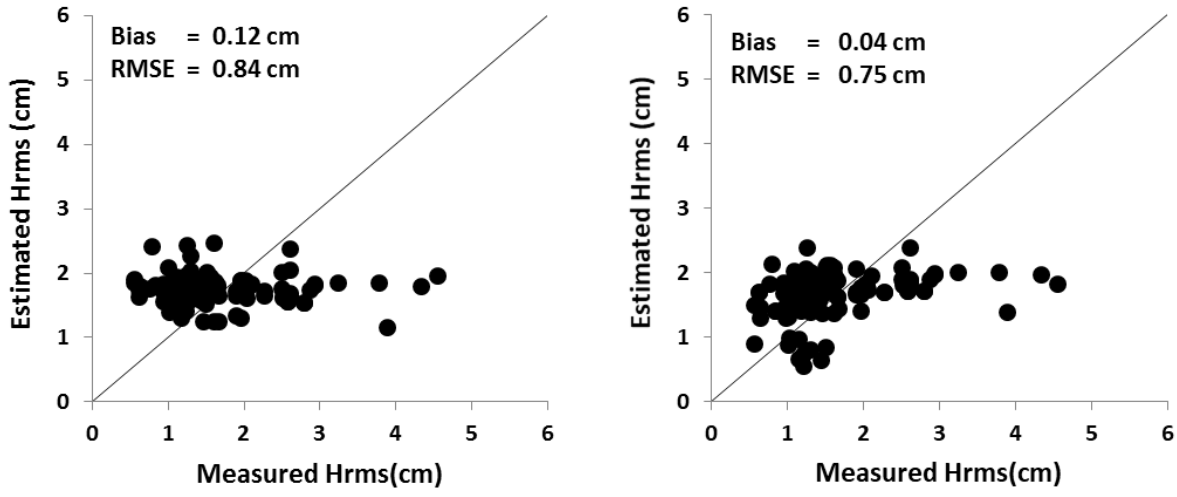


**(a)** **(b)**

**Figure V.38.** Retrieved *Hrms* versus measured measurements in using the NNs trained with synthetic data simulated from the IEM model. VV and VH are used in input to neural networks. *Hrms* and *mv* are the outputs. (a): without a priori information on *mv*; (b): with a priori information on *mv*.

*V.4.3.2.2.2 Using Baghdadi model*

Using Baghdadi model, the precision on the estimates of *Hrms* is approximately the same in using or not a priori information on *mv* (Figure V.39). The RMSE is 1.01 cm with the case of no a priori information on *mv* and 0.97 cm in the case of a priori information on *mv*.

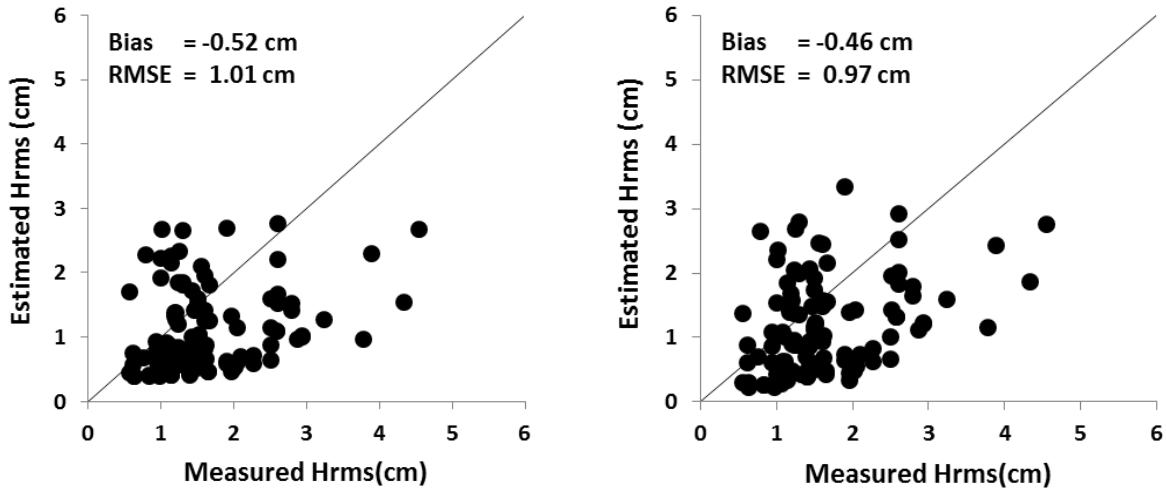


(a) (b)

**Figure V.39.** Retrieved *Hrms* versus measured measurements in using the NN trained with synthetic data simulated from Baghdadi model. VV and VH are used in input to neural networks. *Hrms* and *mv* are the outputs. (a): without a priori information on *mv*; (b): with a priori information on *mv.*

## V.5 Conclusions

The objective of this study was to investigate the potential of Sentinel-1 C-band SAR in several polarizations (VV alone, VH alone, VV and VH together) for estimating the soil roughness over bare agricultural areas using the neural networks technique (NNs). Neural networks were trained with radar backscattering coefficients generated from two models: the Integral Equation Model 'IEM' and the new semi-empirical model developed recently by Baghdadi et al. (2016). An additional simulated dataset and a real dataset composed of Sentinel-1 images and in situ measurements were then used to analyze the performance of the inversion technique for estimating the surface roughness (*Hrms*).

Two inversion configurations were proposed. The first based on estimation of soil roughness at very high spatial resolution ″VHSR″ (plot scale or on a finer scale). Two networks were applied one after the other, the first to estimate the soil moisture (*mv*) and the second using the soil moisture estimates for estimating the soil roughness. Three SAR configurations are

tested: VV alone, VH alone, VV and VH together. In order to improve the soil parameters estimates, a priori knowledge about soil moisture *mv* (dry to slightly wet or very wet soil conditions) is introduced. Three neural networks are developed for the estimation of *mv*, with and without a priori information on the soil moisture state. Next, the soil roughness is estimated at a fine spatial scale (plot or sub-plot scale) using the soil moisture estimated by the first network. The second inversion configuration concerns the estimation of both soil roughness (*Hrms*) and soil moisture (*mv*) at very high spatial resolution ″VHSR″. Both VV and VH polarizations together are used as inputs of these neural networks. Three neural networks are developed, with and without a priori information on the soil moisture state.

Using the first inversion configuration and using the two radar backscattering models, best results are obtained using the VV polarization alone for the IEM Model and the VV and VH polarizations together for Baghdadi model. The soil moisture could be estimated with an RMSE better than 6 vol.% when *a priori* information on *mv* is used in the neural network for the two models. The second neural network uses this estimation of *mv* in order to estimate the soil roughness at the plot scale. Results obtained show estimates of *Hrms* with an RMSE of 0.94 cm using the IEM model (VV polarization alone) and 0.78 cm using Baghdadi model (VV and VH polarizations together). This accuracy on *Hrms* obtained in using the NN built with a priori information on *mv* shows that the use of *mv* estimates with an accuracy of about 6 vol.% is not sufficient to accurately estimate the soil roughness in C-band. Results obtained from the real dataset show that the accuracy on *Hrms* estimates in using the *mv* estimated at the study site scale is better to that in using the *mv* estimated at the plot scale, with an RMSE on *Hrms* about 0.81 cm (RMSE=0.98 cm using *mv* estimated at plot scale) in using the IEM model (VV polarization alone) and an RMSE on *Hrms* about 1.03 cm (RMSE=1.05 cm using *mv* estimated at plot scale) in using Baghdadi model (VV and VH polarizations together).

For the second inversion configuration (VV and VH polarizations together), the use of simulated dataset from the Integral Equation Model ‘IEM’ or the new semi-empirical Baghdadi model show approximately similar results and close to the results obtained in the first inversion configuration. Using the real dataset, the soil moisture *mv* could be estimated with an RMSE better than 6.0 vol.% and 6.6 vol.% for the IEM and Baghdadi models, respectively when *a priori* information on *mv* is used in the neural networks. The RMSEs on *Hrms* are of 0.84 cm without a priori information on *mv* and 0.75 cm with a priori information on *mv* in using the IEM model. Using Baghdadi model, the RMSEs on *Hrms* are about 1.01 cm without a priori information on *mv* and 0.97 cm with a priori information on *mv*. The use

of *mv* estimated at the scale of the study site is possible only when the study site is not irrigated.

This first study on the potential of Sentinel-1 data for estimating the soil roughness shows that the development of an automatic and generalizable inversion procedure of the C-band radar signal does not allow a pertinent estimation of the soil roughness. The accuracy on soil roughness estimates obtained in this study cannot satisfy the requirements of operational users of soil roughness products (in particular to modelers) because the need is at least three roughness classes: smooth (sowing), medium (small plowing) and rough (large plowing).

Only methods based on the use of experimental relationships, which are often difficult to apply to sites other than those for which they were developed and are generally valid only for specific soil conditions, allows the mapping of three roughness classes (Baghdadi et al., 2002a). Indeed, different experimental studies have revealed that the sensitivity of the radar signal to surface roughness (i.e. the slope of the regression lines) can be highly variable from one site to another. In addition, the experimental relationships between the radar signal and *Hrms* are established for a given incidence angle and a range of soil moisture. The soil composition could be also different from one site to another. All these reasons explain why the experimental relationships are not generalizable.

# *VI. General conclusion and perspectives*

## VI.1 General conclusion

The state of the soil surface and in particular through roughness and moisture exerts a fundamental influence on the distribution of rain between infiltration, surface retention and runoff. In addition, it has a key role in surface hydrological processes. The characterization and consideration of these surface conditions is currently an important issue for the physical-based modeling of the processes of infiltration, runoff and erosion. The main objective of this thesis was to evaluate the potential of the new Sentinel-1 SAR for the mapping of surface roughness in bare agricultural areas.

In order to achieve this objective, several steps were followed. The first step was to evaluate the potential of the five most popular radar backscattering models (Oh, Dubois, IEM, AIEM and IEM modified by Baghdadi "IEM_B") using a wide dataset composed of AIRSAR, SIR-C, JERS-1, PALSAR-1, ESAR, ERS, RADARSAT, ASAR, TerraSAR-X, CosmoSky-Med, Sentinel-1 acquisitions over numerous agricultural sites in France, Italy, Germany, Belgium, Luxembourg, Canada and Tunisia. In addition, in situ measurements of soil moisture and surface roughness were carried out simultaneously to SAR acquisitions over bare soil surfaces (soil moisture "*mv*" ranged between 2 vol. % and 47 vol. %, surface roughness "*Hrms*" between 0.2 cm and 9.6 cm which corresponds to *kHrms* from 0.2 and 13.4). The SAR sensors used are in L-, C- and X-bands with incidence angle between 18° and 57°. Results showed that the IEM modified by Baghdadi "IEM_B" using a fitting parameter instead of measured correlation length provides the most accurate SAR simulations with bias (real data − model simulations) lower than 1.0 dB and Root Mean Square Error "RMSE" lower than 2.0 dB. The IEM_B model showed slightly better performance in X-band (RMSE = 1.8 dB) than in L- and C-bands (RMSE between 1.9 and 2.3 dB). The IEM and AIEM models showed better simulations of measured backscattering coefficients using exponential correlation function (RMSE of 5.6 dB for HH and 6.5 dB for VV using the IEM model; RMSE of 4.4 dB for HH and 3.8 dB for VV using the AIEM model) than in using Gaussian correlation function (RMSE about 10 dB for both HH and VV and in using both IEM and AIEM models). The Oh models showed good results in simulations with slightly better performance of the Oh 1992 version with bias less than 1.0 dB and RMSE of 2.6 dB and 2.4 dB respectively for HH and VV. The Oh model showed better agreement in simulations than Dubois model which simulates the backscattering in HH polarization with RMSE of 4.0 dB, and slightly better simulations for VV polarization with RMSE of 2.9 dB.

The second step was to produce a new semi-empirical backscattering model (Baghdadi model) for bare soils based on the formulation of Dubois model. The different terms of Dubois model equations that describe the dependence between the SAR signal and both sensor and soil parameters have been validated or modified to improve the modeling of the radar signal. The new radar backscattering model was developed for HH, VV and HV polarizations. Analysis of this new model showed very good performances in simulating the radar signal. Results showed that this new proposed model improved the performances of simulations (Biases and RMSEs were well decreased) in comparison to the Dubois model for both cases HH and VV polarizations. The radar signal in HV polarization which was not modeled in the Dubois model was added in the new model. The high over- and under-estimations for some ranges of soil moisture, surface roughness and radar incidence angle observed with Dubois model were obviously eliminated with the new backscattering model. The performances of this new model in the L-band were similar to the Dubois model's simulations. For HH and VV, better results were observed with this new model in C- and X-bands (RMSE approximately about 1.9 dB), while the Dubois model simulated the radar backscattering signal with RMSE between 2.6 dB and 4.1 dB in C- and X-bands, respectively. Moreover, the difference between the new model simulations in HV polarization and the real SAR data show an RMSE of 2.1 dB.

The last step was to develop an inversion procedure based on neural networks to estimate the soil surface roughness from C-band Sentinel-1 SAR data in the case of bare agricultural soils. The neural networks were trained using synthetic dataset simulated by the IEM model calibrated by Baghdadi "IEM_B" and the new semi-empirical model developed in the previous step (Baghdadi model). For this purpose, the inversion approach was then validated in using both synthetic and real dataset. The synthetic datasets consist of a wide range of surface roughness "*Hrms*" and soil moisture "*mv*" simulated from IEM-B and Baghdadi models. The real dataset used in the validation of the inversion approach consists of C-band Sentinel-1 images (one in France and one in Tunisia) and in-situ measurements. This work was done in order to evaluate the potential of Sentinel-1 SAR sensors for retrieving soil roughness in several polarizations (VV alone, VH alone, VV and VH together) using the neural networks technique (NNs).

In order to achieve this last step and to estimate the soil roughness, two inversion configurations were proposed. The first configuration is composed of two consecutive neural networks (NNs) that are applied consecutively, the first to estimate the soil moisture (*mv*) and

the second using the soil moisture estimates for estimating the soil roughness (*Hrms*). Three cases were tested: VV alone, VH alone, VV and VH together. The second inversion configuration uses a single NN to estimate both soil roughness (*Hrms*) and soil moisture (*mv*). Both VV and VH polarizations are used as inputs of the neural network. A priori knowledge about soil moisture *mv* (dry to slightly wet or very wet soil conditions) was also introduced in the two inversion configurations in order to improve the soil parameters estimates (soil moisture and surface roughness).

The use of the first inversion configuration showed better estimation of *mv* and *Hrms* in using VV alone and the synthetic dataset simulated from the IEM-B model. When Baghdadi model was used to simulate the synthetic dataset, better results were obtained in using VV and VH together. Results showed that the soil moisture (*mv*) could be estimated at the plot scale with an RMSE better than 6 vol.% using a priori information on *mv*. Then, this estimated soil moisture "*mv*" was used in order to estimate the soil roughness at the plot scale. Results showed an estimation of *Hrm*s with an RMSE of 0.94 cm using the IEM-B model with VV polarization alone and 0.78 cm using Baghdadi model with both VV and VH. This result is not sufficient to accurately estimate the soil roughness in C-band. Using the real dataset, results showed that the RMSE on *Hrms* is of 0.98 cm in using the IEM model (VV alone) and of 1.05 cm in using Baghdadi model (VV and VH together).

The use of the second inversion configuration (VV and VH together for estimating both *mv* and *Hrms* by the same neural network) showed close performances in using synthetic datasets simulated from the two backscattering models. Moreover, the performances are similar with the two inversion configurations. Using the real dataset, the soil moisture *mv* could be estimated with an RMSE about 6.0 vol.% and 6.6 vol.% respectively for the IEM-B and Baghdadi models, when a priori information on *mv* is used in the neural networks. Using a priori information on *mv* and using the IEM_B model, the RMSEs on *Hrms* are of 0.84 cm without a priori information on *mv* and 0.75 cm with a priori information on *mv*. Using Baghdadi model, the RMSEs on *Hrms* are 1.01 cm without a priori information on *mv* and 0.97 cm with a priori information on *mv*.

In general, at least three roughness classes (smooth, medium and rough) are needed in order to fulfill the operational users of soil roughness products. This first study on the potential of Sentinel-1 data for estimating the soil roughness didn't satisfy these requirements. Results show that the inversion procedure of the C-band radar signal does not permit an accurate estimation of the soil roughness. Thus, the three roughness classes are not achievable with an

incidence of about 40° (nominal incidence of Sentinel-1). Indeed, the incidence angles used in this study, between 37° and 41° using VV, VH or VV and VH together, are not optimal for the characterization of the soil roughness. Fung, (1994) has shown that HH polarization is more sensitive to soil roughness than VV for high incidence angles. Moreover, Baghdadi et al., (2002a) indicated that the high incidence angles (about 45°) are more suitable to discriminate various roughness classes (smooth, medium and rough) over bare agricultural fields. So that, the results obtained by the Sentinel-1 SAR sensor for the estimation of surface roughness are logical with such medium incidence angles. Moreover, the use of two polarizations does not improve the estimation of the soil roughness.

## VI.2 Perspectives

In general, the work of this thesis focused on several research sectors (evaluation, modeling and estimation of soil parameters). This thesis showed the potential of radar images (i.e. Sentinel-1 radar sensor) to estimate soil surface parameters. The results obtained could be used as a guide to support research in several fields.

Several research fields emerge from this work. These axes relate, on the one hand, to the potential of SAR sensors to estimate soil parameters (soil moisture and surface roughness) and, on the other hand, the best use the SAR's instrumental parameters (i.e. wavelengths) and configurations (i.e. incidence angles) in order to attain better accurate estimations.

The results obtained in this thesis lead to indicate that the C-band Sentinel-1 SAR data with incidence angle about 40° are not suitable to retrieve surface roughness. So, It is essential to further develop multi-sensor methods combining radar data acquired from two radar wavelengths (L and C bands, or C and X bands). Indeed, the three frequencies L, C and X have complementary capabilities for estimating soil moisture and surface roughness. As the radar signal in X-band is more sensitive to soil moisture than the radar signal in C-band (accuracy on soil moisture estimates in X-band is twice greater than the once obtained in C-band, Aubert et al. (2011)), it might be relevant to combine SAR data in C and X bands to estimate both soil parameters (i.e. soil moisture and surface roughness). The X-band data will be used to estimate soil moisture and the C-band data will be used to estimate the surface roughness. The use of the higher radar wavelengths (L-band) may also be relevant due to the high potential of higher wavelengths for the estimation of soil roughness. In this context, different spatial missions with L band SAR systems are in preparation, as NISAR (NASA and

ISRO mission). European Space Agency also discusses the possibility of adding a new L band SAR to the constellations of Sentinels. The arriving of these missions will open a serious opportunity to develop studies based on the combination of multi-sensor acquired data, particularly with Sentinel-1 & Sentinel-2 missions. The multi-sensor, and particularly multi-frequency algorithms will be essential to reach the operational algorithms which are able to separate effects of different surface parameters on radar signals. This is particularly the case of covered vegetation surface, for which, retrieving of roughness is still very complicated with one frequency configuration. The final objective is to reach in next years the assimilation of roughness maps, as for soil moisture in different surface process models, as runoff and erosion models.

***Annex 1:*** *Results on soil roughness estimates using synthetic dataset generated from the IEM model*

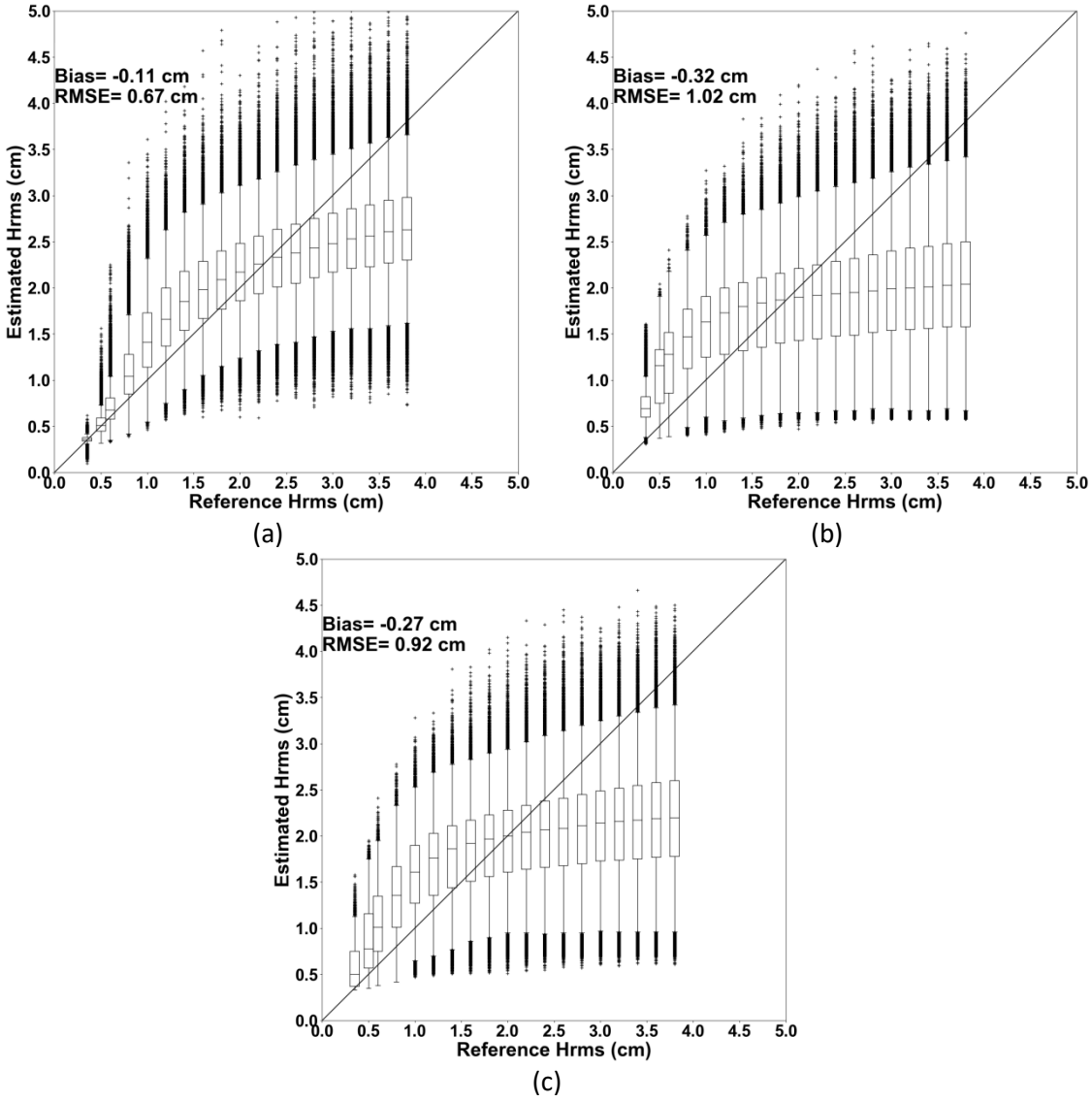


**Figure A1.1.** Box plots of *Hrms* (cm) retrieved from the synthetic dataset generated from the IEM model in using VH polarization. (a) the input *mv* to the network corresponds to real *mv*, (b) the input *mv* to the network corresponds to *mv* estimated by the NN built for estimating *mv* without a priori information on *mv*, (c) the input *mv* to the network corresponds to *mv* estimated by the NN built for estimating *mv* with a priori information on *mv*.

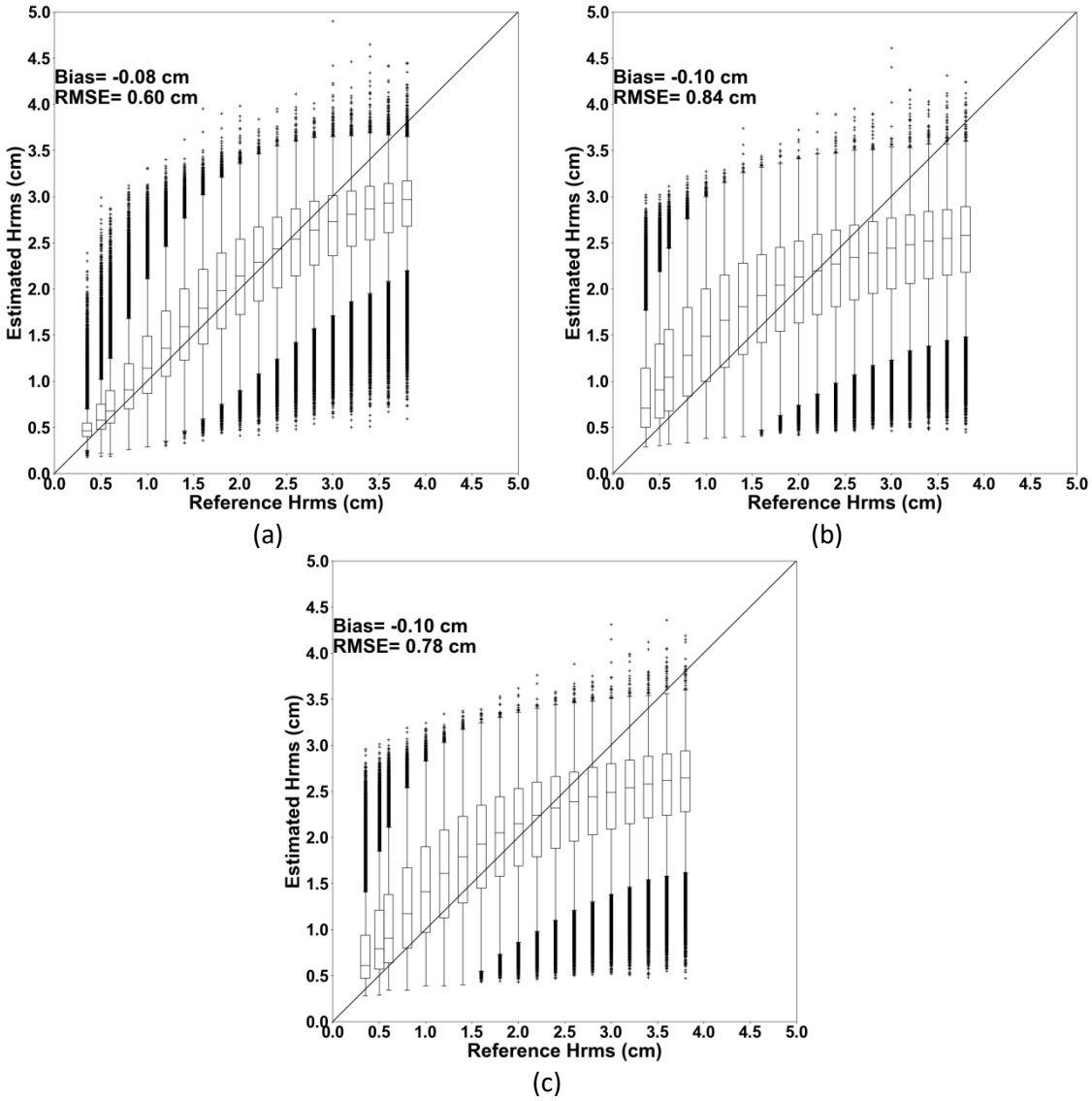


**Figure A1.2.** Box plots of *Hrms* (cm) retrieved from the synthetic dataset generated from IEM model in using VV and VH polarizations together. (a) the input *mv* to the network corresponds to real *mv* (those that are in the validation dataset), (b) the input *mv* to the network corresponds to *mv* estimated by the NN built for estimating *mv* without a priori information on *mv*, (c) the input *mv* to the network corresponds to *mv* estimated by the NN built for estimating *mv* with a priori information on *mv*.

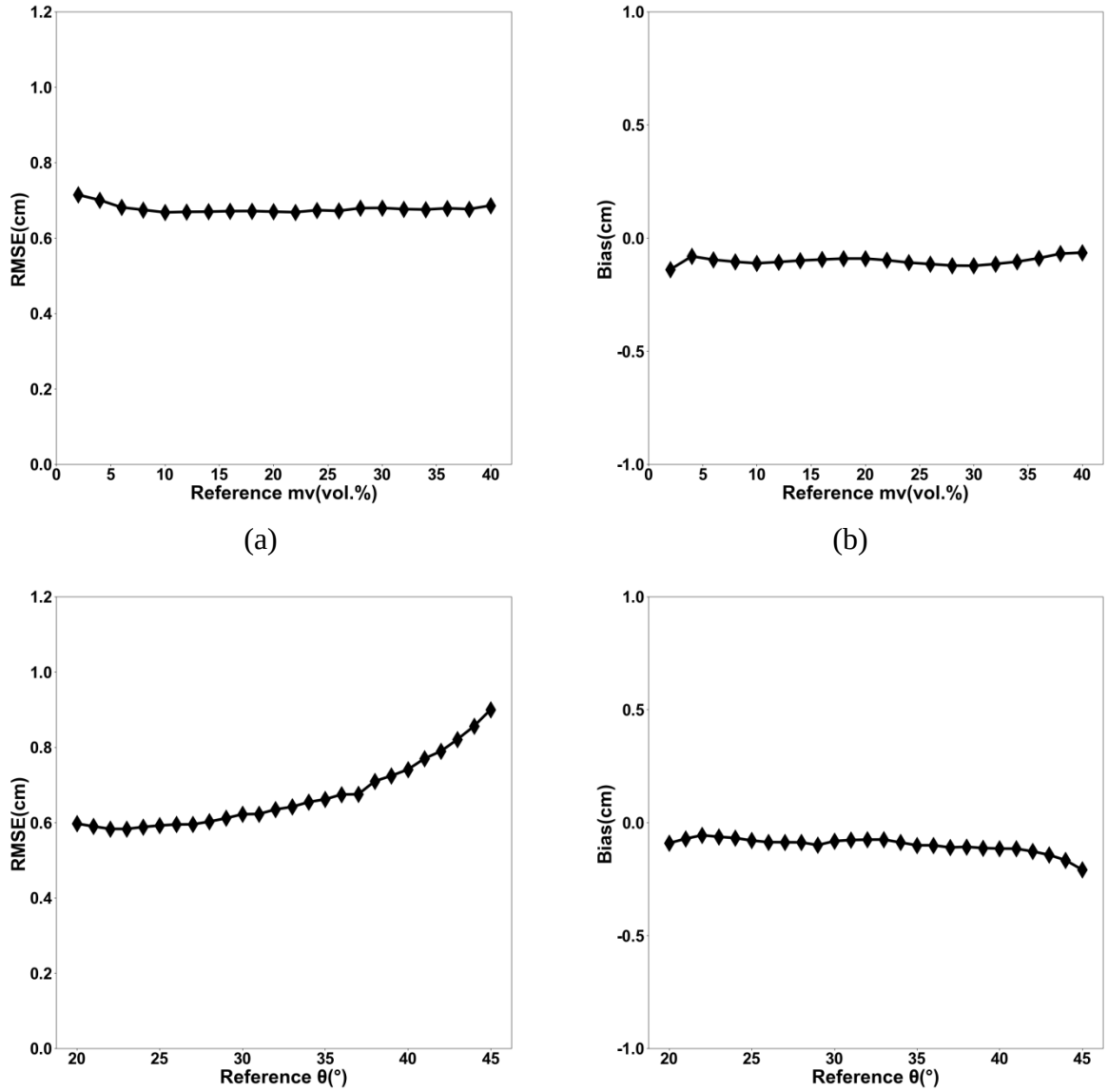


**Figure A1.3.** Accuracy on *Hrms* estimates (RMSE and Bias) as a function of the soil moisture and the incidence angle for VH polarization alone. The *mv* in input to the NN corresponds to the exact *mv* (without estimation error).

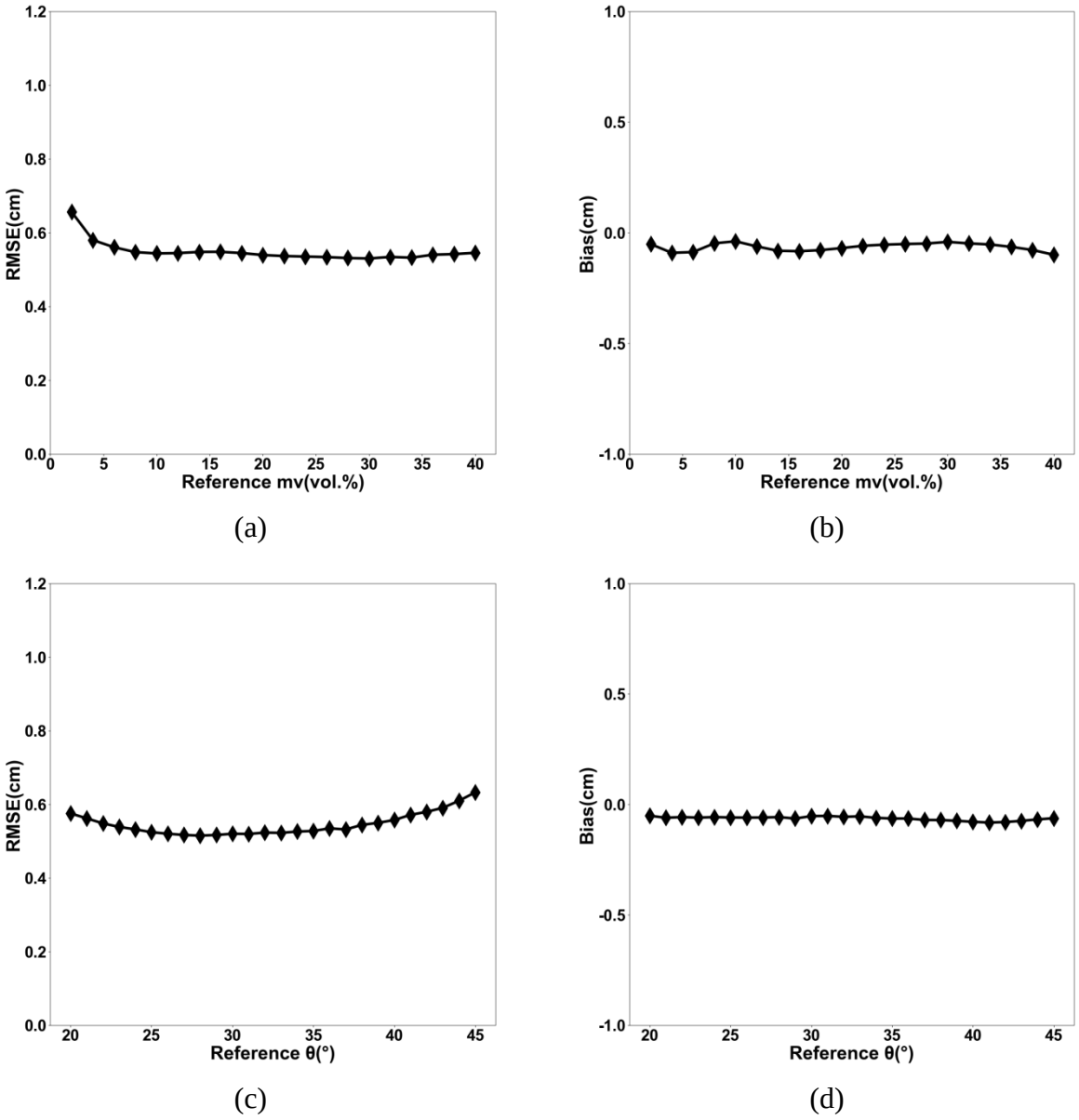


**Figure A1.4.** Accuracy on *Hrms* estimates (RMSE and Bias) as a function of the soil moisture and the incidence angle using VV and VH together. The *mv* in input to the NN corresponds to the exact *mv* (without estimation error).

***Annex 2:*** *Results on soil roughness estimates using synthetic dataset generated from Baghdadi model*

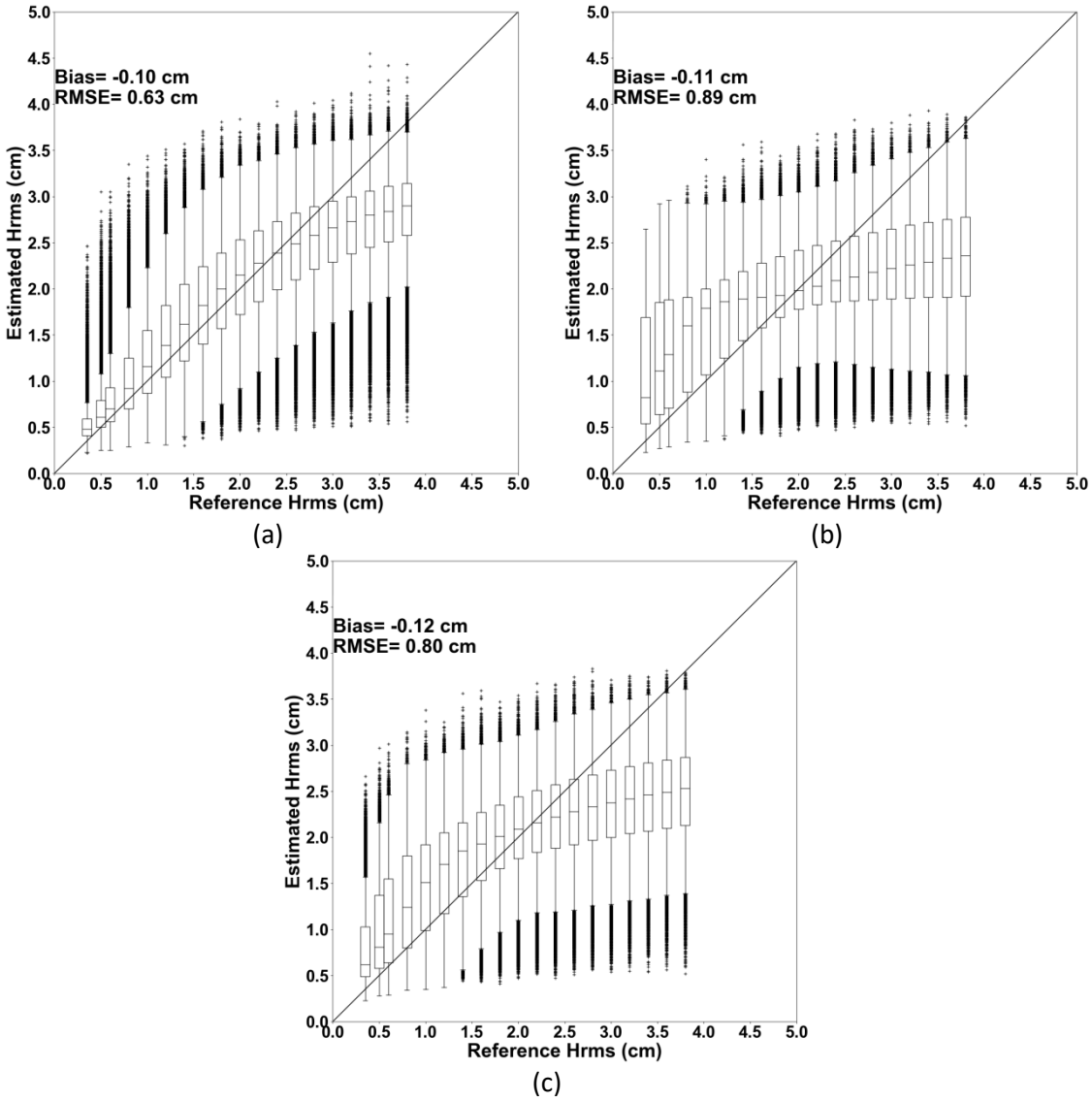


**Figure A2.1.** Box plots of *Hrms* (cm) retrieved from the synthetic dataset generated from Baghdadi model in using VV polarization alone. (a) the input *mv* to the network corresponds to real *mv* (those that are in the validation dataset), (b) the input *mv* to the network corresponds to *mv* estimated by the NN built for estimating *mv* without a priori information on *mv*, (c) the input *mv* to the network corresponds to *mv* estimated by the NN built for estimating *mv* with a priori information on *mv*.

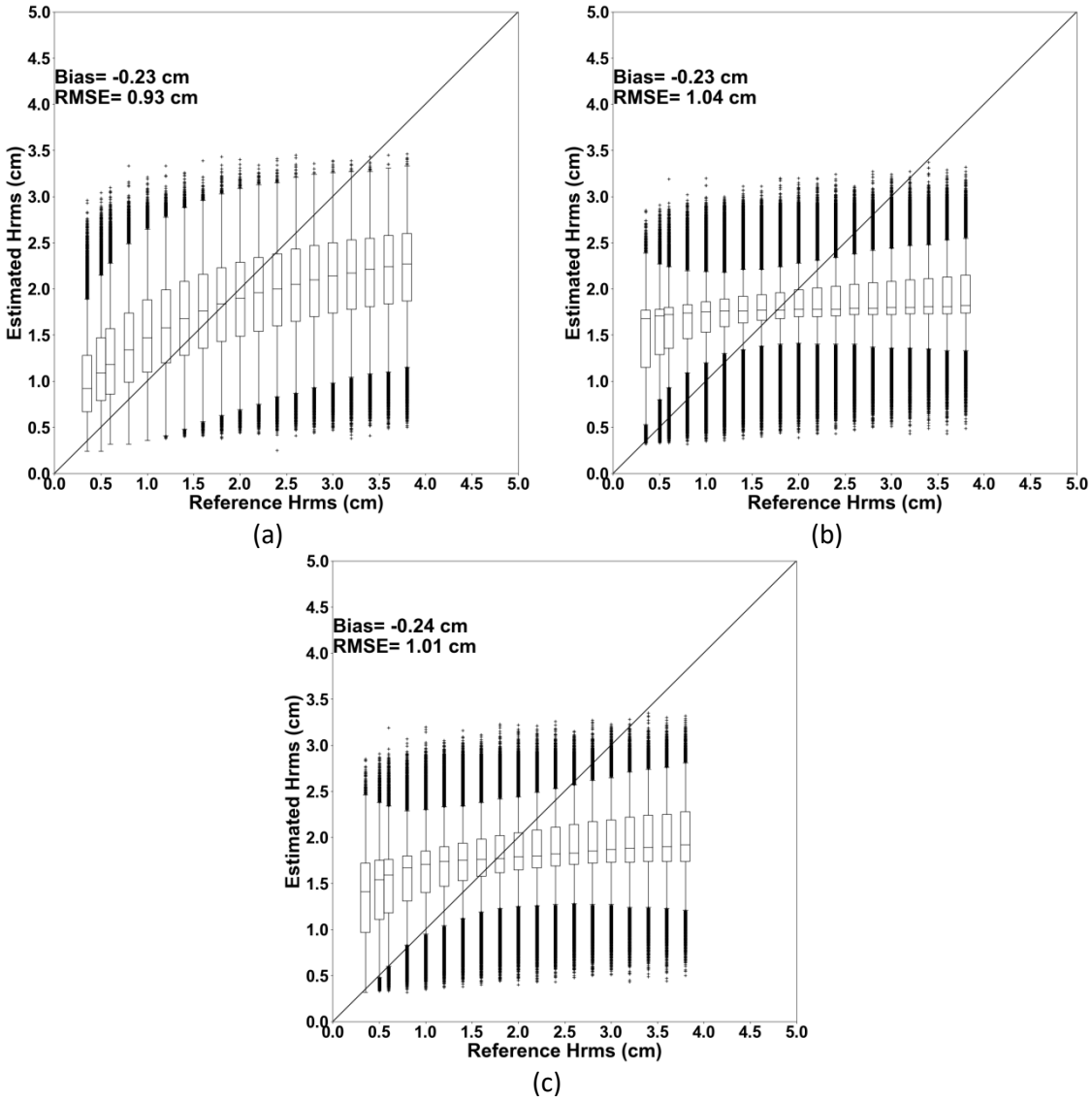


**Figure A2.2.** Box plots of *Hrms* (cm) retrieved from the synthetic dataset generated from Baghdadi model in using VH polarization alone. (a) the input *mv* to the network corresponds to real *mv* (those that are in the validation dataset), (b) the input *mv* to the network corresponds to *mv* estimated by the NN built for estimating *mv* without a priori information on *mv*, (c) the input *mv* to the network corresponds to *mv* estimated by the NN built for estimating *mv* with a priori information on *mv*.

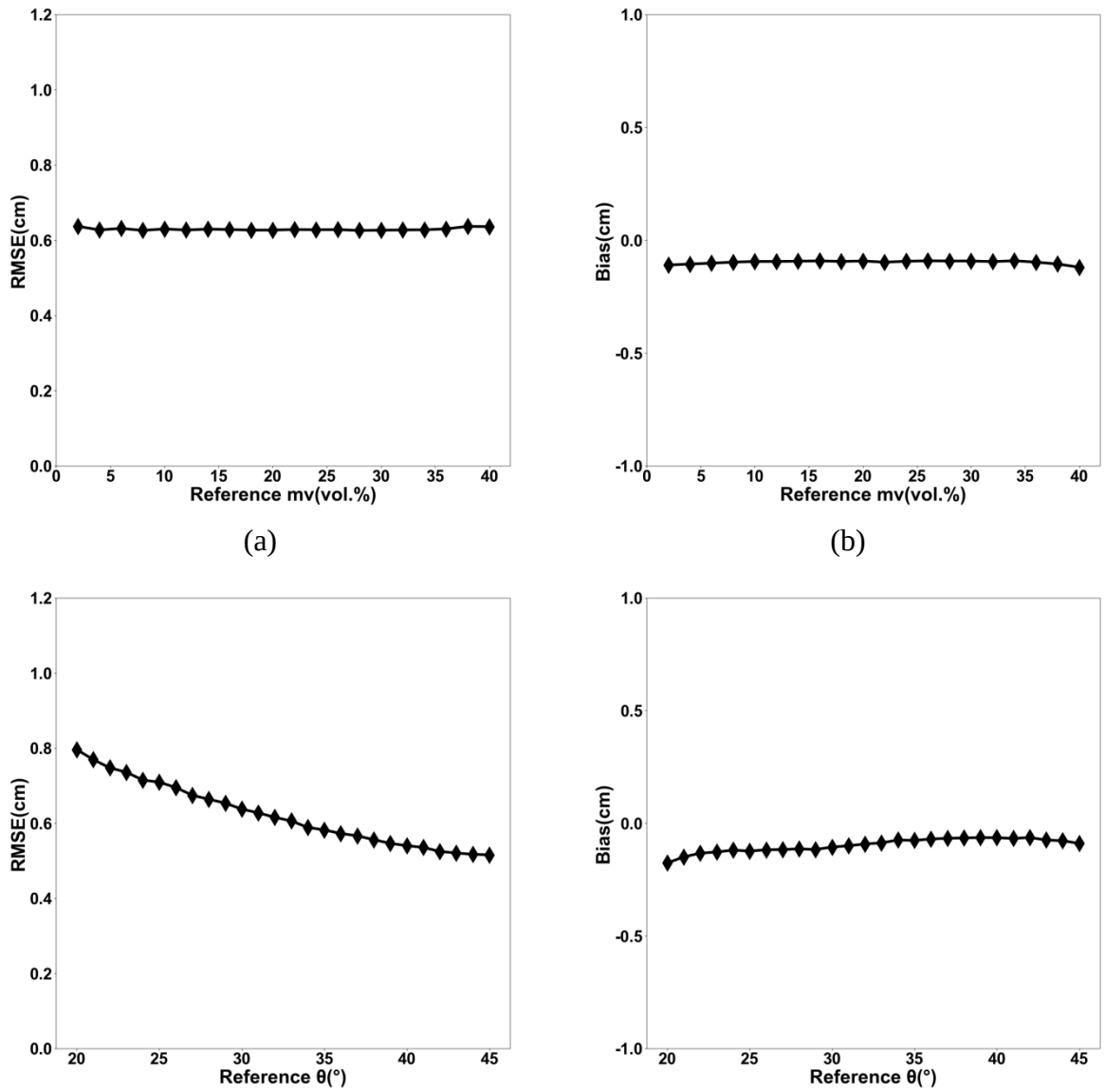


**Figure A2.3.** Accuracy on the *Hrms* estimates (RMSE and Bias) as a function of the soil moisture and the incidence angle for VV polarization alone. The *mv* in input to the NN corresponds to the exact *mv* (without estimation error).

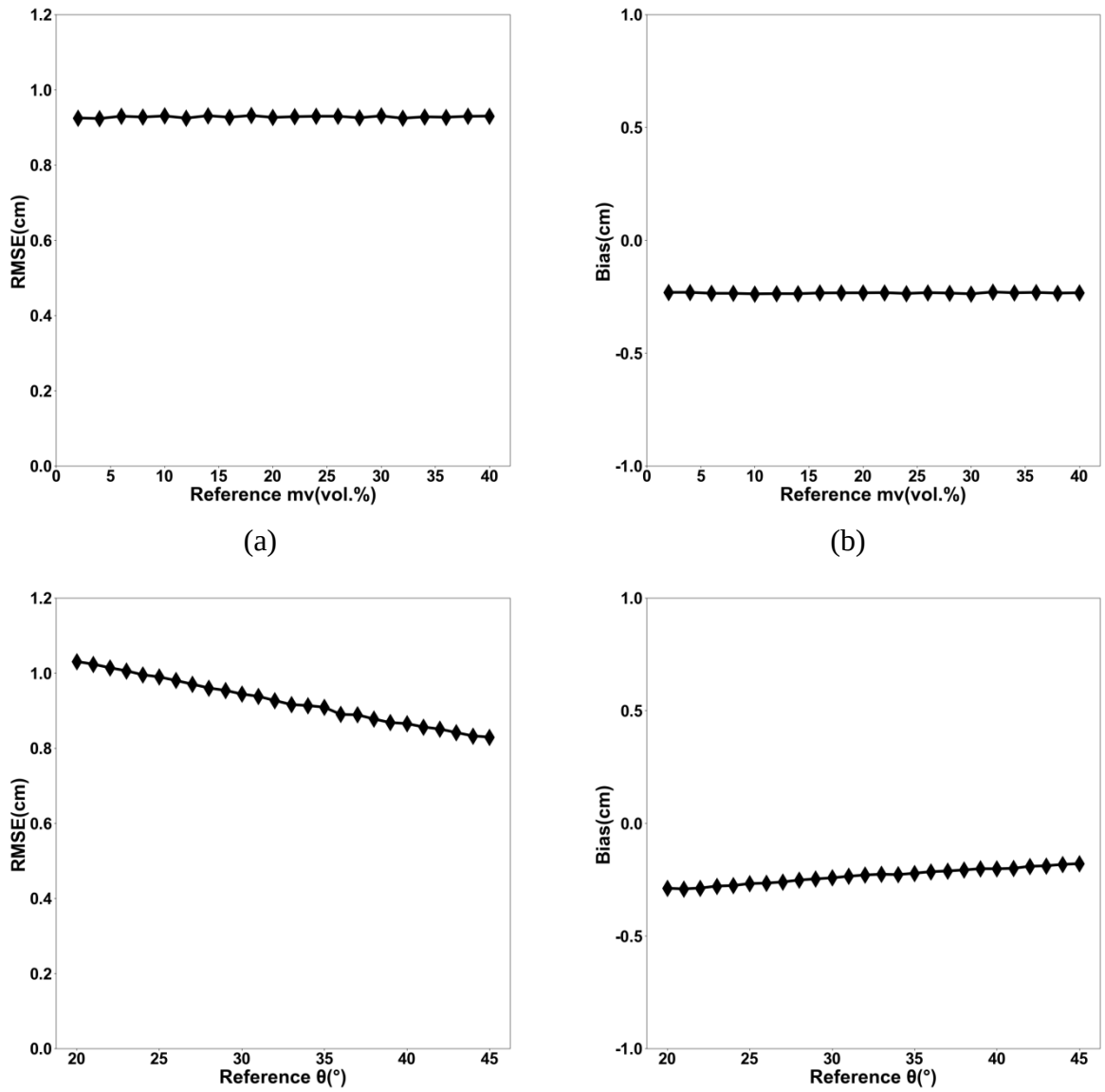


**Figure A2.4.** Accuracy on the *Hrms* estimates (RMSE and Bias) as a function of the soil moisture and the incidence angle for VH polarization alone and using the synthetic data generated from Baghdadi model. The *mv* in input to the NN corresponds to the exact *mv* (without estimation error).

# *List of figures and tables*

# List of figures

## Chapter 2- Generalities



## Chapter 3- Evaluation of radar backscattering models

## Chapter 4- A New Empirical Model for Radar Scattering from Bare Soil Surfaces

## Chapter 5- Estimation of soil roughness using neural networks from sentinel-1 SAR data

# List of tables

## Chapter 2- Generalities



## Chapter 3- Evaluation of radar backscattering models



## Chapter 4- A New Empirical Model for Radar Scattering from Bare Soil Surfaces



## Chapter 5- Estimation of soil roughness using neural networks from sentinel-1 SAR data

# *References*

Alexakis, D.D., Mexis, F.-D.K., Vozinaki, A.-E.K., Daliakopoulos, I.N., and Tsanis, I.K. (2017). Soil Moisture Content Estimation Based on Sentinel-1 and Auxiliary Earth Observation Products. A Hydrological Approach. Sensors *17*, 1455.

Altese, E., Bolognani, O., Mancini, M., and Troch, P.A. (1996). Retrieving soil moisture over bare soil from ERS 1 synthetic aperture radar data: Sensitivity analysis based on a theoretical surface scattering model and field data. Water Resour. Res. *32*, 653–661.

Ambroise, B. (1999). La dynamique du cycle de l'eau dans un bassin versant: processus, facteurs, modèles (HGA).

Anguela, T.P., Zribi, M., Baghdadi, N., and Loumagne, C. (2010). Analysis of local variation of soil surface parameters with TerraSAR-X radar data over bare agricultural fields. IEEE Trans. Geosci. Remote Sens. *48*, 874–881.

Attema, E.P.W., and Ulaby, F.T. (1978). Vegetation modeled as a water cloud. Radio Sci. *13*, 357–364.

Aubert, M., Baghdadi, N., Zribi, M., Douaoui, A., Loumagne, C., Baup, F., El Hajj, M., and Garrigues, S. (2011). Analysis of TerraSAR-X data sensitivity to bare soil moisture, roughness, composition and soil crust. Remote Sens. Environ. *115*, 1801–1810.

Aubert, M., Baghdadi, N.N., Zribi, M., Ose, K., El Hajj, M., Vaudour, E., and Gonzalez-Sosa, E. (2013). Toward an operational bare soil moisture mapping using TerraSAR-X data acquired over agricultural areas. IEEE J. Sel. Top. Appl. Earth Obs. Remote Sens. *6*, 900–916.

Auzet, A.-V., Kirkby, M.J., and Van Dijk, P. (2005). Surface characterisation for soil erosion forecasting. Catena *62*, 77–78.

Baghdadi, N., and Zribi, M. (2006). Evaluation of radar backscatter models IEM, OH and Dubois using experimental observations. Int. J. Remote Sens. *27*, 3831–3852.

Baghdadi, N., and Zribi, M. (2016). Characterisation of soil surface properties using radar remote sensing. Chapitre book: Baghdadi N. and Zribi M. (eds), Land surface remote sensing in continental hydrology, p. 1-40, Septembre 2016, Elsevier, 502 pp. (Elsevier).

Baghdadi, N., Paillou, P., Grandjean, G., Dubois, P., and Davidson, M. (2000). Relationship between profile length and roughness variables for natural surfaces. Int. J. Remote Sens. *21*, 3375–3381.

Baghdadi, N., Bernier, M., Gauthier, R., and Neeson, I. (2001). Evaluation of C-band SAR data for wetlands mapping. Int. J. Remote Sens. *22*, 71–88.

Baghdadi, N., King, C., Bourguignon, A., and Remond, A. (2002a). Potential of ERS and RADARSAT data for surface roughness monitoring over bare agricultural fields: application to catchments in Northern France. Int. J. Remote Sens. *23*, 3427–3442.

Baghdadi, N., King, C., Chanzy, A., and Wigneron, J.P. (2002b). An empirical calibration of the integral equation model based on SAR data, soil moisture and surface roughness measurement over bare soils. Int. J. Remote Sens. *23*, 4325–4340.

Baghdadi, N., Gaultier, S., and King, C. (2002c). Retrieving surface roughness and soil moisture from synthetic aperture radar (SAR) data using neural networks. Can. J. Remote Sens. *28*, 701–711.

Baghdadi, N., Gherboudj, I., Zribi, M., Sahebi, M., King, C., and Bonn, F. (2004). Semi-empirical calibration of the IEM backscattering model using radar images and moisture and roughness field measurements. Int. J. Remote Sens. *25*, 3593–3623.

Baghdadi, N., Holah, N., and Zribi, M. (2006a). Calibration of the Integral Equation Model for SAR data in C-band and HH and VV polarizations. Int. J. Remote Sens. *27*, 805–816.

Baghdadi, N., Holah, N., and Zribi, M. (2006b). Soil moisture estimation using multi-incidence and multi-polarization ASAR data. Int. J. Remote Sens. *27*, 1907–1920.

Baghdadi, N., Aubert, M., Cerdan, O., Franchistéguy, L., Viel, C., Eric, M., Zribi, M., and Desprats, J.F. (2007). Operational mapping of soil moisture using synthetic aperture radar data: application to the Touch basin (France). Sensors *7*, 2458–2483.

Baghdadi, N., Zribi, M., Loumagne, C., Ansart, P., and Anguela, T.P. (2008a). Analysis of TerraSAR-X data and their sensitivity to soil surface parameters over bare agricultural fields. Remote Sens. Environ. *112*, 4370–4379.

Baghdadi, N., Cerdan, O., Zribi, M., Auzet, V., Darboux, F., El Hajj, M., and Kheir, R.B. (2008b). Operational performance of current synthetic aperture radar sensors in mapping soil surface characteristics in agricultural environments: application to hydrological and erosion modelling. Hydrol. Process. *22*, 9–20.

Baghdadi, N., Saba, E., Aubert, M., Zribi, M., and Baup, F. (2011a). Evaluation of radar backscattering models IEM, Oh, and Dubois for SAR data in X-band over bare soils. IEEE Geosci. Remote Sens. Lett. *8*, 1160–1164.

Baghdadi, N., Chaaya, J.A., and Zribi, M. (2011b). Semiempirical calibration of the integral equation model for SAR data in C-band and cross polarization using radar images and field measurements. IEEE Geosci. Remote Sens. Lett. *8*, 14–18.

Baghdadi, N., Saba, E., Aubert, M., Zribi, M., and Baup, F. (2011c). Comparison between backscattered TerraSAR signals and simulations from the radar backscattering models IEM, Oh, and Dubois. IEEE Geosci. Remote Sens. Lett. *6*, 1160–1164.

Baghdadi, N., Cresson, R., El Hajj, M., Ludwig, R., and La Jeunesse, I. (2012a). Estimation of soil parameters over bare agriculture areas from C-band polarimetric SAR data using neural networks. Hydrol. Earth Syst. Sci. *16*, 1607–1621.

Baghdadi, N., Aubert, M., and Zribi, M. (2012b). Use of TerraSAR-X data to retrieve soil moisture over bare soil agricultural fields. IEEE Geosci. Remote Sens. Lett. *9*, 512–516.

Baghdadi, N., Dubois-Fernandez, P., Dupuis, X., and Zribi, M. (2013). Sensitivity of main polarimetric parameters of multifrequency polarimetric SAR data to soil moisture and surface roughness over bare agricultural soils. IEEE Geosci. Remote Sens. Lett. *10*, 731–735.

Baghdadi, N., Zribi, M., Paloscia, S., Verhoest, N.E., Lievens, H., Baup, F., and Mattia, F. (2015). Semi-empirical calibration of the integral equation model for co-polarized L-band backscattering. Remote Sens. *7*, 13626–13640.

Baghdadi, N., Choker, M., Zribi, M., Hajj, M.E., Paloscia, S., Verhoest, N.E., Lievens, H., Baup, F., and Mattia, F. (2016a). A New Empirical Model for Radar Scattering from Bare Soil Surfaces. Remote Sens. *8*, 920.

Baghdadi, N.N., El Hajj, M., Zribi, M., and Fayad, I. (2016b). Coupling SAR C-band and optical data for soil moisture and leaf area index retrieval over irrigated grasslands. IEEE J. Sel. Top. Appl. Earth Obs. Remote Sens. *9*, 1229–1243.

Baronti, S., Del Frate, F., Ferrazzoli, P., Paloscia, S., Pampaloni, P., and Schiavon, G. (1995). SAR polarimetric features of agricultural areas. Int. J. Remote Sens. *16*, 2639–2656.

Beauchemin, M., Thomson, K.P., and Edwards, G. (1995). Modelling forest stands with MIMICS: implications for calibration. Can. J. Remote Sens. *21*, 518–526.

Beaudoin, A., Le Toan, T., and Gwyn, Q.H.J. (1990). SAR observations and modeling of the C-band backscatter variability due to multiscale geometry and soil moisture. IEEE Trans. Geosci. Remote Sens. *28*, 886–895.

Beckmann, P., and Spizzichino, A. (1987). The scattering of electromagnetic waves from rough surfaces. Norwood MA Artech House Inc 1987 511 P.

Le Bissonnais, Y. (1990). Experimental study and modelling of soil surface crusting processes. Catena Suppl. 13–28.

Le Bissonnais, Y., and Singer, M.J. (1992). Crusting, runoff, and erosion response to soil water content and successive rainfalls. Soil Sci. Soc. Am. J. *56*, 1898–1903.

Bockheim, J.G., and Gennadiyev, A.N. (2000). The role of soil-forming processes in the definition of taxa in Soil Taxonomy and the World Soil Reference Base. Geoderma *95*, 53–72.

Boiffin, J. (1984). La dégradation structurale des couches superficielles du sol sous l'action des pluies.

Boisvert, J.B., Gwyn, Q.H.J., Chanzy, A., Major, D.J., Brisco, B., and Brown, R.J. (1997). Effect of surface soil moisture gradients on modelling radar backscattering from bare fields. Int. J. Remote Sens. *18*, 153–170.

Bruckler, L., Witono, H., and Stengel, P. (1988). Near surface soil moisture estimation from microwave measurements. Remote Sens. Environ. *26*, 101–121.

Brun, C., Bernard, R., Vidal-Madjar, D., Gascuel-Odoux, C., Merot, P., Duchesne, J., and Nicolas, H. (1990). Mapping saturated areas with a helicopter-borne C band scatterometer. Water Resour. Res. *26*, 945–955.

Callens, M., Verhoest, N.E., and Davidson, M.W. (2006). Parameterization of tillage-induced single-scale soil roughness from 4-m profiles. IEEE Trans. Geosci. Remote Sens. *44*, 878–888.

Casenave, A., and Valentin, C. (1989). Les états de surface de la zone sahélienne: influence sur l'infiltration.

Chai, S.-S., Walker, J.P., Makarynskyy, O., Kuhn, M., Veenendaal, B., and West, G. (2009). Use of soil moisture variability in artificial neural network retrieval of soil moisture. Remote Sens. *2*, 166–190.

Chai, X., Zhang, T., Shao, Y., Gong, H., Liu, L., and Xie, K. (2015). Modeling and mapping soil moisture of plateau pasture using RADARSAT-2 imagery. Remote Sens. *7*, 1279–1299.

Champagne, C., Rowlandson, T., Berg, A., Burns, T., L'Heureux, J., Tetlock, E., Adams, J.R., McNairn, H., Toth, B., and Itenfisu, D. (2016). Satellite surface soil moisture from SMOS and Aquarius: Assessment for applications in agricultural landscapes. Int. J. Appl. Earth Obs. Geoinformation *45*, 143–154.

Chan, S.K., Bindlish, R., O'Neill, P.E., Njoku, E., Jackson, T., Colliander, A., Chen, F., Burgin, M., Dunbar, S., and Piepmeier, J. (2016). Assessment of the SMAP passive soil moisture product. IEEE Trans. Geosci. Remote Sens. *54*, 4994–5007.

Chen, K.-S., Wu, T.-D., Tsang, L., Li, Q., Shi, J., and Fung, A.K. (2003). Emission of rough surfaces calculated by the integral equation method with comparison to three-dimensional moment method simulations. IEEE Trans. Geosci. Remote Sens. *41*, 90–101.

Choker, M., Baghdadi, N., Zribi, M., El Hajj, M., Paloscia, S., Verhoest, N.E., Lievens, H., and Mattia, F. (2017). Evaluation of the oh, dubois and iem backscatter models using a large dataset of sar data and experimental soil measurements. Water *9*, 38.

Condrea, P., and Bostan, I. (2008). Environmental issues from an economic perspective. Environ. Eng. Manag. J. *7*, 843–849.

Davidson, M.W., Le Toan, T., Mattia, F., Satalino, G., Manninen, T., and Borgeaud, M. (2000). On the characterization of agricultural soil roughness for radar remote sensing studies. IEEE Trans. Geosci. Remote Sens. *38*, 630–640.

De Roo, R.D., Du, Y., Ulaby, F.T., and Dobson, M.C. (2001). A semi-empirical backscattering model at L-band and C-band for a soybean canopy with soil moisture inversion. IEEE Trans. Geosci. Remote Sens. *39*, 864–872.

Dong, L., Baghdadi, N., and Ludwig, R. (2013). Validation of the AIEM through correlation length parameterization at field scale using radar imagery in a semi-arid environment. IEEE Geosci. Remote Sens. Lett. *10*, 461–465.

Dubois, P.C., Van Zyl, J., and Engman, T. (1995). Measuring soil moisture with imaging radars. IEEE Trans. Geosci. Remote Sens. *33*, 915–926.

El Hajj, M., Baghdadi, N., Belaud, G., Zribi, M., Cheviron, B., Courault, D., Hagolle, O., and Charron, F. (2014). Irrigated grassland monitoring using a time series of terraSAR-X and COSMO-skyMed X-Band SAR Data. Remote Sens. *6*, 10002–10032.

Entekhabi, D., Njoku, E.G., O'Neill, P.E., Kellogg, K.H., Crow, W.T., Edelstein, W.N., Entin, J.K., Goodman, S.D., Jackson, T.J., and Johnson, J. (2010). The soil moisture active passive (SMAP) mission. Proc. IEEE *98*, 704–716.

Fieuzal, R., Duchemin, B., Jarlan, L., Zribi, M., Baup, F., Merlin, O., Hagolle, O., and Garatuza-Payan, J. (2011). Combined use of optical and radar satellite data for the monitoring of irrigation and soil moisture of wheat crops. Hydrol. Earth Syst. Sci. *15*, 1117–1129.

François, J.B. (1988). Influence des systèmes de culture sur les risques d'érosion par ruissellement concentré. I. — Ana-lyse des conditions de déclenchement de l'érosion.

Fung, A.K. (1994). Microwave Scattering and Emission Models and their Applications (Boston, London: Artech House, Inc.). Norwood MA Artech House 573.

Fung, A.K., Li, Z., and Chen, K.-S. (1992). Backscattering from a randomly rough dielectric surface. IEEE Trans. Geosci. Remote Sens. *30*, 356–369.

Galarneau, M., Leconte, R., Brissette, F., Pultz, T.J., and Rousselle, J. (2001). Utilization of Radarsat in integrated catchment management. IAHS Publ. 321–326.

Gardner, W.H. (1986). Water content. Methods Soil Anal. Part 1—Physical Mineral. Methods 493–544.

Gherboudj, I., Magagi, R., Berg, A.A., and Toth, B. (2011). Soil moisture retrieval over agricultural fields from multi-polarized and multi-angular RADARSAT-2 SAR data. Remote Sens. Environ. *115*, 33–43.

Gilliot, J.-M., Vaudour, E., and Michelin, J. (2017). Soil surface roughness measurement: A new fully automatic photogrammetric approach applied to agricultural bare fields. Comput. Electron. Agric. *134*, 63–78.

Gorrab, A., Zribi, M., Baghdadi, N., Mougenot, B., and Chabaane, Z.L. (2015a). Potential of X-band TerraSAR-X and COSMO-SkyMed SAR data for the assessment of physical soil parameters. Remote Sens. *7*, 747–766.

Gorrab, A., Zribi, M., Baghdadi, N., Mougenot, B., Fanise, P., and Chabaane, Z.L. (2015b). Retrieval of both soil moisture and texture using TerraSAR-X images. Remote Sens. *7*, 10098–10116.

Govers, G., Takken, I., and Helming, K. (2000). Soil roughness and overland flow. Agronomie *20*, 131–146.

Hajnsek, I., Jagdhuber, T., Schon, H., and Papathanassiou, K.P. (2009). Potential of estimating soil moisture under vegetation cover by means of PolSAR. IEEE Trans. Geosci. Remote Sens. *47*, 442–454.

Hallikainen, M.T., Ulaby, F.T., Dobson, M.C., El-Rayes, M.A., and Wu, L.-K. (1985). Microwave dielectric behavior of wet soil-part 1: empirical models and experimental observations. IEEE Trans. Geosci. Remote Sens. 25–34.

He, B., Xing, M., and Bai, X. (2014). A synergistic methodology for soil moisture estimation in an Alpine prairie using radar and optical satellite data. Remote Sens. *6*, 10966–10985.

Hégarat-Mascle, L. (2000). Estimation of Watershed Soil Moisture Index from ERS/SAR Data. Remote Sens. Environ. *3*, 290–303.

Holah, N., Baghdadi, N., Zribi, M., Bruand, A., and King, C. (2005). Potential of ASAR/ENVISAT for the characterization of soil surface parameters over bare agricultural fields. Remote Sens. Environ. *96*, 78–86.

Hosseini, M., and Saradjian, M.R. (2011). Soil moisture estimation based on integration of optical and SAR images. Can. J. Remote Sens. *37*, 112–121.

Jackson, T.J., Bindlish, R., Cosh, M.H., Zhao, T., Starks, P.J., Bosch, D.D., Seyfried, M., Moran, M.S., Goodrich, D.C., and Kerr, Y.H. (2012). Validation of Soil Moisture and Ocean Salinity (SMOS) soil moisture over watershed networks in the US. IEEE Trans. Geosci. Remote Sens. *50*, 1530–1543.

Joughin, I.R., Percival, D.B., and Winebrenner, D.P. (1993). Maximum likelihood estimation of K distribution parameters for SAR data. IEEE Trans. Geosci. Remote Sens. *31*, 989–999.

King, D., and Le Bissonnais, Y. (1992). Rôle des sols et des pratiques culturales dans l'infiltration et l'écoulement des eaux. Exemple du ruissellement et de l'érosion sur les plateaux limoneux du nord de l'Europe. CR Acad Agric Fr *78*, 91–105.

King, C., Lecomte, V., Le Bissonnais, Y., Baghdadi, N., Souchère, V., and Cerdan, O. (2005). Remote-sensing data as an alternative input for the 'STREAM'runoff model. Catena *62*, 125–135.

Kirimi, F., Kuria, D.N., Thonfeld, F., Amler, E., Mubea, K., Misana, S., and Menz, G. (2016). Influence of Vegetation Cover on the Oh Soil Moisture Retrieval Model: A Case Study of the Malinda Wetland, Tanzania.

Kseneman, M., Gleich, D., and Potočnik, B. (2012). Soil-moisture estimation from TerraSAR-X data using neural networks. Mach. Vis. Appl. *23*, 937–952.

Kweon, S.-K., Hwang, J.-H., and Oh, Y. (2012). COSMO SkyMed AO projects-soil moisture detection for vegetation fields based on a modified water-cloud model using COSMO-SkyMed SAR data. In 2012 IEEE International Geoscience and Remote Sensing Symposium, (IEEE), pp. 1204–1207.

Lakhankar, T., Ghedira, H., Azar, A., and Khanbilvardi, R. (2006). Effect of sub-pixel variability and land-cover on soil moisture retrieval from RADARSAT-1 data. In IEEE MicroRad, 2006, (IEEE), pp. 187–192.

Le Hégarat-Mascle, S., Zribi, M., Alem, F., Weisse, A., and Loumagne, C. (2002). Soil moisture estimation from ERS/SAR data: Toward an operational methodology. IEEE Trans. Geosci. Remote Sens. *40*, 2647–2658.

Le Toan, T., Davidson, M., Mattia, F., Borderies, P., Chenerie, I., Manninen, T., and Borgeaud, M. (1999). Improved observation and modelling of bare soil surfaces for soil moisture retrieval. Earth Obs. Q. *62*, 62, 20–24.

Lee, J.-S., Jurkevich, L., Dewaele, P., Wambacq, P., and Oosterlinck, A. (1994). Speckle filtering of synthetic aperture radar images: A review. Remote Sens. Rev. *8*, 313–340.

Lievens, H., Vernieuwe, H., Alvarez-Mozos, J., De Baets, B., and Verhoest, N.E. (2009). Error in radar-derived soil moisture due to roughness parameterization: An analysis based on synthetical surface profiles. Sensors *9*, 1067–1093.

Lievens, H., Verhoest, N.E.C., Keyser, E.D., Vernieuwe, H., Matgen, P., Alvarez-Mozos, J., and Baets, B.D. (2011). Effective roughness modelling as a tool for soil moisture retrieval from C-and L-band SAR. Hydrol. Earth Syst. Sci. *15*, 151–162.

Ludwig, B., Boiffin, J., Chad, J., and Auzet, A.-V. (1995). Hydrological structure and erosion damage caused by concentrated flow in cultivated catchments. Catena *25*, 227–252.

Macelloni, G., Paloscia, S., Pampaloni, P., Sigismondi, S., De Matthaeis, P., Ferrazzoli, P., Schiavon, G., and Solimini, D. (1999). The SIR-C/X-SAR experiment on Montespertoli: sensitivity to hydrological parameters. Int. J. Remote Sens. *20*, 2597–2612.

Marquardt, D.W. (1963). An algorithm for least-squares estimation of nonlinear parameters. J. Soc. Ind. Appl. Math. *11*, 431–441.

Mattia, F., Le Toan, T., Souyris, J.-C., De Carolis, C., Floury, N., Posa, F., and Pasquariello, N.G. (1997). The effect of surface roughness on multifrequency polarimetric SAR data. IEEE Trans. Geosci. Remote Sens. *35*, 954–966.

Mattia, F., and Le Toan, T. (1999). Backscattering properties of multi-scale rough surfaces. J. Electromagn. Waves Appl. *13*, 493–527.

Mattia, F., Davidson, M.W., Le Toan, T., D'Haese, C.M., Verhoest, N.E., Gatti, A.M., and Borgeaud, M. (2003). A comparison between soil roughness statistics used in surface scattering models derived from mechanical and laser profilers. IEEE Trans. Geosci. Remote Sens. *41*, 1659–1671.

McNairn, H., Merzouki, A., and Pacheco, A. (2010). Estimating surface soil moisture using Radarsat-2. Int. Arch. Photogramm. Remote Sens. Spat. Inf. Sci. *38*, 576–579.

Merzouki, A., McNairn, H., and Pacheco, A. (2011). Mapping soil moisture using RADARSAT-2 data and local autocorrelation statistics. IEEE J. Sel. Top. Appl. Earth Obs. Remote Sens. *4*, 128–137.

Mohanty, B.P., Cosh, M.H., Lakshmi, V., and Montzka, C. (2017). Soil moisture remote sensing: State-of-the-science. Vadose Zone J. *16*.

Narvekar, P.S., Entekhabi, D., Kim, S.-B., and Njoku, E.G. (2015). Soil moisture retrieval using L-band radar observations. IEEE Trans. Geosci. Remote Sens. *53*, 3492–3506.

Notarnicola, C., Angiulli, M., and Posa, F. (2006). Use of radar and optical remotely sensed data for soil moisture retrieval over vegetated areas. IEEE Trans. Geosci. Remote Sens. *44*, 925–935.

Ogilvy, J.A., and Ogilvy, J.A. (1991). Theory of wave scattering from random rough surfaces (Hilger Bristol et al.).

Oh, Y. (2004). Quantitative retrieval of soil moisture content and surface roughness from multipolarized radar observations of bare soil surfaces. IEEE Trans. Geosci. Remote Sens. *42*, 596–601.

Oh, Y., and Kay, Y.C. (1998). Condition for precise measurement of soil surface roughness. IEEE Trans. Geosci. Remote Sens. *36*, 691–695.

Oh, Y., Sarabandi, K., and Ulaby, F.T. (1992). An empirical model and an inversion technique for radar scattering from bare soil surfaces. IEEE Trans. Geosci. Remote Sens. *30*, 370–381.

Oh, Y., Sarabandi, K., and Ulaby, F.T. (1994). An inversion algorithm for retrieving soil moisture and surface roughness from polarimetric radar observation. In Geoscience and Remote Sensing Symposium, 1994. IGARSS'94. Surface and Atmospheric Remote Sensing: Technologies, Data Analysis and Interpretation., International, (IEEE), pp. 1582–1584.

Oh, Y., Sarabandi, K., and Ulaby, F.T. (2002). Semi-empirical model of the ensemble-averaged differential Mueller matrix for microwave backscattering from bare soil surfaces. IEEE Trans. Geosci. Remote Sens. *40*, 1348–1355.

Paloscia, S., Macelloni, G., Pampaloni, P., and Sigismondi, S. (1999). The potential of C-and L-band SAR in estimating vegetation biomass: the ERS-1 and JERS-1 experiments. IEEE Trans. Geosci. Remote Sens. *37*, 2107–2110.

Paloscia, S., Pampaloni, P., Pettinato, S., and Santi, E. (2008). A comparison of algorithms for retrieving soil moisture from ENVISAT/ASAR images. IEEE Trans. Geosci. Remote Sens. *46*, 3274–3284.

Paloscia, S., Pettinato, S., and Santi, E. (2012). Combining L and X band SAR data for estimating biomass and soil moisture of agricultural fields. Eur. J. Remote Sens. *45*, 99–109.

Paloscia, S., Pettinato, S., Santi, E., Notarnicola, C., Pasolli, L., and Reppucci, A. (2013). Soil moisture mapping using Sentinel-1 images: Algorithm and preliminary validation. Remote Sens. Environ. *134*, 234–248.

Panciera, R., Tanase, M.A., Lowell, K., and Walker, J.P. (2014). Evaluation of IEM, Dubois, and Oh radar backscatter models using airborne L-band SAR. IEEE Trans. Geosci. Remote Sens. *52*, 4966–4979.

Prakash, R., Singh, D., and Pathak, N.P. (2012). A fusion approach to retrieve soil moisture with SAR and optical data. IEEE J. Sel. Top. Appl. Earth Obs. Remote Sens. *5*, 196–206.

Prevot, L., Champion, I., and Guyot, G. (1993). Estimating surface soil moisture and leaf area index of a wheat canopy using a dual-frequency (C and X bands) scatterometer. Remote Sens. Environ. *46*, 331–339.

Quesney, A., Le Hégarat-Mascle, S., Taconet, O., Vidal-Madjar, D., Wigneron, J.P., Loumagne, C., and Normand, M. (2000). Estimation of watershed soil moisture index from ERS/SAR data. Remote Sens. Environ. *72*, 290–303.

Rahman, M.M., Moran, M.S., Thoma, D.P., Bryant, R., Sano, E.E., Holifield Collins, C.D., Skirvin, S., Kershner, C., and Orr, B.J. (2007). A derivation of roughness correlation length for parameterizing radar backscatter models. Int. J. Remote Sens. *28*, 3995–4012.

Rahman, M.M., Moran, M.S., Thoma, D.P., Bryant, R., Collins, C.H., Jackson, T., Orr, B.J., and Tischler, M. (2008). Mapping surface roughness and soil moisture using multi-angle radar imagery without ancillary data. Remote Sens. Environ. *112*, 391–402.

Rakotoarivony, L., Taconet, O., Vidal-Madjar, D., Bellemain, P., and Benallegue, M. (1996). Radar backscattering over agricultural bare soils. J. Electromagn. Waves Appl. *10*, 187–209.

Rao, S.S., Das, S.N., Nagaraju, M.S.S., Venugopal, M.V., Rajankar, P., Laghate, P., Reddy, M.S., Joshi, A.K., and Sharma, J.R. (2013). Modified Dubois model for estimating soil moisture with dual polarized SAR data. J. Indian Soc. Remote Sens. *41*, 865–872.

Remond, A. (1997). Image SAR: potentialités d'extraction d'un paramètre physique du ruissellement, la rugosité (modélisation et expérimentation). Ph. D. thesis, University of Bourgogne, Pub. BRGM.

Rice, S.O. (1951). Reflection of electromagnetic waves from slightly rough surfaces. Commun. Pure Appl. Math. *4*, 351–378.

Roose, E. (1996). Méthodes de mesure des états de surface du sol, de la rugosité et des autres caractéristiques qui peuvent aider au diagnostic de terrain des risques de ruissellement et d'érosion, en particulier sur les versants cultivés des montagnes. Bull Réseau Eros. *16*, 87–97.

Sahebi, M.R., Angles, J., and Bonn, F. (2002). A comparison of multi-polarization and multi-angular approaches for estimating bare soil surface roughness from spaceborne radar data. Can. J. Remote Sens. *28*, 641–652.

Schwerdt, M., Schmidt, K., Tous Ramon, N., Klenk, P., Yague-Martinez, N., Prats-Iraola, P., Zink, M., and Geudtner, D. (2017). Independent System Calibration of Sentinel-1B. Remote Sens. *9*, 511.

Sikdar, M., and Cumming, I. (2004). A modified empirical model for soil moisture estimation in vegetated areas using SAR data. In Geoscience and Remote Sensing Symposium, 2004. IGARSS'04. Proceedings. 2004 IEEE International, (IEEE), pp. 803–806.

Srivastava, H.S., Patel, P., Manchanda, M.L., and Adiga, S. (2003). Use of multiincidence angle RADARSAT-1 SAR data to incorporate the effect of surface roughness in soil moisture estimation. IEEE Trans. Geosci. Remote Sens. *41*, 1638–1640.

Srivastava, H.S., Patel, P., Sharma, Y., and Navalgund, R.R. (2009). Large-area soil moisture estimation using multi-incidence-angle RADARSAT-1 SAR data. Geosci. Remote Sens. IEEE Trans. On *47*, 2528–2535.

TOAN, L. (1982). Active microwave signatures of soil and crops- Significant results of three years of experiments. In 1982 International Geoscience and Remote Sensing Symposium, Munich, West Germany, p. 1982.

Topp, G.C., Davis, J.L., and Annan, A.P. (1980). Electromagnetic determination of soil water content: Measurements in coaxial transmission lines. Water Resour. Res. *16*, 574–582.

Ulaby, F.T., Batlivala, P.P., and Dobson, M.C. (1978). Microwave backscatter dependence on surface roughness, soil moisture, and soil texture: Part I-bare soil. IEEE Trans. Geosci. Electron. *16*, 286–295.

Ulaby, F.T., Moore, R.K., and Fung, A.K. (1982). Microwave remote sensing: Active and passive. Volume 2-Radar remote sensing and surface scattering and emission theory.

Ulaby, F.T., Moore, R.K., and Fung, A.K. (1986). Microwave remote sensing active and passive-volume III: from theory to applications.

Ulaby, F.T., Sarabandi, K., Mcdonald, K., Whitt, M., and Dobson, M.C. (1990). Michigan microwave canopy scattering model. Int. J. Remote Sens. *11*, 1223–1253.

Vaudour, E., Baghdadi, N., and Gilliot, J.-M. (2014). Mapping tillage operations over a peri-urban region using combined SPOT4 and ASAR/ENVISAT images. Int. J. Appl. Earth Obs. Geoinformation *28*, 43–59.

Vaudour, E., Costantini, E., Jones, G.V., and Mocali, S. (2015). An overview of the recent approaches to terroir functional modelling, footprinting and zoning. Soil *1*, 287.

Verhoest, N.E., Lievens, H., Wagner, W., Álvarez-Mozos, J., Moran, M.S., and Mattia, F. (2008). On the soil roughness parameterization problem in soil moisture retrieval of bare surfaces from synthetic aperture radar. Sensors *8*, 4213–4248.

Wang, H., Méric, S., Allain, S., and Pottier, E. (2014). Adaptation of Oh Model for soil parameters retrieval using multi-angular RADARSAT-2 datasets. J. Surv. Mapp. Eng. *2*, 65–74.

Wang, J.R., Hsu, A., Shi, J.C., O'neill, P.E., and Engman, E.T. (1997). A comparison of soil moisture retrieval models using SIR-C measurements over the Little Washita River watershed. Remote Sens. Environ. *59*, 308–320.

Wang, S.G., Li, X., Han, X.J., and Jin, R. (2011). Estimation of surface soil moisture and roughness from multi-angular ASAR imagery in the Watershed Allied Telemetry Experimental Research (WATER). Hydrol. Earth Syst. Sci. *15*, 1415–1426.

WEISSE, A., OUDIN, L., and LOUMAGNE, C. (2003). Assimilation of soil moisture into hydrological models for flood forecasting: comparison of a conceptual. Rev. Sci. L'EAU *173*, 197.

Wigneron, J.-P., Chanzy, A., Calvet, J.-C., and Bruguier, N. (1995). A simple algorithm to retrieve soil moisture and vegetation biomass using passive microwave measurements over crop fields. Remote Sens. Environ. *51*, 331–341.

Wigneron, J.-P., Jackson, T.J., O'Neill, P., De Lannoy, G., de Rosnay, P., Walker, J.P., Ferrazzoli, P., Mironov, V., Bircher, S., and Grant, J.P. (2017). Modelling the passive microwave signature from land surfaces: A review of recent results and application to the L-band SMOS & SMAP soil moisture retrieval algorithms. Remote Sens. Environ. *192*, 238–262.

Wu, T.-D., Chen, K.-S., Shi, J., and Fung, A.K. (2001). A transition model for the reflection coefficient in surface scattering. IEEE Trans. Geosci. Remote Sens. *39*, 2040–2050.

Yang, G., Shi, Y., Zhao, C., and Wang, J. (2012). Estimation of soil moisture from multi-polarized SAR data over wheat coverage areas. In Agro-Geoinformatics (Agro-Geoinformatics), 2012 First International Conference On, (IEEE), pp. 1–5.

Yu, F., and Zhao, Y. (2011). A new semi-empirical model for soil moisture content retrieval by ASAR and TM data in vegetation-covered areas. Sci. China Earth Sci. *54*, 1955–1964.

Zobeck, T.M., and Onstad, C.A. (1987). Tillage and rainfall effects on random roughness: a review. Soil Tillage Res. *9*, 1–20.

Zribi, M. (1998). Développement de nouvelles méthodes de modélisation de la rugosité pour la rétrodiffusion hyperfréquence de la surface du sol.

Zribi, M., and Dechambre, M. (2002). A new empirical model to inverse soil moisture and roughness using two radar configurations. In Geoscience and Remote Sensing Symposium, 2002. IGARSS'02. 2002 IEEE International, (IEEE), pp. 2223–2225.

Zribi, M., and Dechambre, M. (2003). A new empirical model to retrieve soil moisture and roughness from C-band radar data. Remote Sens. Environ. *84*, 42–52.

Zribi, M., Taconet, O., Le Hégarat-Mascle, S., Vidal-Madjar, D., Emblanch, C., Loumagne, C., and Normand, M. (1997). Backscattering behavior and simulation comparison over bare soils using SIR-C/X-SAR and ERASME 1994 data over Orgeval. Remote Sens. Environ. *59*, 256–266.

Zribi, M., Baghdadi, N., Holah, N., and Fafin, O. (2005a). New methodology for soil surface moisture estimation and its application to ENVISAT-ASAR multi-incidence data inversion. Remote Sens. Environ. *96*, 485–496.

Zribi, M., Baghdadi, N., Holah, N., Fafin, O., and Guérin, C. (2005b). Evaluation of a rough soil surface description with ASAR-ENVISAT radar data. Remote Sens. Environ. *95*, 67–76.

Zribi, M., Chahbi, A., Shabou, M., Lili-Chabaane, Z., Duchemin, B., Baghdadi, N., Amri, R., and Chehbouni, A. (2011). Soil surface moisture estimation over a semi-arid region using ENVISAT ASAR radar data for soil evaporation evaluation. Hydrol. Earth Syst. Sci. Discuss. *15*, 345–358.

Zribi, M., Gorrab, A., and Baghdadi, N. (2014a). A new soil roughness parameter for the modelling of radar backscattering over bare soil. Remote Sens. Environ. *152*, 62–73.

Zribi, M., Gorrab, A., Baghdadi, N., Lili-Chabaane, Z., and Mougenot, B. (2014b). Influence of radar frequency on the relationship between bare surface soil moisture vertical profile and radar backscatter. IEEE Geosci. Remote Sens. Lett. *11*, 848–852.

Résumé en Français

Thèse de doctorat

M. Mohammad Choker

UMR TETIS, Irstea, France

Mohammad.choker@teledetection.fr

## Introduction

Le sol n'est pas seulement la surface sur laquelle nous marchons, nous construisons, ni la terre que nous cultivons; c'est la source de notre vie et une richesse que nous devons préserver. À partir des années 1950, l'intensification des terres agricoles n'a fait qu'accélérer les processus de dégradation des sols, affectant ainsi leurs propriétés biophysico-chimiques. La fertilité des sols (matière organique et stabilité structurale du sol) est le premier élément directement affecté par l'intensification.

Le sol se caractérise par son taux d'humidité et la rugosité de sa surface. L'humidité du sol est un paramètre clé dans les différents processus impliqués dans le cycle hydrologique (cycle de l'eau). La cartographie de la distribution spatio-temporelle de l'humidité du sol permet d'optimiser la réattribution de l'eau pendant les sécheresses et fournit un soutien pour la prévision et la gestion des inondations. D'un point de vue agronomique, l'humidité du sol est une variable cruciale pour le développement des cultures. Ainsi, la cartographie de l'humidité des sols permet un meilleur suivi et une meilleure gestion de l'irrigation, conduisant à un rendement optimal.

Une autre caractéristique du sol à considérer est la rugosité de surface. C'est un paramètre physique qui caractérise l'état de la surface du sol. Pour les sols agricoles, la rugosité définit le microrelief de la surface du sol à l'échelle des mottes et est due à de petits accidents sur le terrain (naturels, techniques de culture ou les deux). Cartographier la rugosité de la surface est nécessaire pour comprendre les différents processus physiques. C'est un paramètre principal dans l'estimation de la capacité de stockage de l'eau dans les horizons pédologiques ainsi que dans le modèle de ruissellement. Ce dernier phénomène a une grande influence sur les processus d'érosion et détermine les crues suite à un événement pluvieux.

La télédétection spatiale est d'une importance primordiale pour la cartographie et la surveillance des problèmes environnementaux. Son intérêt réside dans la capacité des capteurs satellitaires spatiaux à fournir des informations globales et permanentes de la planète, aux échelles locale à globale. La télédétection radar a montré son grand potentiel ces dernières années dans la caractérisation des états de la surface du sol. L'état de la surface du sol, et en particulier l'humidité et la rugosité, exerce une influence fondamentale sur la répartition de la pluie entre infiltration, rétention superficielle et ruissellement. Il a un rôle essentiel dans les processus hydrologiques de surface et ceux associés à l'érosion et aux processus d'évapotranspiration. La caractérisation et la prise en compte de ces conditions de surface

constituent actuellement un enjeu important pour la modélisation à base physique des processus hydrologiques et pour le couplage surface-atmosphère. Dans ce cadre et depuis plusieurs années, plusieurs études scientifiques ont montré le potentiel des données micro-ondes actives dans l'estimation de l'état hydrique du sol et de la rugosité de sa surface.

Les nouveaux systèmes radar (SAR ″Synthetic Aperture Radar″) ont permis d'ouvrir de nouvelles perspectives pour l'observation de la terre grâce à l'amélioration de la résolution spatiale (métrique sur TerraSAR-X et COSMO-SkyMed) et temporelle (TerraSAR-X, COSMO-SkyMed, Sentinel-1). La disponibilité depuis peu des nouveaux capteurs radar en bande C Sentinel-1 (Sentinel-1A et Sentinel-1B) rend indispensable l'évaluation des données Sentinel-1 pour la caractérisation des états de surface du sol et en particulier la rugosité du sol.

Les données radar à synthèse d'ouverture (SAR) sont utilisées depuis longtemps pour estimer et cartographier les paramètres du sol, en particulier l'humidité et la rugosité du sol. Plusieurs modèles de rétrodiffusion radar ont été développés pour estimer l'humidité et la rugosité du sol. La disponibilité des hautes résolutions spatiales et temporelles des données SAR Sentinel-1 et l'utilisation des modèles de rétrodiffusion radar permettent d'estimer avec précision les paramètres du sol. Dans le cas des sols nus ou avec peu de végétation, l'estimation de l'humidité et de la rugosité du sol est effectuée en inversant la rétrodiffusion SAR mesurée au moyen de modèles de rétrodiffusion SAR (empiriques ou physiques). Contrairement aux modèles physiques, les modèles empiriques ou semi-empiriques doivent être étalonnés chaque fois que la zone d'étude change en utilisant des mesures in-situ spécifiques au site d'étude et des observations SAR. Les modèles semi-empiriques les plus couramment utilisés sont les modèles Oh et Dubois. Quant aux modèles physiques, les modèles les plus populaires sont le modèle d'équations intégrales (IEM), IEM calibré par Baghdadi, appelé dans cette thèse "IEM_B", et le modèle avancé d'équations intégrales (AIEM).

L'objectif général de cette thèse est d'évaluer le potentiel du capteur radar Sentinel-1 pour estimer la rugosité du sol sur des parcelles nues (sans végétation ou avec peu de végétation) en milieux agricoles. Peu d'études ont été réalisées pour estimer la rugosité du sol à partir des données SAR. De plus, le potentiel des données Sentinel-1 pour l'estimation de la rugosité du

sol n’a jamais été évalué. L’arrivée de la constellation Sentinel-1 (SAR en bande C) récente, offrant des données libres et gratuites avec une couverture terrestre complète à des hautes résolutions spatiales et temporelles, justifie ce travail.

Le travail de la présente thèse se structure en trois parties. La première partie consiste à évaluer la précision des modèles de rétrodiffusion radar les plus utilisés (Oh, Dubois, IEM, IEM_B, et AIEM) en utilisant une grande base de données SAR et des mesures expérimentales des paramètres du sol. Cette évaluation permet de trouver le modèle de rétrodiffusion le plus robuste qui simule le mieux le signal radar afin de l'utiliser par la suite dans les procédures d'inversion du signal radar pour estimer la rugosité du sol. Le deuxième axe de recherche de cette thèse consiste à proposer un modèle de rétrodiffusion radar semi-empirique pour les polarisations HH, HV et VV. Ce nouveau modèle a été construit avec la même base de données utilisée précédemment (chapitre d’évaluation des modèles de rétrodiffusion radar). Ce nouveau modèle sera également utilisé dans la procédure d'inversion du signal radar pour estimer la rugosité du sol. Le dernier axe de cette thèse consiste à construire une méthode d’inversion du signal radar en utilisant la technique des réseaux de neurones. Ces réseaux de neurones ont été entraînés à l'aide d'une base de données synthétiques élaborée à partir des modèles de rétrodiffusion radar choisis (IEM-B et le nouveau modèle semi-empirique proposé dans cette thèse). Ensuite, la méthode d’inversion du signal radar a été appliquée en utilisant des données Sentinel-1. La base de données de validation a été collectée sur un site en Tunisie (Kairouan) et un autre France (Versailles).
Cette thèse est composée de plusieurs chapitres. Le premier chapitre décrit l'importance des paramètres du sol et le potentiel des techniques de télédétection pour leur estimation. Le deuxième chapitre décrit la technique de télédétection radar et présente l'interaction des ondes électromagnétiques avec les sols agricoles nus, et aussi les paramètres de surface du sol (rugosité et l’humidité) ainsi que les différentes méthodes d'estimation de ces paramètres. Ensuite, les modèles de rétrodiffusion radar les plus populaires (semi-empiriques et physiques) ont été décrits et évalués dans le chapitre 3. Un nouveau modèle de rétrodiffusion radar semi-empirique est proposé dans le chapitre 4. Enfin au chapitre 5, les réseaux de neurones entraînés sur des données simulées à partir du modèle de rétrodiffusion radar IEM_B et du nouveau modèle semi-empirique proposé dans le chapitre 4 ont été utilisés pour estimer la rugosité du sol à partir d'images radar Sentinel-1. Les principaux résultats obtenus dans cette thèse ainsi que les travaux de recherche futurs sont présentés dans le chapitre 6.

**Chapitre 2**

Dans le **chapitre 2,** une introduction à la télédétection radar est exposée. Des rappels sont présentés sur les propriétés des ondes électromagnétiques et leurs interactions avec la surface des zones agricoles. Les paramètres descriptifs du sol (humidité et rugosité) sont également présentés ainsi que la sensibilité du signal radar à l'humidité et à la rugosité du sol. Dans cette thèse, notre étude se concentre sur les sols nus en zones agricoles. De plus, les modèles de rétrodiffusion électromagnétiques, qui simulent le signal radar en fonction des paramètres géophysiques du sol, sont introduits.

**Chapitre 3**

Dans le **chapitre 3,** l'évaluation des modèles de rétrodiffusion SAR les plus populaires (Oh, Dubois, IEM, IEM_B et AIEM) en utilisant une grande base de données SAR et des mesures in situ est effectuée. La base de données utilisée a été acquise sur de nombreux sites agricoles en France, Italie, Allemagne, Belgique, Luxembourg, Canada et Tunisie. Ainsi, cette étude est d'une grande importance pour la communauté scientifique parce qu'elle aide à comprendre les performances des modèles de rétrodiffusion en utilisant une grande gamme de conditions de surface du sol, acquises sur plusieurs sites d'étude à travers le monde, et par de nombreux capteurs SAR (plusieurs incidences, polarisations et longueurs d'onde radar). Jamais auparavant tous ces modèles de rétrodiffusion radar n'ont été évalués ensemble avec une aussi importante base de données (humidité "*mv*" entre 2 et 47 vol.%, rugosité "*Hrms*" entre 0.2 cm et 9.6 cm, angle d'incidence entre 18 ° et 57°). De plus, cette étude est la première à évaluer les modèles de rétrodiffusion en utilisant ensemble les bandes L, C et X.

Les résultats montrent que le modèle IEM modifié par Baghdadi (IEM_B), qui utilise un paramètre de calibration plutôt que la longueur de corrélation mesurée (fonction de corrélation gaussienne), fournit les simulations SAR les plus précises. En utilisant toutes les données ensemble (bandes L, C et X), le biais (différence entre simulations et mesures SAR) est inférieur à 1.0 dB et le RMSE sur l'estimation du signal radar est inférieur à 2.0 dB. Les performances du modèle IEM_B sont légèrement meilleures en bande X (RMSE = 1.8 dB) qu'en bandes L et C (RMSE entre 1.9 et 2.3 dB).

En utilisant les modèles IEM et AIEM avec la fonction de corrélation gaussienne, le RMSE sur l'estimation du signal radar est très élevé. En utilisant toutes les données (bandes L, C et X), le RMSE sur l'estimation du signal radar avec le modèle IEM est de 10.5 dB en polarisation HH et de 9.2 dB en polarisation VV. Avec le modèle AIEM, le RMSE est de 12.2 dB en HH et de 10.8 dB en VV. Les mauvaises simulations du signal radar correspondent aux faibles valeurs de rugosité (écart type des hauteurs, *Hrms*), principalement pour des *kHrms* inférieurs à 3 (*k* est le nombre d'onde radar). L'utilisation de la fonction de corrélation exponentielle en entrée des modèles IEM et AIEM conduit à des meilleures simulations du coefficient de rétrodiffusion radar. Le RMSE sur l'estimation du signal radar est d'environ 5.6 dB avec IEM et 4.4 dB avec AIEM en polarisation HH et d'environ 6.5 dB avec IEM et 3.8 dB avec AIEM en polarisation VV. Les résultats montrent que le modèle AIEM simule mieux la rétrodiffusion radar que le modèle IEM (version originale) seulement avec la fonction de corrélation exponentielle. De plus, les résultats sont légèrement meilleurs dans la bande X que dans les bandes C et L. En revanche, le modèle IEM simule mieux la rétrodiffusion radar dans la bande L que dans les bandes C et X. En polarisation HV, les résultats du modèle IEM montrent des erreurs très élevées avec un RMSE sur l'estimation du signal radar supérieur à 30.0 dB en utilisant à la fois la fonction de corrélation gaussienne et la fonction de corrélation exponentielle en entrée du modèle.

En utilisant les modèles de rétrodiffusion radar semi-empiriques, les résultats montrent que toutes les versions du modèle Oh fournissent des bonnes estimations du signal radar (RMSE inférieur à 3.0 dB) avec une performance légèrement meilleure de la version Oh 1992 aux polarisations HH et VV (biais inférieur à 1.0 dB et RMSE inférieur à 2.6 dB). De plus, nous observons que le modèle Oh fournit des meilleurs résultats que le modèle de Dubois qui simule la rétrodiffusion en HH avec un RMSE de 4.0 dB, et en VV avec un RMSE de 2.9 dB. En polarisation HV, la version Oh 2002 simule correctement la rétrodiffusion radar avec une différence entre les données réelles et simulées d'environ +0.7 dB et RMSE de 2.9 dB. La performance de la version Oh 1992 avec les polarisations HH et VV est meilleure dans les bandes C et X (biais compris entre -1.2 et +0.4 dB avec un RMSE inférieur à 2.5 dB) que dans la bande L (biais supérieur à +2.0 avec un RMSE inférieur à 3.0 dB).

En conclusion, le modèle IEM_B est le modèle qui fournit les meilleures simulations du signal radar. Ainsi, il est préférable de l'utiliser dans la procédure d'inversion du coefficient de rétrodiffusion SAR afin d'estimer les paramètres d'humidité et de rugosité du sol.

**Chapitre 4**

Dans le chapitre 4, un modèle empirique de rétrodiffusion radar basé sur le modèle de Dubois a été proposé. Les différents termes des équations de Dubois qui décrivent la dépendance entre le signal SAR et les paramètres du capteur et du sol ont été analysés et certains modifiés pour améliorer la modélisation du signal radar. Au final, un nouveau modèle semi-empirique de rétrodiffusion radar pour des sols nus a été développé pour les polarisations HH, VV et HV.

Les expérimentations montrent que le nouveau modèle fournit des résultats améliorés par rapport au modèle Dubois (cas de HH et VV). Les biais et RMSE ont diminué pour les polarisations HH et VV. De plus, les fortes sur-estimations et sous-estimations observées avec le modèle Dubois pour certaines gammes d'humidité du sol, de rugosité et d'angle d'incidence radar ont clairement diminué avec le nouveau modèle. L'analyse des performances du nouveau modèle pour chaque longueur d'onde radar séparément (L, C et X) montre que dans la bande L, les performances du nouveau modèle sont similaires à celles du modèle Dubois. Le nouveau modèle semi-empririque montre une amélioration significative des simulations en bandes C et X (RMSE d'environ 1.9 dB avec le nouveau modèle dans les bandes C et X, de 2.6 dB dans la bande C et 4.1 dB dans la bande X avec le modèle de Dubois).

La même formulation utilisée en HH et VV a été adoptée pour modéliser le signal radar en polarisation HV. La comparaison entre les simulations du nouveau modèle en polarisation HV et les données réelles (données SAR) montrent une valeur de RMSE de 2.1 dB (1.6 dB dans la bande L, 2.2 dB dans la bande C et 1.9 dB dans la bande X). Le biais est de -1.3 dB dans la bande L, de 0.2 dB dans la bande C et de -1.3 dB dans la bande X. Enfin, le nouveau modèle empirique proposé dans cette partie de la thèse a été testé dans le chapitre 5 pour l'estimation de la rugosité du sol à partir des nouvelles données SAR Sentinel-1A/B.

**Chapitre 5**

Le but du chapitre 5 est de développer une approche pour estimer la rugosité de la surface du sol (écart type des hauteurs, *Hrms*) à partir des données SAR Sentinel-1 en bande C dans le cas des sols agricoles nus. Cette approche d'inversion est basée sur la technique des réseaux de neurones multi-couches. L'entrainement des réseaux de neurones a été réalisé à l'aide de données synthétiques simulées par le modèle d'équation intégrale calibré par Baghdadi (IEM_B) et le nouveau modèle semi empirique (chapitre 4). L'approche d'inversion a ensuite

été validée en utilisant des données Sentinel-1 et des mesures in-situ (collectées en France et en Tunisie).

Deux configurations d'inversion ont été proposées. La première configuration d'inversion est basée sur l'estimation de la rugosité du sol à très haute résolution spatiale "THSR" (échelle de la parcelle ou à plus petite échelle). Deux réseaux ont été appliqués l'un après l'autre, le premier pour estimer l'humidité du sol (*mv*) et le second pour estimer la rugosité de la surface du sol (*Hrms*) en utilisant en entrée l'humidité du sol estimée par le premier réseau. Deux tests ont été effectués, le premier est utilisé en entrée pour le second réseau de neurones (celui pour estimer *Hrms*) le *mv* estimé à très haute résolution spatiale "THSR" (l'échelle de la parcelle). Le second test utilise comme entrée dans le second réseau l'humidité moyenne du sol estimée par le premier réseau (celui pour estimer *mv*) à l'échelle du site d'étude (une zone de quelques km²) en utilisant le coefficient de rétrodiffusion moyenne de tous les pixels agricoles nus du site d'étude. Trois configurations SAR ont été testées: VV seul, HV seul, VV et VH ensemble. Afin d'améliorer les estimations des paramètres du sol, une connaissance a priori sur l'humidité du sol *mv* est introduite (sols secs à légèrement humides ou très humides). L'information a priori sur l'humidité du sol (*mv*) est fournie par un expert qui utilise les données météorologiques (précipitations, température). En effet, après une forte pluie le sol est supposé être humide. En l'absence de pluie depuis quelques jours, le sol est supposé être sec ou légèrement humide. L'utilisation d'une connaissance a priori sur l'humidité du sol (sec à légèrement humide ou très humide) améliore les estimations de l'humidité du sol.

La deuxième configuration d'inversion concerne l'estimation en même temps de la rugosité du sol (*Hrms*) et de l'humidité du sol (*mv*). Les deux polarisations VV et VH sont utilisées ensemble en entrée du réseau.

En utilisant la première configuration d'inversion du signal radar (estimation de la rugosité du sol à très haute résolution spatiale "THSR" utilisant VV seul, VH seul ou VV et VH ensemble) et en utilisant les deux modèles de rétrodiffusion radar (IEM_B et Baghdadi), les meilleurs résultats sont obtenus en utilisant la polarisation VV seule pour le modèle IEM_B et les polarisations VV et VH ensemble pour le modèle semi-empirique de Baghdadi. L'humidité du sol pourra être estimée avec un RMSE de l'ordre de 6 vol.% quand une information a priori sur l'humidité est utilisée dans les réseaux de neurones (construits à partir du modèle IEM_B ou du nouveau modèle semi-empirique). Le deuxième réseau de neurones utilise cette estimation de *mv* pour estimer la rugosité du sol (*Hrms*) à l'échelle de la parcelle. Les résultats

obtenus montrent des estimations de *Hrms* avec un RMSE de 0.94 cm en utilisant le modèle IEM_B (polarisation VV seule) et 0.78 cm en utilisant le modèle semi-empirique Baghdadi (polarisations VV et VH ensemble). Cette précision sur *Hrms* obtenue en utilisant le réseau de neurones construit avec des informations a priori sur *mv* montre que l'utilisation des estimations de *mv* avec une précision d'environ 6 vol.% n'est pas suffisante pour estimer avec une bonne précision la rugosité du sol avec des données SAR en bande C.

Les résultats obtenus à partir du jeu de données Sentinel-1 montrent que la précision sur les estimations de la rugosité *Hrms* en utilisant les humidités estimées à l'échelle du site d'étude est meilleure qu'en utilisant les humidités estimées à l'échelle de la parcelle. Le modèle IEM_B estime la rugosité de surface *Hrms* avec un RMSE de 0.81 cm quand l'humidité utilisée est estimée à l'échelle du site d'étude et en utilisant la polarisation VV seul (RMSE = 0.98 cm en utilisant *mv* estimé à l'échelle de la parcelle). En utilisant le modèle semi-empirique Baghdadi, le RMSE sur *Hrms* est de 1.03 cm quand l'humidité utilisée est estimée à l'échelle du site d'étude et en utilisant les polarisations VV et VH confondues (RMSE = 1.05 cm en utilisant *mv* estimé à l'échelle de parcelle).

Pour la seconde configuration d'inversion (polarisations VV et VH utilisées ensemble en entrée du réseau), l'utilisation d'une base de données simulées à partir du modèle IEM_B ou du nouveau modèle semi-empirique Baghdadi montre des résultats proches des résultats obtenus avec la première configuration d'inversion. En utilisant pour la validation de cette configuration d'inversion la base de données réelles de Sentinel-1, l'humidité du sol *mv* pourra être estimée avec un RMSE de l'ordre 6.0 vol.% et de 6.6 vol.% en utilisant respectivement les modèles IEM_B et Baghdadi avec une information a priori sur *mv*. Le RMSE sur l'estimation de *Hrms* en utilisant le modèle IEM_B dans l'entrainement du réseau de neurones est de 0.84 cm sans information a priori sur *mv* et 0.75 cm avec une information a priori sur *mv*. En utilisant le modèle Baghdadi, le RMSE sur *Hrms* est d'environ 1.01 cm sans information a priori sur *mv* et de 0.97 cm avec une information a priori sur *mv*.

Cette première étude sur le potentiel des données Sentinel-1 (incidence de l'ordre de 40°) pour l'estimation de la rugosité du sol montre que le développement d'une procédure d'inversion automatique et généralisable du signal radar en bande C ne permet pas une estimation pertinente de la rugosité du sol. Les estimations de la rugosité du sol obtenues dans cette étude ne peuvent pas satisfaire les exigences des utilisateurs de la rugosité du sol (en

particulier pour les modélisateurs) car il faut au moins trois classes de rugosité: lisse (semis), moyen (petit labour) et rugueux (gros labour).

Seules les méthodes basées sur l'utilisation de relations expérimentales, souvent difficiles à appliquer à des sites autres que ceux pour lesquels elles ont été développées et qui ne sont généralement valables que pour des conditions pédologiques spécifiques, permettent de cartographier trois classes de rugosité. En effet, différentes études expérimentales ont révélé que la sensibilité du signal radar à la rugosité du sol (c'est-à-dire la pente des droites de régression) peut être très variable d'un site à l'autre. En outre, les relations expérimentales entre le signal radar et *Hrms* sont établies pour un angle d'incidence donné et une gamme d'humidité du sol. La composition du sol pourrait également être différente d'un site à l'autre. Toutes ces raisons expliquent pourquoi les relations expérimentales ne sont pas généralisables.

**Chapitre 6**

Les travaux de cette thèse ont porté sur plusieurs secteurs de recherche (évaluation, modélisation et estimation des paramètres du sol). Cette thèse a montré le potentiel des images radar du capteur radar Sentinel-1 pour estimer les paramètres de la surface du sol. Les résultats obtenus pourraient servir de guide pour soutenir la recherche dans plusieurs domaines.

Ces résultats permettent de conclure que les données SAR des capteurs Sentinel-1 (1A et 1B) en bande C avec un angle d'incidence d'environ 35 ° ne sont pas appropriées pour récupérer la rugosité de surface du sol. Il est donc essentiel de développer davantage des méthodes multi-capteurs combinant des données radar acquises à partir de deux longueurs d'onde radar : bandes L et C, ou bandes C et X. En effet, les trois fréquences L, C et X ont des capacités complémentaires pour estimer l'humidité du sol et la rugosité de sa surface. Comme le signal radar dans la bande X est plus sensible à l'humidité du sol que le signal radar dans la bande C (estimations d'humidité du sol dans la bande X deux fois supérieure à celle obtenue en bande C), il pourrait être pertinent de combiner les données SAR dans les bandes C et X pour estimer les paramètres du sol (c.-à-d. l'humidité du sol et la rugosité de la surface). Les données de la bande X seront utilisées pour estimer l'humidité du sol et les données de la bande C seront utilisées pour estimer la rugosité de la surface. L'utilisation des grandes longueurs d'onde radar (bande L par exemple) peut également être pertinente en raison du fort potentiel des grandes longueurs d'onde pour l'estimation de la rugosité du sol. Dans ce

contexte, différentes missions spatiales avec des systèmes SAR en bande L sont en préparation, comme NISAR (mission de la NASA et de l'ISRO). L'Agence spatiale européenne discute également de la possibilité d'ajouter une nouvelle bande SAR aux constellations des Sentinelles. L'arrivée de ces missions offrira une opportunité prometteuse pour développer des études basées sur la combinaison de données acquises par plusieurs capteurs, en particulier avec les missions Sentinel-1 et Sentinel-2. Les algorithmes multi-capteurs, et en particulier multi-fréquences seront essentiels pour atteindre les algorithmes opérationnels capables de séparer les effets de différents paramètres de surface sur les signaux radar. C'est notamment le cas de la surface de végétation couverte, pour laquelle la récupération de la rugosité est encore très compliquée avec une configuration de fréquence. L'objectif final est d'atteindre dans les prochaines années l'assimilation des cartes de rugosité, comme pour l'humidité du sol dans différents modèles de processus de surface, en tant que modèles d'écoulement et d'érosion.